NASA Conference Publication 2147

Research in Nonlinear Structural and Solid Mechanics

Research-in-progress papers presented
at a symposium held at Washington, D.C.,
October 6-8, 1980

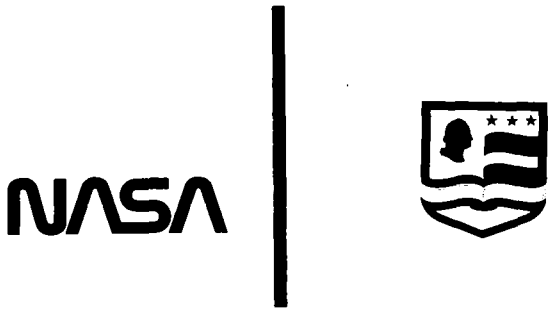

NASA Conference Publication 2147

Research in Nonlinear Structural and Solid Mechanics

Compiled by
Harvey G. McComb, Jr.,
NASA Langley Research Center

Ahmed K. Noor
The George Washington University
Joint Institute for Advancement of Flight Sciences
NASA Langley Research Center

Research-in-progress papers presented at a symposium sponsored by NASA Langley Research Center, Hampton, Virginia, and The George Washington University, Washington, D.C., in cooperation with the National Science Foundation, the American Society of Civil Engineers, and the American Society of Mechanical Engineers, and held at Washington, D.C., October 6-8, 1980

NASA
National Aeronautics
and Space Administration

Scientific and Technical
Information Branch

1980

FOREWORD

"The Engineer Grapples With Nonlinear Problems" was the title of the Fifteenth Josiah Willard Gibbs Lecture by Theodore von Karman published in August 1940 in the Bulletin of the American Mathematical Society. With his characteristic clarity and insight, Von Karman presented key aspects of nonlinear problems in selected fields of engineering and concisely described the mathematics available to address them. In May 1956, the entire issue of the Journal of the Aeronautical Sciences was comprised of papers written by former students of Von Karman and dedicated to him on the occasion of his 75th birthday. In this issue was a paper by Francis Clauser entitled "The Behavior of Nonlinear Systems."

We recommend Von Karman's 1940 paper and Clauser's 1956 paper for their illuminating discussions of fundamental nonlinear problems in engineering. Both papers include brief treatments of nonlinear problems in structural and solid mechanics. Notable advancements, dominated by the remarkable growth of computer technology, have been made in these fields in recent years. Nevertheless, in structural and solid mechanics the kinds of nonlinearities and the theories involved are diverse and complex enough to require large investments in computer resources or to pose significant analytical difficulties. Forty years after Von Karman's classic Gibbs Lecture, engineers in structural and solid mechanics continue to grapple with nonlinear problems.

A Symposium on Computational Methods in Nonlinear Structural and Solid Mechanics was held in Washington, D.C., on October 6-8, 1980. NASA Langley Research Center and The George Washington University sponsored the symposium in cooperation with the National Science Foundation, the American Society of Civil Engineers, and the American Society of Mechanical Engineers. The purpose of the symposium was to communicate recent advances and foster interaction among researchers and practitioners in structural engineering, mathematics (especially numerical analysis), and computer technology. The symposium was organized into 21 sessions with a total of 85 papers. Most of these papers are contained in the proceedings:

Noor, Ahmed K.; and McComb, Harvey G., Jr. (eds.): Computational Methods in Nonlinear Structural and Solid Mechanics. Pergamon Press, Ltd., 1980.

Topics discussed in the symposium included

(1) Nonlinear mathematical theories and formulation aspects

(2) Computational strategies for nonlinear problems

(3) Time integration techniques and numerical solution of nonlinear algebraic equations

(4) Material characterization and nonlinear fracture mechanics

(5) Nonlinear interaction problems

(6) Seismic response and nonlinear analysis of reinforced concrete structures

(7) Nonlinear problems for nuclear reactors

(8) Crash dynamics and impact problems

(9) Nonlinear problems of fibrous composites and advanced nonlinear applications

(10) Computerized symbolic manipulation and nonlinear analysis software systems

This NASA Conference Publication primarily contains papers presented in four research-in-progress sessions of the symposium which were reserved for reporting unfinished research for timely communication of the status of the work. The first five papers in this publication, however, are not research-in-progress papers, but were presented in other sessions.

The included papers are largely as submitted. Some authors did not adhere to the NASA policy of expressing all dimensional quantities in the International System of Units (SI). This requirement has been waived, and a table of conversion factors between U.S. Customary Units and SI is provided on page viii. Use of trade names or manufacturers' names does not constitute an official endorsement of such products or manufacturers, either expressed or implied, by NASA.

Harvey G. McComb, Jr.
Ahmed K. Noor
Compilers

CONTENTS

FORMULATION ASPECTS AND SPECIAL SOFTWARE FOR NONLINEAR ANALYSIS

(RESEARCH IN PROGRESS)

CONVERSION FACTORS FOR UNITS OF MEASUREMENTS

To convert from U.S. Customary Unit	To SI Unit	Multiply by
atmosphere (atm)	pascal (Pa)	$1.013\ 25 \times 10^{5}$
calorie (cal)	joule (J)	4.184
dyne	newton (N)	10^{-5}
foot (ft)	meter (m)	3.048×10^{-1}
inch (in.)	meter (m)	2.54×10^{-2}
inch-pound (in-lb or in-lbf)	newton-meter (N-m)	$1.129\ 848 \times 10^{-1}$
inch per second (in/sec)	meter per second (m/s)	2.54×10^{-2}
kips per square inch (ksi)	pascal (Pa)	$6.894\ 757 \times 10^{6}$
poise	pascal-second (Pa-s)	10^{-1}
pound force (lb or lbf)	newton (N)	4.448 222
pound mass (lb or lbm)	kilogram (kg)	$4.535\ 924 \times 10^{-1}$
pound per square inch (psi)	pascal (Pa)	$6.894\ 757 \times 10^{3}$

ANALYSIS OF REINFORCED CONCRETE STRUCTURES WITH OCCURRENCE OF DISCRETE CRACKS AT ARBITRARY POSITONS

J. Blaauwendraad, H.J. Grootenboer
Rijkswaterstaat, the Netherlands

A.L. Bouma, H.W. Reinhardt
Delft University of Technology, the Netherlands

SUMMARY

A nonlinear analysis of in-plane loaded plates is presented, which eliminates the disadvantages of the smeared crack approach. The paper discusses the elements used and the computational method. An example is shown in which one or more discrete cracks are dominant.

1. INTRODUCTION

In reinforced and prestressed concrete structures the post cracking behaviour, the collapse mechanism and the magnitude of the failure load are in most cases highly determined by the system of cracks that develops in the concrete. It is therefore not surprising that in finite element programs for the analysis of the nonlinear behaviour of concrete structures, besides the modelling of the constitutive relations, considerable attention is devoted to the inclusion in these programs of the occurrence of concrete cracks. In the literature two methods of schematizing the cracks are to be distinguished, namely: a method based on the possibility of discrete cracks along the boundaries of the elements and a method in which the cracks are assumed to be distributed over the element or over parts thereof. Each method has certain advantages and disadvantages. The aim of the reported study was to develop a model in which the advantages of both methods were combined (ref. 1). The model has been set up for the analysis of two-dimensional in-plane loaded reinforced or prestressed concrete structures. In the model are considered the various types of nonlinear material time-independent and time-dependent behaviour, the performance of the boundary layer between steel and concrete and the occurrence of discrete cracks within the structure.

The model is based on the finite element approach. For describing the structure two types of elements have been developed: a triangular thin plate element for schematizing the concrete and a bar element for describing the reinforcing steel or prestressing steel plus the bond zone with the surrounding concrete. Both these elements are based on the hybrid method with (what has been called) natural boundary displacements. It is characteristic of these elements that the stresses at their boundaries are always in equilibrium with one another and with the internal loading.

Besides taking account of the discontinuity in the displacements on each side of a crack, the model also takes account of discontinuity across a crack of the normal stresses in the direction of the crack. The method of initial strains is used for dealing with the nonlinear behaviour of the materials, the displacements at the crack and the slip of the reinforcement.

The development of this model, which has been called the MICRO-model, forms a part of the Dutch research project "Concrete Mechanics" (in Dutch: Betonmechanica). In this project concrete structures are studied along two parallel lines of basic experiments and computational methods. The subprojects for basic experiments concentrate on the fundamental behaviour of bond zones and on the phenomenon of force transfer in cracks. The results of this experimental work is fed into the subproject for computational methods. Apart of the here described model for two-dimensional in-plane loaded structures, also a model has been derived for the special case of plane framed structures in which linear elements are used allowing for normal strains, bending strains and shear strains. Because of the use of greater elements, this last model was called the MACRO-model. This paper will be restricted to the MACRO-model.

Discrete cracks versus "smeared-out" cracks

The method with discrete cracks:
- gives better insight into the relative displacements at a crack and the crack spacing;
- offers the possibility of describing the stress peaks and the dowel forces in the steel at a crack;
- can take account of the relationship between aggregate interlock and displacements at a crack;
- is often better able to schematize dominant cracks and their effect on behaviour.

A serious disadvantage of this method was that cracking was restricted to occur only along the element boundaries (ref. 2,3). This results in a high degree of schematization of the cracking pattern and considerable dependence on the subdivision into elements. Also in consequence of the detachment of the elements the system of equations must each time be re-established and inverted or decomposed.

Because of these disadvantages, in general, the discrete crack model has been abandoned in favour of the approach in which a crack is smeared or spread out over a whole element or over part of an element. The crack is thus incorporated into the stiffness properties of the concrete, which becomes anisotropic in consequence (refs. 4,5). Its great advantage is that cracking is conceived as a phenomenon like plastic deformation and can therefore be analyzed by the same methods, with which a good deal of experience has already been gained. The disadvantages of this method are due to "smearing out" the cracks. Especially the assumption about the stiffness perpendicular to the crack in an element with few or no reinforcement forms a problem. The reason is that in reality this stiffness not only depends on the element and the position of the crack herein but also on the circumstance if the element

is a link in a series connection of elements or a link in a parallel connection of elements. With this model the crack spacings and displacements at the cracks are difficult to calculate, even if a fine-meshed network of elements is used. This has its repercussions on the modelling of the aggregate interlock which highly depends on the displacements at the crack. Whether these drawbacks constitute a serious objection will depend on the kind of structure to be analysed.

In the MICRO-model a method of crack schematization is adopted which combines the advantages of both methods by treating cracks as (what they in reality are) discrete material boundaries for which the displacements and the normal stresses in the crack direction may be different on both sides. These "discrete" cracks may pass through the element mesh at any place in any direction and are continuous over the element boundaries.

Hybrid element model and natural boundary displacements

The hybrid element model with natural boundary displacements is used for the derivation of the force-deformation relations per element. In this model an assumption is made with regard to the distribution of the stresses in the element. The distribution of the displacements of the element boundaries is likewise assumed. This model offers the following advantages:

- the distribution of the stresses in the various types of element can be suitably interadjusted;
- discontinuous distribution of the displacements in an element can be taken into account quite simply in this model. Such discontinuity occurs if a crack passes through the element;
- the favourable experience previously gained with this type of finite element model can be used;
- the model offers the possibility of adding extra stress functions for describing special situations to the stress functions already existing;
- by adjusting the description of the displacements of element boundaries to the stress distribution at these boundaries it is ensured that the conditions of equilibrium are exactly satisfied at the boundaries. The advantage of this is that the stresses at a section along the element boundaries are always in equilibrium with the external loads.

The method of adjusting the description of the displacements of the element boundaries to the stress field so that inter-edge equilibrium is achieved is also called the method of natural boundary displacements (ref. 6). In this method we use for the description of the element boundary displacements a separate set of degrees of freedom per element boundary instead of the usually employed degrees of freedom in the element corners. In the next chapter the characteristics of the developed elements will be briefly discussed. For an extensive derivation see reference 1.

2. USED ELEMENT

Triangular plate element

The concrete is described by triangular thin plate elements. For the uncracked element we use per element boundary four degrees of freedom for the description of a linear displacement distribution in normal and tangential direction. In the element linear interpolation functions are used for the description of the stresses.To restrict in an element with twelve degrees of freedom the number of stressless displacement possibilities to the three rigid-body displacement modes, it is necessary to have at least nine independent stress parameters. A linearly distributed stress field for a thin plate which satisfies the internal equilibrium conditions in every point of the element only has seven independent stress parameters. So to satisfy the condition of nine independent stress parameters the second equation of Cauchy which states that σ_{xy} equals σ_{yx} in every point of the plate, is relaxed into the condition that the area integral per element of the shear stresses σ_{xy} and σ_{yx} must be equal ($\int_{v_e} \sigma_{xy}\, dv = \int_{v_e} \sigma_{yx}\, dv$).

Because the linear stress distribution per element boundary is uniquely represented by the four stress resultants per element boundary,full inter-edge equilibrium is achieved.

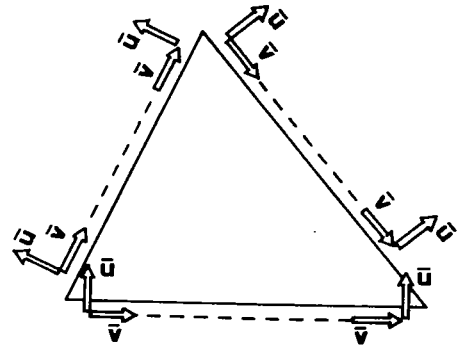

Figure 2.1 Degrees of freedom of an uncracked plate element.

If a crack has to occur in an element, this crack is assumed to form, in a straight line from one boundary of the element to another. Within a crack three additional degrees of freedom are introduced, two for the description of a linear varying crack opening (u_i , u_j) and one for the description of the parallel shift (v). (See figs. 2.1 to 2.4.)

In the vicinity of a crack the stresses may vary greatly due to dowel forces in the rebars or bond stresses between rebars and concrete.
To take account of these stress variations and the possibility of a discontinuity at a crack of the normal stress in the crack direction , the linear stress field of the uncracked element is extended for a cracked element with a stress field which is discontinuous across the crack.

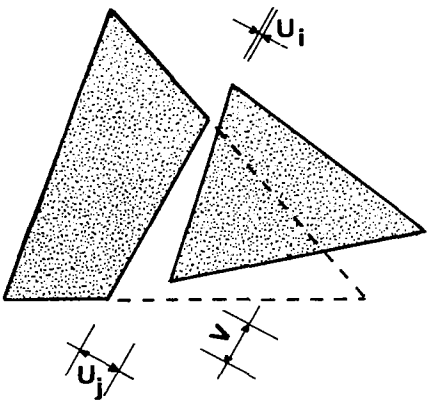

Figure 2.2 Displacement possibilities at a crack.

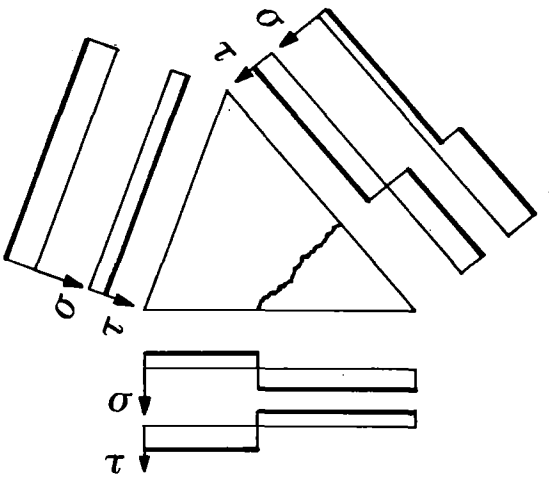

Figure 2.3 Distribution of the stresses, from the additional stress field, along the boundaries of a plate element with one crack.

To preserve full inter-edge equilibrium in a crack-crossed element boundary it is necessary to add to the linear displacement interpolation a discontinuous displacement interpolation. This is done per crack-crossed element boundary with the additional degrees of freedom Δu^0 and Δv^0.

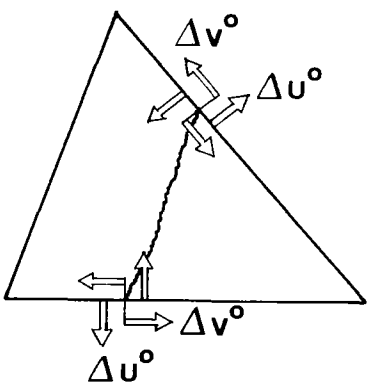

Figure 2.4 Extra degrees of freedom at cracked element boundaries.

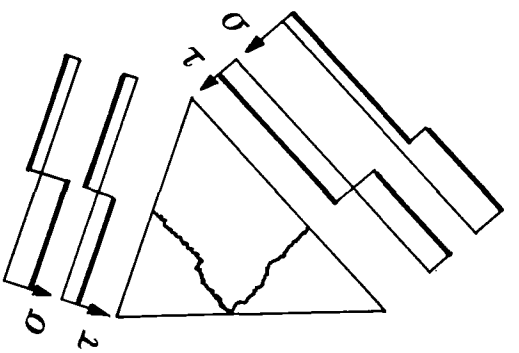

Figure 2.5 Distribution of the stresses, from the additional stress field, along the boundaries of a plate element with two cracks.

In an element a second crack is permitted only if this crack runs from the uncracked edge to the intersection of the first crack and the element boundary (see figure 2.5). Now the additional stress field is discontinuous over both cracks and we find additional degrees of freedom along all three element boundaries.

Rebar element

A linear bar element is used for the schematization of the embedded steel and the properties of the contact zone for bond between steel and concrete. The distribution of the forces in the bar element is adjusted for the distribution of the stresses along the boundaries of the triangular plate element with which these bar elements are to be associated. In the uncracked plate element a linear stress distribution has been adopted . So the shear stress τ along the rebar and the normal stress σ are also linear, which corresponds to a quadratic distribution for the normal force (F) and shear force (S) in the bar element. The distribution of the shear force in an element has been so chosen that the average shear force is always zero. This ensures that the bending moments in the bar remain small and that they are zero at the ends of the bar. It is still a point of discussion if this is permitted for all situations.

This assumption was necessary to restrict the number of stressless displacement modes to three. Because of the small influence of the shear flexibility on the structural behaviour it seems to be an allowable assumption.

$$\begin{bmatrix} F \\ \tau \\ S \\ \sigma \end{bmatrix} = \begin{bmatrix} 1 & s & s^2 & 0 & 0 \\ 0 & 1 & 2s & 0 & 0 \\ 0 & 0 & 0 & l^2-3s^2 & 2sl-3s^2 \\ 0 & 0 & 0 & -6s & 2l-6s \end{bmatrix} \begin{bmatrix} \beta(1) \\ \\ \\ \beta(5) \end{bmatrix}$$

Stress interpolation for uncracked rebar element; s is the coordinate along the element edge and l the length of the edge

In expectation of the results of the other study on the real properties of the boundary layer the constitutive equations for the combined steel/ boundary layer element are taken as

$$\begin{bmatrix} \varepsilon \\ \Delta_{||} \\ \gamma \\ \Delta_{\perp} \end{bmatrix} = \begin{bmatrix} \frac{1}{AE} & 0 & 0 & 0 \\ 0 & \frac{1}{K} & 0 & 0 \\ 0 & 0 & \frac{1}{D} & 0 \\ 0 & 0 & 0 & \frac{1}{B} \end{bmatrix} \begin{bmatrix} F \\ \tau \ (\frac{dF}{ds}) \\ S \\ \sigma \ (\frac{dS}{ds}) \end{bmatrix}$$

where:
- ε = strain of the steel
- $\Delta_{||}$ = slip in boundary layer
- $\gamma_{||}$ = deformation in steel due to shear force
- $\Delta_{\perp}$ = indentation of boundary layer
- $A^{\perp}$ = cross-sectional area of steel
- E = modules of elasticity of steel
- K = elastic stiffness of boundary layer with respect to slip
- D = dowel rigidity of steel
- B = elastic stiffness of boundary layer with respect to indentation

The displacements at the element boundaries are described with the aid of the displacement quantities $\overline{u}$ and $\overline{v}$ along the outside of the boundary layer and the displacements u and v at the outer ends of the steel bar.

The first set of degrees of freedom corresponds with the degrees of freedom of the plate element while the second set provides for the continuity of the normal and shear force over the length of the reinforcement.

If the bar element is intersected by a crack, then -as in the plate element- the stress functions and displacement function are extended by adding extra fields. These fields are compatible with the extra stresses and displacements used in the plate element.

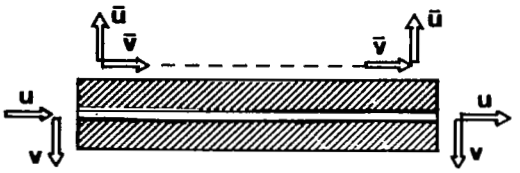

Figure 2.6 Degrees of freedom of an uncracked bar element.

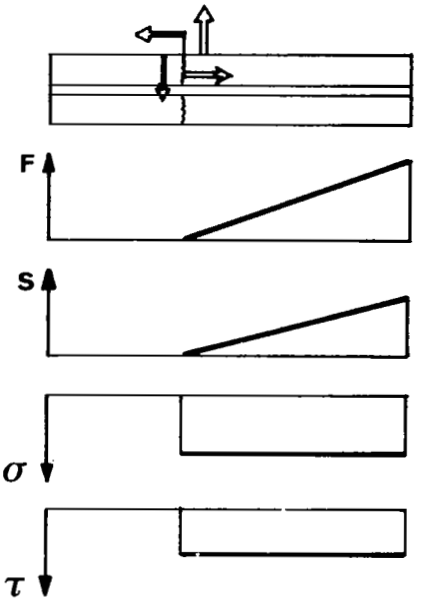

Figure 2.7 Extra stress fields and degrees of freedom in a bar element intersected by a crack.

3. COMPUTATIONAL METHOD

The finite element stiffness relations and equations were derived by using a Galerkin approach for the kinematic relations and the equilibrium conditions (see reference 1). This results for a structure without any cracks in the next set of equations:

$$S\underline{v}^0 = \underline{k} + A\underline{\varepsilon}^I - B\underline{q}$$

Herein v^0 are the degrees of freedom, k represents the applied load, ε^I is the sum of all initial strains and q is the volume load. In the method of analysis envisaged in the MICRO-model, the strains are split up into an elastic part and an initial part. The elastic strains are those which would occur if the material displayed ideal linearly elastic behaviour. The initial strains are used to account for all nonlinearities such as plastic deformation, creep, shrinkage, etc. When a load increment is applied the set of equations is solved iteratively by adjusting the initial strains until all criteria of nonlinearity are fulfilled to a certain accuracy.

When cracks occur, an additional stress field with stress parameters $\bar{\beta}$ and additional degrees of freedom $\bar{v}^0$ are introduced (v.s.).
Now it can be shown that the set of equations is replaced by two systems of equations:

$$S\underline{v}^0 = \underline{k} + A\underline{\varepsilon}^I - B\underline{q} - C\underline{v}^{cr} - D\underline{\bar{\beta}}$$

$$\bar{S}\underline{\bar{v}}^0 = \bar{A}\underline{\varepsilon}^I - \bar{C}\underline{v}^{cr} - E\underline{v}^0$$

Herein v^{cr} are the number of degrees of freedom on the crack faces (vs.) and v^0 the additional degrees of freedom on the element boundaries at the point of intersection with a crack.
The split up of the equations in two sets is done to avoid the alteration of the origional system matrix S and the renumbering of the degrees of freedom v^0 . During the iterative solution procedure both sets of equations are solved in sequence. In this procedure we calculate $\underline{v}^0$ from the first set of equations using for the additional stress parameters $\bar{\beta}$ the value from the preceding iteration. In each iteration the initial strains ε^I and the internal crack displacements v^{cr} are adjusted to the criteria of nonlinearity c.q. the stress conditions for a crack.
To take into account the internal stress redistribution due to a crack, one element crack at a time is allowed to occur. Only when the normal stresses on the crack surfaces have become sufficiently low, can another cracked element occur.
Each time when a new crack is formed the matrix $\bar{S}$ has to be formed and decomposed again.
Because the bandwidth of this matrix stays very small this requires much less time than a reformation and decompositon of matrix S would take.

To decide when an element is cracked and to determine the direction of the crack we use the average stresses over an element. When these stresses are in the range in which the crack criterion is valid and supercedes the criterion more than will occur in other elements, a crack is assumed to form (with the restriction that the normal stresses on the existing crack faces are small enough). A crack is placed through the centre of the triangular element, except if a crack already ends on the boundary of the element. In that case the new crack proceeds from this existing crack.
In reality there is a local stress peak near the tip of a crack. This causes further spreading of a crack, even if the average stresses in the vicinity thereof -apart from the stress peaks- are below the cracking criterion. In the MICRO-model these highly localized stress fields are not included. The effect that, in an element adjacent to the end of an existing crack, a crack will develop at lower average stresses than it would if there were no cracks present, is here dealt with by reducing the cracking criterion for these elements. The calculations that have been performed show a reduction to about 0.7 to be satisfactory. A crack, once it has been introduced into the model, remains in existence. The procedure does however take account of the possibility that, on further loading or unloading the structure, it may occur that a crack closes up again by compression, but as soon as tensile stresses act across a closed crack, the latter opens again. Transfer of compressive stresses across a crack is possible only for zero crack width.

For determining the displacements in the cracks and the initial strain for the elasto-plastic materials a fictitious visco-plastic model is used. By doing this the iteration process can be conceived as a fictitious creep process with a time interval Δt between each two successive iterations and a loading of the viscous element equal to the unbalanced stresses $(\Delta\sigma)$. Per iteration the increase in the internal crack displacements or initial strains is

$$\Delta v^{CR} \ (\Delta\varepsilon^{I}) = K\Delta\sigma$$

To ensure that the iteration process is stable the value of K must not be taken too large (see reference 7). The number of iterations needed per load increment is highly influenced by the number of cracks present in the structure. In order to speed up the iteration process, whenever a number of cracks have formed, the system matrices S and $\bar{S}$ are changed in order to take into account the condition that the normal stresses on the faces of open cracks must become zero.

4. EXAMPLE OF REINFORCED BEAM WHICH FAILS IN SHEAR

After several calculations in which the MICRO-model had proven its ability to simulate bending failure (see reference 1), a reinforced beam which fails in shear was analysed with the model. This beam is one of a series of beams which were tested in the Stevin Laboratory of the Delft University of Technology in the Netherlands in a program of research to investigate the influence of beam depth and crack roughness on the shear failure load (ref. 8). The beam was loaded as shown in figure 4.1.

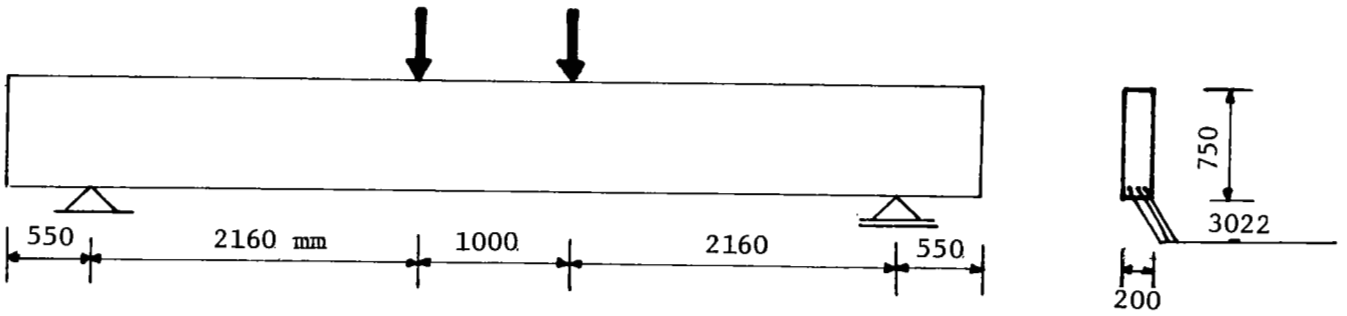

Figure 4.1 Shape and manner of loading of tested beam.

On account of symmetry of the structure, the boundary conditions and the loading, it was sufficient to confine the analysis to one half of the structure. The network of elements, the restraints and support and the external loading of this half structure have been shown in figure 4.2.

In the experiment as well as in the analysis abrupt failure occured, caused by crushing of the concrete at the tip of an inclined (shear) crack. At failure the stresses in the rebars were still below the yield stress.

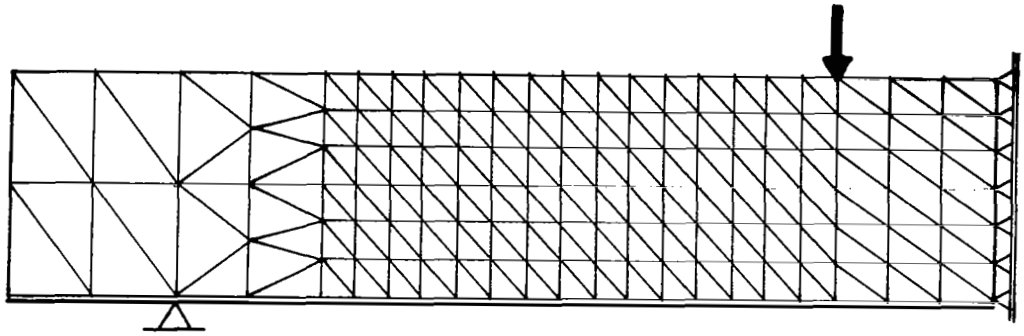

Figure 4.2 Network of element.

The experimentally determined failure load and the failure load found from the analysis were very close to each other (112,1kN and 112,4kN). The load deflection curves for the experiment and the analysis are given in Fig. 4.3.

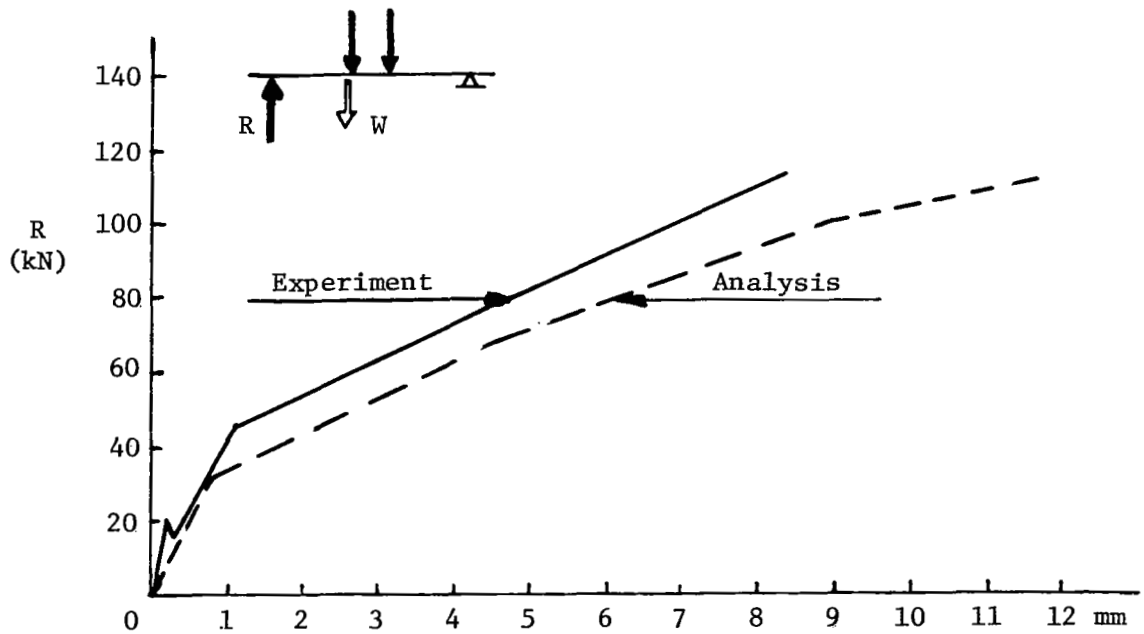

Figure 4.3 Load-deflection diagram.

It follows from the load-deflection curves that the analysis leads to a somewhat lower stiffness than was registered in the experiment. An explanation for this lower stiffness may be a too low tensile strength for the concrete in the analysis, which results in the premature occurrence of cracks and a bend in the load-deflection curve at a lower value of the load than in the test. The maximum bond stress between steel and concrete may have been chosen too low as well.

Fig. 4.4 shows the crack patterns, just before failure, according to experiment and analysis. For convenience of comparison the reflection of the right part of the beam has been displayed in this figure.

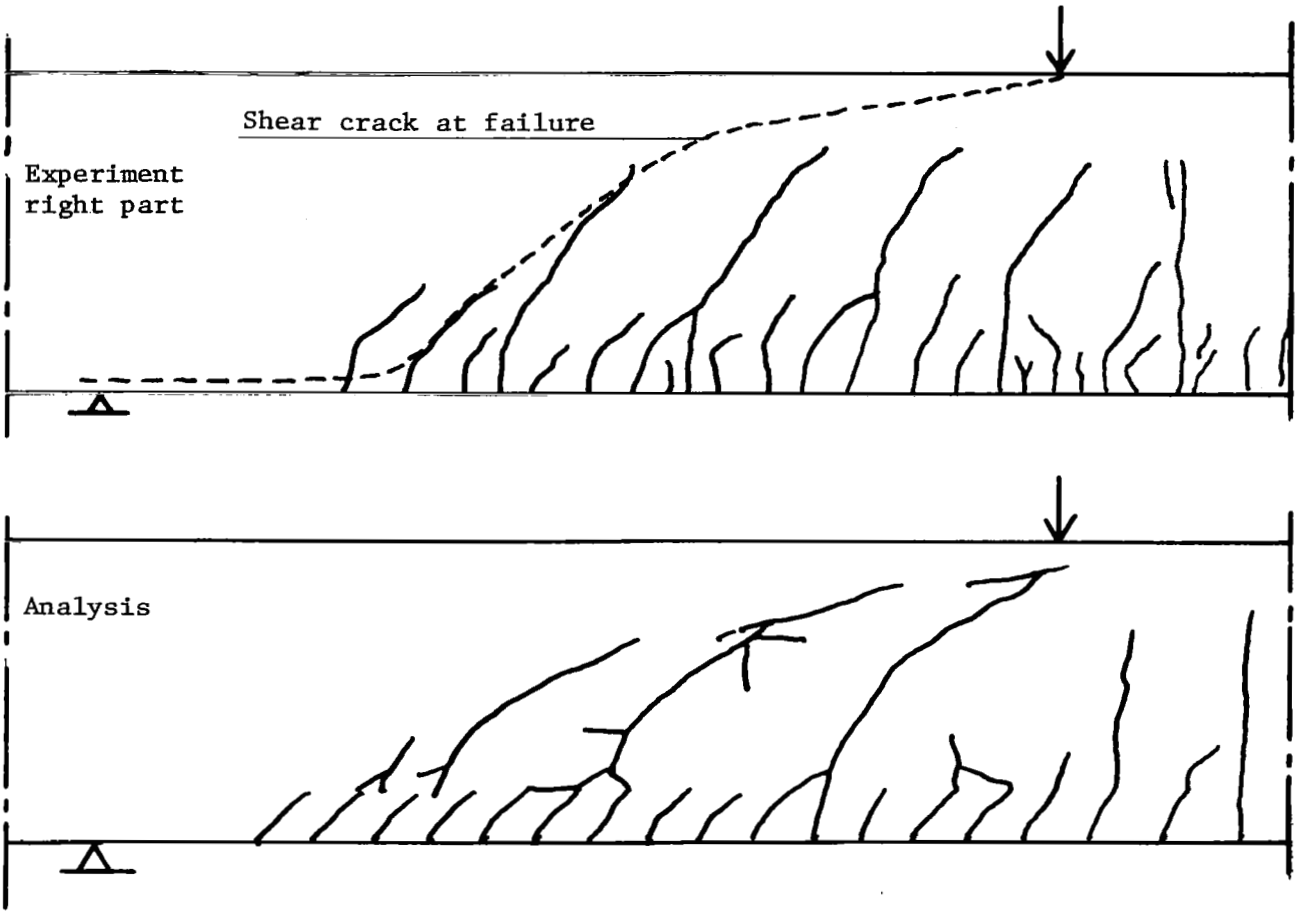

Figure 4.4 Crack pattern experiment and analysis.

It can be seen from these crack patterns that the beam fails due to an inclined shear crack in the experiment. This inclined crack was also found in the analysis. In fact there is a very good agreement between the crack patterns of the test and the analysis. Although not much information about the width of the cracks in the experiment is available, it seems that in the analysis somewhat larger crackwidths were found than in reality. This corresponds with the smaller stiffness as discussed above and can also be the result of a slightly low value for tensile strength of concrete and maximum bond stress.

5. SUMMARY AND CONCLUSIONS

A finite element program has been presented for the analysis of two-dimensional in-plane loaded concrete structures. The program makes use of seperate elements for the description of the concrete and the rebars including the bond zone with the surrounding concrete. When cracks occur they are handled as being discrete. Displacements and stresses may be discontinuous across a crack. Cracks may pass through the finite element mesh at any place in any direction and are continuous over the element boundaries.

The elements are based on the hybrid method with natural boundary displacements, resulting in stresses at the inter-element boundaries which are always in equilibrium with one another and with the external loading. The model takes care of the different types of nonlinear material behaviour. Comparison of the results of experiments with the results of analyses shows that the model is capable of obtaining a good prediction of the deformation, crack pattern, crack widths, failure load and internal stress distribution of concrete structures under in-plane static loading.

REFERENCES

1. GROOTENBOER H.J.
   "Finite element analysis of two-dimensional reinforced concrete structures, taking account of nonlinear physical behaviour and the development of discrete cracks".
   Dissertation, Delft, 1979.
2. NGO D/SCORDELIS A.C.
   "Finite element analysis of reinforced concrete beams". ACI Journal, Proceedings Vol. 64 no.3,
   March 1967 p.p 152-163.
3. STAUDER W.
   "Ein Beitrag zur Untersuchung von Stahlbetonscheiben mit Hilfe finiter Elemente unter Berücksichtigung eines wicklichkeits nahen Werkstoffverhaltes" (in German)
   Dissertation, Darmstadt, 1973.
4. FRANKLIN H.A.
   "Nonlinear analysis of reinforced concrete frames and panels".
   Dissertation, Berkeley, 1970.
5. SCHNOBRICH W.C.
   "Behaviour of reinforced concrete structures predicted by the finite element method". Computers & Structures, Vol. 7, no. 3.
   June 1977 p.p 365-376.
6. BLAAUWENDRAAD J.
   "Systematic derivation of models in mechanics using direct methods and variational techniques" (in Dutch).
   Dissertation, Delft 1973.
7. CARMEAU I.
   "Numerical stability in quasistatic elasto/viscoplasticity".
   International Journal for numerical methods in engineering, 1975, vol. 9, p.p 109-127.
8. WALRAVEN J.C.
   "The influence at depth on the shear strength of lightweight concrete beams without shear reinforcement".
   Stevin Laboratory, Delft University of Technology, report nr. 5-78-4.

COMPUTATIONAL MODELS FOR THE NONLINEAR ANALYSIS OF REINFORCED CONCRETE PLATES

E. Hinton, H.H. Abdel Rahman and M.M. Huq

University College of Swansea

SUMMARY

A finite element computational model for the nonlinear analysis of reinforced concrete solid, stiffened and cellular plates is briefly outlined. Typically, Mindlin elements are used to model the plates whereas eccentric Timoshenko elements are adopted to represent the beams. The layering technique, common in the analysis of reinforced concrete flexural systems, is incorporated in the model.

INTRODUCTION

The present studies were motivated by the need to develop finite element computational models suitable for the efficient and accurate nonlinear analysis of reinforced concrete bridge decks and flexural systems. In particular solid as well as stiffened and cellular plates are of interest and the full load-displacement history is required.

Previous studies have generally been based on Kirchhoff plate and Euler-Bernouilli beam representation and one novel feature of the present studies is the use of Mindlin plate and Timoshenko beam theories. Apart from the fact that transverse shear deformation effects are then automatically taken into account, the use of Mindlin/Timoshenko models allows the adoption of $C^{(o)}$ rather than $C^{(1)}$ finite elements in the discretisation process.

In the nonlinear analysis of reinforced concrete plates it is important to allow for the gradual spread of cracking and yielding of the concrete over the plate thickness as well as the yielding of the steel in the reinforcement. To cater for these effects the well-known layered approach is adopted. Tension stiffening, which will be described later, is included in the concrete model and various unloading curves are considered. As well as providing a better representation of the reinforced concrete behaviour during cracking, tension stiffening appears to have a beneficial effect on the numerical stability of the nonlinear solution scheme.

The authors have successfully experimented with a variety of nonlinear solution schemes. In the present context, experience points to the use of either the Quasi-Newton method with large load increments and a fine convergence tolerance or the initial stiffness method with small load increments and a coarser convergence tolerance. The results quoted here have been obtained using the initial stiffness method with small load increments after

initial cracking has occurred and a coarse convergence tolerance (1%) on the displacements norm.

Also quoted in this paper are results from a numerical experiment with a tentative cellular plate model based on a beam-plate representation. A layered beam models the webs whereas a layered plate with zero rigidity in the void region is used to model the flanges. The transverse shear rigidity of the plate in the plane perpendicular to voids is suitably modified. For cylindrical voids the beams have variable width over the cross-section.

The basic formulation is now described in a little more detail.

BASIC FORMULATION

Main assumptions In Table I the main features of the Mindlin plate formulation are indicated. (NB: The Timoshenko beam formulation, which is based on similar concepts, is omitted.) In the usual Mindlin plate representation integration through the plate thickness is performed explicitly prior to discretisation and therefore the present model is really a degenerated 3D model with restricted (flat) geometry. The main assumption is that normals to the plate midsurface remain straight but not necessarily normal after deformation. Thus the displacements u, v and w at any point in the plate with coordinates (x,y,z) can be expressed as

$$\begin{bmatrix} u(x,y,z) \\ v(x,y,z) \\ w(x,y,z) \end{bmatrix} = \begin{bmatrix} u_o(x,y) - z\,\theta_x(x,y) \\ v_o(x,y) - z\,\theta_y(x,y) \\ w_o(x,y) \end{bmatrix} \qquad (1)$$

where u_o, v_o and w_o are the displacements at the plate midsurface (xy plane) in the x,y and z directions respectively and θ_x and θ_y are the rotations of the normal in the xz and yz planes respectively.

The strain-displacement relationships may therefore be expressed as

$$\underline{\varepsilon} = \begin{bmatrix} \underline{\varepsilon}_m \\ \underline{0} \end{bmatrix} + \begin{bmatrix} z\,\underline{\varepsilon}_f \\ \underline{\varepsilon}_s \end{bmatrix} \qquad (2)$$

in which the membrane strains $\underline{\varepsilon}_m = [u_{o,x},\ v_{o,y},\ u_{o,y} + v_{o,x}]^T$

the flexural strains $\underline{\varepsilon}_f = [-\theta_{x,x},\ -\theta_{y,y},\ -(\theta_{x,y} + \theta_{y,x})]^T$

and the shear strains $\underline{\varepsilon}_s = [w_{o,x} - \theta_x,\ w_{o,y} - \theta_y]^T$

and where $u_{o,x} \equiv \partial u_o / \partial x$ etc.

Elasto-plastic behaviour of concrete Concrete is idealised as an elastic-perfectly plastic material in uniaxial compression. The behaviour of concrete in biaxial stress states is described by an idealised version of the failure envelope obtained by Kupfer et al. (Ref.1). A Von Mises failure surface is used in the biaxial compression zone. See also reference 2. Concrete which has yielded can sustain compressive strains smaller than a limiting strain ε_{cu}. However, when the concrete reaches this strain it is assumed to crush. The crushing surface adopted here is given as

$$c(\underline{\varepsilon}) = \varepsilon_x^2 - \varepsilon_x \varepsilon_y + \varepsilon_y^2 + \frac{3}{4}\gamma_{xy} - \varepsilon_{cu} = 0 \qquad (3)$$

where ε_x and ε_y are the strains in x and y directions and γ_{xy} is the shear strain.

In tension, the concrete is assumed to behave elastically until the tensile strength (f_t') is reached. The concrete then cracks in a direction orthogonal to the stress direction and loses strength. An unloading curve is assumed to account for tension stiffening in the cracked concrete. The stress level in the cracked concrete is interpolated using the tension stiffening curve depending on the degree of straining in the concrete. Concrete cracked in one direction is assumed to have uniaxial properties in that direction only. Concrete cracked in two directions is assumed to lose all of its strength.

The constitutive relations of the concrete are continuously updated according to the stress state in the concrete. However, it must be noted that the shear rigidities always retain their elastic values. The constitutive relations can also be written in partitioned form by separating out the membrane-flexure and shear strain energy terms.

Yielding of steel The steel reinforcement is smeared into steel layers which are assumed to be in a state of uniaxial tension or compression. When the longitudinal stress exceeds the proportionality limit, the steel starts to yield. Strain hardening of the steel can be included if the strain hardening parameter, H' is known. The constitutive relation for yielded steel is given as

$$\sigma_s = \sigma_y + \varepsilon_s E\left[1 - \left(\frac{E}{E+H'}\right)\right] \qquad (4)$$

in which σ_s and ε_s are the stress and strain in steel, E is the Young's Modulus and σ_y is the yield stress.

Slab-beam idealisation The first step in the analysis of a slab-beam system such as the one shown in figure 1 is to discretize the structure into a suitable number of plate and beam elements. In order to simplify the analysis, the stiffeners must be attached along the mesh lines of the plate elements.

The selectively integrated, isoparametric 9-node Heterosis element (Ref.3) is used to model the plate. A hierarchical formulation is adopted to represent all degrees of freedom. Thus the shape functions $\underline{N}_i$ in Table I

are constructed as follows:

$N_1^{(e)}$ ... to $N_8^{(e)}$ are the 8-node Serendipity shape functions and $N_9^{(e)}$ is the bubble shape function $(1-\xi^2)(1-\eta^2)$ associated with the 9^{th} internal node. Note that $\underline{a}_i^{(e)} = [u_i^{(e)}, v_i^{(e)}, w_i^{(e)}, \theta_{xi}^{(e)}, \theta_{yi}^{(e)}]$, $\underline{a}_1^{(e)}$ to $\underline{a}_8^{(e)}$ are the vectors of displacements at nodes 1 to 8 on the boundary of the element and $\underline{a}_9^{(e)}$ is the vector of the degrees of freedom at the hierarchical central node 9. To obtain the displacement vector at node 9 the following expression is used

$$\underline{a}_9' = \sum_{i=1}^{8} \underline{N}_i^{(e)}(0,0)\, \underline{a}_i^{(e)} + \underline{a}_9^{(e)} \qquad (5)$$

The 8-node Serendipity representation can be obtained if all degrees of freedom at node 9 are constrained to zero. If they are all left free, a 9-node Lagrangian representation is obtained. For the Heterosis type representation, only the hierarchical lateral deflection at node 9 is restrained to zero and (5) is used to interpret displacements at node 9.

The 3-node isoparametric Timoshenko beam element is adopted for the beams. The reader should consult reference (4) for further details regarding this element. Beam elements can be located along the mesh lines of the plate elements. The properties of each element are calculated first in the local direction and then transformed to the global coordinate system.

Since the stiffener element is assumed to be monolithically connected to the plate, compatibility of deformation along the junction line between the beam and the plate is enforced since a related system of displacement functions is used for the plate and beam elements. As the details of the stiffness matrix evaluation are standard they are not included here.

The layered beam and plate elements are shown in figure 2.

Nonlinear solution A very small load increment is first applied to the structure, and the cracking load is then estimated. The size of the successive load increments is chosen to be equal to 0.1 times the cracking load as suggested by Johnarry (Ref.5); this improves the rate of convergence since nonlinearities are induced gradually in the structure. For each linearised increment, the unknown displacements are obtained using the initial uncracked stiffness matrix. Strains calculated at the centre of each layer are taken as representative for the whole layer. Stresses are then calculated using the material properties from the previous material state. After checking the state of stress for possible yielding, cracking or crushing, the internal nodal resisting forces can then be calculated and compared with the external forces. The lack of equilibrium between internal and external forces is corrected by applying the out-of-balance or residual forces. The out-of-balance forces are successively applied through a series of iterations of the solution and new corrections to the unknown displacements are obtained until the equilibrium and the constitutive relations are satisfied within a certain allowable limit.

The following convergence criterion is used:

$$(\delta \underline{a}^T \delta \underline{a})^{\frac{1}{2}} / (\underline{a}^T \underline{a})^{\frac{1}{2}} \leq 0.01 \qquad (6)$$

where $\delta \underline{a}$ and $\underline{a}$ are the vectors of iterative and total displacements respectively.

The analysis is terminated when convergence is not achieved within a specified number of iterations. This usually occurs when a structure is about to fail. An estimate of the failure load can then be obtained.

SOLID AND STIFFENED PLATES

Corner supported slab A corner supported doubly reinforced concrete slab (Ref.6) is analysed using a 3x3 mesh in a symmetric quadrant. Initially it is assumed that there is no tension stiffening. Crack patterns on the lower surface of the slab for two load levels (12 kN and 62 kN) are shown in figure 3. Figure 4 shows the load displacement curve. After the steel yields the norm of the out-of-balance membrane forces is rather large even though the displacement convergence tolerance is satisfied. When the displacement tolerance is decreased from 1% to 0.1% after the steel yields, an improved result is obtained as shown in figure 4.

When tension stiffening is used, improved displacement values are obtained. However, this results in higher failure loads. When the unloading part of the tension stiffening curve is extended, better results are obtained for the displacements but the failure loads are still high. When a finer tolerance is used after steel yielding, excellent results are obtained as shown in figure 5.

Stiffened slab The load-central deflection curve predicted by the present model for a reinforced concrete T-beam tested by Cope and Rao (Ref.7) are given in figure 6, which also includes some geometric details of the beam. The load-deflection graphs obtained by Cope and Rao, both experimentally and using a finite element shell formulation, are also reproduced in figure 6. The good agreement between the load-deflection graphs predicted by the present analysis and both Rao's experimental and numerical analyses shows that the proposed approach provides an inexpensive yet fairly accurate analysis for reinforced concrete slabs with RC beam stiffeners.

REINFORCED CONCRETE VOIDED PLATES

Voided reinforced concrete and prestressed concrete plates are widely used for their economic advantages. Although the behaviour of such structures has been studied in the elastic range (Ref.8 , Ref.9), very little experimental and analytical work appears to have been carried out on the behaviour of these structures in the overloading and ultimate stages. In the elastic analysis, equivalent values of the flexural, torsional and shear rigidities of a voided plate can be calculated in different ways (Ref.9 , Ref.10) and used in a finite difference or a finite element analysis of an equivalent orthotropic solid plate. The nonlinear analysis is, however, rather more complex. The spread of plasticity and nonlinearities due to cracking and crushing of concrete

through the depth of the plate must be taken into account. A nonlinear finite element analysis using a 3D or shell formulation to represent different structural elements of the voided plate seems ideal. Unfortunately such a formulation, though feasible, is very expensive. In the present approach, a less expensive approach to the nonlinear analysis of RC voided plates is tentatively suggested. The analysis is based on the formulation of RC stiffened plates described earlier, where the voided plate is assumed to consist of voided plate elements representing the upper and lower flanges and beam stiffeners representing the webs.

The basic assumption is basically that of Mindlin: a transverse plane normal to the middle plane of the plate remains plane but not necessarily normal after deformation, thus implying that the deformations of both flanges are related. This assumption may be justified for voided slabs with large numbers of voids, which have an overall bending behaviour predominantly in the longitudinal direction. In situations where the upper flange is directly loaded by a concentrated load, better results can be achieved if an overlapped mesh is used for a small part around the loaded area to represent the upper flange solely while the original mesh in this part represents the lower flange.

Documented experimental evidence for such structures is provided by Elliott, Clark and Symmons (Ref.11). In this work the results of a quarter scale model reinforced concrete voided bridge have been reported. The geometrical details of the slab are summarised in figure 7. A number of tests were made to study the performance of the slab in the service as well as the over-loading stages and finally an ultimate load test was carried out. This example has been solved using the proposed approach for voided slabs. The discretization and cross section representation of a symmetric quarter of the plate is given in figure 8, while the load-central deflection graphs obtained experimentally and analytically are compared in figure 9. It is reported that the cracking load was nearly equal to the working load which is in agreement with that predicted by the proposed model. The agreement between the experimental and analytical graphs shown in figure 9 is very encouraging. The experimental results show that the slab failed by the formation of a mechanism which involved longitudinal shear/flexural yield lines and transverse hogging flexural yield lines. The analytical study, however, slightly overestimates the failure load since shear failures cannot be predicted by the present model.

CONCLUSIONS

The proposed computational model for the nonlinear analysis of solid and stiffened reinforced plates provides an inexpensive and reasonably accurate approach which can be extended for use with voided plates.

REFERENCES

1. Kupfer, H.; Hilsdorf, H. K, and Rusch, H.: Behaviour of Concrete Under Biaxial Stresses. J. Am. Conc. Inst., Vol.66, No. 8, 1969,pp.656-666.

2. Abdel Rahman, H. H.; Hinton, E.; and Huq, M. M.: Nonlinear Finite Element Analysis of Reinforced Concrete Slab and Slab-beam Structures. Proceedings of Int. Conf. on Numerical Methods for Nonlinear Problems, University College, Swansea, Pineridge Press, 1980, pp. 493-512.

3. Hughes, T.J.R.; and Cohen, M.: The Heterosis Finite Element for Plate Bending, Computers and Structures, vol. 9, 1978, pp. 445-450.

4. Hinton, E.; and Owen, D.R.J.: Finite Element Programming, Academic Press, 1977.

5. Johnarry, T.: Elasto-plastic Analysis of Concrete Structures. Ph.D. Thesis, University of Strathclyde, 1979.

6. Mueller, G.: Numerical Problems in Nonlinear Analysis of Reinforced Concrete. UC-SESM Report No. 77-5, University of California, Sept. 1977.

7. Cope, R. J.; and Rao, P.V.: Nonlinear Finite Element Analysis of Concrete Slab Structures, Proc. Inst. Civ. Engrs., Part 2, vol.63, 1977, pp. 159-179.

8. Hinton, E.; Razzaque, A.; Zienkiewicz, O. C.; and Davies, J. D.: A Simple Finite Element Solution for Plates of Homogeneous, Sandwich and Cellular Construction. Department of Civil Engineering, University of Wales, Swansea, C/R/217/74, 1974.

9. Basu, A. K.; and Dawson, J. M.: Orthotropic Sandwich Plates, Proc. Inst. Civ. Engrs., 1970, Supplementary Paper 7275S, pp. 87-115.

10. Highway Engineering Computer Branch, Department of Transport, User Guide, Slab and Pseudo-slab Bridge Decks, HECB/B1/7.

11. Elliott, G.; Clark, L. A.; and Symmons, R. M.: Test of a Quarter-scale Reinforced Concrete Voided Slab Bridge. Cement and Concrete Association, Dec. 1979, Technical Report 527 (Publication 42.527).

TABLE I.- MINDLIN PLATE FORMULATION

Virtual work equation

$$\int_V \delta \underline{\varepsilon}_1^T \underline{\sigma}_1 \, dV + \int_V \delta \underline{\varepsilon}_2^T \underline{\sigma}_2 \, dV - \int_V \delta \underline{u}^T \underline{b} \, dV - \int_{S_t} \delta \underline{u}^T \underline{t} \, dS = 0$$

where

displacements $\underline{u} = [u, v, w]^T$

virtual displacement $\delta\underline{u} = [\delta u, \delta v, dw]^T$

in-plane strains $\underline{\varepsilon}_1 = [u_{,x}, v_{,y}, u_{,y} + v_{,x}]^T$

$\delta\underline{\varepsilon}_1 = [\delta u_{,x}, dv_{,y}, du_{,y} + dv_{,x}]^T$

shear strains $\underline{\varepsilon}_2 = [w_{,x} - \theta_x, w_{,y} - \theta_y]^T$

$\delta\underline{\varepsilon}_2 = [\delta w_{,x} - \delta\theta_x, \delta w_{,y} - \delta\theta_y]^T$

in-plane stresses $\underline{\sigma}_1 = [\sigma_x, \sigma_y, \tau_{xy}]^T$

$\delta\underline{\sigma}_1 = [\delta\sigma_x, \delta\sigma_y, \delta\tau_{xy}]^T$

shear stresses $\underline{\sigma}_2 = [\tau_{xz}, \tau_{yz}]^T$

$\delta\underline{\sigma}_2 = [\delta\tau_{xz}, \delta\tau_{yz}]^T$

Incremental stress/strain relationships

$$d\underline{\sigma}_1 = \underline{D}_1 \, d\underline{\varepsilon}_1$$

$$d\underline{\sigma}_2 = \underline{D}_2 \, d\underline{\varepsilon}_2$$

Elastic

$$\underline{D}_1 = \underline{D} = \frac{E}{(1-\nu^2)} \begin{bmatrix} 1 & \nu & 0 \\ \nu & 1 & 0 \\ 0 & 0 & \frac{1-\nu}{2} \end{bmatrix}$$

$$\underline{D}_2 = \frac{E}{2(1+\nu)\alpha} \begin{bmatrix} 1 & 0 \\ 0 & 1 \end{bmatrix}$$

α is a modification factor (usually $\alpha = 1.2$)

Plastic

$$\underline{D}_1 = \underline{D} - \underline{D} \left[\frac{\partial F}{\partial \underline{\sigma}_1}\right] \left[\frac{\partial F}{\partial \underline{\sigma}_1}\right]^T \underline{D} \left[\bar{A} + \frac{\partial F}{\partial \underline{\sigma}_1} \underline{D} \frac{\partial F}{\partial \underline{\sigma}_1}\right]^{-1}$$

in which F is the yield function

$F = F(\underline{\sigma}_1, H)$, $\bar{A} = -\frac{1}{\lambda} \frac{\partial F}{\partial H} dH$

λ is the proportionality constraint

H is the hardening parameter

Finite element discretization

$$\underline{u} = \sum_i \underline{N}_i \underline{a}_i$$

$$\underline{\varepsilon}_1 = \sum_i \underline{B}_{1i} \underline{a}_i$$

$$\underline{\varepsilon}_2 = \sum_i \underline{B}_{2i} \underline{a}_i$$

where $\underline{N}_i = N_i \begin{bmatrix} 1 & 0 & 0 & -z & 0 \\ 0 & 1 & 0 & 0 & -z \\ 0 & 0 & 1 & 0 & 0 \end{bmatrix}$

$\underline{a}_i = [u_i, v_i, w_i, \theta_{xi}, \theta_{yi}]^T$

$$\underline{B}_{1i} = \begin{bmatrix} N_{i,x} & 0 & 0 & -zN_{i,x} & 0 \\ 0 & N_{i,y} & 0 & 0 & -zN_{i,y} \\ N_{i,y} & N_{i,x} & 0 & -zN_{i,y} & -zN_{i,x} \end{bmatrix} \qquad \underline{B}_{2i} = \begin{bmatrix} 0 & 0 & N_{i,x} & -N_i & 0 \\ 0 & 0 & N_{i,y} & 0 & -N_i \end{bmatrix}$$

Stiffness Matrices

$$\underline{K}_{ij} = \int_V \underline{B}_{1i}^T \underline{D}_1 \underline{B}_{1j} \, dV + \int_V \underline{B}_{2i}^T \underline{D}_2 \underline{B}_{2j} \, dV$$

Residual forces

$$\underline{\psi}_i = \int_V \underline{B}_{1i}^T \underline{\sigma}_1 \, dV + \int_V \underline{B}_{2i}^T \underline{\sigma}_2 \, dV - \underline{f}_i$$

where the consistent nodal forces $\underline{f}_i = \int_V \underline{N}_i^T \underline{b} \, dV + \int_{S_t} \underline{N}_i^T \bar{\underline{t}} \, dS$

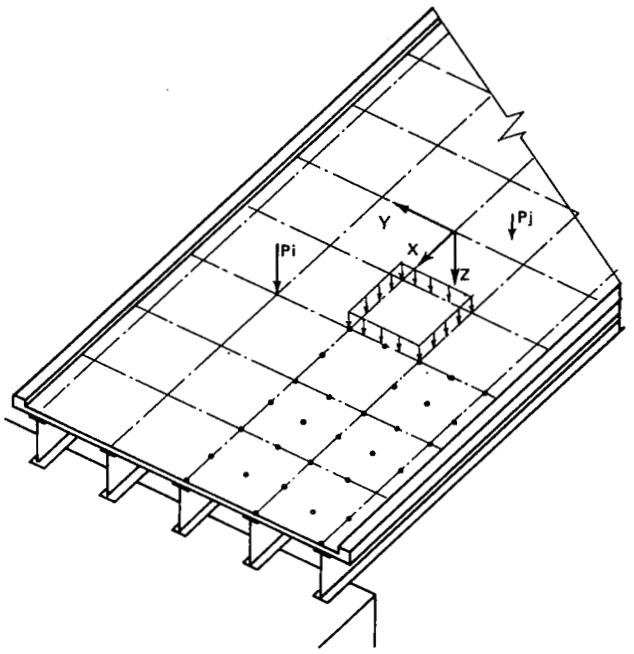

Figure 1.- Typical slab-beam system and its structural idealisation.

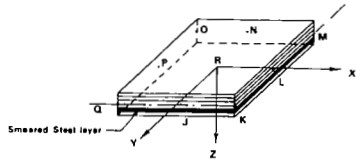

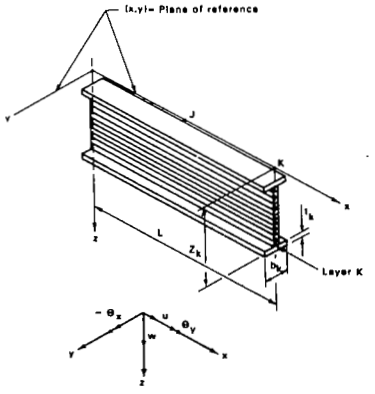

(a) Layered finite plate element.

(b) Layered beam element.

Figure 2.- Layered plate and beam elements.

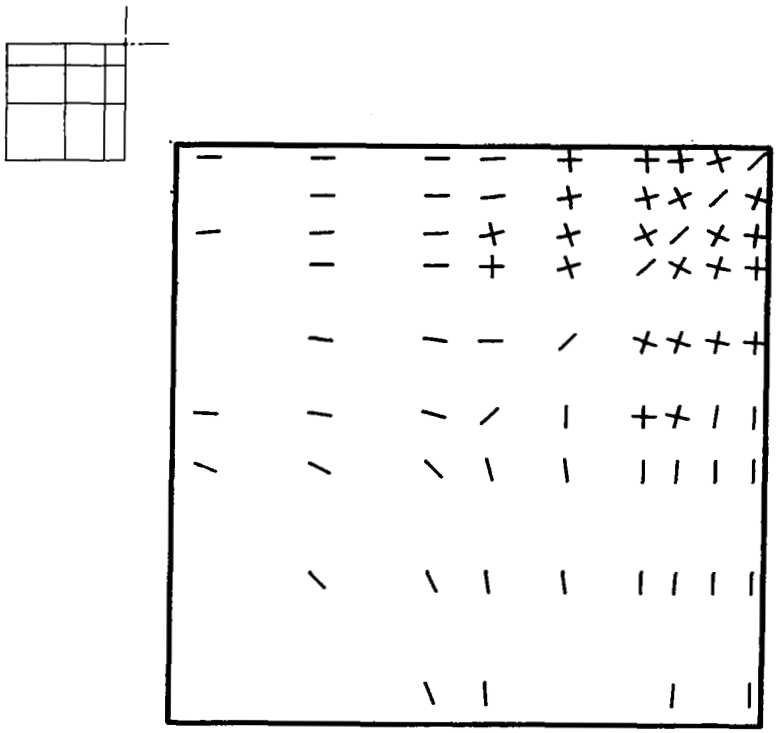

(a) P : 12.0 kN.

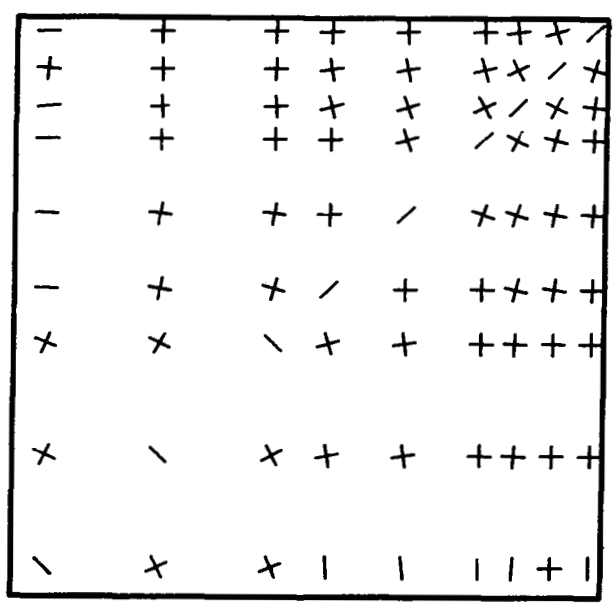

(b) P : 62.0 kN

Figure 3.- Crack patterns on the lower side of Mueller's slab.

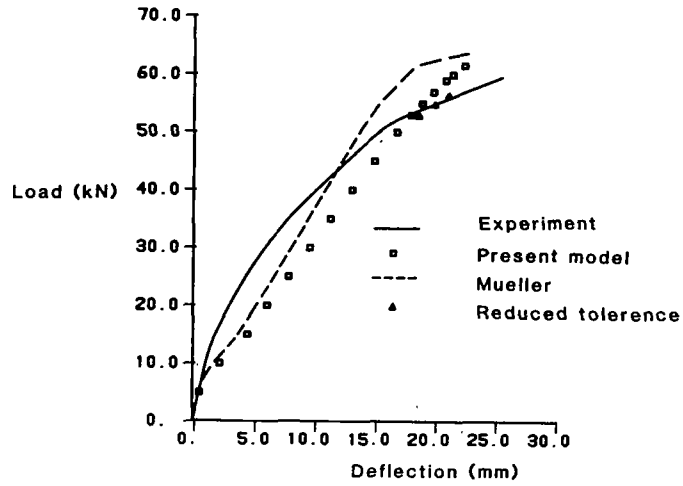

Figure 4.- Load-central deflection curves for Mueller's slab.

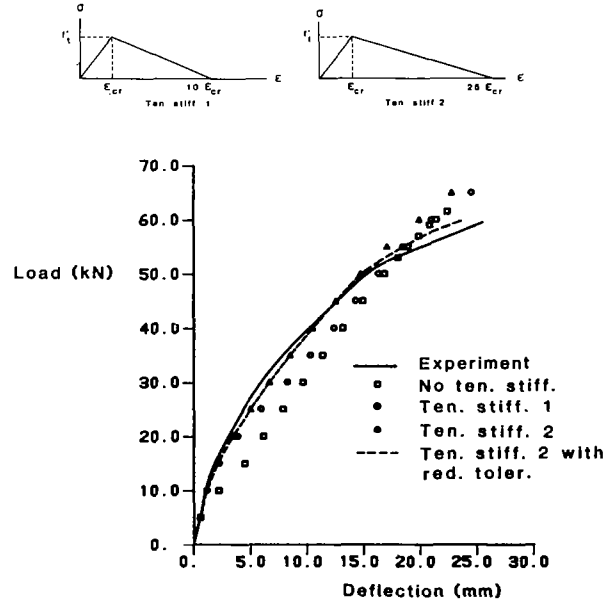

Figure 5.- Effect of tension stiffening on Mueller's slab.

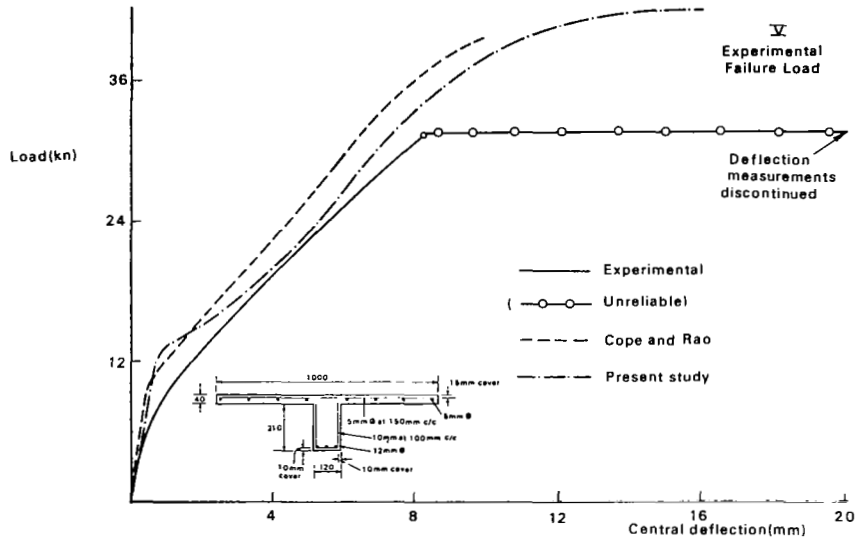

Figure 6.- Load-central deflection curves for T-beam.

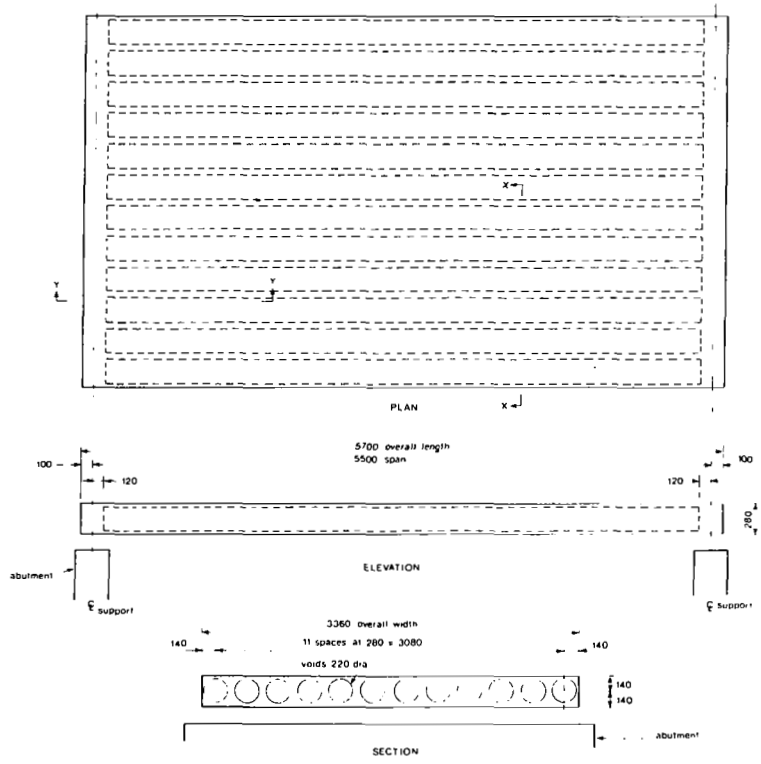

Figure 7.- Details of voided bridge deck model.

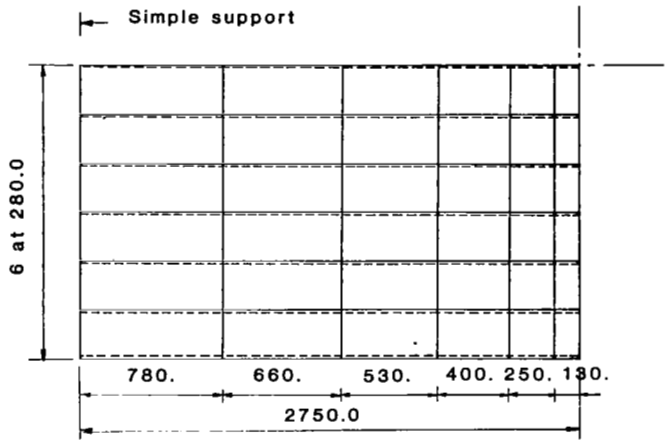

(a) Discretisation of voided plate.

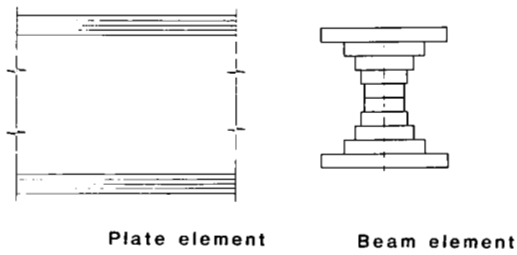

(b) Cross-section representation.

Figure 8.- Finite element discretisation of voided plate.

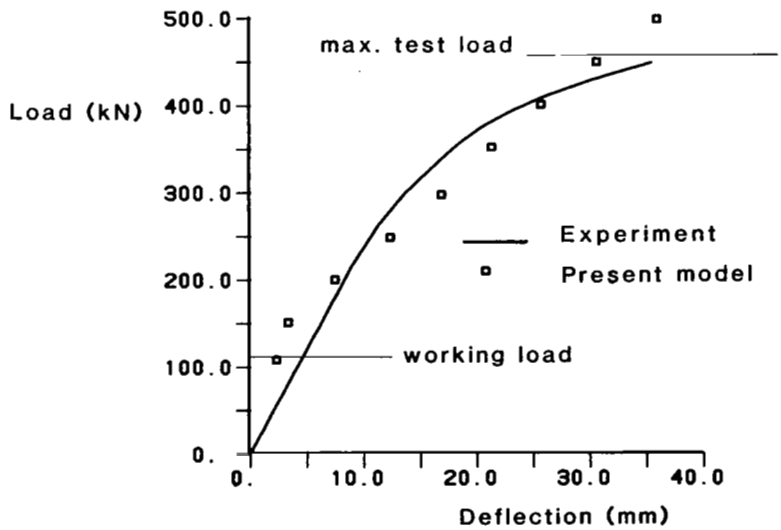

Figure 9.- Load-central deflection curves for voided plate model.

NEWTON'S METHOD: A LINK BETWEEN CONTINUOUS AND DISCRETE SOLUTIONS OF NONLINEAR PROBLEMS

Gaylen A. Thurston
Langley Research Center

ABSTRACT

Newton's method for nonlinear mechanics problems replaces the governing nonlinear equations by an iterative sequence of linear equations. When the linear equations are linear differential equations, the equations are usually solved by numerical methods. The iterative sequence in Newton's method can exhibit poor convergence properties when the nonlinear problem has multiple solutions for a fixed set of parameters, unless the iterative sequences are aimed at solving for each solution separately. The theory of the linear differential operators is often a better guide for solution strategies in applying Newton's method than the theory of linear algebra associated with the numerical analogs of the differential operators. In fact, the theory for the differential operators can suggest the choice of numerical linear operators. In this paper the method of variation of parameters from the theory of linear ordinary differential equations is examined in detail in the context of Newton's method to demonstrate how it might be used as a guide for numerical solutions.

INTRODUCTION

Nonlinear mechanics problems can be formulated as nonlinear differential equations and associated boundary conditions. One approach to solving these nonlinear equations is Newton's method. Newton's method replaces the nonlinear equations with an iterative sequence of linear differential equations. The present paper emphasizes that each iteration step consists of two separate operations. The first operation, referred to as linearization, is the derivation of the linear differential equations. The second operation is the solution of the linear equations and is referred to by the name of the method of solution for the linear system (e.g., power series, asymptotic series, finite-differences, finite-elements, successive approximations, or boundary integrals).

The emphasis on defining the iteration in Newton's method as two successive operations is to prevent confusion between Newton's method and the familiar Newton-Raphson method for a set of nonlinear algebraic equations. The confusion arises when the second operation is purely numerical and depends on a discretization operation. In this case, the operation of discretization can be applied to the nonlinear differential operators followed by the linearization of the Newton-Raphson method. Ortega and Rheinboldt, (ref. 1), prove that the operations of linearization and discretization commute. The operations

result in the same set of linear algebraic equations for each iteration step for both the Newton-Raphson method and Newton's method. The proof that the two operations commute requires that "the discretizations are carried out in the same way."

The present paper examines problems where the discretizations are not carried out in the same way. The choice of discrete model is affected by the theory of the linear differential equations. Examples of these problems are boundary-value problems where multiple solutions exist for a fixed set of parameters. This class of problems includes periodic solutions of nonlinear dynamics problems and static buckling problems with bifurcation points and with limit points.

Newton's method, that is, the operation of linearization before discretization, supplies two kinds of information for problems with multiple solutions. The first kind is qualitative information which is related to the convergence of the iterative procedure and is useful in itself. The second kind of information is quantitative information that directly affects the discrete model. The literature for linear differential equations is vast and much of it provides insight into the convergence properties of Newton's method. Rather than attempting a general review of applicable theory, this paper examines one method in detail as it relates to Newton's method. The method examined is variation of parameters as it is applied to systems of ordinary differential equations. The theory is examined first, followed by a discussion of the application of the theory to discrete solutions of nonlinear problems with multiple solutions.

The main body of the paper on variation of parameters is preceded by a preliminary section. This section discusses the linearization operation in Newton's method. Once the equations are linearized, different versions of Newton's method receive different names in the literature. These versions are briefly reviewed. The section also discussed convergence of Newton's method as it pertains to nonlinear problems with multiple solutions. The theoretical results from variation of parameters suggest changes in dependent variables that are determined by the given problem and, therefore, are applicable to adaptive computer solutions. A final section indicates the general nature of such adaptive computer solutions.

NEWTON'S METHOD

Fundamental Concepts

Nonlinear mechanics problems that are formulated as nonlinear ordinary or nonlinear partial differential equations can be solved using Newton's method. The basic idea in Newton's method is to expand the nonlinear operator about an assumed or an approximate solution. This expansion yields a new nonlinear operator that operates on an unknown correction to the approximate solution. It is assumed in Newton's method that nonlinear terms in the correction are small compared to linear terms, and the nonlinear terms are temporarily neglected. The resulting linear differential equations are

solved for an approximate correction which is added to the assumed solution to make a new approximation. The procedure is repeated until the corrections are small. At each iteration step, the residual error in the solution of the nonlinear problem is a function of the nonlinear terms neglected in the previous iteration step. Convergence of the iterative sequence is almost assured if the nonlinear problem has a unique solution. When the nonlinear problem has multiple solutions, convergence is not assured in Newton's method unless provisions are made to converge to only one solution for each iteration sequence. Examples of problems with multiple solutions are static buckling problems with bifurcation points and with limit points and certain nonlinear vibrations problems. The theory of linear differential operators is useful in guiding numerical computations so that Newton's method converges to the desired solution branch.

The linear operator in Newton's method is called the Frechet derivative, and it is derived from the nonlinear differential operator for the problem. Let the nonlinear differential operator be P operating on a scalar function or vector function y. The nonlinear problem is

$$P(y) = 0 \tag{1}$$

plus associated initial conditions or two-point boundary conditions. Denote by y_m the approximation to the solution of equation (1) after the mth iteration step, and denote by δy_{m+1} the correction to y_m. Then the Newton iteration process solves recursively the equations

$$P'[y_{m-1}](\delta y_m) = -P[y_{m-1}] \tag{2a}$$

$$y_m = y_{m-1} + \delta y_m \qquad m = 1,2,3,.... \tag{2b}$$

The operator $P'[y_{m-1}]$ in equation (2a) is the Frechet derivative. Formal definitions of the Frechet derivative appear in texts on functional analysis, reference (2). For nonlinear differential operators operating on continuous functions, the Frechet derivative consists of the linear operators that appear in a Taylor series expansion in several variables. The expansion is in terms of the dependent variables rather than the independent variables, reference (3).

Examples of Frechet Derivatives

For example, consider a single nonlinear equation.

$$\frac{d^2y}{dt^2} + C\left(\frac{dy}{dt}\right)^2 + \lambda \sin y - F \sin wt = 0 \tag{3}$$

with C, λ, F and w constants. The linear variational equation, equation (2a), for equation (3) is

$$\frac{d^2\delta y_m}{dt^2} + 2C\left(\frac{dy_{m-1}}{dt}\right)\frac{d\delta y_m}{dt} + \lambda\,(\cos\, y_{m-1})\,\delta y_m = -P[y_{m-1}] \tag{4a}$$

$$P[y_{m-1}] = \frac{d^2 y_{m-1}}{dt^2} + C\left(\frac{dy_{m-1}}{dt}\right)^2 + \lambda \sin y_{m-1} - F \sin wt \tag{4b}$$

The Frechet derivative for the nonlinear operator is the operator

$$P'[y_{m-1}]( ) = \frac{d^2( )}{dt^2} + 2C\,\frac{dy_{m-1}}{dt}\,\frac{d}{dt}( ) + \lambda \cos y_{m-1}\,( ) \tag{5}$$

The Taylor series expansion in Newton's method is readily extended to partial differential operators. A second example is a nonlinear strain expression

$$\varepsilon_{xz} = \frac{\partial u}{\partial z} + \frac{\partial w}{\partial x} + \frac{\partial u}{\partial z}\frac{\partial u}{\partial z} + \frac{\partial v}{\partial x}\frac{\partial v}{\partial z} + \frac{\partial w}{\partial x}\frac{\partial w}{\partial z} \tag{6}$$

Then

$$\begin{aligned}\varepsilon'_{xz}[y_{m-1}](\delta y_m) = {} & \frac{\partial \delta u_m}{\partial z} + \frac{\partial \delta w_m}{\partial x} + \frac{\partial u_{m-1}}{\partial x}\,\frac{\partial \delta u_m}{\partial z} \\ & + \frac{\partial u_{m-1}}{\partial z}\,\frac{\partial \delta u_m}{\partial x} + \frac{\partial v_{m-1}}{\partial x}\,\frac{\partial \delta v_m}{\partial z} + \frac{\partial v_{m-1}}{\partial z}\,\frac{\partial \delta v_m}{\partial x} \\ & + \frac{\partial w_{m-1}}{\partial x}\,\frac{\partial \delta w_n}{\partial z} + \frac{\partial w_{m-1}}{\partial z}\,\frac{\partial \delta w_m}{\partial x}\end{aligned} \tag{7}$$

In addition to the linear variational equations of Newton's method, the Frechet derivative appears as part of the chain rule of differentiation. If the nonlinear operator is written $P(y(x),x)$ to emphasize that y is a function of the independent variable, the total derivative of P is

$$\frac{dP}{dx} = P'[y]\left(\frac{dy}{dx}\right) + \frac{\partial P}{\partial x} = 0 \tag{8}$$

The derivative of equation (3) with respect to t can be written

$$\frac{d^2}{dt^2}\left(\frac{dy}{dt}\right) + 2C\,\frac{dy}{dt}\,\frac{d}{dt}\left(\frac{dy}{dt}\right) + \lambda\,(\cos y)\,\frac{dy}{dt} = wF\cos wt \tag{9}$$

It is often useful to think of y as a function of parameters in addition to the independent variables and the operator as $P(y(\lambda,x),x,\lambda)$. Then

$$\frac{\partial P}{\partial \lambda} = P'[y]\left(\frac{\partial y}{\partial \lambda}\right) + \dot{P} = 0 \tag{10}$$

where the dot notation denotes partial differentiation with respect to a parameter while holding both the independent and dependent variables fixed. If y is considered as a function of t and λ is equation (3),

$$\frac{d^2}{dt^2}\left(\frac{\partial y}{\partial \lambda}\right) + 2C\,\frac{dy}{dt}\,\frac{d}{dt}\left(\frac{\partial y}{\partial \lambda}\right) + \lambda\cos y\,\frac{\partial y}{\partial \lambda} + \sin y = 0 \tag{11}$$

Some versions of Newton's method make use of equation (10) in solving for particular solutions of equations (2a).

Different Versions of Newton's Method

In this paper, the iterative procedure defined by equations (2) is called Newton's method. Bellman (refs. 4 and 5) gave the procedure the name quasilinearization. McGill and Kenneth (ref. 6) use the terminology generalized Newton-Raphson operator for the Frechet derivative of nonlinear differential operators. The three different names are synonymous for the general iterative method.

When the linear variational equations, equations (2a), are solved by a specific algorithm, different writers have coined different names for specialized versions of Newton's method. Perrone and Kao (refs. 7 and 8) transform equations (2) to finite difference equations and solve the resulting linear algebraic equations by relaxation. This algorithm is called nonlinear relaxation by Perrone and Kao.

Other versions of Newton's method are connected with solutions of the linear variational equations depending on a parameter. In mechanics, it is usual to compute a set of solutions for the nonlinear problems for a given set of loads or other parameters. It soon becomes apparent to a user of Newton's method that a solution for one load or parameter is a good zeroth approximation for a solution for a nearby parameter (ref. 9). If $P(u,\lambda) = 0$, then u is a good zeroth approximation for the solution for $P(y,\lambda + \Delta\lambda) = 0$. The first iteration of Newton's method, $m = 1$ in equations (2), is then

$$P'[u](\delta y_1) = -P(u,\lambda + \Delta\lambda) = -[\dot{P}(u)\Delta\lambda + \frac{P(u)(\Delta\lambda)^2}{2!} + \ldots] \tag{12}$$

If the nonlinear operator is linear in the parameter so that quadratic and higher order terms in $\Delta\lambda$ do not appear, a particular solution of equation (12) follows directly from equation (10). For this case,

$$\delta y_1 = \frac{\partial u}{\partial \lambda}\Delta\lambda \tag{13}$$

$$y_1 = u + \frac{\partial u}{\partial \lambda}\Delta\lambda \tag{14}$$

If Newton's method is terminated after one iteration, $m = 1$, equation (14) becomes the zeroth approximation for the next increment on λ. Na and Turski (ref. 10) call this version of Newton's method a solution by parameter differentiation. When the parameter λ is a load parameter and the iteration in equations (2) is continued for the iteration counter $m > 1$, Newton's method is also known as the incremental method. Stricklin and Haisler (ref. 11) review various versions of this approach when the linear variational equations, equations (2a), are solved by the finite element method.

The idea of continuing known solutions of nonlinear problems into nearby neighborhoods gives rise to higher order forms of Newton's method. These forms retain higher order derivatives in the Taylor series about a known solution. These higher order methods stem from Taylor series expansions in the independent variable for initial value problems. Davis (ref. 12) designated this method as a solution by analytic continuation because the solutions are capable of extension around singular points in the complex domain. Weinitschke (ref. 13) applied a similar approach to solve axisymmetric shallow shell equations for particular solutions starting at one boundary. He used the Newton-Raphson method to satisfy boundary conditions at a second boundary.

Stricklin, et al., (refs. 14 and 15) and Noor and Peters (ref. 16) combine the idea of analytic continuation with parameter differentiation by computing higher partial derivatives with respect to a parameter. Stricklin and Haisler (ref. 11) refer to the general scheme as a self-correcting

incremental approach to nonlinear problems. Noor does not substitute the high partial derivatives in a Taylor series in $\Delta\lambda$, but uses them as basis vectors in a Rayleigh-Ritz solution of the original nonlinear problem.

The modified Newton's method uses the same Frechet derivative for each iteration. Instead of equations (2), the iterative sequence is

$$P'[y_o](\delta y_m) = -P(y_{m-1}) \tag{15a}$$

$$y_m = y_{m-1} + \delta y_m \qquad m = 1,2,3... \tag{15b}$$

Convergence

The advantage of having the same linear operator for each iteration step in the modified Newton's method is offset by slower convergence to the solution of the nonlinear problem. Parameter differentiation exhibits slow convergence near limit points where $\partial u/\partial\lambda$ is infinite.

Kantorovich (ref. 2) proves sufficient conditions for the convergence of Newton's method. The sufficient conditions are restrictive, but, when they apply, the nonlinear problem has a unique solution near the zeroth approximation.

In practical applications of Newton's method, there is not enough information to apply Kantorovich's convergence criterion. However, it is a useful guide because nonlinear problems with unique solutions for a fixed range of parameters will exhibit rapid convergence of Newton's method. When the solutions are not unique, Newton's method can still converge. The lack of uniqueness in the nonlinear solutions is reflected by lack of uniqueness in δy_m at some iteration step m. A decision on which solution branch to pursue must be made before continuing the iteration.

The theory of the linear differential operators is a guide for making these decisions. Application of the theory of linear ordinary differential equations in finding multiple solutions of nonlinear problems is the topic of the next section.

VARIATION OF PARAMETERS

One method of analysis is examined here in detail to show how linearization can influence discretization. The method is variation of parameters which is used for finding particular solutions for systems of linear ordinary differential equations. The theory for linear ordinary differential equations is well understood and is a reliable guide for computing their solutions. The variational equations of Newton's method are linear ordinary differential

equations when the nonlinear problem is governed by a system of nonlinear ordinary differential equations.

Assume that the nonlinear problem can be written as

$$P(y) = \frac{dy}{dx} + F(y,x,\lambda) = 0 \qquad a \leq x \leq b \tag{16}$$

plus two-point boundary conditions,

$$U(y\ (a),\ y(b),\lambda) = 0 \tag{17}$$

The dependent variable y is a vector function with n component functions of the independent variable x. There are n boundary conditions which may be nonlinear.

The sequence for the mth iteration step, equations (2), is

$$\frac{d\delta y_m}{dx} + F'[y_{m-1},x,\lambda]\delta y_m = -P(y_{m-1},x,\lambda) \tag{18a}$$

$$\underset{\sim}{U}'_{m-1} \begin{pmatrix} \delta y_m(a) \\ \hline \delta y_m(b) \end{pmatrix} = -\underset{\sim}{U}_{m-1} \tag{18b}$$

$$y_m = y_{m-1} + \delta y_m \qquad m = 1,2,3,\ldots \tag{18c}$$

The Frechet derivative $F'[y_{m-1},x,\lambda]$ for this case is the Jacobian of the function $F(y_{m-1},x,\lambda)$. The shorthand notation

$$J_{m-1} = F'[y_{m-1},x,\lambda] \tag{19}$$

will be used in subsequent equations.

The solution of the linear variational equations, equation (18a), can be written in matrix notation as (see ref. 17, for example)

$$\delta y_m = \Phi_m \underset{\sim}{C}_m + \delta y_{mp} \tag{20}$$

The matrix Φ_m contains n columns, each column contains a linearly independent solution $\phi(x)$ of the homogeneous differential equations.

$$\frac{d\phi}{dx} + J_{m-1}\,\phi = 0 \tag{21}$$

The vector $\underset{\sim}{C}_m$ is constant. The vector function δy_{mp} is the particular solution of the differential equation system. The method of variation of parameters is a method of deriving the particular solution using the solutions of the homogeneous equations Φ_m. The method introduces the change in variables

$$\delta y_m = \Phi_m z_m \tag{22}$$

where z_m is a vector function. In the new variables z_m, equation (21a) is

$$\frac{d\Phi_m}{dx} z_m + \Phi_m \frac{dz_m}{dx} + J_{m-1}\Phi_m z_m = -P(y_{m-1},x,\lambda) \tag{23}$$

The terms multiplying z_m vanish identically from equation (23) since each column Φ_m satisfies the homogeneous equations, equation (21). The equations

$$\Phi_m \frac{dz_m}{dx} = -P(y_{m-1},x,\lambda) \tag{24}$$

are solved by inverting the matrix Φ_m and integrating each equation.

$$z_m = \underset{\sim}{C}_m - \int_a^x \Phi_m^{-1}(\zeta)\; P(y_{m-1},\zeta,\lambda)\; d\zeta \tag{25}$$

Substituting equation (25) back into equation (22) completes the solution for δy_m. Comparing like terms with equation (20) shows that the particular solution is

$$\delta y_{mp} = -\Phi_m(x) \int_a^x \Phi_m^{-1}(\zeta)\; P(y_{m-1},\zeta,\lambda)\; d\zeta \tag{26}$$

Whenever the integrals in equation (26) exist, the particular solution always exists and depends on both the residual error and the solutions of the homogeneous equations, equation (21).

Boundary Conditions and Compatability

Determining the values of the constants of integration $\underset{\sim}{C}_m$ completes the mth iteration step. The constants depend on the linearized boundary conditions, equation (18b). Substitution of equation (25) into equation (18b) yields a set of linear algebraic equations

$$\underset{\sim}{B}_m \underset{\sim}{C}_m = \underset{\sim}{D}_m \tag{27}$$

$$\underset{\sim}{B}_m = \underset{\sim}{U}'_m \begin{bmatrix} \Phi_m(a) \\ - - - \\ \Phi_m(b) \end{bmatrix} \tag{28a}$$

$$\underset{\sim}{D}_m = -\underset{\sim}{U}_{m-1} - U'_{m-1}[\delta y_{mp}(a);\ \delta y_{mp}(b)]^T \tag{28b}$$

Assume that the boundary conditions are posed so that $\underset{\sim}{B}_m$ is an $n \times n$ square matrix. Then three possible conditions exist for the solution of equations (27). Let the rank of matrix $\underset{\sim}{B}_m$ be $(n - k)$ where the number k is the index of compatibility (Ince, ref. 18). Let the rank of the matrix obtained by augmenting $\underset{\sim}{B}_m$ with the column vector $\underset{\sim}{D}_m$ be $(n - p)$. The three conditions are the following:

1. $k = 0$ There is a unique solution of equations (27) for the constants of integration $\underset{\sim}{C}_m$. The mth iteration step is complete with a unique correction vector δy_m given by equation (20).

2. $k < p$ The algebraic equations are incompatible (also referred to as inconsistent) and no solution exists for the constants of integration, $\underset{\sim}{C}_m$.

3. $k = p$ There are k arbitrary constants in the solutions of equations (27)

$$\underset{\sim}{B}_m \underset{\sim}{C}^j_m = 0 \qquad j = 1,2, \ldots k \leq n \tag{29}$$

The solution of the linear variational equations, equation (18), contains k arbitrary constants A_j.

$$\delta y_m = \sum_{j=1}^{k} A_j V_{mj} + \delta y_{m1} \tag{30}$$

The V_{mj} are linear combinations of the solutions of the homogeneous equations,

$$V_{mj} = \Phi_m \underset{\sim}{C}_m^j \qquad j = 1,2, \ldots k \leq n \tag{31}$$

The particular solution δy_{m1} is completely determined and satisfies the boundary conditions,

$$\delta y_{m1} = \Phi_m \underset{\sim}{C}_m + \delta y_{mp} \tag{32}$$

The constants of integration $\underset{\sim}{C}_m$ in equations (32) are solutions of a reduced $(n - k)$ square matrix.

The theory for the compatibility of the boundary conditions is related to Kantorovich's convergence criteria for Newton's method. The first condition $k = 0$ is part of the sufficient conditions for convergence of Newton's method to a unique solution. Problems with unique solutions converge rapidly using Newton's method and the numerical solution strategy for the zeroth approximation and incrementing parameters is not crucial for convergence.

The second condition $k < p$ indicates a break in the iteration sequence. This condition is not usually met in practice. The matrix $\underset{\sim}{B}_m$ becomes ill-conditioned near limit points and approaches the condition $k < p$, but does not satisfy the condition exactly. If the assumed solution y_{m-1} is modified, the boundary conditions may be shifted to make $k = 0$ or $k = p$. This modification follows the same lines as the procedure for the third condition, $k = p$, which is considered next.

When $k = p$, there are k arbitrary constants of integration A_j in the correction function δy_m in equation (30). If the A_j can be assigned values, the iteration can be continued.

Multiple Solutions

If k constants of integration A_j are arbitrary after m iteration steps, the nonlinear problem can have multiple solutions for a fixed set of input parameters. The procedure for determining the different solutions depends on the details of the problem, but the analysis contains general guidelines for assigning values for the A_j. The discussion here considers the (m+1)th iteration for the case $\delta y_{m1} = 0$ in equation (30). In other words, it is assumed that convergence has been obtained for a solution y_{m-1} of the nonlinear problem for a certain value of $\lambda = \bar{\lambda}$ when the A_j are zero.

The next step is to investigate continuing the iteration with at least one of the A_j small but finite. The residual error for the (m+1)th iteration using δy_m from equation (30) is

$$P(y_m, x, \bar{\lambda}) = F''[y_{m-1}, x, \bar{\lambda}] \left(\frac{\delta y_m^2}{2!}\right) + F'''[y_{m-1}, x, \bar{\lambda}] \left(\frac{\delta y_m^3}{3!}\right) + \ldots \quad (33)$$

The residual is nonlinear in the constants A_j. The lowest order terms are quadratic in the constants unless $F''[y_m, x, \bar{\lambda}]$ containing second derivatives in the Taylor series vanishes. The linear variational equation for the (m+1) iteration becomes

$$\frac{d\delta y_{m+1}}{dx} + J_m \, \delta y_{m+1} = -P(y_m, x, \bar{\lambda}) \quad (34)$$

The Jacobian J_m is shifted from J_{m-1} and is also a function of the A_j. The difference in the two Jacobians appears if the transformation from the mth iteration is applied to the (m+1)th step

$$\delta y_{m+1} = \Phi_m z_{m+1} \quad (35)$$

Then, equation (34) is transformed to

$$\frac{dz_{m+1}}{dx} + \Phi_m^{-1}[J_m - J_{m-1}]\Phi_m z_{m+1} = -\Phi_m^{-1} P(y_m, x, \bar{\lambda}) \quad (36)$$

The difference in the Jacobians is a matrix

$$[J_m - J_{m-1}] = F'[y_{m-1} + \delta y_m, x, \lambda] - F'[y_{m-1}, x, \lambda]$$

$$= F''[y_{m-1}, x, \lambda](\delta y_m) + \ldots \tag{37}$$

The leading terms in an expansion for each coefficient of the matrix is linear in the A_j when the residual error expansion starts with quadratic terms. The leading exponent is always one less than the leading exponent in the residual.

In theory, equation (36) can be solved by variation of parameters. A new set of constants of integration $\underset{\sim}{C}_{m+1}$ appears in the solution to be determined by a new set of boundary conditions.

$$\underset{\sim}{B}_{m+1}\ \underset{\sim}{C}_{m+1} = \underset{\sim}{D}_{m+1} \tag{38}$$

The formal solutions contain the undefined A_j as parameters. In numerical solutions, the explicit dependence of the solution on the A_j is not known. A procedure that can be implemented for numerical solutions is to partition the problem of determining the constants of integration $\underset{\sim}{C}_{m+1}$, equation (38).

The partitioning identifies k constants of integration as corrections δA_j on the A_j and partitions equation (38) into a k by k problem to fix the A_j and δA_j. An iterative procedure is to use trial values for the A_j and solve for the δA_j. The k by k problem is solved when the δA_j vanish for finite real A_j.

The δA_j appear as the first k variables of $\underset{\sim}{C}_{m+1}$ when the V_{mj} from equation (30) are arranged in the first k columns of Φ_m in equation (35). Once the A_j and δA_j are determined, the remaining $(n - k)$ equations in equation (38) are a linear set of algebraic equations in the remaining $(n - k)$ constants in $\underset{\sim}{C}_{m+1}$.

To avoid converging back to the solution y_{m-1} with the $A_j = 0$, a shift in λ is introduced to provide for nonzero, real solutions for the constants A_j.

The shift in λ is introduced in the right side of equation (34) which is replaced by

$$P(y_m, x, \lambda) = P(y_m, x, \overline{\lambda}) + \dot{P}(y_m, x, \overline{\lambda})(\lambda - \overline{\lambda}) + \ldots \tag{39}$$

and the right side of equation (36) is

$$-\Phi_m^{-1}P(y_m,x,\lambda) = -\Phi_m^{-1}P(y_m,x,\bar{\lambda}) - \Phi_m^{-1}\dot{P}(y_m,x,\bar{\lambda})(\lambda - \bar{\lambda}) + \ldots \qquad (40)$$

Introducing λ as a free parameter allows iterating on the reduced k by k problem by assigning a value to one A_j and using λ as part of the minimization on δy_{m+1} by making δA_j zero or small compared to A_j.

Which A_j to replace as a variable by λ depends on the modal coupling in the given problem. When $k = 1$, there is only one $A_j = A_1$ so the choice is not arbitrary.

The case $k = 1$ is a common case for problems with limit points or isolated bifurcation points. Therefore, the general iterative procedure for $k = 1$ will be examined further.

Isolated Bifurcation Point

For an isolated bifurcation point, y_{m-1} is identified as a solution of the nonlinear problem at $\lambda = \bar{\lambda}$ and $k = p = 1$. In applications of Newton's method, the solution y_{m-1} can be generated by simply incrementing the parameter λ in numerical solutions to approach the bifurcation point and continue past it. As λ is varied in increments in any numerical solution using Newton's method, the boundary condition matrix $\underset{\sim}{B}$ approaches $\underset{\sim}{B}_m$ in equation (29). The rows of $\underset{\sim}{B}$ can be rearranged by elementary operations so that the coefficients of at least one row, say row $k = 1$, are small as λ approaches $\bar{\lambda}$. For a bifurcation point, the element k of the D vector is identically zero for λ near $\bar{\lambda}$.

For a limit point, the kth component of D may be small but the small divisors of B prevent convergence at $\lambda = \bar{\lambda}$ without analysis similar to the bifurcation analysis described here.

When y_{m-1} is a solution at the bifurcation point $\lambda = \bar{\lambda}$, setting $A_1 = 0$ so that $y_m = y_{m-1}$ and varying λ continues the solution so that

$$\delta y_{m+1} \cong \frac{\delta y_{m-1}}{d\lambda}(\lambda - \bar{\lambda}) \qquad (41)$$

as noted in the discussion on parameter differentiation and equation (13).

Having one solution near $\bar{\lambda}$, the problem is to investigate the second solution of the nonlinear problem whose existence is identified by V_1, the nontrivial solution of the linear variational equations.

A simple procedure for Newton's method is to assign a value to A_1 so that $y_m = y_{m-1} + A_1V_1$ is a known function. Solve the first scalar equation

of the set of equations (36) where the equations are arranged so that the first element of z_{m+1} multiplies the vector function V_1. The right side of the single differential equation is the first element of equation (40). The constant of integration δA_1 for this equation can be set to zero if $(\lambda - \bar{\lambda})$ is selected to make the first component of $\underset{\sim}{D}_{m+1}$ in the boundary conditions, equation (38), vanish.

For numerical solutions, the analysis required by the expansion in equation (40) can be circumvented by recognizing that while the solution for δA_1 is nonlinear in A_1, it is approximately linear in $(\lambda - \bar{\lambda})$. The constant of integration for δA_1 can be minimized by interpolating linearly between solutions for residuals $P(y_m, x, \bar{\lambda} + \Delta\lambda_{m+1})$ and $P(y_m, x, \bar{\lambda})$ where $\Delta\lambda_{m+1}$ is small but arbitrary. This interpolation on λ to determine $\lambda = \lambda_{m+1}$ for fixed A_1 is shown schematically in figure 1. The figure represents the surface $\delta A_1 = \delta A_1(A_1, \lambda)$. It is desired to compute intersections of the surface and the $A_1 - \lambda$ plane. The surface is tangent to the plane along the λ axis, but solutions with $A_1 = 0$ are already assumed known by equation (41). Curves on the surface for constant λ are nonlinear in A_1 while curves for constant A_1 are assumed to be nearly linear. Therefore, one can fix $(A_1)_m \pm 0$ and approximate $\lambda_{m+1} = \lambda_m + \Delta\lambda$ by interpolating on λ between the calculated points $\delta A_1[(A_1)_m, \lambda_m]$ and $\delta A_1[(A_1)_m, \bar{\lambda}]$ to approximate $\delta A_1[(A_1)_m, \lambda_{m+1}] = 0$.

Once A_1 is determined and $\lambda = \lambda_{m+1}$ the remaining $(n - 1)$ equations of equation (38) can be solved to complete the $(m+1)$th iteration. When A_1 is small, the terms in $[J_m - J_{m-1}]$ can be neglected in these equations or handled by successive approximations.

Since $[J_m - J_{m-1}]$ is of lower degree than the residual, successive approximations should converge rapidly for the remaining $(n - 1)$ equations, (ref. 18).

If the linearized boundary conditions are no longer singular because of a finite A_1, the usual Newton method iteration can be continued with λ prescribed as an independent parameter. If the boundary conditions are nearly singular, another interpolation on λ may be required.

Once the analysis shows how to start the Newton's method iteration with a finite value of A_1, different implicit or explicit numerical integration methods can be used to find λ as a function of A_1.

NUMERICAL SOLUTIONS

In applying the results of the theory, numerical solutions do not need to follow the analysis in every detail. For example, "shooting" methods (ref. 19) are used for computing particular solutions rather than variation of parameters. When the problem is partitioned into a reduced k by k problem, the complete transformation indicated by equation (35) need not be carried out. The transformation

$$\delta y_{m+1} = w\, z_{m+1} \tag{42}$$

is sufficient where w is not singular and contains the k eigenfunctions V_{mj} as its first k columns.

The interpolation on λ for fixed A_1 can be carried over to nonlinear partial differential equations which are solved by matrix methods. A finite-element code for general shell problems was used to generate the end-shortening u as a function of center deflection w for an isotropic square plate in compression. The amplitude $w = A_1$ was held constant at $1.7h$ where h is the thickness while u was varied in the role of λ. The interpolation on λ is indicated by the dashed lines in figure 2. One iteration cycle of Newton's method ($m = 1$) with input $w_o = 1.7h$ and $u = 1.0\ u_{cr}$ (point A in the figure) shifted the output to $w_1 = w_o + \delta w_1 = 1.32h$ (point B). Another separate iteration with input at point C shifted the output to $w_1 = 1.99h$ and $u = 4.47\ u_{cr}$ (point D). Interpolating on u gives $\delta w_1 = 0$ at $u = 2.97\ u_{cr}$ (point E). The latter value of u was sufficiently accurate to obtain convergence of Newton's method at point F on the solid curve. The solid curve was generated by varying u in increments starting at point F using the standard Newton iteration of the computer program. Varying the end-shortening with $w = 0$ over all the plate would merely change the in-plane solution which does not couple with the transverse equilibrium equation for an initially flat plate. Starting the iteration on the computer solution with an assigned amplitude of the lowest buckling mode shape is sufficient to achieve convergence on the postbuckled curve.

When matrix methods are used for the numerical solution of static boundary-value problems, a similarity transformation on the tangent stiffness matrix is analogous to the change of variables in variations of parameters. When the equations are partitioned using only k modes, equations (42), the analog is an equivalence transformation in matrix theory.

The numerical analogies will not be developed in this paper, but the general development should parallel the discussion here. Eigenvectors of the numerical analog to the Prechet derivative replace eigenfunctions. A k by k reduced problem has been suggested by Almroth, et al., (ref. 20). Solving the remaining $(n - k)$ equation by successive approximations as suggested here preserves linear independence.

CONCLUDING REMARKS

Linearization before discretization in Newton's method allows classical linear theory to be applied to nonlinear mechanics problems. The linear theory provides useful qualitative information that can affect convergence of the iterative solution.

The example in the paper, variation of parameters from the theory of linear ordinary equations, shows clearly the interdependence of the residual

error and the properties of the linearized operator in Newton's method. Variation of parameters suggests a change of dependent variables for computing particular solutions. The change in variables is also a means of partitioning the problem to speed convergence of Newton's method when the nonlinear problem has multiple solutions for a given set of parameters.

The change of variables can be extended to numerical solutions using matrix methods by an equivalence transformation. The new variables arise naturally in the problem which is an advantage for writing computer codes for matrix solutions. No prior quantitative information on choice of variables is required by the program user.

REFERENCES

1. Ortega, J. M.; and Rheinboldt, W. D.: On Discretization and Differentiation of Operators with Application to Newton's Method, J. SIAM Numerical Analysis, Vol. 3, No. 1, 1966, pp. 143-156.

2. Kantorovich, L. V.: and Akilov, G. P.: Functional Analysis in Normed Spaces, Macmillan Company, New York, 1964.

3. Thurston, G. A.: Newton's Method Applied to Problems in Nonlinear Mechanics, Journal of Applied Mechanics, Vol. 32, Series E, No. 2, 1965, pp. 383-388.

4. Bellman, R.: Kagiwada, H.; and Kalaba, R.: Orbit Determination as a Multipoint Boundary Value Problem and Quasilinearization, Proceedings of the National Academy of Sciences, Vol. 48, 1962, p. 1327.

5. Bellman, R.; and Kalaba, R.: Quasilinearization and Nonlinear Boundary Value Problems, Elsevier, New York, 1965.

6. McGill, R.; and Kenneth, P.: Solution of Variational Problems by Means of a Generalized Newton-Raphson Operator, AIAA Journal, Vol. 2, No. 10, 1964, pp. 1761-1766.

7. Perrone, N.; and Kao, R.: A General Nonlinear Relaxation Iteration Technique for Solving Nonlinear Problems in Mechanics, Journal of Applied Mechanics, Vol. 38, Series E, No. 2, 1971, pp. 371-376.

8. Kao, R.; and Perrone, N.: Asymmetric Buckling of Spherical Caps with Asymmetrical Imperfections, Journal of Applied Mechanics, Vol. 38, Series E, No. 1, 1971, pp. 172-178.

9. Thurston, G. A.: A Numerical Solution of the Nonlinear Equations for Axisymmetric Bending of Shallow Spherical Shells, Journal of Applied Mechanics, Vol. 28, Series E, No. 4, 1961, pp. 557-562.

10. Na, T. Y.; and Turski, C. E.: Solution of the Nonlinear Differential Equations for Finite Bending of a Thin-Walled Tube by Parameter Differentiation, Aeronautical Quarterly, Feb. 1974, pp. 14-18.

11. Stricklin, J. A.; and Haisler, W. E.: Evaluation of Solution Procedures for Material and/or Geometrically Nonlinear Structural Analysis, AIAA Journal, Vol. 11, No. 3, 1973, pp. 292-299.

12. Davis, H. T.: Introduction to Nonlinear Differential and Integral Equations, Dover Publications, New York, 1962.

13. Weinitschke, H. J.: On the Nonlinear Theory of Shallow Spherical Shells, SIAM Journal, Vol. 6, No. 3, 1958, pp. 209-231.

14. Massett, D. A.; and Stricklin, J. A.: Self-Correcting Incremental Approach in Nonlinear Structural Mechanics, AIAA Journal, Vol. 9, No. 12, 1971, pp. 2464-2466.

15. Stricklin, J. A.; Haisler, W. D.; and Von Riesemann, W. A.: Geometrically Nonlinear Structural Analysis by the Direct Stiffness Method, J. Structural Division, ASCE, Vol. 97, No. ST9, 1971, pp. 2299-2314.

16. Noor, A.; and Peters, J.: Reduced Basis Technique for Nonlinear Analysis of Structures, AIAA Journal, Vol. 18, No. 4, April 1980, pp. 455-462.

17. Coddington, F. A.; and Levinson, N.: Theory of Ordinary Differential Equations, McGraw-Hill, New York, 1955.

18. Ince, E. L.: Ordinary Differential Equations (1926), reprinted by Dover Publications, Inc., New York (1956), Chap. IX.

19. Roberts, S. M.; and Shipman, J. S.: Two-Point Boundary Value Problems: Shooting Methods, Elsevier, NY, 1972.

20. Almroth, B. O.; Stern, P.; and Brogan, F. A.: Automatic Choice of Global Shape Functions in Structural Analysis, AIAA Journal, Vol. 16, May 1978, pp. 525-528.

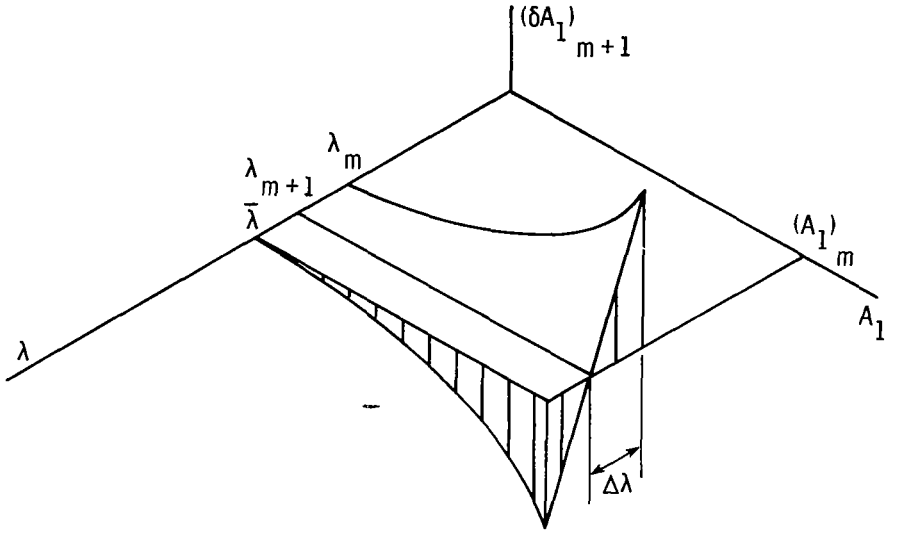

Figure 1.- Schematic diagram of calculation of parameter increment $\Delta\lambda_{m+2}$.

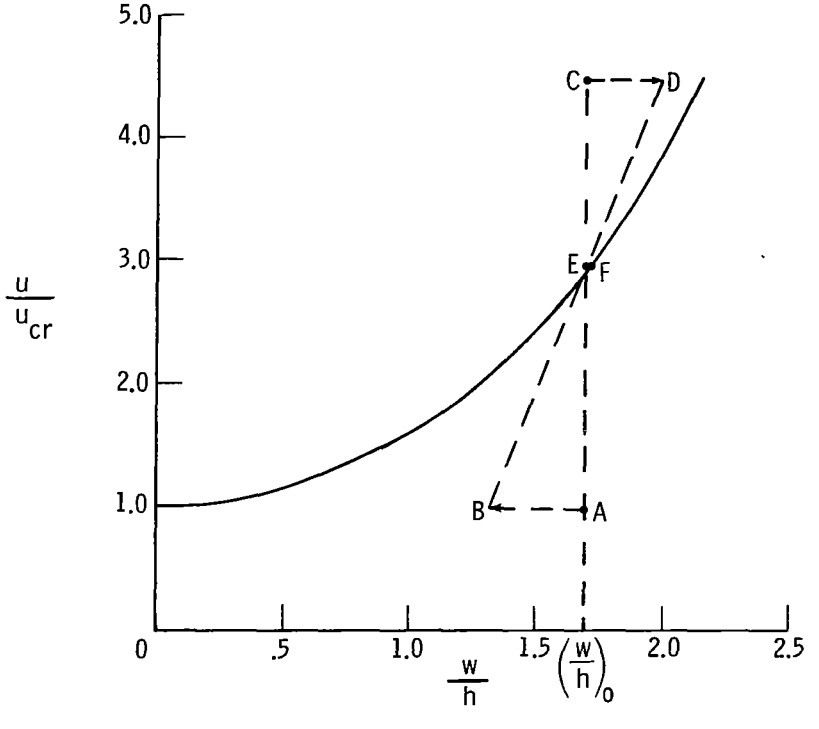

Figure 2.- Variation of end shortening with transverse deflection of plate in compression.

NONLINEAR SOIL-STRUCTURE INTERACTION CALCULATIONS

SIMULATING THE SIMQUAKE EXPERIMENT USING STEALTH 2D

H. T. Tang
Electric Power Research Institute
Palo Alto, California 94304

R. Hofmann and G. Yee
Science Applications, Inc.
San Leandro, California 94577

D. K. Vaughan
Weidlinger Associates
Menlo Park, California 94025

SUMMARY

Transient, nonlinear soil-structure interaction (SSI) simulations of an Electric Power Research Institute (EPRI), SIMQUAKE experiment were performed using the large strain, time domain STEALTH 2D code and a cyclic, kinematically hardening cap soil model. Results from the STEALTH simulations have been compared to identical simulations performed with the TRANAL code.

INTRODUCTION

Transient, nonlinear soil-structure interaction (SSI) simulations of an Electric Power Research Institute (EPRI), SIMQUAKE experiment (ref. 1) were performed using the large strain, time domain STEALTH 2D code (ref. 2) and a cyclic, kinematically hardening cap soil model (ref. 3). Results from the STEALTH simulations have been compared to identical simulations performed with the TRANAL code (ref. 4) and will be compared to field data at a later time.

The desirability of using a large strain, nonlinear time domain approach to do certain types of SSI simulations has been established by several investigators. In particular, two studies prior to this one and also sponsored by EPRI have explored (1) the limitations of the equivalent linear method (ELM) to calculate large strain nonlinear response (ref. 5) and (2) the effect of a soil model to allow for debonding and rebonding around a rocking structure (ref. 6).

A primary emphasis in the current study was the application to SSI simulations of a mesh-interaction (slideline) algorithm developed for impact (ref. 7) and penetration events (ref. 8). The interaction algorithm is based on explicit numerical equations developed by Wilkins (ref. 9). The interaction algorithm formulation in STEALTH 2D is "strongly coupled" in that interface motion equations are centered in both time and space.

To simulate SIMQUAKE using the interaction algorithm, a modified soil island approach used by previous studies (ref. 6) was adopted. The input excitation histories around the fictitious soil island boundary were obtained by linearly interpolating the measured time-dependent ground motion data in the free field. A free-field calculation using coarse meshes in a large domain to obtain soil island input histories was therefore not required. Furthermore, the available measured data around the structure provided a validation check of the STEALTH 2D code and the interaction algorithm.

Several types of analyses were performed. One type compared calculations in which the structure was omitted and the effects of the cap versus a simple elastic model were considered. Both velocity and stress responses within the domain of the soil island were monitored. These cases provided insight into the transient wave characteristics between linear and nonlinear soil models. These calculations also provided a preliminary test of the mesh-interaction logic in which interface nodes were constrained to act as interior nodes. Another type of analysis included both the structure and the soil (cap and elastic) but did not allow debonding and rebonding. Again, velocity and stress responses surrounding the structure were compared to each other and to the previous calculations without the structure. Basic characteristics of the soil-structure interaction are revealed through such comparisons. The last class of calculations included the comparison of two debonding-rebonding logics -- one based on the mesh-interaction algorithm and the other on a constitutive tension-cutoff model.

Next are described the SIMQUAKE field tests, the soil island methodology, the STEALTH 2D code, and the slideline logic used for various aspects of the problem. Finally, the results of various calculations are presented.

DESCRIPTION OF SIMQUAKE

The purpose of the SIMQUAKE field-test series was to impose strong earthquake-like ground motions on structural models in order to evaluate (1) soil response characteristics (through laboratory and field studies) and (2) soil-structure interaction phenomenology. For the former, endochronic (ref. 10) and cap constitutive models were developed, while in the latter

category, different numerical models were used to perform pretest and post-test analyses.

The simulated earthquake test conditions were achieved by detonating two planar arrays of explosives in such a way as to yield several cycles of planar, p- and s-wave motion passing by the structures. The amplitudes and frequencies of these motions were chosen to approximate a given undamped spectrum. A plan view of the two planar arrays of explosives and five of the structural models used in the second SIMQUAKE test series is shown in figure 1a.

During the test, measurements were taken on and near the structure and in the free field. Figure 1b shows schematically the locations of the various free-field bore holes in which instruments were located. It was intended that these free field measurements would be used as "soil-island" input boundary conditions for the various calculations. The measurements taken on or near the structure were intended to be used to validate the codes and analytic methodology.

The structural models were subjected to planar test conditions. Figure 2 is a schematic of a typical axisymmetric structure. The nominal dimensions of the various structural models are listed below.

Structure Type	Diameter (ft)	Height (ft)
1.	15	22-1/2
2.	10	15
3.	5	7-1/2

One each of the type 1, 2 and 3 structural models were imbedded to 1/4 of their height in the soil using native backfill. Two type 2 structures were included -- each at a different range location. A second type 3 structure was constructed to test a seismic isolation design. A third type 3 model was free standing and filled with water to test fluid-structure interaction. The different conditions chosen intended to shed light on questions of response, scaling, backfill and depth of burial.

SOIL ISLAND METHODOLOGY

The soil island approach is a method for coupling free-field ground motions to analyses of structure-medium interaction. It allows the analyst the freedom to develop free-field ground motion in any manner which is consistent with equations of dynamic equilibrium. This includes either field

measurements or computations or both. The soil island approach has been successfully applied to a range of problems involving wave effects on protective structures.

In the first step of the soil island approach, a fictitious boundary is designated in the free field which surrounds the location of a structure; the free-field ground motions along this boundary are stored for later use. In the second step, this volume of soil referred to as the soil island is analyzed in detail using the stored free-field ground motions as boundary conditions. This reduces the structure-medium interaction model to manageable size.

The soil island concept was initially developed to analyze the response of a surface-flush military structure in a layered site subjected to outrunning ground shock from traveling airblast loading, to local airblast induced ground motion, and to the airblast itself. The outrunning response contained predominantly low frequencies because the high frequency component was filtered out by propagation over long distances through hysteretic soil. To apply the soil island method to this case, the outrunning motion was calculated with a coarse grid (adequate up to about 1 Hz) which extended about 3 miles in length and about 1 mile in depth. A fictitious soil island was defined and motions on its boundary were stored. These were subsequently applied to the boundaries of a soil island, which included the structure. The soil island consisted of sufficiently small elements to insure that the high frequency response (up to about 30 Hz), produced by the airblast and the local airblast induced ground motion, was properly represented.

A modification of the soil island approach is adopted when simulating a physical experiment such as the SIMQUAKE series of field tests. In this case the free-field calculation is eliminated and free-field velocity and acceleration gages are installed on the boundaries of the fictitious soil island. After processing, the time-phased records are used first as input to a calculation of the response of a soil island without structure. The motions in the interior of this soil island can be compared with free-field measurements at corresponding locations. The degree of favorable comparison gives valuable insight into the adequacy of the site model. Then the structural model is inserted into the soil island and the procedure is repeated to obtain soil-structure response. Due to practical limitations on the number of channels of instrumentation, there are never input time history records at all mesh points on the soil island boundaries as is required for the soil island analysis. Studies involving input from coarse mesh free-field calculations into fine mesh soil island models indicate that satisfactory input motion at a fine mesh node can be obtained by linear spatial interpolation between the two adjacent coarse mesh nodes.

Comparison between motions in the interior of the soil island and at corresponding points of the parent free-field calculation, illustrates the success of the method.

Regardless of the methods used to define free-field ground motion, the second step in the soil island approach is to designate fictitious soil islands surrounding possible structures of interest. The free-field velocity-time histories at all points on the boundary of the island are stored for future use. The boundaries of this island are chosen sufficiently far from the eventual position of the structure that, when it is included, it causes only a slight perturbation of the boundary motion. Of course the boundaries must be chosen close enough to the structure to ensure that the eventual structure-medium interaction problem is of manageable size.

The final step is to apply the free-field motions to the boundaries of a soil island including the model of the structure. Since the soil model is the same in the island and in the free field, the time phasing of the applied motion would exactly satisfy the wave equations governing motion within the island if it were not for the structure, which disturbs the free-field motions in two ways. First, there is scattering of waves which is caused by the impedance mismatch between the soil and the structure. Although the authors are unaware of prior work which would shed light on the wave lengths associated with the scattered waves, it is speculated that they are determined by the input ground motion and possibly by the characteristic length and embedment depth of the structure. The second type of disturbance arises from waves induced in the soil by motion of the structure, such as rocking and relative translation, which is commonly recognized as structure-medium interaction. The wave lengths associated with these disturbances presumably are governed by the periods of the principal modes of structure-medium interaction. In some approaches, nonreflecting boundaries are used to absorb both types of waves so that they are not reflected back to the structure and become confused with the primary structure-medium interaction. One benefit of an energy absorbing boundary is that the boundaries may be moved close to the structure with resulting savings in computer time.

In the soil island approach, the island is presumed to be sufficiently large that reflections between the boundaries and the structure are small. Reliance is placed on dispersion, geometrical attenuation and absorption of energy by material damping to reduce the error to an acceptable level.

A simple site model involving uniform properties or horizontal layering and uniform horizontal bedrock motion was adopted for this study. Though this is not necessarily a complete picture of earthquake ground

motion, it is nevertheless one which is familiar to many workers in the area of finite element simulation of structure-medium interaction. It is also simple, which helps in identifying structure-medium interaction effects.

STEALTH 2D AND SLIDELINES

STEALTH 2D is a two-dimensional, large-strain, explicit finite-difference Lagrange computer code. The most important feature of STEALTH 2D that was tested in the SIMQUAKE simulations was the multigrid slideline capability. Slideline is an historical term which identifies the logic necessary to couple two object meshes together to simulate a penetration or impact event in which relative sliding, debonding and redebonding occurs. Numerically this means that each of the interacting objects gets its interface boundary conditions from the other object. When relative motion between the objects occurs, interface boundary node locations on one object do not necessarily coincide with the locations of interface boundary nodes on the other object. In scenarios of relative sliding, the locations of interface boundary nodes are constantly changing. In cases in which debonding and rebonding occur, the interface boundary nodes are not only changing their position along their relative interface but are often spaced by regions of void.

Slidelines are also used to effect a discontinuous change in nodalization within a particular material. This capability is called "tied sliding" because nodal points are tied to the slideline, that is, no relative sliding or debonding is allowed after the original placing of the interface nodes. The nodes act as if they were interior nodes. Figure 3 shows an example of tied sliding nodes.

For the SIMQUAKE soil island geometry, there are a number of ways in which STEALTH 2D can be used to model the event. Each has distinct physical and economic advantages and disadvantages. The simplest, most rudimentary use of STEALTH 2D does not require slidelines. In this case, a rectangular domain is chosen which is bounded by the soil island boundaries on the bottom and two sides and a horizontal free surface boundary at the elevation of the top of the structure. This is shown in figure 4a. One grid is used which includes explicit air (void) regions on either side of the structure and above the ground surface. This model has one major economic disadvantage -- that of having to compute air nodes, which could just as easily be handled by using an appropriate boundary condition and by using two grids coupled through one tied slideline to define the structure. Figure 4b shows this arrangement. Neither the mesh in figure 4a nor the one in figure 4b allows for debonding and rebonding of the structure. These effects can be handled through special logic in the constitutive model for the soil zones

next to the structure. These zones can be made very small (by STEALTH mesh), and the tension-cutoff and recompression constitutive parameters can be chosen to give the effect of gap regions. One set of calculations was performed using the STEALTH mesh. A disadvantage to this approach can occur if the "gap" zones are so small that they control the time step. In SIMQUAKE, this was not the case -- the zones in the very stiff structure controlled the time step.

Another approach for modeling debonding and rebonding involves multiple grids connected by both tied and free slidelines. Several variations of this approach are shown in figures 5a and 5b. The variation shown in figure 5a was used in several SIMQUAKE simulations. Slideline #1 is tied and is used to effect a change in zoning. Slideline #2 is located at a depth coincident with the bottom of the structure. The nodalization above and below slideline #2 is identical but debonding/rebonding is allowed to occur at the base of the structure. Everywhere else the slideline is tied. A third tied slideline exists at the ground surface connecting the bottom 1/4 of the structure to the top 3/4. A potential flaw of the approach shown in figure 5a is that no kinematic debonding is allowed at the sides of the structure. If it is necessary to achieve debonding at these locations, then zone gap models would again be necessary.

To have kinematic debonding all around the structure would require the mesh shown in figure 5b. Here, slideline #1 is the same as in figure 5a, but slideline #2 is placed at the surface of the ground and around the structure as shown. This arrangement has two advantages over the previous one -- it will require slightly less computer time because there are fewer total nodes and there is no need for gap zones. The disadvantages are that the zones are not rectangles and are less accurate than their rectangular equivalents.

Two other STEALTH 2D options which can significantly reduce cost and possibly increase accuracy are available. The primary assumption required is that the structure can be treated as a rigid body. In all the meshes shown so far, the time step is controlled by zones in the structure. The sound speed in the structure is about ten times that of the soil, so that for equivalently sized zones, the global (problem) time step is 1/10th of what would be required for the soil were it to control the global time step. Assuming that the structure is at least elastic and almost rigid allows for two options to be considered -- (1) subcycling the nodalized structure at its smaller time step or (2) using a rigid body model for the structure.

One approach using the rigid body assumption for the structure is shown in figure 6. Figure 6 is a variation of figure 5b, in which the flexible structure is replaced by a rigid body model.

DESCRIPTION OF CALCULATIONS

Several SIMQUAKE calculations have been performed using three different codes -- TRANAL, FLUSH (ref. 11) and STEALTH 2D. The results presented in this paper are primarily from the STEALTH 2D calculations. However, the STEALTH results have been compared to results from TRANAL, so where necessary, TRANAL results are also presented. TRANAL and STEALTH are both explicit time domain codes. Though TRANAL is a finite-element code and STEALTH is a finite-difference code, the only major difference is that TRANAL utilizes a small strain assumption while STEALTH does not.

Table 1 summarizes the calculations presented in this paper. These include several variations of the same boundary conditions and geometry in order to determine among other things, the effect of (1) material properties and (2) debonding-rebonding logic. Two material models were used -- elastic and kinematic cap. Two debonding-rebonding logics were used -- one involved a tension-cutoff parameter in the cap material model while the other used a distinct kinematic surface.

In order to verify the STEALTH 2D tied sliding logic, three free field calculations were made. These calculations used the same soil island volume but slightly different boundary conditions from those used in subsequent SSI calculations, in which the structure was included in the mesh. Figure 7a shows the mesh used both by TRANAL and by STEALTH. Figure 7a has no slidelines. Figure 7b is the STEALTH mesh which makes use of tied sliding in order to get a greater number of zones in the region where the structure will be placed. Notice that in both cases the soil island boundary nodes are identical.

Results from these cases for the elastic material model are shown in figures 8a and 8b. These are velocity histories at the A and B locations, respectively, noted in figures 7.

The next set of calculations that were performed included the structure. The TRANAL and STEALTH meshes are shown in figures 9a and 9b. These two meshes use gapping logics in the thin zones bordering the structure. Two other STEALTH meshes were shown in figures 5a and 5b. Figure 5a displayed a grid which uses a horizontal slideline at the base of the structure. In figure 5b, a slideline separating the entire structure from the soil was used. Characteristic results from these cases are shown in figure 10. Due to page limitations for this paper, other comparisons are not shown. The results shown are typical. Detailed results will be available in the near future as an EPRI publication.

CONCLUSIONS AND SUMMARY

The results shown indicate relatively good agreement between all the STEALTH and TRANAL calculations. The differences that are seen can probably be attributed to (1) large (STEALTH) vs small (TRANAL) strain formulation and/or (2) grid discretization differences.

REFERENCES

1. C. Chan and H. T. Tang, EPRI Research Project 810 - Soil-Structure Interaction, 1976.

2. R. Hofmann, "STEALTH - A Lagrange Explicit Finite-Difference Code for Solids, Structural, and Thermohydraulic Analysis", EPRI NP-260, Vol. 1, August 1976.

3. I. S. Sandler, F. L. DiMaggio and G. Y. Baladi, "Generalized Cap Model for Geological Material", J. of Geotechnical Engineering Division, ASCE, Vol. 102, No. GT7, July 1976.

4. J. L. Baylor, J. P. Wright, C. F. Chung, "TRANAL User's Guide, Part I, (Small Strain, Small Displacement Version)", Weidlinger Assoc., Final Report Under Contract DNA 001-76-C-0125, Report No. DNA 4960F, March 1979.

5. Julio E. Valera, et al., "Study of Nonlinear Effects on One-Dimensional Earthquake Response", EPRI NP-865, August 1978.

6. J. Isenberg, D. K. Vaughan and I. Sandler, "Nonlinear Soil-Structure Interaction", EPRI NP-945, December 1978.

7. R. Hofmann, S. L. Hancock, R. L. Puthoff and M. Wohl, "Computed Response of Spherical Shielding to Impact Loading", TCAM 72-7, May 1972.

8. M. L. Wilkins, "Penetration Mechanics", UCRL-7211, November 1969.

9. M. L. Wilkins, "Calculation of Elastic-Plastic Flow", UCRL-7322-Rev. 1, January 1969.

10. H. E. Read, K. C. Valanis, "An Endochronic Constitutive Model for General Hysteretic Response of Soils", EPRI NP-957, January 1979.

11. Dilip Jhaveri, et al., "Applications in Soil-Structure Interaction", EPRI NP-1091, June 1979.

TABLE 1. - SUMMARY OF CALCULATIONS PRESENTED

Type	Code	Comments
Free Field	TRANAL	elastic
Free Field	STEALTH 2D	elastic
Free Field	STEALTH 2D	elastic, with tied slidelines
SSI	TRANAL	kinematic cyclic cap, gapping elements (Figure 9a)
SSI	STEALTH 2D	kinematic cyclic cap, gapping zones (Figure 9b)
SSI	STEALTH 2D	kinematic cyclic cap, rigid body debonding/rebonding (Figure 6)

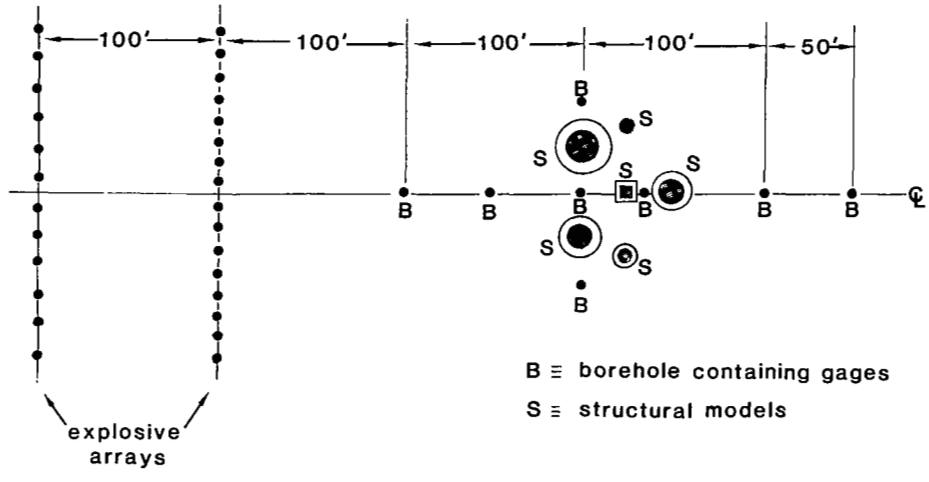

(a) Plan view.

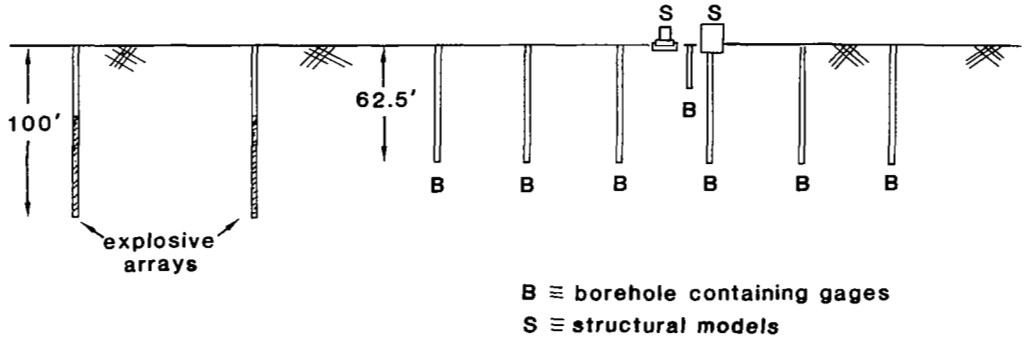

(b) Vertical cut through SIMQUAKE II centerline.

Figure 1.- SIMQUAKE II field test.

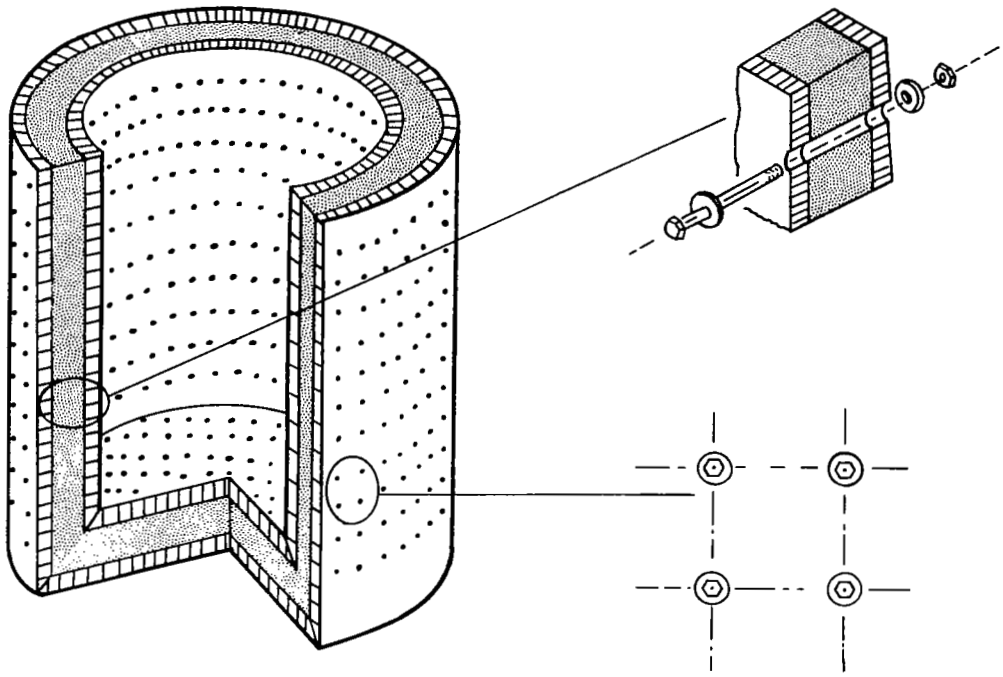

Figure 2.- Typical scaled structure.

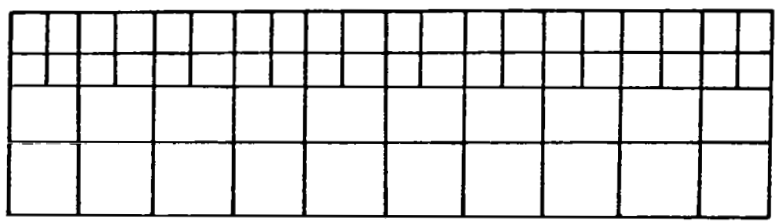

Figure 3.- Two-dimensional multi-grid example.

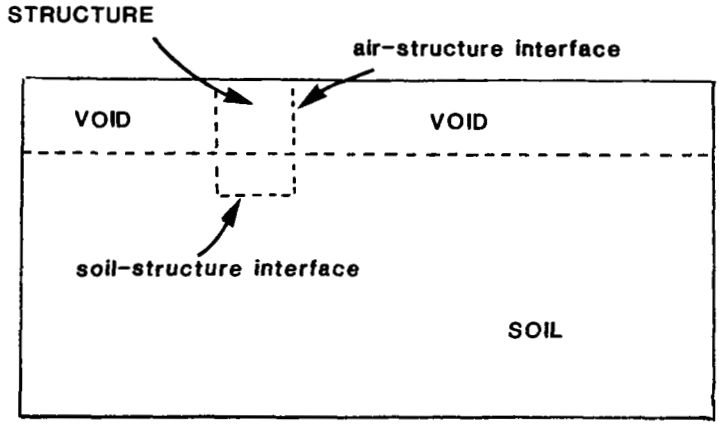

(a) Schematic using no slidelines and one grid.

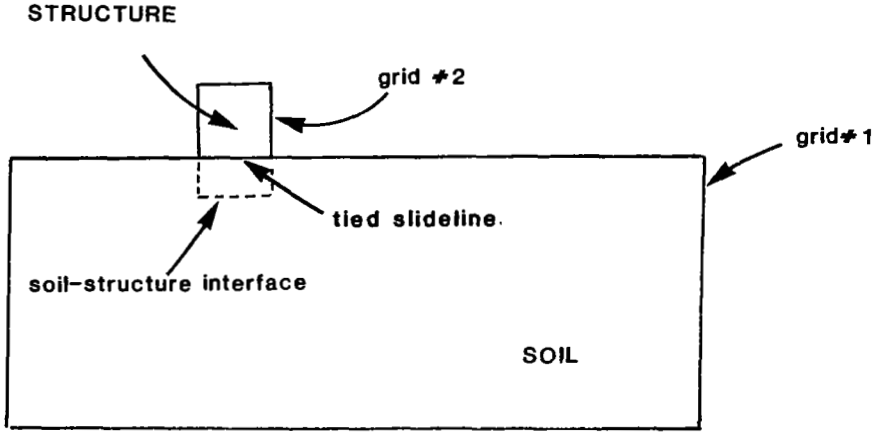

(b) Schematic using one slideline and two grids.

Figure 4.- Schematics of SIMQUAKE mesh.

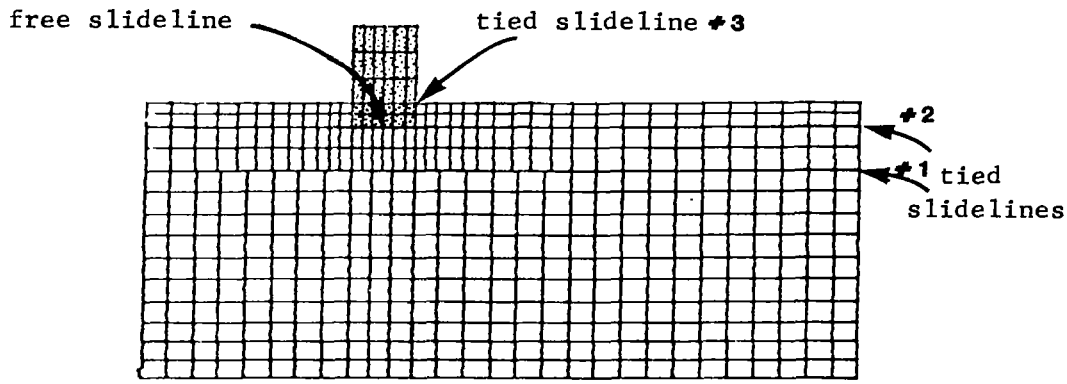

(a) At bottom of flexible structure only.

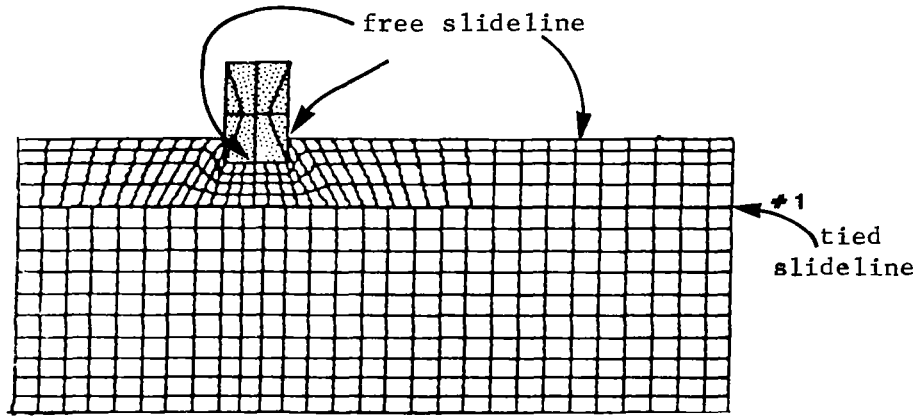

(b) All around flexible structure.

Figure 5.- Debonding/rebonding of a flexible structure.

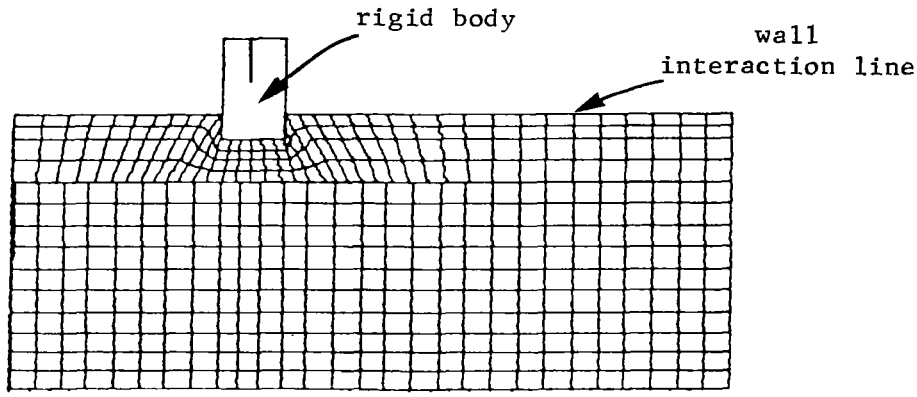

Figure 6.- Debonding/rebonding all around rigid structure.

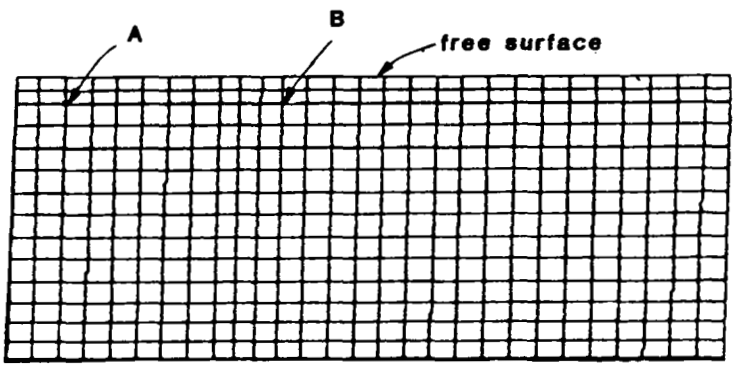

(a) TRANAL and STEALTH free field, soil island mesh using no slidelines.

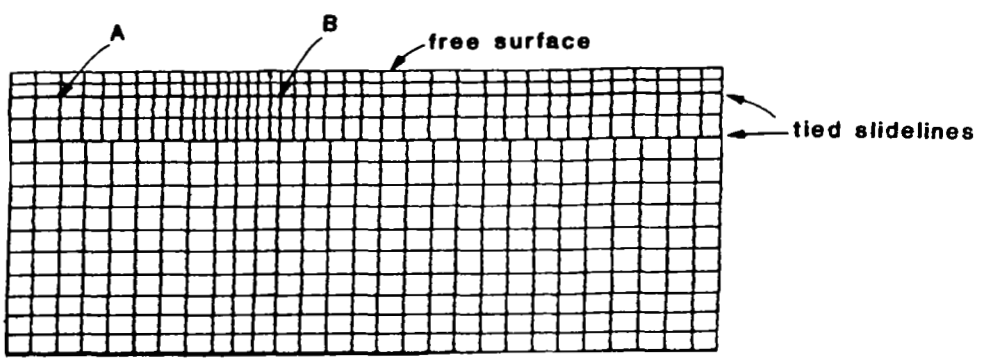

(b) STEALTH free field, soil island mesh using two tied slidelines.

Figure 7.- TRANAL and STEALTH free fields.

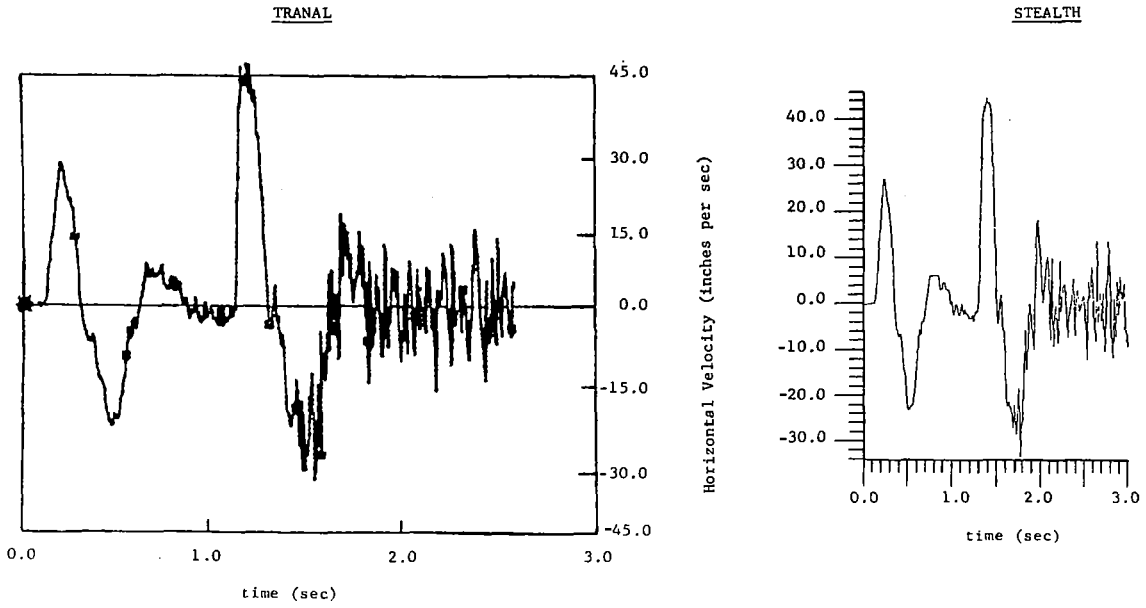

(a) Horizontal velocity histories for 3.0 seconds from TRANAL and STEALTH output at location A (see Fig. 7).

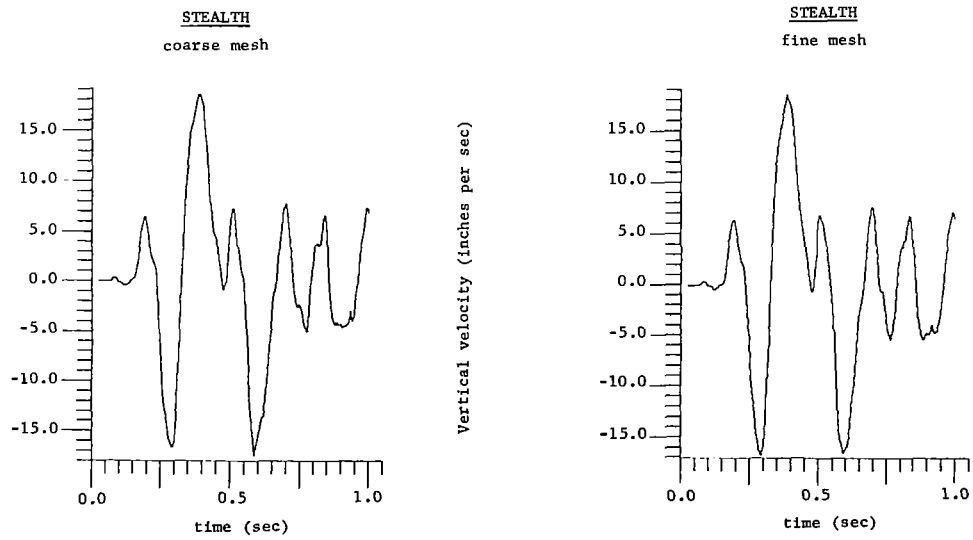

(b) Vertical velocity histories for 1.0 second from two STEALTH meshes at location B (see Fig. 7).

Figure 8.- Comparison of velocity histories for elastic free field simulations.

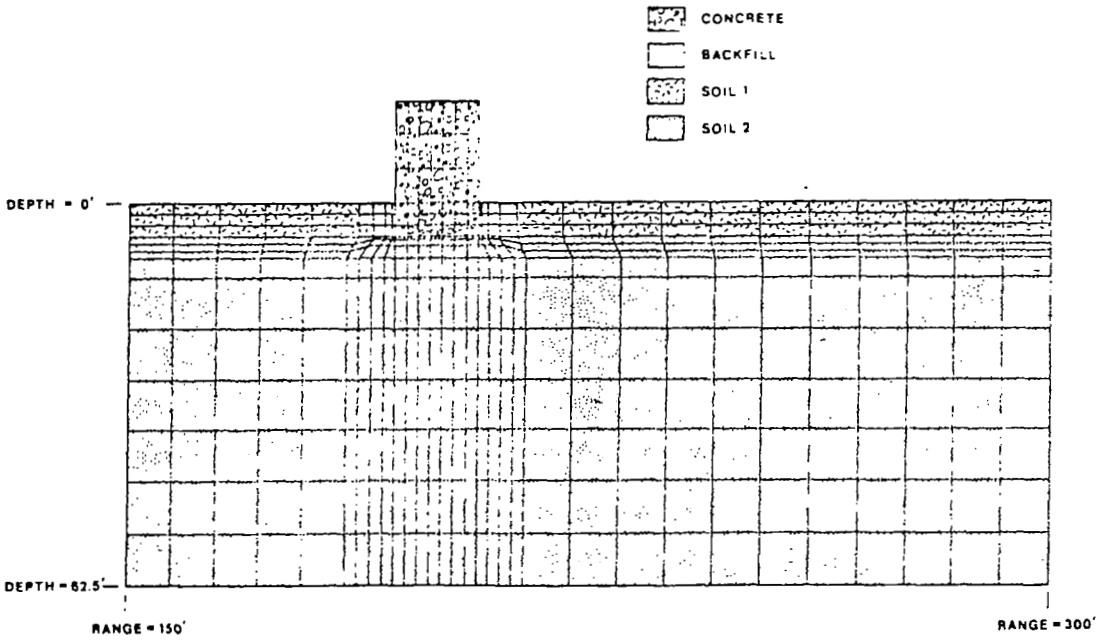

(a) TRANAL mesh.

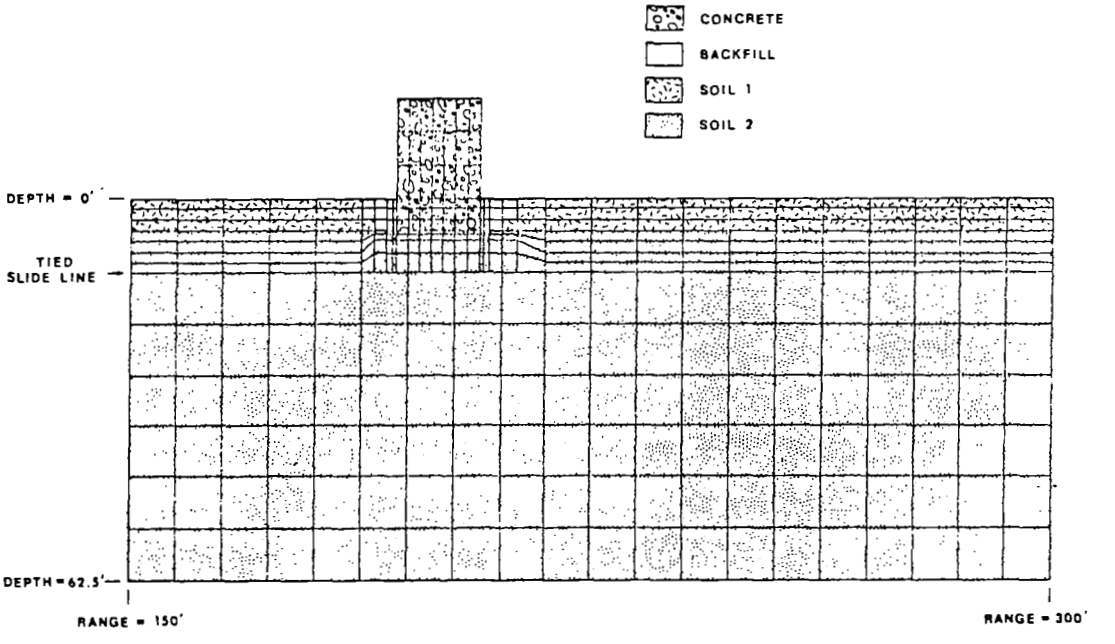

(b) STEALTH mesh.

Figure 9.- Comparison of TRANAL and STEALTH meshes with gapping elements, or zones, next to flexible structure.

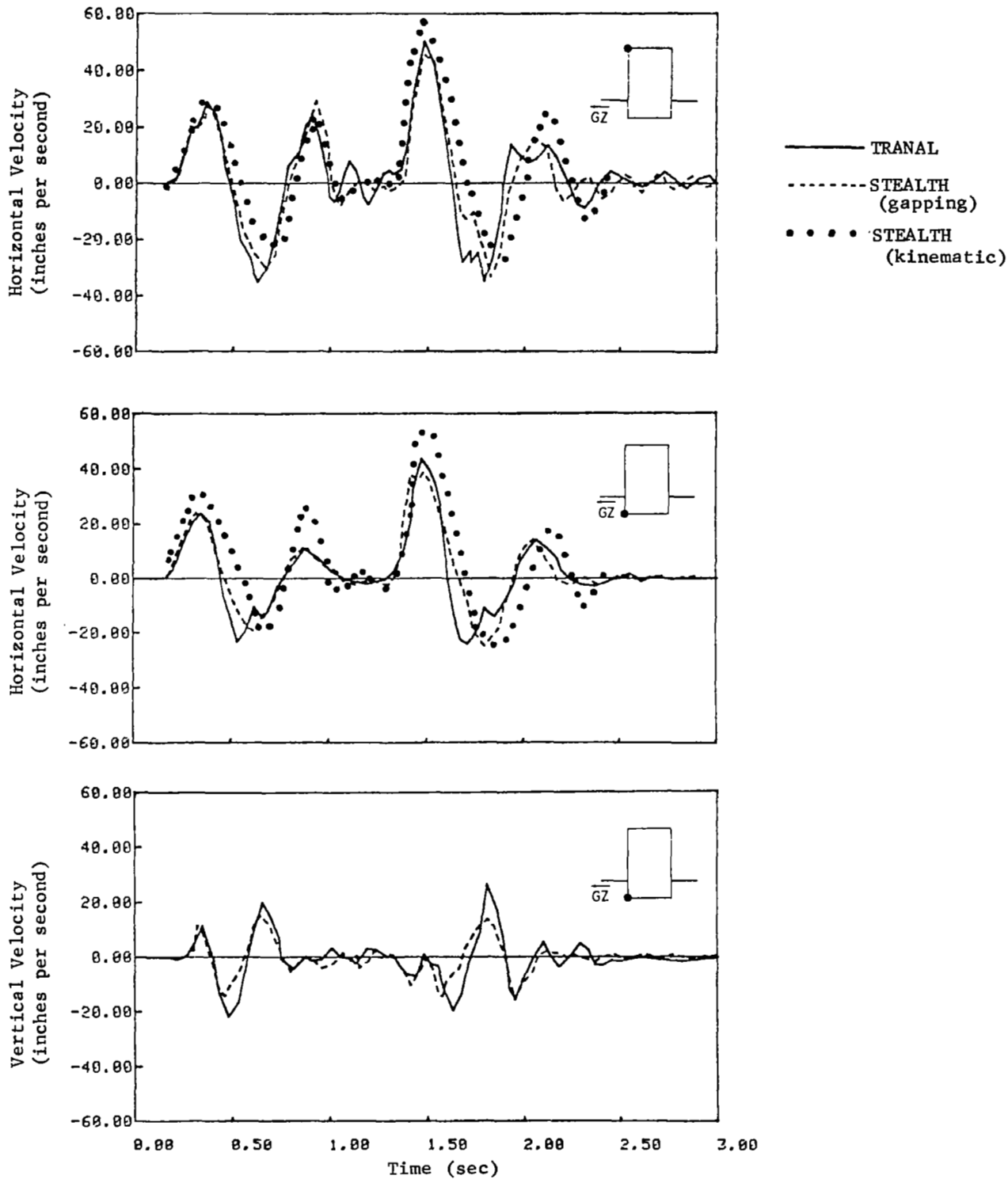

Figure 10.- Comparison of three velocity histories on the flexible structures.

COMBUSTION - STRUCTURAL INTERACTION IN A VISCOELASTIC MATERIAL*

T. Y. Chang and J. P. Chang
Department of Civil Engineering
The University of Akron, Akron, Ohio

M. Kumar and K. K. Kuo
Department of Mechanical Engineering
The Pennsylvania State University
University Park, Pennsylvania

SUMMARY

The effect of interaction between combustion processes and structural deformation of solid propellant was considered. The combustion analysis was performed on the basis of deformed crack geometry, which was determined from the structural analysis. On the other hand, input data for the structural analysis, such as pressure distribution along the crack boundary and ablation velocity of the crack, were determined from the combustion analysis. The interaction analysis was conducted by combining two computer codes, a combustion analysis code and a general purpose finite element structural analysis code.

INTRODUCTION

In recent years, much attention has been focused on the investigation of the coupling effect between combustion phenomenon and mechanical behavior of solid propellant. The solution of problems of this type can further better understanding of the transient combustion processes inside solid propellant cracks, which may significantly affect the performance of a rocket motor. The combustion phenomenon inside the crack of solid propellant is strongly influenced by the crack geometry as the material is being deformed and burned away. Generally, there are two major reasons for alteration of the crack geometry: 1) mass loss due to gasification of propellant surface along the crack during the combustion process, and 2) mechanical deformation of the propellant due to pressure.

On one hand, both the burning rate and mechanical deformation are governed by pressure acting on the crack surface. On the other hand, a change in crack size will cause the pressure distribution to vary. The pressure distribution will strongly influence the deformation and stress concentration at the crack

*Research sponsored by the Power Program of the Office of Naval Research Arlington, Va., under Contract No. N00014-79-C-0762. The support of Dr. R. S. Miller is gratefully acknowledged. A part of this work was performed under a previous contract sponsored by Dr. R. L. Derr of NWC. His support is also appreciated.

tip, which in turn will affect the manner of the crack propagation. It is, therefore, apparent that the pressure distribution and the change in crack geometry are strongly interdependent.

In the past, combustion and structural analyses of solid propellant were conducted independently, with the result that interaction effects were completely ignored. As noted above, such interaction effects can be quite important, especially when the deformation is large as compared to the original crack-gap width. The deformation response of the material is categorized as linearly viscoelastic. It is, therefore, the intent of this paper to present a method of analysis for the combustion-structural interaction in a linear viscoelastic medium. To this end, three major tasks are involved: 1) combustion analysis to model the transient combustion process, 2) viscoelastic analysis in conjunction with moving boundary, and 3) linkage of the two analyses.

For the combustion analysis, investigations of certain aspects of combustion processes have been made. Taylor [1] conducted experimental tests to study the convective burning of porous propellants with closed- and open-end boundary conditions. Belyaev et al. [2] showed that the burning of propellant inside a narrow pore may lead to an excess pressure buildup. In a later study, Belyaev et al. [3] made a series of experimental tests to determine the dependence of flame-spreading rate on crack geometry, propellant properties, boundary conditions, and combustion chamber pressures. Cherepanov [4] stated that as a result of the impeded gas flow in a sufficiently narrow and long cavity, the pressure reaches such high values that the system becomes unstable. From his work, Godai [5] indicated that there is a threshold diameter or critical width of a uniform cavity below which flame will not propagate into the crack. Krasnov et al. [6] investigated the rate of penetration of combustion into the pores of an explosive charge. Jacobs et al. [7,8] studied the pressure distribution in burning cracks that simulate the debonding of solid propellant from the motor casing.

Although results of previous experiments were of interest, no sound theoretical model was developed. In this study, a theoretical model was established for predicting rate of flame propagation, pressure distribution, and pressurization rate inside the crack. Two sets of coupled partial differential equations were obtained: one from mass, momentum, and energy conservation of the gas phase of the propellant product in the void region adjacent to the crack surface; the other from consideration of solid-phase heat conduction. Due to the mathematical complexity of governing equations and boundary conditions involved, the finite difference method was used to obtain the solution for the combustion analysis. In the numerical solution, the boundary conditions, which vary with time, are specified in terms of the changing crack geometry, which in turn is found from the structural analysis. In addition, the pressure distribution along the crack surface, varying as a function of time, was obtained from the analysis and was used as input for the structural analysis.

For structural analysis, different approaches have been taken previously in solving (analytically or numerically) several moving boundary problems in linear viscoelasticity. Lee et al. [9] obtained a solution for the pressurization of an annihilating viscoelastic cylinder contained by an elastic casing in which the material was assumed to be a Kelvin model in shear and incompressible in bulk. Arenz et al. [10] performed a similar analysis for a sphere. Corneliussen et

al. [11,12] presented solutions for a spinning, annihilating, viscoelastic cylinder with free outer boundary. Since the constraining case was not included in their analyses, the stress distribution was independent of the material properties. With the assumption of a standard linear solid model, Shinozuka [13] presented the analytical solution for a case-bonded pressurized viscoelastic cylinder. More generalized solutions were obtained by Rogers et al. [14] for a class of linear viscoelastic problems by using the numerical integration scheme. Schapery [15] also developed a general method for solving moving boundary problems. In his approach, the moving boundary condition was replaced by a fictitious non-moving boundary subjected to a time-dependent pressure. Later, Christensen et al. [16] obtained a series solution for the stresses of the same problem. As noted above, most of the analytical solutions were available for viscoelastic problems of simple geometry. For complex geometry, the finite element method has proven to be most useful.

Application of the finite element method for solving viscoelastic problems is not new; reports of such work can be found, for instance, in references [17-20]. However, most of the previous work did not consider the effect of moving boundary, an important feature for the structural analysis of solid propellant. Sankaran and Jana [21] presented a technique for the solving of axisymmetric viscoelastic solids with moving boundary. In their approach, the finite element mesh corresponding to the new boundary was re-generated, while the stress-strain histories and material properties were assumed to be carried over from those of the previous time increment. This assumption is valid only if the time increment is very small. An algorithm for automatically tracking ablating boundaries was given by Weeks and Cost [22]. All previous work dealing with moving boundary viscoelastic problems lacks both the appropriate treatment of material properties, and stress-strain histories for the newly generated mesh. It is the purpose of this paper to present such a treatment.

Three major features must be included in the structural analysis for a solid propellant: 1) proper modeling of viscoelastic behavior, 2) tracking of ablating boundary in order to generate new finite element meshes, and 3) treatment of the material responses (i.e., stress-strain histories and material properties) for the new mesh. All of these features have been incorporated into a nonlinear finite element program called NFAP [23]. Combustion and structural programs were combined in order to make possible an interaction analysis. Numerical results are presented to demonstrate the effect of interaction between combustion and structural responses of the material.

COMBUSTION ANALYSIS

The theoretical model was developed to simulate the combustion phenomenon inside a propellant crack, which is located in a transverse direction to the main flow of the rock chamber. During the course of derivation, the following assumptions are made:

1) All chemical reactions occur near the propellant crack surface, and the combustion zone is so thin that it is considered a plane.

2) Rate processes at the propellant surface are quasi-steady in the sense that characteristic times associated with the gaseous flame and preheated propellant are short in comparison to that of pressure transient variation.

3) Gases flowing in the propellant crack obey the Clausius or Noble-Abel equation of state.

4) Bulk flow in the pore is one-dimensional [24].

To describe gas-phase behavior inside a solid propellant crack, mass, momentum, and energy equations in unsteady, quasi-one-dimensional forms have been developed, based upon the balance of fluxes in a control volume within the propellant crack.

The mass conservation equation is

$$\frac{\partial(\rho A_p)}{\partial t} + \frac{\partial(\rho u A_p)}{\partial x} = r_b \rho_{pr} P_b \tag{1}$$

The momentum conservation equation is

$$\frac{\partial}{\partial t}(\rho u A_p) + \frac{\partial}{\partial x}(\rho A_p u^2) = - A_p \frac{\partial p}{\partial x} + \frac{\partial}{\partial x}(A_p \tau_{xx})$$

$$- \tau_w P_w \cos \Theta_w + \rho A_p B_x - (\rho_{pr} r_b P_b) V_{gf} \sin \Theta_w \tag{2}$$

The energy conservation equation written in terms of the total stored energy (internal and kinetic) per unit mass, E, is

$$\frac{\partial}{\partial t}(\rho A_p E) + \frac{\partial}{\partial x}(\rho A_p u E) = \frac{\partial}{\partial x}(\lambda A_p \frac{\partial T}{\partial x}) - \frac{\partial}{\partial x}(A_p pu)$$

$$+ \frac{\partial}{\partial x}(\tau_{xx} A_p u) + \rho_{pr} r_b P_b h_f - \bar{h}_{cp} P_b (T - T_{ps}) \tag{3}$$

$$+ B_x \rho A_p u - \bar{h}_{cw} (P_w - P_b)(T - T_{ws})$$

The conservation equations are further simplified by an order of magnitude analysis in which the following terms are negligible: 1) forces between molecules due to viscous normal stress in axial direction; 2) viscous dissipation and rate of work done by the force caused by viscous normal stresses in the energy equation; and 3) axial heat conduction between gas molecules in the energy equation.

The propellant surface temperature at a fixed location along the crack before the attainment of ignition is calculated from the solid-phase heat conduction equation written in unsteady one-dimensional form:

$$\frac{\partial T_{pr}(t,y)}{\partial t} = \alpha_{pr} \frac{\partial^2 T_{pr}(t,y)}{\partial y^2} \tag{4}$$

where the length variable y is measured perpendicular to the local propellant crack surface. Initial and boundary conditions are

$$T_{pr}(0, y) = T_{pi} \tag{5}$$

$$T_{pr}(t, \infty) = T_{pi} \tag{6}$$

$$\frac{\partial T_{pr}}{\partial y}(t, 0) = - \frac{\bar{h}_c(t)}{\lambda_{pr}} [T(t) - T_{ps}(t)] \tag{7}$$

The heat conduction equation is solved by using an integral method [25] which employs a third-order polynomial, or by direct numerical solution of Eqs. (4-7) with variable mesh size in the subsurface.

For the gas phase, the Noble-Abel equation is used for the equation of state:

$$p(\frac{1}{\rho} - b) = RT \tag{8}$$

The gas-phase equations, i.e. Eqs. (1), (2) and (3), are non-linear, inhomogeneous, partial differential equations. Along with the partial differential equation for the solid phase (Eq. (4)), they are solved simultaneously, using the finite difference method. The derivation described above was implemented into a computer program, crack combustion code (CCC) by Kuo et al. [26].

STRUCTURAL ANALYSIS

To conduct the structural analysis of the solid propellant, three main features must be included in the numerical formulations: 1) modeling of viscoelastic material behavior, 2) simulation of ablating boundary, and 3) treatment of material responses by an interpolation scheme. Each feature is outlined below.

Viscoelastic Material Model

The material behavior of the solid propellant is assumed to be viscoelastic in shear and elastic in bulk. Only the isothermal condition is considered. The stress-strain relations with zero initial conditions are written in two parts.

1) Shear behavior:

$$S_{ij} = \int_0^t G_1(t-t') \frac{d}{dt'} e_{ij}(t')dt' \tag{9}$$

where G_1 is the relaxation modulus in shear. For most viscoelastic materials, it is usually considered

$$G_1 = g_o + \sum_{m=1}^{M} g_m \, e^{-\beta_m t} \tag{10}$$

2) Bulk behavior:

$$\sigma_{kk} = 3K \, \varepsilon_{kk} \tag{11}$$

As discussed in [27], the incremental stress-strain relations in matrix form are written as

$$\{\Delta\sigma\} = [D_{VE}]\{\Delta\varepsilon\} - \{\sigma_0\} \tag{12}$$

where

$$\{\Delta\sigma\}^T = \{\Delta\sigma_{22}, \Delta\sigma_{33}, \Delta\tau_{23}, \Delta\sigma_{11}\} \tag{13}$$

$$\{\Delta\varepsilon\}^T = \{\Delta\varepsilon_{22}, \Delta\varepsilon_{33}, \Delta\varepsilon_{23}, \Delta\varepsilon_{11}\} \tag{14}$$

$$\{\sigma_0\}^T = \sum_{m=1}^{M} B_m \, \{{}_mC_{22}^t, \, {}_mC_{33}^t, \, {}_mC_{23}^t, \, {}_mC_{11}^t\} \tag{15}$$

and

$$[D_{VE}] = \begin{bmatrix} (K+\frac{2}{3}A) & (K-\frac{1}{3}A) & 0 & (K-\frac{1}{3}A) \\ & (K+\frac{2}{3}A) & 0 & (K-\frac{1}{3}A) \\ \text{symmetric} & & \frac{A}{2} & 0 \\ & & & (K+\frac{2}{3}A) \end{bmatrix} \tag{16}$$

Furthermore,

$$A = g_o + \sum_{m=1}^{M} g_m \, (1 - e^{-\beta_m \Delta t})/(\beta_m \Delta t) \tag{17}$$

$$B_m = 1 - e^{-\beta_m \Delta t} \tag{18}$$

and the term ${}_mC_{ij}^t$ has a recursive relationship, i.e.,

$$ {}_{m}C_{ij}^{t} = e^{-\beta_m \Delta t} \, {}_{m}C_{ij}^{t-\Delta t} + \frac{g_m (1-e^{-\beta_m \Delta t})}{\beta_m \Delta t} \, e'_{ij} \tag{19} $$

$$ e'_{ij} = e_{ij}^{t} - e_{ij}^{t-\Delta t} \tag{20} $$

The advantage of Eq. (19) is that all of the strain history can be obtained by referring only to information in the previous time step, thus reducing computer storage and numerical calculations.

From the virtual work principle and the relationship of Eq. (12), the finite element equilibrium equations for a typical time interval [t, t + Δt] can be derived as

$$ [K] \{\Delta v\} = \{\Delta f\} - \{f_o\} \tag{21} $$

where

$$ [K] = \int [B]^T [D_{VE}] [B] \, dv \tag{22} $$

and

$$ \{f_o\} = \int [B]^T \{\sigma_o\} \, dv \tag{23} $$

Simulation of Ablating Boundary and Mesh Generation

Burning of the propellant causes a significant change in geometry, thus presenting complications in finite element structural analysis. The effect of ablating boundary is accounted for by redefining the finite element mesh at specified time intervals. This involves two stages of calculations: 1) tracking of the ablating boundary, and 2) generation of new finite element mesh. With some modifications, the procedures adopted herein are similar to those presented in [22].

Consider a structural geometry with ablating boundary. The spatial positions of the ablating boundary are determined by the ablation velocities which are found from the combustion analysis at discrete times. It is assumed that the ablation occurs always in the directon normal to the boundary. For structural analysis, the entire surface is divided into an ablating part and a non-ablating part; each part is formed by discrete line segments joining at the nodes of the finite element mesh. The new position of each line segment is located from the given ablating velocity. Consequently, the new boundary nodes are determined by calculating the intersections of two subsequent new line segments. Likewise, the nodes at the intersections of new ablating and non-ablating boundaries are then determined.

During the locating process, however, some of the boundary nodes may not lie on the new boundary and thus must be eliminated. If the distance from the tip of the normal vector at a new nodal position to any node on the original boundary is less than the value of the normal itself, the node is removed.

In general, the total number of nodes on the boundary at discrete times will be different because some of the nodes have been removed. However, in the analysis it is more convenient to generate a finite element mesh similar to the original one so that interpolation of material response can be made. One way to accomplish this is by keeping the number of boundary nodes constant. Consequently, the boundary nodes are redistributed between two discontinuity points which are specified in the input data in such a way that the lengths of the new line segments have the same ratio as those of the original lines.

Once the new boundary nodes are defined, an automatic mesh generation scheme is used to create the interior nodes for further analysis. Because of its flexibility in obtaining a desirable mesh, a Laplacian-isoparametric grid generation scheme [28] is utilized. However, this method is limited to a geometry bounded by four sides. A finite element mesh is shown in Fig. 1. The coordinates of the i-th interior node can be expressed in terms of those of neighboring nodes by

$$y_i = \frac{1}{4(2-w)} [2(y_{i1} + y_{i2} + y_{i3} + y_{i4}) - w(y_{i5} + y_{i6} + y_{i7} + y_{i8})] \tag{24}$$

$$z_i = \frac{1}{4(2-w)} [2(z_{i1} + z_{i2} + z_{i3} + z_{i4}) - w(z_{i5} + z_{i6} + z_{i7} + z_{i8})] \tag{25}$$

where w is the weighting factor for adjusting the distribution of interior nodes, and $0 \leq w \leq 1$.

Setting up the equations for each interior node yields two systems of simultaneous equations. It is observed that the resulting systems of equations are banded and symmetric. The Gaussian elimination scheme is employed to solve for the coordinates of the interior nodes.

Interpolation of Material Responses

As seen from Eq. (16), the stress increment $\Delta\sigma$ for the time interval $[t, t+\Delta t]$ varies with material properties and with the strain history at both current and previous time steps. When the region of an element changes over a period of time due to ablation, the material response history of the new elements is lost and must be determined by an interpolation procedure from the old elements at previous time steps. Accordingly, the interpolation procedure is carried out on the element level. For calculations, the material responses are separated into two groups: the first includes such variables evaluated at the Gaussian integration points, i.e., $\Delta\sigma_{ij}$, $\Delta\varepsilon_{ij}$ and C^t_{ij}; the second includes the nodal displacements which are evaluated at nodal points. In the present calculations, two limitations are imposed: 1) eight-node quadrilateral elements are used throughout the analysis; and 2) the four sides of each element remain straight before and after ablation.

1) Interpolation of Gaussian variables - It is noted that the quadratic displacement approximation of an eight-node element yields a linear strain variation. With this fact in mind, the quantities of Gaussian variables at nodal points are first evaluated for every old element. As shown in Fig. 2a, b, this can be done by using the linear isoparametric shape functions, namely,

$$\bar{w}_k' = \sum_{i=1}^{4} h_i(r_k', S_k') * w_i' \quad k = 1, 2, 3, 4 \tag{26}$$

where $h_i = 1/4(1 + r_i r)(1 + s_i s) \quad i = 1, 2, 3, 4$

For each new element, the local coordinates (r_k, s) of the k-th Gaussian point are known. The global coordinates, $(\bar{y}_k, \bar{z}_k)$, of that point are, therefore, computed by using the following equations:

$$\bar{y}_k = \sum_{i=1}^{4} h_i(r_k, s_k) * y_i$$

$$\bar{z}_k = \sum_{i=1}^{4} h_i(r_k, s_k) * z_i \tag{27}$$

After $(\bar{y}_k, \bar{z}_k)$ are found, the old element to which the point belongs must be identified. A search process based upon the values of r' and s' is developed for this purpose. The search starts from the old element which corresponds to the neighboring elements. Equations for such calculations are given by

$$\bar{y}_k = \sum_{i=1}^{4} h_i(r', s') * y_i'$$

$$\bar{z}_k = \sum_{i=1}^{4} h_i(r', s') * z_i' \tag{28}$$

Fig. 2c shows how to identify the element to which the points, (r', s'), belong. Once the location of the point is verified, an interpolation procedure is performed, using the relationship

$$\bar{w}_k = \sum_{i=1}^{4} h_i(r', s') * w_i' \tag{29}$$

2) Interpolation of nodal displacements - A similar procedure to that explained above is also used to determine the position of the node in question with reference to the old element. However, the interpolation procedure in Eq. (26) is no longer necessary since the nodal displacements are known. The nodal displacements of the new mesh are computed from

$$d_i = \sum_{i=1}^{8} h_i(r', s') * d_i' \tag{30}$$

where h_i are the standard quadratic isoparametric shape functions.

All formulations discussed in this section have been implemented into a general purpose nonlinear finite element program called NFAP for conducting viscoelastic analysis of solid propellant with ablating boundary. Some numerical examples are presented in a later section.

COUPLING EFFECT

For structural analysis, the boundary condition along the crack geometry is defined by pressure distribution which varies with time, and ablation velocity; both are determined from combustion analysis. In the combustion analysis, the regression rate of the propellant is dependent on the deformed crack geometry. Therefore, the two processes are strongly interdependent. Such a coupling effect is obtained by combining the analysis of two computer programs: a crack combustion code (CCC) and a structural analysis code (NFAP). Both codes were developed independently to facilitate program verifications. Linkage of the two codes was made subsequently.

The coupling effect considered in the present analysis is limited to the major parameters, namely pressure loading, ablation velocity, and crack deformation. Pressure and ablation velocity are calculated by the CCC at each nodal point located on a one-dimensional grid along the length of the crack. The analysis of crack combustion incorporates the crack geometry variation caused by both mechanical deformation and mass loss through gasification of the propellant surface. Once the gas-phase equations are solved and the pressures and ablation velocities along the crack are calculated for a given time t, the data are transferred to the NFAP as the input information. NFAP then simulates the updated crack geometry from the ablation velocities and generates a new finite element mesh. With the new mesh and pressure data, NFAP updates the stiffness matrix and interpolates material responses for conducting a quasi-static analysis at time t. After obtaining the deformation, the change in the crack width at each finite different node is calculated and added to the existing crack width. Since the crack width is the input of the combustion analysis, one cycle of calculations is thus completed. The same procedure is followed for every specified time increment.

EXAMPLES

For program verification and demonstration of its analysis capability, three sample problems were run either by NFAP alone or in the combined NFAP/CCC program. The results of the analysis are discussed in the following. The numerical results obtained from CCC alone are contained in reference [26].

1. A Reinforced Thick-walled Cylinder

Figure 3 shows a cylinder of viscoelastic material bonded by a steel casing and subjected to a step-function internal pressure. The example was selected because it is composed of two different materials and the analytical results are readily available for comparison. Only five eight-node axisymmetric elements were used to model the cylinder. The material properties of the elastic casing are

$$E = 2.068 \times 10^6 \text{ MPa} \qquad \nu = 0.3015$$

The material properties of the viscoelastic core are defined by

$$K = 689.5 \text{ MPa} \qquad G_1 = 51.71 * \exp(-0.1t) \text{ MPa}$$

In Fig. 4, the variations of circumferential stresses with time are plotted for comparison with the analytical solution obtained in [9]. It is observed that both solutions agree very closely. This problem was analyzed previously by Zienkiewicz et al. [18], using strain rate formulation of the finite element method. However, the formulation presented in the present paper is more easily incorporated into the NFAP program.

2. A Star-shaped Solid Rocket Motor

As an application of the present approach in dealing with the moving boundary, a star-shaped solid rocket motor was analyzed by assuming both a constant and ablating inner boundary. The configuration and finite element mesh are shown in Fig. 5, and the material properties of outer casing and inner propellant are identical to those of the first example. Taking advantage of the symmetry condition, only a 30^{o}-sector was modeled by finite element mesh. The contours of maximum compressive stress analyzed by constant inner boundary at various times are shown in Fig. 5. Comparing the present results with those of [18], it is evident that the general pattern is quite similar but that some small differences do exist. Since the geometry of the rocket motor in [18] was not clearly defined, the difference in dimension used in these two analyses could be the cause of such deviations.

The actual case of a solid rocket motor can be modeled more closely by considering the inner boundary being ablated. Figure 6 shows the contours of maximum compressive stress predicted by NFAP, using the option of moving boundary. The results obtained are quite different from those of [18]. However, observing the differences between Figs. 5 and 6, we can conclude that the results obtained by NFAP are quite reasonable. The solution reveals that the high stress region obtained for ablating boundary propagates faster than that with non-ablating boundary.

3. A Propellant Crack Specimen

As a final example, a propellant crack sample was analyzed, using the combined NFAP/CCC program to demonstrate the coupling effect. The initial geometry and finite element mesh generated by NFAP is given in Fig. 7. The crack is 0.15 m long and the initial gap-width is 0.89 mm. The web thickness is 8 mm along the crack and 20 mm at the tip. Because of symmetry, only half of the sample was modeled by 80 plane strain elements. The shear relaxation modulus of the propellant was assumed to be

$$G_1(t) = 1.461 + 7.43 * \exp(-.095t) \text{ MPa; and } K = 4{,}826 \text{ MPa}.$$

Calculated pressure distributions at various times, from the CCC alone, are given in Fig. 7. The burning phenomenon of the propellant can be briefly described as follows. The pressure in the chamber increases with time, causing the hot gases to penetrate further into the crack. As time passes, the pressure wave travels along the crack and is reflected from the closed end. At about

200 μs, the pressure front has already reached the tip and is reflected, causing pressure at the tip to increase.

Figure 8 shows the results obtained from the combined NFAP/CCC program. During the initial period, the general trend of the pressure distribution is similar to that from convective burning analysis alone. However, as time progresses, noticeable differences between the two cases begin to appear. Up to 200 μs, the pressures obtained from the combined analysis are lower, except near the crack entrance region. At t = 300 μs, two pressure peaks appear. At t = 325 μs, three pressure peaks appear. These pressure peaks are caused by the partial closure of the gap. The deformation pattern of the propellant is quite irregular because of the uneven distribution of the pressure along the crack surface. The elements at the crack entrance are compressed by the high chamber pressure, which results in the propellant being pushed into the crack. Since chamber pressure increases more quickly than pressure inside the crack, the propellant is pushed toward the lower pressure region inside the crack. The mechanical deformation of the propellant causes narrowing of the crack width, and consequently results in a local crack closure. This local gap closure manifests itself in a pressure peak. The localized pressure peaks or gap closures move along the crack. At t = 325 μs, this localized pressure phenomenon becomes evident at x/L = 0.167, 0.433, and 0.633.

CONCLUSION

The computer program for evaluating the coupling effect between convective burning and structural deformation was developed by combining the Crack Combustion Code and a Nonlinear Finite-Element Analysis Program. In structural analysis, the linear viscoelastic material model, together with the capabilities of simulating ablating boundary and interpolating material responses, was considered. Also, the coupling effect estimated by the combined analysis shows some significant interaction between the combustion and mechanical deformation. This phenomenon will be verified further by future experiments.

SYMBOLS

1. Combustion Analysis

A_p = cross-sectional area of crack

B_x = body force

b = co-volume

c_p = specific heat at constant pressure

E = total stored energy

$\bar{h}_c$ = local convective heat-transfer coefficient

$\bar{h}_{cp}$ = local convective heat-transfer coefficient over propellant surface

$\bar{h}_{cw}$ = local convective heat-transfer coefficient over nonpropellant port wall

h_f = enthalpy of combustion gas at adiabatic flame temperature

P_h = burning perimeter

P_w = wetted perimeter of port

p = static pressure

R = specific gas constant for combustion gases

r_b = burning rate of solid propellant, including erosive burning contribution

T = temperature (without subscript, static gas temperature)

T_f = adiabatic flame temperature of solid propellant

T_{pi} = initial propellant temperature

T_{ps} = propellant surface temperature

T_{ws} = nonpropellant wall surface temperature

t = time

u = gas velocity

V_{gf} = velocity of propellant gas at burning surface

x = axial distance from propellant crack opening

y = perpendicular distance from propellant surface into solid

α = thermal diffusivity

γ = ratio of specific heats

λ = thermal conductivity

μ = gas viscosity

ρ = density (without subscript, gas density)

τ_w = shear stress on port wall

τ_{xx} = normal viscous stress

Θ_w = angle measure, in a counterclockwise direction, at lower side of propellant, degree

Subscripts

i = initial value

pr = solid propellant (condensed phase)

c = rocket chamber

2. Structural Analysis

S_{ij} = stress deviators

e_{ij} = strain deviators

σ_{ij} = stress tensor

G_1 = shear relaxation modulus

K = bulk modulus

$( )^t$ = a quantity at time t

$\{\Delta\sigma\}$ = incremental stress

$\{\Delta\varepsilon\}$ = incremental strain

$\{\sigma_o\}$ = equivalent initial stress vector due to viscoelastic behavior

[K] = stiffness matrix

$[ ]^T$ = transpose of matrix

M = number of terms of series in relaxation modulus

g_o =
g_m = } material constants in relaxation modulus
β_m =

$\{\Delta v\}$ = increment of nodal displacement vector

$[D_{VE}]$ = viscoelastic material matrix

$[B]$ = strain-nodal displacement transformation matrix

$\bar{w}_k'$ = values of Gaussian variables at k-th integration point referred to old element

w_i' = values of Gaussian variables at i-th nodal point referred to old element

(r_k', s_k') = local coordinates of k-th integration point referred to old element

(y_i, z_i) = global coordinates of i-th nodal point referred to new element

D_i = i-th nodal displacement referred to new element

D_i' = i-th nodal displacement referred to old element

(r', s') = local coordinates of point in equation referred to old element

REFERENCES

1. Taylor, J.W.: The Burning of Secondary Explosive Powders by a Convective Mechanism. Trans. Farad. Soc. 58, 1962, p. 561.

2. Belyaev, A.F.; Korotkov, A.I.; Sulimov, A.A.; Sukoyan, M.K.; and Obemin, A.V.: Development of Combustion in an Isolation Pore. Combustion, Explosion and Shock Waves, Vol. 5, Jan.-March 1969, pp. 4-9.

3. Belyaev, A.F.; Bobolev, V.K.; Korotkov, A.A.; Sulimov, A.A.; and Chuiko, S.V.: Development of Burning in a Single Pore, Transition of Combustion of Condensed Systems to Detonation, Chap. 5, Pt.A., Science Publisher, 1973, pp. 115-134.

4. Cherepanov, G.P.: Combustion in Narrow Cavities. J. of Appl. Mech., Vol. 11, 1970, pp. 276-281.

5. Godai, T.: Flame Propagation into the Crack of a Solid-Propellant Grain. AIAA Journal, Vol. 8, July 1970, pp. 1322-1327.

6. Krasnov, Yu. K.: Margulis, V.M.; Margolin, A.D.; and Pokhil, P.F.: Rate of Penetration of Combustion into the Pores of an Explosive Charge. Combustion, Explosion, and Shock Waves, Vol. 6, July-Sept. 1970, pp. 262-265.

7. Jacobs, H.R.; Williams, M.L.; and Tuft, D.B.: An Experimental Study of the Pressure Distribution in Burning Flaws in Solid Propellant Grains. Univ. of Utah, Salt Lake City, Utah, Final Report to Air Force Rocket Propulsion Laboratory, AFRPL-TR-72-108, UTEC DO 72-130, Oct. 1972.

8. Jacobs. H.R.; Hufferd, W.L.; and Williams, M.L.: Further Studies of the Critical Nature of Cracks in Solid Propellant Grains, AFRPL-TR-75-14, March 1975.

9. Lee, E.H.; Radok, J.R.M.; and Woodward, W.B.: Stress Analysis for Linear Viscoelastic Material. Trans. Soc. Rheol., Vol. 3, 1959, pp. 41-59.

10. Arenz, R.J.; and Williams, M.L.: The Stresses in an Elastically Reinforced Pressurized Viscoelastic Sphere with an Eroding Boundary. Proceedings 20th Meeting Joint Army-Navy-Air Force Physical Properties Panel, Johns Hopkins Univ., Baltimore, Md., 1961, p. 143.

11. Corneliussen, A.H.; and Lee, E.H.: Stress Distribution Analysis for Linear Viscoelastic Materials. International Union of Theoretical and Applied Mechanics Symposium on Creep, 1960, pp. 1-20.

12. Corneliussen, A.H.; Kamowitz, E.F.; Lee, E.H.; and Radok, J.R.M.: Viscoelastic Stress Analysis of a Spinning Hollow Circular Cylinder with an Ablating Pressurized Cavity. Trans Soc. Rheol., Vol. 7, 1963, pp. 357-390.

13. Shinozuka, M.: Stresses in a Linear Incompressible Viscoelastic Cylinder with Moving Inner Boundary. J. Appl. Mech., Vol. 13, 1963, pp. 335-341.

14. Rogers, T.G.; and Lee, E.H.: The Cylinder Problem in Viscoelastic Stress Analysis. Quart. Appl. Math., Vol. 22, 1964, pp. 117-131.

15. Schapery, R.A.: An Approximate Method of Stress Analysis for a Large Class of Problems in Viscoelasticity. Purdue Univ. Rept. A. and ES62-18, 1963.

16. Christensen, R.M.; and Schreiner, R.N.: Response to Pressurization of a Viscoelastic Cylinder with an Eroding Internal Boundary, AIAA Journal, Vol. 3, 1965, pp. 1451-1455.

17. Chang, T.Y.: Approximate Solutions in Linear Viscoelasticity. Ph.D. Dissertation, Dept. of Civil Eng., Univ. of California, Berkeley, 1966.

18. Zienkiewicz, O.C.; Watson, M.; and King, I.P.: A Numerical Method of Viscoelastic Stress Analysis. Int. J. Mech. Sci., Vol. 10, 1968, pp. 807-827.

19. White, J.L.: Finite Element in Linear Viscoelasticity. Proceedings of 2nd Conference on Matrix Method in Structural Mechanics, Airforce Flight Dynamics Lab, Wright Patterson AFB, Ohio, AFFDL-TR-68-150, 1968, pp. 489-516.

20. Gupta, K.K.; and Heer, E.: Viscoelastic Structures. Structural Mechanics Computer Programs, Univ. Press of Virginia, Charlottesville, 1974, pp. 207-225.

21. Sankaran, G.V.; and Jana, M.K.: Thermoviscoelastic Analysis of Axisymmetric Solid Propellant Grains. J. Spacecraft, Vol. 13, 1976, pp. 641-642.

22. Weeks, G.E.; and Cost, T.L.: An Algorithm for Automatically Tracking Ablating Boundary. Int. J. Num. Method. Engr., Vol. 14, 1979, pp. 441-449.

23. Chang, T.Y.; and Prachuktam, S.: NFAP - A Nonlinear Finite-Element Analysis Program. Dept. of Civil Engr., Univ. of Akron, Rept. No. SE76-3, 1976.

24. Kuo, K.K.; Chen, A.T.; and Davis, T.R.: Transient Flame Spreading and Combustion Process Inside a Solid Propellant Crack. AIAA Paper 77-14, AIAA 15th Aerospace Science Meeting, Jan. 1977.

25. Goodman, T.R.: Application of Integral Methods to Transient Nonlinear Heat Transfer. Advances in Heat Transfer, Vol. 1, Academic Press, New York, 1964, pp. 51-122.

26. Kuo, K.K.; Chen, A.T.; and Davis, T.R.: Convective Burning in Solid-Propellant Cracks. AIAA Journal, Vol. 16, June 1978, pp. 600-607.

27. Chang, J.P.: Finite Element Analysis of Linear Viscoelastic Solids. M.S. Thesis, Dept. of Civil Engr., Univ. of Akron, 1980.

28. Herrmann, L.R.: Laplacian-Isoparametric Grid Generation Scheme. J. of Engr. Mech. Div., Proc. of the ASCE, Vol. 102, Oct. 1976, pp. 749-756.

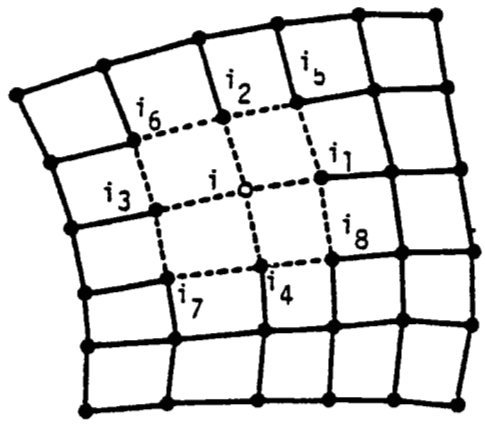

Figure 1.- Neighborhood of node i.

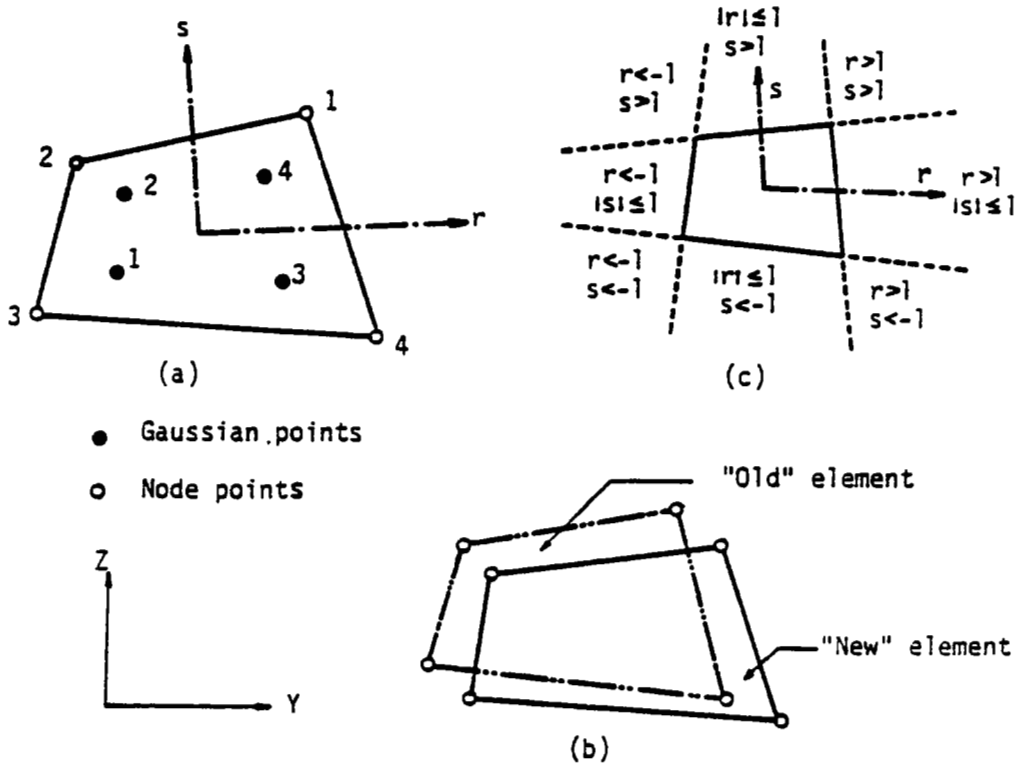

Figure 2.- Interpolation scheme.

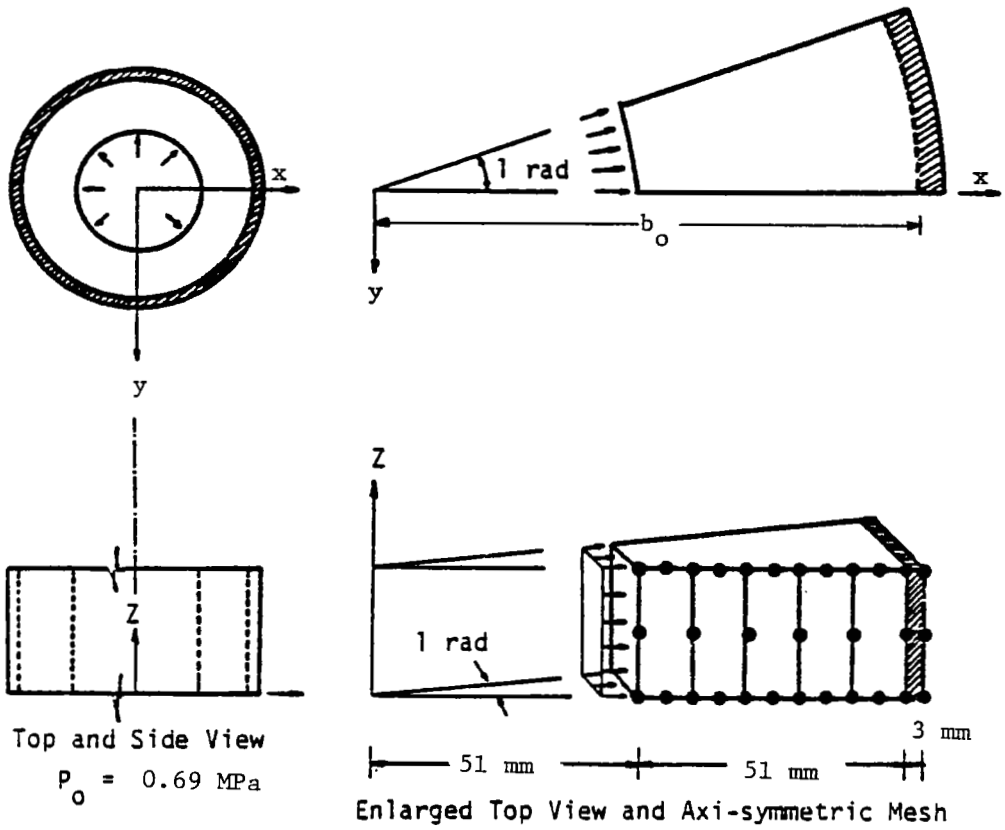

Figure 3.- Finite element mesh of a reinforced thick-walled cylinder.

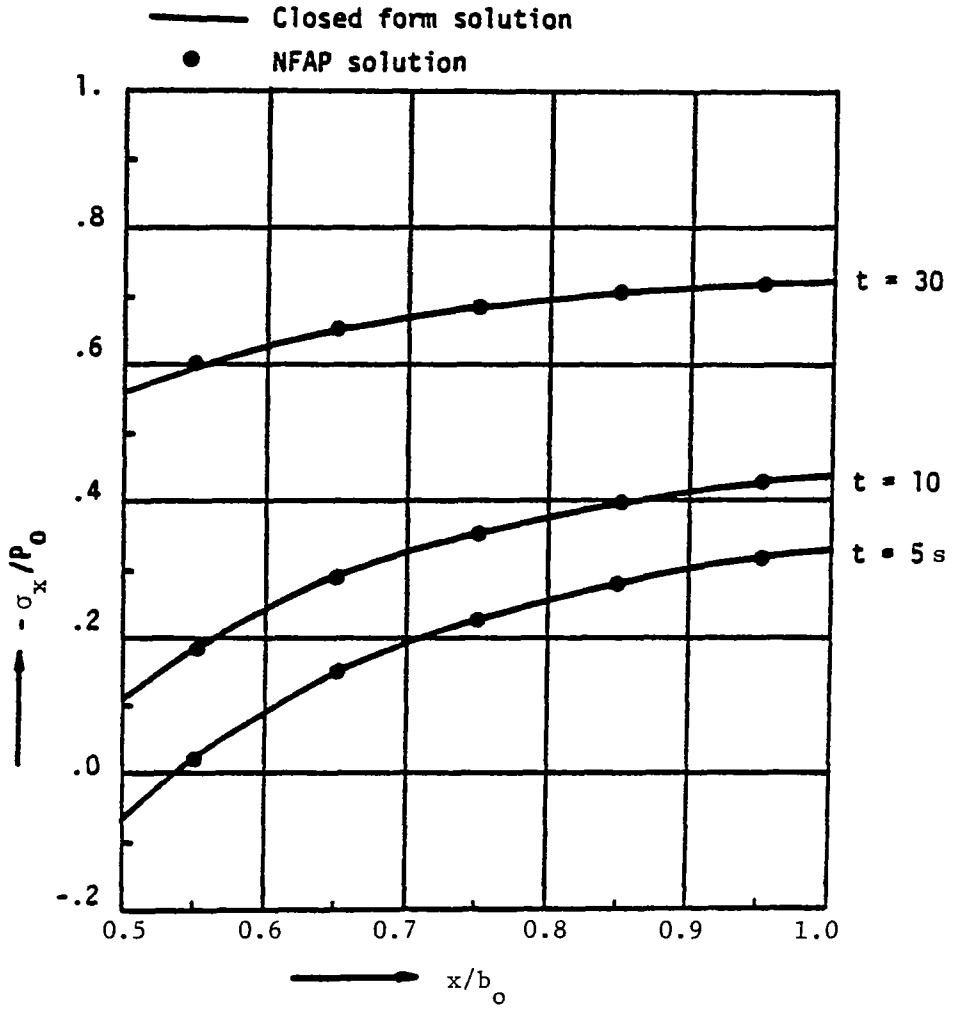

Figure 4.- Reinforced cylinder under internal pressure variation of hoop stress.

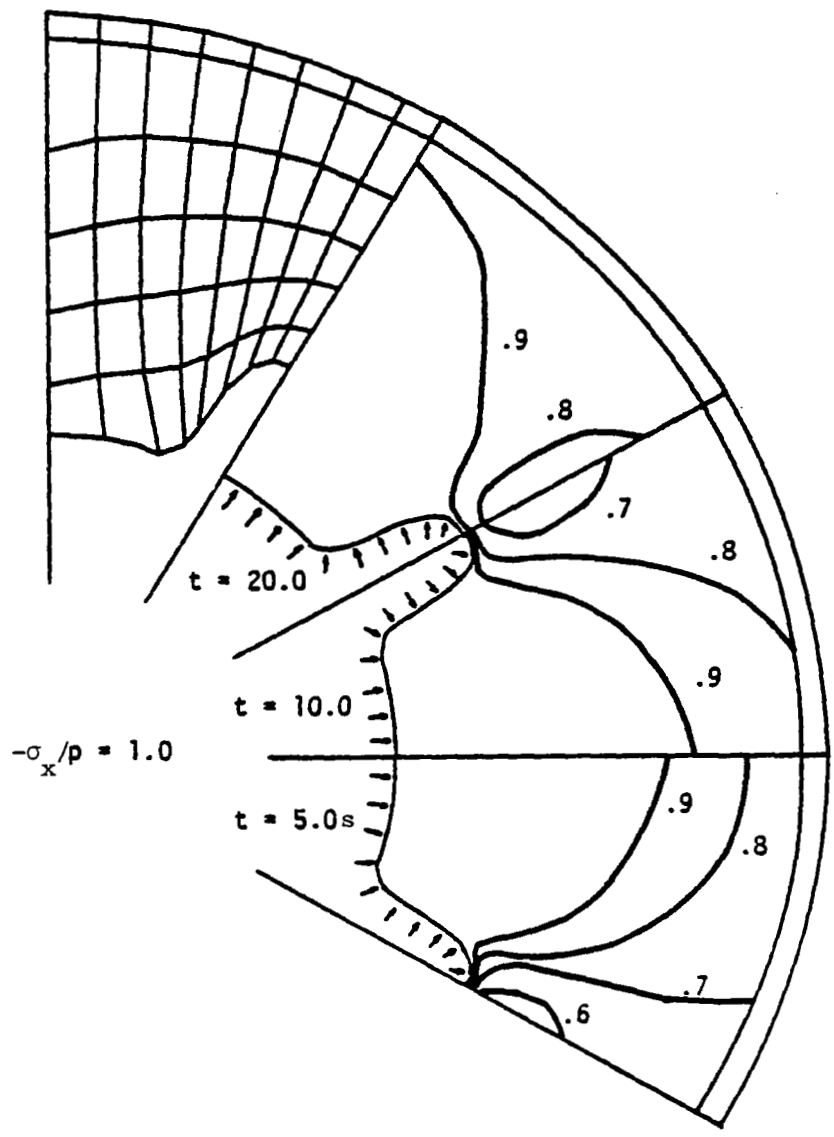

Figure 5.- Finite element mesh and contours of maximum principal stress of a star-shaped rocket motor with fixed boundary.

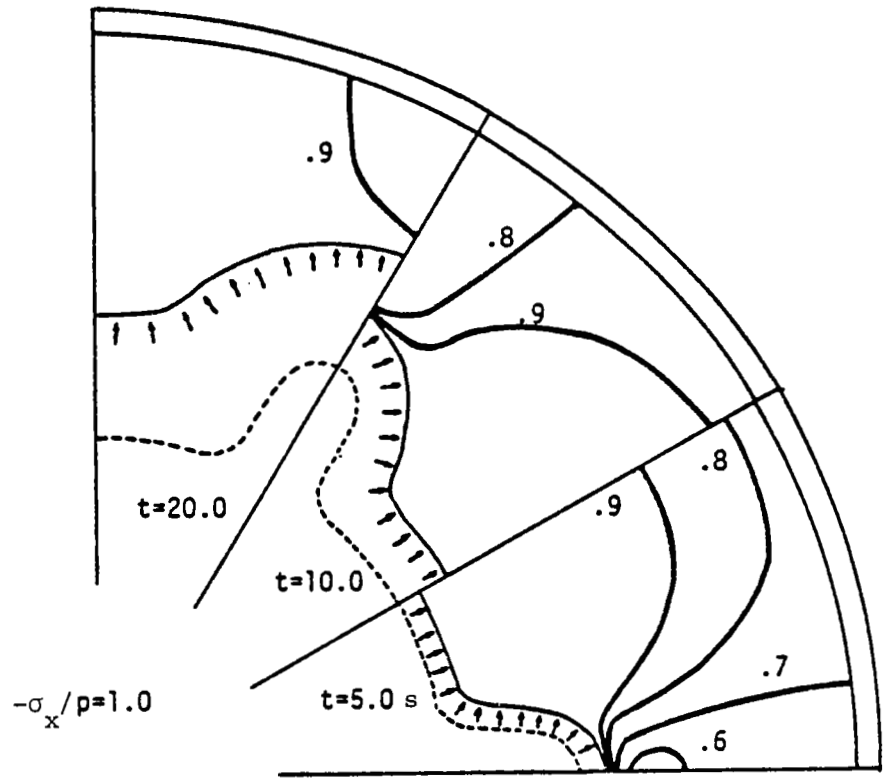

Figure 6.- Contours of maximum principal compressive stress of a star-shaped rocket motor with moving boundary.

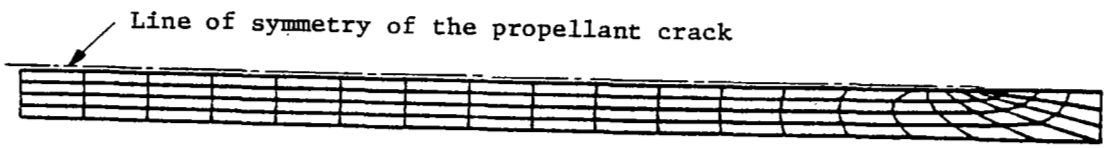

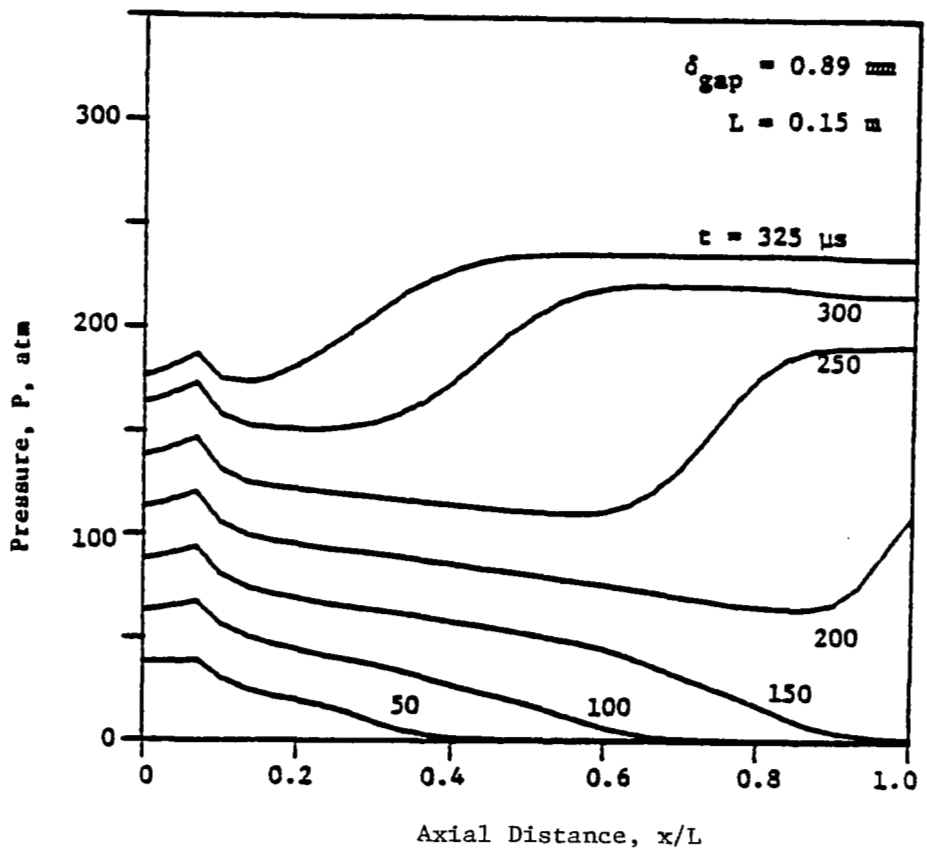

Figure 7.- Finite element mesh of a propellant crack and calculated pressure distributions for various times from the crack combustion code.

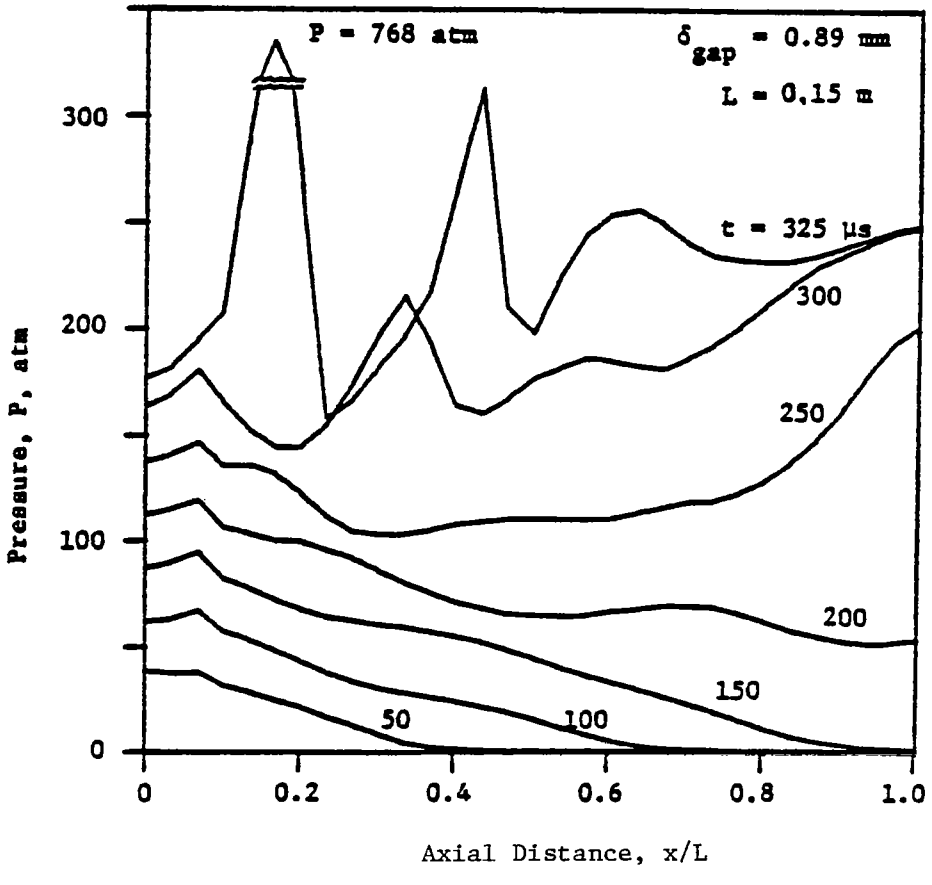

Figure 8.- Calculated pressure distributions for various times from the combined crack combustion and non-linear finite-element analysis program.

ITERATIVE METHODS BASED UPON RESIDUAL AVERAGING

J. W. Neuberger

This paper concerns iterative methods for solving boundary value problems for systems of nonlinear partial differential equations. The methods involve subtracting an average of residuals from one approximation in order to arrive at a subsequent approximation.

The paper is divided into five parts. The first part gives two abstract methods in Hilbert space. The second part shows how to apply these methods to quasilinear systems to give numerical schemes for such problems. The third section contains some specific applications. The fourth part contains a discussion of some potential theoretic matters related to the iteration schemes. The final part indicates work in progress concerning extensions and improvements of the above.

1. Two abstract iterative schemes. Suppose H is a Hilbert space, H' a closed subspace of H and P is an orthogonal projection on H whose range is a subset of H'. Suppose also that L is a strongly continuous function from H to L(H,H) so that L(U) is an orthogonal projection for each U in H. It will be seen how a variety of boundary value problems for nonlinear systems may be reduced to the problem of finding $U \in H'$ so that

$$L(U)U = 0, \quad P(U-W) = U-W \tag{1}$$

where W is a given element of H'. It will be seen that the first part of (1) represents a quasilinear system and the second part of (1) is a way of asserting that U satisfies boundary conditions described by the given element W.

For $\delta > 0$ an iterative scheme for attempting to find U satisfying (1) is

$$W_0 = W, \; W_{n+1} = W_n - \delta PL(W_n)W_n, n = 0,1,2, \ldots . \tag{2}$$

If $\{W_n\}_{n=0}^{\infty}$ converges to $U \in H'$, then

$$P(U-W) = U-W \text{ and } PL(U)U = 0. \tag{3}$$

A solution U to (3) is called a quasisolution to the problem (1). See ref. 1 for a discussion concerning quasisolutions vs. actual solutions.

A second scheme uses a continuous iteration parameter but is otherwise similar to (2): Define $Z : (0,\infty) \to H$ so that

$$Z(0) = W, Z'(t) = -PL(Z(t))Z(t), \; t \geq 0. \tag{4}$$

If $U = \lim_{t \to \infty} Z(t)$ exists, then U satisfies (3).

For numerical schemes one is interested in finite dimensional choices for (2) under fairly unrestrictive hypothesis on P and L. In ref. 2 it is shown that (2) always converges in the linear (L(x) independent of $x \in H$) for $\delta = 1$. Similar results may be obtained for (4) by noting that (4) is a limiting case of (2) as $\delta \to 0$.

2. Quasilinear systems; use of finite differences. It is first indicated how a fairly general second order quasilinear system may be placed in a setting to which the iterative schemes (2), (4) apply. Extensive generalizations will be evident.

Suppose Ω is a bounded open subset of R^2 and each of R,S,T is a continuous real-valued function on R^3. Functions z,u,v on Ω are sought so that

$$(5) \qquad \begin{cases} R(z,u,v)u_1 + S(z,u,v)(u_2 + v_1) + T(z,u,v)v_2 = 0 \\ z_1 - u = 0 \\ z_2 - v = 0 \end{cases}$$

where $u_1 = \delta u/\delta x$, $u_2 = \delta u/\delta y$ etc.

If appropriate derivatives exist and (5) holds, then

$$(6) \qquad R(z,z_1,z_2)z_{11} + 2S(z,z_1,z_2)z_{12} + T(z,z_1,z_2)z_{22} = 0 .$$

Pick two piecewise smooth one-dimensional curves Γ and Γ' in $\overline{\Omega}$ and a function $W \in C(\overline{\Omega})$. Consider boundary conditions for (5):

$$z(p) = w(p), p \in \Gamma$$

$$(7) \qquad \left\langle \begin{pmatrix} u(p) \\ v(p) \end{pmatrix}, \begin{pmatrix} f(p) \\ g(p) \end{pmatrix} \right\rangle = \left\langle \begin{pmatrix} w_1(p) \\ w_2(p) \end{pmatrix}, \begin{pmatrix} f(p) \\ g(p) \end{pmatrix} \right\rangle, p \in \Gamma$$

where $\begin{pmatrix} f(p) \\ g(p) \end{pmatrix}$ denotes the direction normal to Γ' at p.

Define $A: R^3 \to L(R^9, R^3)$ modeled on (5) so that

$$A(r,s,t)(a,a_1,a_2,b,b_1,b_2,c,c_1,c_2) =$$
$$\begin{cases} R(r,s,t)b_1 + S(r,s,t)(b_2 + c_1) + T(r,s,t)c_2 \\ a_1 - b \\ a_2 - c \\ (r,s,t),(a,a_1,a_2),(b,b_1,b_2),(c,c_1,c_2) \in R^3 . \end{cases}$$

Note that if $z,u,v \in C^{(1)}(\overline{\Omega})$ and

$$A(z(p),u(p),v(p))$$
$$(z(p),z_1(p),z_2(p),u(p),u_1(p),u_2(p),v(p),v_1(p),v_2(p)) = 0,$$

then z,u,v satisfy (5).

Denote $L_2(\Omega)^9$ by H, denote by H′ the set of all $(z,z',u,u',v,v') \in H$ where $z' = (z_1,z_2)$ etc. and all indicated derivatives are L_2 generalized derivatives (cf ref. 3). Denote by H_0' the set of all $(z,z',u,u',v,v') \in H'$ so that

$$z(p) = 0, \quad p \in \Gamma$$
$$\left\langle \begin{pmatrix} u(p) \\ v(p) \end{pmatrix}, \begin{pmatrix} f(p) \\ g(p) \end{pmatrix} \right\rangle = 0, p \in \Gamma'$$

and denote by P the orthogonal projection of H onto H_0'.

To complete a description of how (5), (7) are carried over to (1) a description of L is required. Denote $L_2(\overline{\Omega})^3$ by K and define $C:H \to L(H,K)$ so that if $U,Z \in H$, then for almost all $p \in \Omega$,

$$(C(U)Z)(p) = (A(q)A(q)^*)^{-\frac{1}{2}}A(q)'z_1(p)$$

where $q \equiv (r,s,t)$ and r,s,t are the first, fourth and seventh elements respectively of U(p). Finally for $U \in H$, $L(U) \equiv C(U)^*C(U)$.

For w as above, define $W = (w,w_1,w_2)$. Start iteration (2) with W. Then for $n = 0,1,2, \ldots$, W_n has the property that the triple consisting of the first, fourth and seventh elements of W_n satisfy (7). Similar statements hold for the iteration (4).

It is now indicated how a finite difference scheme for (5),(7) may be constructed by defining finite dimensional spaces $\underline{H}$ and $\underline{K}$ which approximate H and K above. Suppose G_0 is a rectangular grid with even spacing δ so that $G \equiv G_0 \cap \overline{\Omega}$ has the property that if $p \in G$, then at least one of $p + \delta e_i$ is in G, $i = 1,2$, where e_1,e_2 is the standard basis for R^2. Define $\underline{K}$ to be a vector space of all real-valued functions on the grid G. For $u \in \underline{K}$, define

$$(D_i u)(p) = \begin{cases} (u(p+\delta e_i) - u(p-\delta e_i))/(2\delta) & \text{if } p+\delta e_i, p-\delta e_i \in G \\ (u(p+\delta e_i) - u(p))/\delta & \text{if } p-\delta e_i \notin G \\ (u(p) - u(p-\delta e_i))/\delta & \text{if } p+\delta e_i \notin G, \end{cases} \quad i = 1,2, \; p \in G.$$

Define $\underline{H} = \underline{K}^9$. For $(z,u,v) \in \underline{K}^3$, define $D(z,u,v) = (z,D_1z,D_2z,u,D_1u,D_2u,v,D_1v,D_2v)$. Denote by $\underline{H}'$ the range of D. Define $\underline{\Gamma},\underline{\Gamma}'$ subsets of G approximating Γ and Γ' respectively. Denote by H_0' the set of all $D(z,u,v) \in H'$ such that

$$z(p) = 0, \quad p \in \underline{\Gamma}$$
$$\left\langle \begin{pmatrix} u(p) \\ v(p) \end{pmatrix}, \begin{pmatrix} f(p) \\ g(p) \end{pmatrix} \right\rangle = 0, \quad p \in \underline{\Gamma}' \tag{8}$$

Denote by $\underline{P}$ the orthogonal projection of $\underline{H}$ onto H_0'. Pick $\underline{w} \in K$ approximating w above. Define $\underline{z} = \underline{w}$, $\underline{u} = D_1\underline{w}$, $\underline{v} = D_2\underline{w}$ and choose $\underline{W}_0 = (\underline{z},D_1\underline{z},D_2\underline{z},\underline{u},D_1\underline{u},D_2\underline{u},\underline{v},D_1\underline{v},D_2\underline{v})$ and

$$\underline{W}_{n+1} = \underline{W}_n - PL(\underline{W}_n)\underline{W}_n, n = 0,1,2, \ldots \tag{9}$$

where L is defined essentially as above. Condition (8) on $\underline{P}$ implies that boundary conditions are preserved under the iteration (9) and hence are satsified by a limit of $\{W_n\}_{n=0}^{\infty}$.

Similar statements hold for a finite dimensional counterpart to the iteration (4).

Process (4) in this finite dimensional setting becomes a variant of the "method of lines". It specifies one equation and one 'unknown' for each point in the grid G. The 'time' parameter is iteration number, not a distinguished variable in the system of differential equations. Use of (4) then may extend the use of the 'method of lines' to a larger class of problems.

3. Applications.

Take Ω to be a bounded region in R^2. Define R,S,T in (5) so that

$$R(z,u,v) = 1+v^2$$
$$S(z,u,v) = -uv$$
$$T(z,u,v) = 1+u^2.$$

System (5) then is

$$(1+v^2)u_1 - uv(u_2+v_1) + (1+u^2)v^2 = 0$$
$$z_1 - u = 0$$
$$z_2 - v = 0$$

As a single second order equation this is

$$(1+z_2^2)z_{11} - 2z_1z_2z_{12} + (1+z_1^2)z_{22} = 0,$$

the minimal surface equation for real-valued functions on a region in R^2. Conditions are specified by

$$z(p) = f(p), p \in \partial\Omega,$$

for some given function f. The FORTRAN code listed in ref. 4 may be easily modified to deal with this equation.

If $\gamma, a_\infty, u_\infty$ are given positive numbers and R,S,T are chosen so that

$$R(z,u,v) = a_\infty^2 + ((\gamma-1)/2)(u_\infty^2-u^2-v^2) - u^2$$
$$S(z,u,v) = -uv$$
$$T(z,u,v) = a_\infty^2 + ((\gamma-1)/2(u_\infty^2-u^2-v^2) - v^2$$

then (5) reduces to the transonic flow equation used in reference 4 (and taken from reference 5). For numerical computations, boundary conditions at infinity are replaced by appropriate boundary conditions on the boundary of a large box. One also has zero normal derivative conditions on an airfoil inside

the box. See references 4, 5 for details. The FORTRAN listing in reference 4 is specifically for this problem. Printouts of results for various mach numbers (u_∞/a_∞) are given there.

4. Finite dimensional potential theory. The main computational effort connected with (9) is the calculation of Px for various $x \in H$. Denote by $\underline{J}_0$ all $(z,u,v) \in K^3$ satisfying (8) and denote by π the orthogonal projection of $\underline{K}^3$ onto J_0. From ref. 2 it follows that $P = DE^{-1}\pi D^*$ where $E \equiv \pi D^* D\big|_{\underline{J}_0}$. Hence the main work in calculating the action of $\underline{P}$ is the solving for x (given y) in linear systems

$$Ex = y. \tag{10}$$

Now $\underline{J}_0$ is a Dirichlet space in the sense of ref. 6 and E is the corresponding Laplacian for $\underline{J}_0$. So, E^{-1} being the inverse of a Laplacian, the effect of multiplying a vector y by E^{-1} is to take a certain nonnegative weighted average of the components of y. References 2 and 4 contain descriptions of methods for solving (10).

5. Extensions and Improvements.

A promising replacement for (4) is given by

$$z(0) = w z'(t) = -(\nabla\phi)(z(t)),\ t \geq 0 \tag{11}$$

where $\sigma(x) \equiv \tfrac{1}{2} \| A(x)x \|^2, x \in H$, A being defined as in section 3. One has the following explicit expression for the gradient of ϕ:

$$(\nabla\phi)(x) = P[A(x)^* + C(x)^*]\, A(x)x,\ x \in H.$$

Then (11) becomes a steepest descent process. In a number of examples, the only critical points of ϕ seem to be solutions to (3). Furthermore, solutions z to (3) remain bounded and so converge to a solution u to (3).

Work is in progress concerning the adaptation of (2), (4) and (11) to finite element spaces rather than finite difference schemes. It is expected that methods will be developed which use finite element spaces but have little else in common with conventional finite element methods. See reference 7 for some preliminary results.

REFERENCES

1. J. W. Neuberger: An Iterative Method for Approximating Solutions to Nonlinear Partial Differential Equations, Applied Nonlinear Analysis, Academic Press, 1979.

2. J. W. Neuberger: Finite Dimensional Potential Theory Applied to Numerical Analysis of Linear Systems, Linear Algebra and Applications, 35(1981). (To be published.)

3. P. G. Ciarlet: The Finite Element Method for Elliptic Problems, North Holland (1978).

4. J. W. Neuberger: A Type-independent Method for Systems of Nonlinear Partial Differential Equations: Application to the Problem of Transonic Flow, Computers Math. Appl. 6(1980), 67-78.

5. G. F. Carey: Variational Principles for the Transonic Airfoil Problem, Compt. Math. Appl. Mech. Engng. 13(1978), 129-140.

6. A. Beurling el J. Deny: Espaces de Dirichlet, I. Le Cas Elementaire, Acta Math. 99 (1958).

7. J. W. Neuberger: A Type-independent Iterative Method Using Finite Elements, Proceedings of Third International Conference on Finite Elements in Flow Problems, D. H. Nome, ed., Univ. of Calgary, Calgary, Alberta, Canada, 1980.

Department of Mathematics
North Texas State University
Denton, Texas 76203

COMPUTATIONAL STRATEGY FOR THE SOLUTION OF LARGE STRAIN NONLINEAR PROBLEMS USING THE WILKINS EXPLICIT FINITE-DIFFERENCE APPROACH

R. Hofmann

Science Applications, Incorporated
2450 Washington Avenue, Suite 120
San Leandro, California 94577

SUMMARY

The STEALTH code system, which solves large strain, nonlinear continuum mechanics problems, has been rigorously structured in both overall design and programming standards. The design is based on the "theoretical elements of analysis" while the programming standards attempt to establish a parallelism between physical theory, programing structure and documentation. These features have made it easy to maintain, modify and transport the codes. It has also guaranteed users a high level of quality control and quality assurance.

INTRODUCTION

A computer code system called "STEALTH" (ref. 1)*, has been developed for the Electric Power Research Institute (EPRI) for the primary purpose of solving nonlinear, static, quasi-static and transient problems involving both fluids and solids. The numerical technology for this computer program is based on the developments of Wilkins (ref. 2) and Herrmann (ref. 3). Although this technology was originally developed for large deformation, fast-transient defense-oriented applications (figure 1), it has been adapted to be quite useful for studying thermal-hydraulic mechanical transients (figure 2), nuclear waste isolation geologic burial stability (figure 3) and a variety of structure-medium interaction (SMI) problems (figures 4 and 5). The design and development of general-purpose

---

*"Solids and Thermal hydraulics codes for EPRI Adapated from Lagrange TOODY and HEMP", developed for Electric Power Research Institute by Science Applications, Inc., under contract RP307.

STEALTH involved extensive planning in order to make it adaptive enough to handle this wide variety of nonlinear problems. This paper describes the strategy that was (and still is) used.

ARCHITECTURAL OVERVIEW

The overall structure of the STEALTH nonlinear code system has been built around a particular view of the physical equations being solved. This view is based on the "theoretical elements of analysis of a physical system" which are summarized in Table 1. The theoretical elements of analysis are a convenient conceptulization for solid and fluid mechanics problems. It separates physics laws, material response characteristics, geometric aspects (e.g., boundary conditions) and initial conditions. These distinct categories are not only convenient theoretical groupings, but are also useful programming and documentation entities.

The STEALTH architecture based on this view has stood the test of time for over five years and continues to be quite flexible and adaptable to new problems and more complex situations. Among the many adaptive features are (1) the ability to couple other computer programs, (2) a standard procedure for externally developed constitutive models, (3) a modular topdown architecture with a FORTRAN syntax that makes developing and changing subroutines easy, and (4) a general-purpose, special-purpose version arrangement that guarantees good quality assurance. Finally, it has been possible to add new capabilities that were not specifically anticipated when STEALTH was originally designed.

STEALTHs 1D, 2D, and 3D are based on a modular architecture in which many subroutines and COMMON blocks in each code are identical in every detail. The top-down design that was implemented requires each code to have the same calling sequence at its highest levels. Subroutines and COMMON blocks which must be different are found at the lowest (innerrmost) levels of STEALTH. In between, there are subroutines that have identical names, functions, and structure, but different specific programming.

The actual FORTRAN programming utilizes a subset of FORTRAN that is common to IBM, Univac, and CDC computers. The use of these FORTRAN statements is further restricted by format conventions that produce very structured programming. In addition, FORTRAN variable names are formed by combining three-character roots with one- and two-character prefixes and suffixes.

The STEALTH codes have been designed to be most efficient for the occasional user. The standard version combines extensive checking logic which checks and rechecks a user's input and checks and rechecks the status of the calculation as it proceeds. The codes also provide many standard models for materials, boundary conditions, etc.

Computer memory requirements range from 135 000 to 155 000 words of octal storage in CDC 7600. This size has been achieved by overlaying the GENERATOR. Further reduction of code size can be achieved by either overlaying the GENERATOR some more, overlaying the PROCESSOR, or by reducing the size of certain COMMON blocks. Reducing the size of COMMON blocks usually results in a reduction in the number of grid points that can be computed.

Other tailorings of the codes can be made to suit specific computing environments and/or problems. For example, it is simple to put "hardwired" material models into the code to improve code speed. It is also possible to remove the trace and debug options, again improving speed. For short production runs where generation is a larger proportion of the run time, it is possible to write a pregenerator to reduce GENERATOR costs. Finally, special-purpose versions of STEALTH can be created in order to improve efficiency. For example, a hydrodynamic-only version of STEALTH runs 20% faster than the standard version for the same fluids problem.

The FORTRAN coding conventions and the structural modularity make STEALTHs 1D, 2D, and 3D portable and device-independent. Word size and memory storage limitations are determined from the requirements of an actual calculation. For most calculations, it is desirable to use a machine which has a word size greater than 48 bits and memory of at least 30 000 decimal words. However, it is possible to perform STEALTH simulations at a word size of 32 bits and a memory of 20 000 decimal words. The STEALTH code system is made up of more than 100 000 FORTRAN cards.

PROGRAMMING STRUCTURE

The development of a user-oriented, well documented, Wilkins explicit finite-difference computer code is based on the premise that programming structure, input/output, and documentation should be formulated from physical rather than mathematical (or numerical) concepts. Theory, code structure, and documentation are fundamental categories in the discussion of user orientation. Elements of these categories (Table 2) should be as similar in vocabulary and notation as possible. Using the theoretical elements of analysis as the basis for this design, automatically links the physical theory and programming structure in a way in which program development is easily achieved. In the discussion that follows, a standard view of program structure has been adapted to these concepts.

The STEALTH computer programs do numerical simulations as opposed to numerical evaluations. A simulation is carried out through execution of three separate "phase groups". Appropriate names for these phase groups are GENERATOR, PROCESSOR, and OUTPUT ANALYZER. (Analogous processing concepts exist for computer systems. They are: compiler/loader, central

processing unit (CPU), and output devices, respectively.) The conceptual functions of each phase group are summarized below.

- The GENERATOR accepts detailed data (from cards or keyboard) as input for many different types of computer calculations. All input data are checked as thoroughly as possible. If no serious errors are detected, an input file for the appropriate PROCESSOR phase group is prepared.

- The PROCESSOR accepts preresolved (link-edited) data from the GENERATOR as a complete specification for a calculation in order to perform a specific physics calculation. During the calculation, output data are prepared to be input for both the OUTPUT ANALYZER and the GENERATOR. These data take the form of archive files. The file for the GENERATOR is called the restart file, while the data for the OUTPUT ANALYZER are known simply as archive data. The PROCESSOR is analogous to a CPU. Its primary purpose is to compute (crunch numbers) and direct data to output devices.

- The OUTPUT ANALYZER accepts data from the GENERATOR or PROCESSOR phase groups in archive format. It performs analysis functions such as plotting, special printing, data reduction, etc. Output data from the OUTPUT ANALYZER are presented either in hard copy form or as input files for other OUTPUT ANALYZERS. It is exactly analogous to hard copy output functions of a hardware printer, plotter, or other output device.

Figure 6 is a schematic display of the interaction between phase groups.

The GENERATOR phase group is a combination compiler/loader. For example, input to the compiler function of the GENERATOR is the code input for a particular problem. The loader (link-editing) function of the GENERATOR performs the task of resolving several types of input into a single file to be read by an appropriate PROCESSOR. The GENERATOR is capable of setting up (loading) a variety of problems from a spectrum of input modes. There are two GENERATOR input modes, standard and nonstandard.

- Standard Record Format (start or restart)

  cards
  keyboard

- Nonstandard Input (start only)

  library file

The PROCESSOR phase group is analogous to the CPU of a computer. Its purpose is to compute physics from appropriate algorithms. Input data for the PROCESSOR are prepared by the GENERATOR. Output data are in the form of an archive file. The archive file contains a complete summary of all the results of the physics calculations performed. The format of the file is a self-contained, easy-to-read format and is designed to be used by other programs as input (e.g., programs in the OUTPUT ANALYZER phase group can read the archive file as input). An abbreviated form of the archive file, known as the restart file, is created as an input file for the GENERATOR. If a calculation must be restated, it is more convenient to use the abbreviated file than a complete archive file.

The OUTPUT ANALYZER phase group is composed of many different stand-alone computer programs. Among these are plotting programs, Fourier analyzers, data reduction codes, etc. Output analysis may be performed on data from both the GENERATOR and PROCESSOR phase groups. All data are transmitted in archive format but only the PROCESSOR creates a permanent archive file. (The OUTPUT ANALYZER can be used to make a reduced archive file, if required.)

Output from the OUTPUT ANALYZER phase group is usually in the form of hard copy (that is, printed pages, plots, etc.). Files that are produced as output are usually in archive format also so that they can be used as input for other data analyzing functions. These files are not intended to be used as input to the GENERATOR or the PROCESSOR, although it is conceivable that they could be used this way.

Phases are the logical subdivisions of a phase group. They are groups of subroutines which perform a particular logical "macrofunction" which preserves the simplicity of physical concepts. In contrast, subroutines perform "microfunctions" and are defined by a specific functional task such as reading, checking, calculating, etc., or a well defined combination of these tasks.

A phase group can be divided into as many phases as necessary. One special phase known as the Utility phase is part of every phase group. It contains subroutines which are used by more than one phase and which fall into one of the following categories:

(1) System or Machine Dependent
(2) Input Related
(3) Output Related
(4) Enter/Exit
(5) Error
(6) Arithmetic
(7) Miscellaneous

All phases are chosen from logical or conceptual considerations dictated by the tasks to be performed by a particular phase group.

Phases in the OUTPUT ANALYZER cannot be defined a priori. This phase group may require different phase structure for different types of problems and different types of analyses, respectively. However, the GENERATOR and PROCESSOR phases are amenable to a general design concept based on the physical notions associated with the partial differential equations being solved.

The fundamental ideas behind the design of the phase structure for the GENERATOR and PROCESSOR phase groups of STEALTH come directly from the theoretical elements of analysis of a physical system. That is, logically, STEALTH may be viewed in terms of the following distinct subdivisions:

- Conservation Equations

  mass
  momentum
  energy

- Boundary Conditions

  geometric constraints
  boundary values

- Initial Conditions

  intensive
  extensive

- Constitutive Equations

  mechanical
  thermal

Designing the GENERATOR and PROCESSOR for STEALTH from these four categories is relatively straightforward. The conservation equations (equations of change) are the equations to be solved; they are the kernel of the PROCESSOR. They describe the response or motion of a physical system. The initial and boundary values and the constitutive equations supply the conditions or constraints for solution. The computational network is formed from the geometric constraints and the time-dependence specification.

The STEALTH GENERATOR phase group is broken down into nine phases which are further divided into two groups. The first group contains two non-optional phases which must be executed prior to the execution of other GENERATOR phases and the Utility phase. The second group is composed of six

optional phases which are used selectively to satisfy specific processing requirements of a particular PROCESSOR. While the two nonoptional phases in the former group must be executed in a particular order, the phases in the latter group may be executed in any order.

The two phases in the nonoptional group are called CMNGEN and PRBGEN. CMNGEN initializes all common blocks and PRBGEN provides data for a GENERATOR scheduler. The GENERATOR scheduler is a subroutine which determines which of the latter group's optional phases is necessary for a particular PROCESSOR.

The functions of the optional phases in the GENERATOR phase group are (1) material model definition, MATGEN, (2) mesh or grid-point generation, GPTGEN, (3) zone interior initialization, ZONGEN, (4) boundary value specification, BDYGEN, (5) time control, TIMGEN, and (6) edit specification, EDTGEN. Figure 7 is a flow chart of the phases in the GENERATOR phase group. Table 3 shows the correspondence between the six optional GENERATOR phases and the logical elements of design.

Within each GENERATOR phase the subroutine calling structure (logic) is similar. Each phase contains a phase scheduler subroutine which calls all the "mainline" subroutines. The scheduler name is _ _ _GEN, where _ _ _ is the phase name.

The mainline subroutines are an input processing subroutine, _ _ _INP; a subroutine that checks input data, _ _ _CHK; a subroutine that prints out relevant data for the phase, _ _ _PRT; and a subroutine that allows input and computed data to be plotted, _ _ _PLT.

In addition to the mainline subroutines, there is a group of subroutines known as "kernel" subroutines. These subroutines perform generation tasks specific to that phase. Figure 8 shows a conceptual flowchart for a typical GENERATOR phase. Kernel subroutines may be called at any time in the phase, whereas mainline subroutines must be called in the proper order.

All GENERATOR phases may call Utility subroutines from any subroutine. (Utility subroutines are defined as those subroutines which are common to more than one phase in a phase group). However, certain utilities are called from specific locations or only at specific times. For example, ENTER/EXIT utilities are the first and last executable statements in each mainline subroutine; only _ _ _INP and _ _ _CHK call ERROR utilities; INPUT utilities are concentrated in _ _ _INP, etc. A list of typical utilities are shown in Table 4.

Each PROCESSOR phase group is composed of eight phases -- one phase less than the GENERATOR phase group (there is one phase corresponding to each of the GENERATOR phases except the CMN phase). For STEALTH, all phases

are mandatory and all phases must be executed in a precise order. Figure 9 displays the PROCESSOR phase group flowchart for serial STEALTH.

In each PROCESSOR phase there is at least one mainline subroutine called _ _ _PRO. It is analogous to _ _ _GEN in the GENERATOR, where _ _ _ is the phase name identifier. In the GPT and ZON phases there are two other mainline subroutines, _ _ _OLD and _ _ _NEW. Subroutine _ _ _OLD transfers data at times n-1/2 and n from array variable storage locations to storage locations in nonarray variables. These nonarray variables are used in physics calculations to update "old" values of variables (times n-1/2 and n) to "new" values of variables (times n+1/2 and n+1). Subroutine _ _ _NEW then transfers the data at times n+1/2 and n+1 from nonarray storage locations to appropriate array storage locations.

All other subroutines in the PROCESSOR are kernel or utility subroutines. A special group of kernel subroutines, which describes material model response characteristics, is found in the ZON phase of the PROCESSOR.

For a vector mode version of STEALTH, the PROCESSOR would take a slightly different form at the subroutine level and would require a different phase calling order. However, the overall design concepts would remain.

CONCLUSION

Implementing a structured architecture for the STEALTH code system has made it (1) easier to debug and modify logic, (2) simpler for new users to learn how the codes work, and (3) ideal for maintaining versions on different computer hardware. The "theoretical elements of analysis", which are the basis for program design in STEALTH, have proven to be a useful concept for solving general nonlinear equations approximated by the Wilkins explicit finite-difference solution technique.

REFERENCES

1. Ronald Hofmann; "STEALTH, A Lagrange Explicit Finite-Difference Code of Solids, Structural, and Thermo-hydraulic Analysis", EPRI NP-260, Vols. 1-3, Electric Power Research Institute, Palo Alto, California, August 1976. Prepared by Science Applications, Inc., San Leandro, California.

2. Mark L. Wilkins; "Calculation of Elastic-Plastic Flow", UCRL-7322, Lawrence Livermore Laboratory, Livermore, California, April 19, 1963. Also in Methods in Computational Physics, Berni Alder, Sidney Fernbach, and Manual Rotenberg, eds., Vol. 3, Fundamental Methods in Hydrodynamics, Academic Press, New York, 1964 (211-263).

3. Walter Herrmann; "A Lagrangian Finite-Difference Method for Two-Dimensional Motion Including Material Strength", WL-TR-64-107 (AD 609 523), Air Force Weapons Laboratory, New Mexico, November 1964.

TABLE 1. THEORETICAL ELEMENTS OF A PHYSICAL SYSTEM

Conservation laws	physical principles governing all motion
Boundary conditions	geometric constraints and boundary values
Initial conditions	initial state of things
Constitutive relations	material models

TABLE 2. ELEMENTS OF THEORY, CODE STRUCTURE, AND DOCUMENTATION AFFECTING USER ORIENTATION

THEORY

1. Physical Laws
2. Mathematical equations
3. Numerical equations

CODE STRUCTURE	DOCUMENTATION
1. Programming practices	1. Input manual
2. Modular structure	2. Flow charts
3. Input/Output	3. Vocabulary

TABLE 3. CORRESPONDENCE BETWEEN OPTIONAL GENERATOR PHASES AND CONTINUUM MECHANICS ELEMENTS OF ANALYSIS

Constitutive Equations (material models)	MATGEN
Boundary Conditions (control volume definition)	
geometric constraints	GPTGEN
boundary values	BDYGEN
Initial Conditions	ZONGEN
Conservation Equations	TIMGEN
Output	EDTGEN

TABLE 4. TYPICAL UTILITY PHASE SUBROUTINES

SYSTEMS	OUTPUT	ENTER/EXIT	ARITHMETIC
RUNDAT	PGEHDG	SBRENT	FNCONE
RUNTIM	TIMHDG	PHSENT	MYFNO
	PHSHDG	SBREXT	FNCTWO
INPUT	INPHDG*	PHSEXT	MYFNT
	CHKHDG	GENEXT	FDVONE
CRDTTL*	PRTHDG	PROEXT	MYFDO
CRDINP*	PLTHDG	ERREXT	
CRDPRT*			
LIBTTL			
LIBINP			
LIBPRT		ERROR	MISCELLANEOUS
KBDTTL*			
KBDINP*		CHRERR	INPDGT
KBDPRT		FLDERR	FLDCHK*
REWFLS		LIMERR	CNVDTA
RINREC		MDLERR	PHSCHK
GETDTA		RGEERR	
WOTREC		SBRERR	
PUTDTA		TYPERR	

* Uses standard input record format

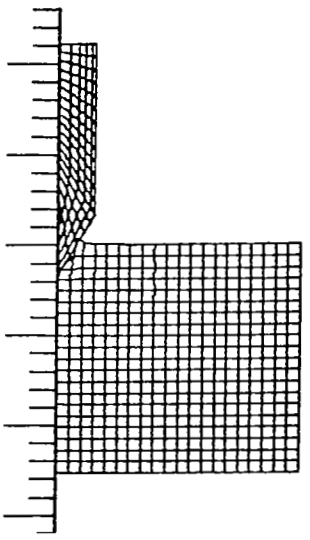

t = 4

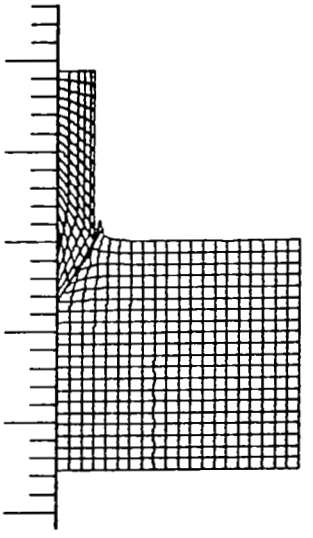

t = 8

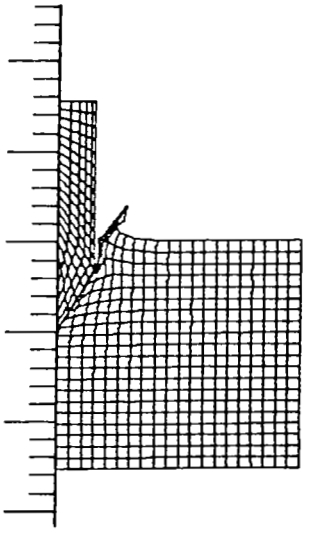

t = 12

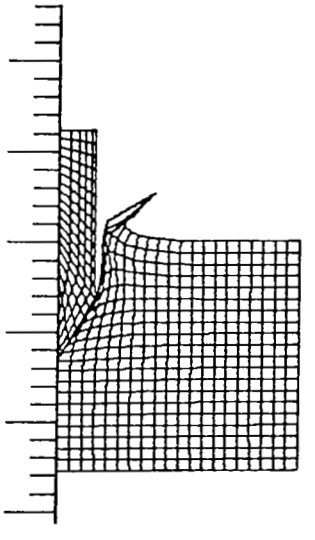

t = 16

Figure 1.- Penetration of steel projectile into aluminum target using STEALTH 2D.

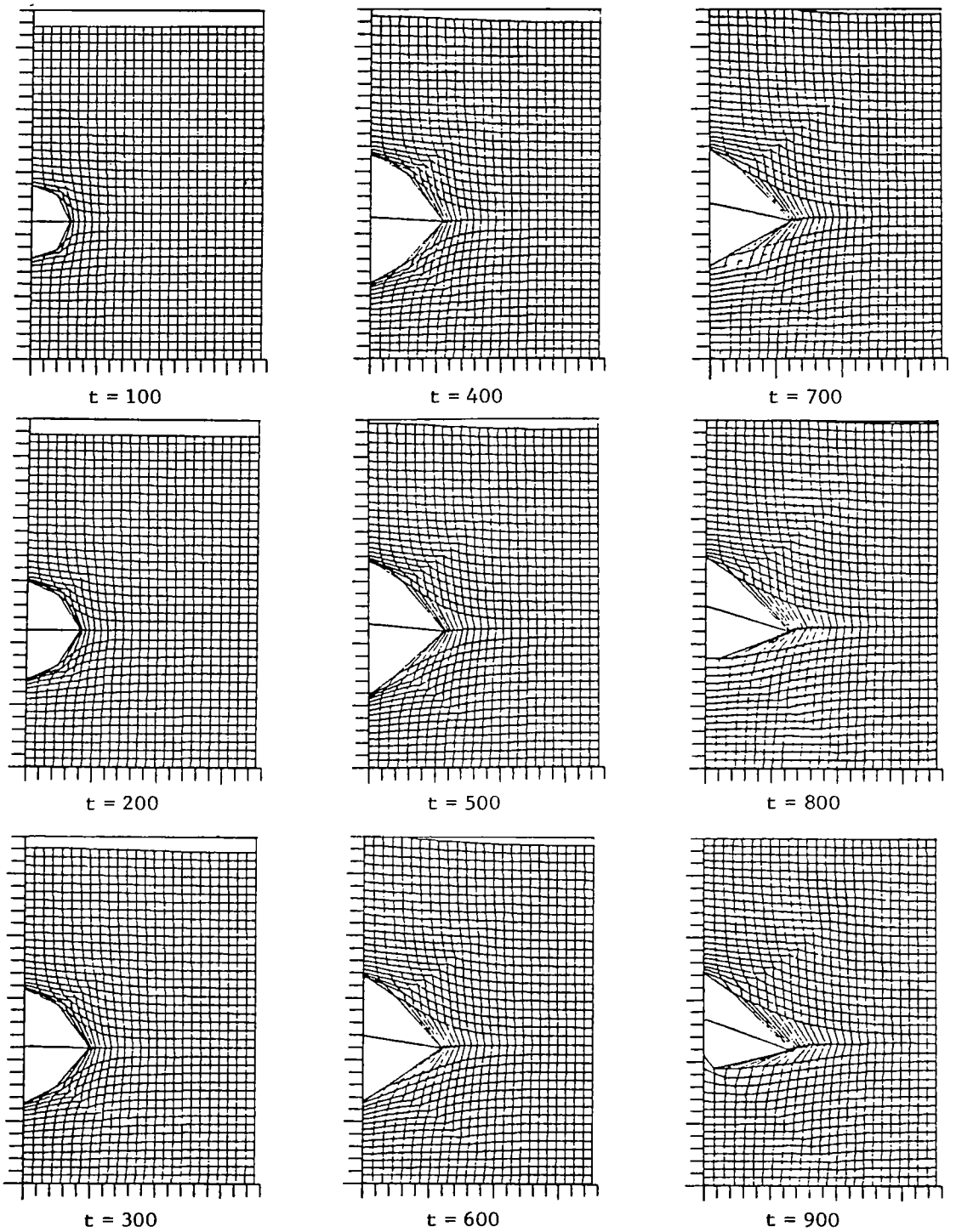

Figure 2.- Axisymmetric STEALTH 2D simulations of energy release in fluid contained in overstrong cylindrical container.

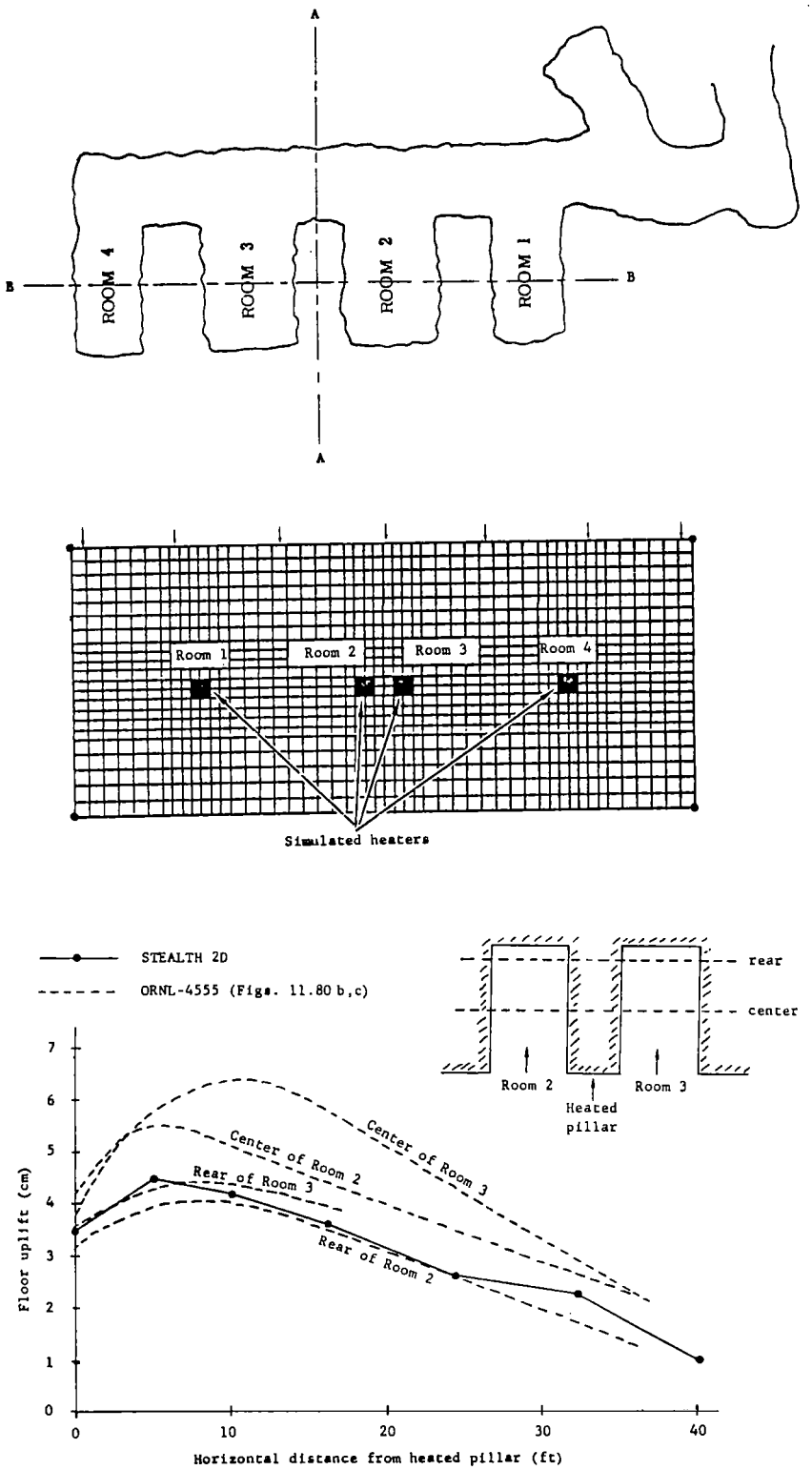

Figure 3.- Nuclear waste repository simulation using STEALTH 2D.

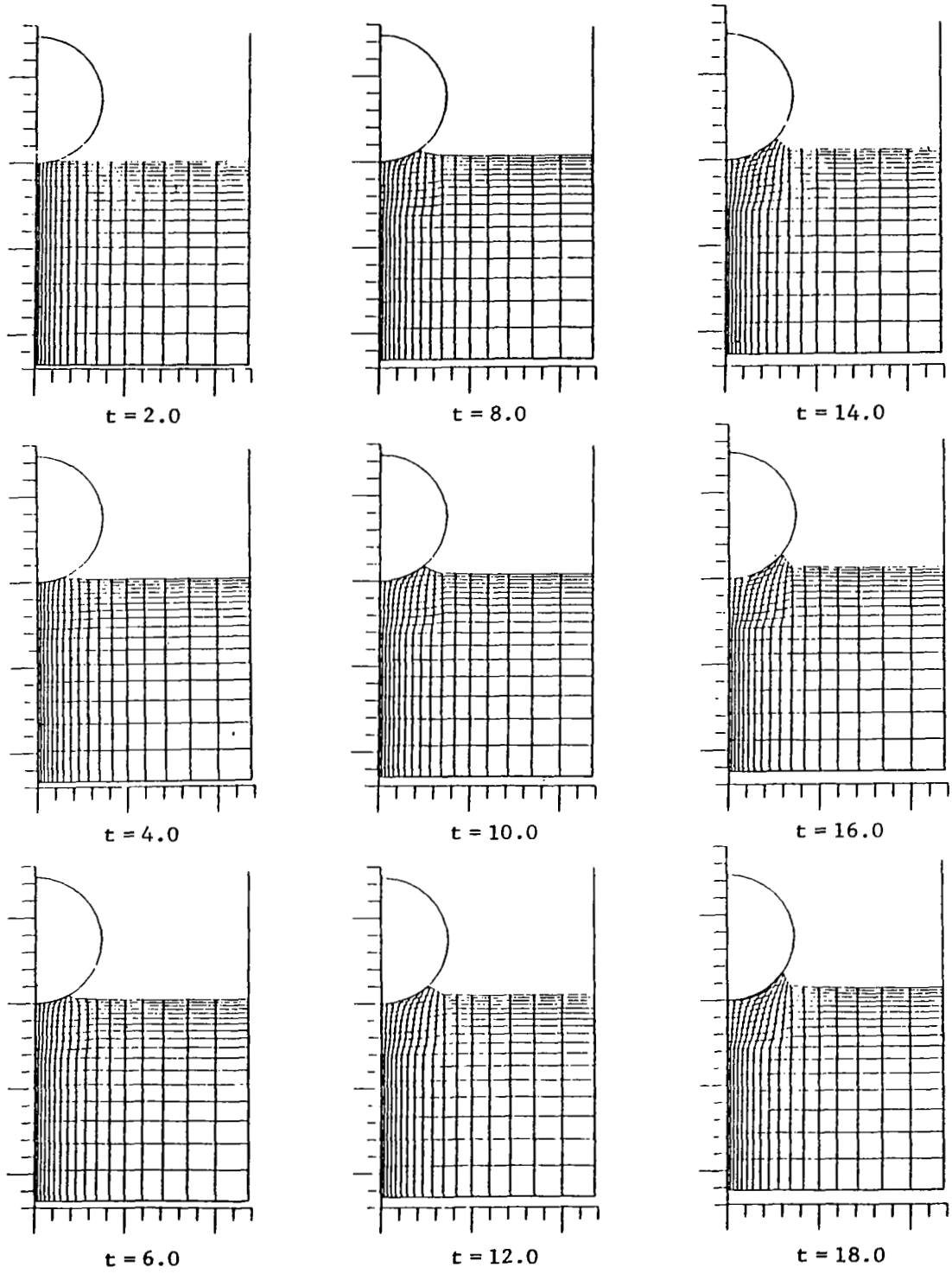

Figure 4.- Translational symmetry STEALTH 2D simulation of long rigid pipe being pushed down into tank of water.

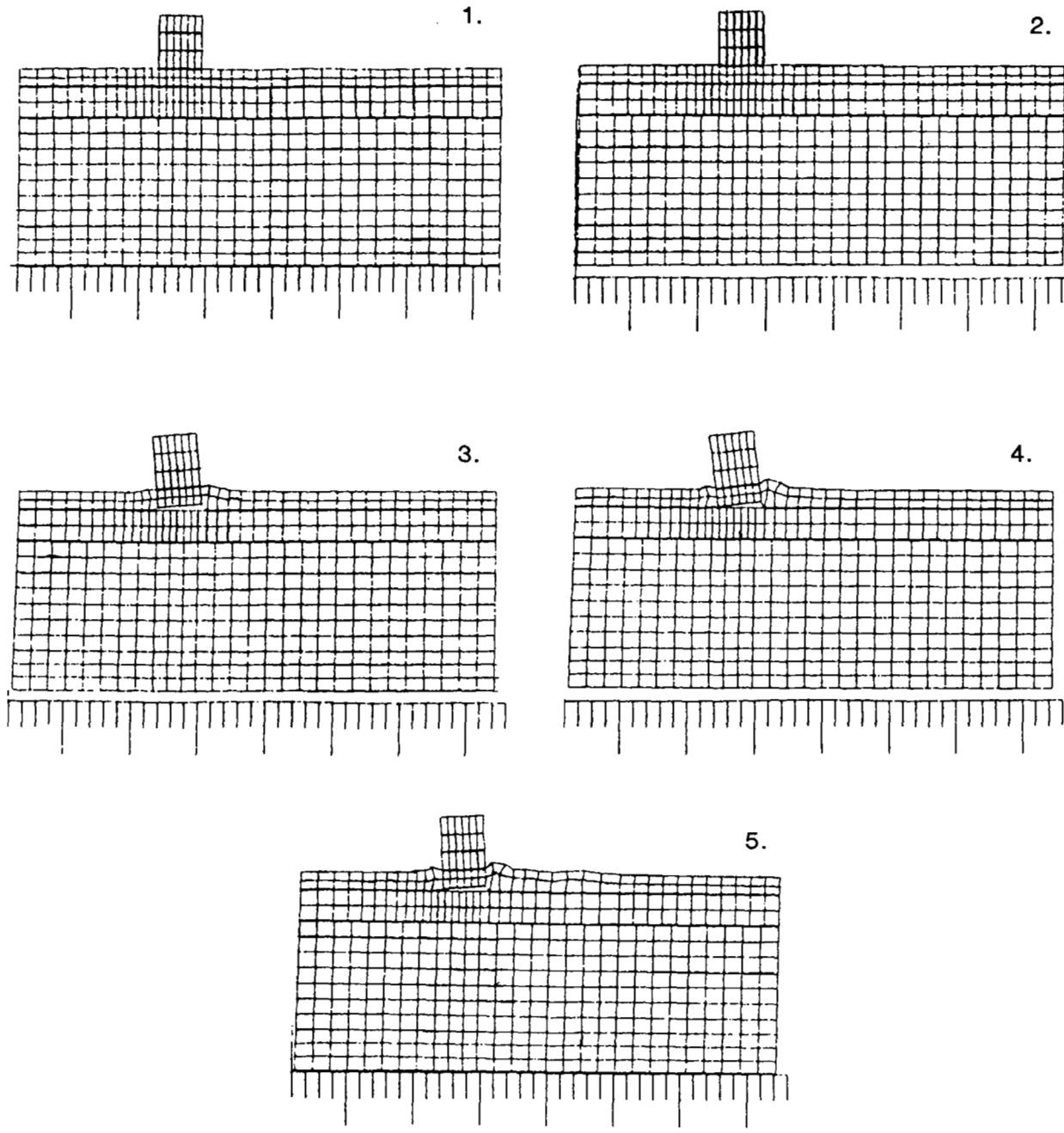

Figure 5.- Rocking of building on soil island using STEALTH 2D.

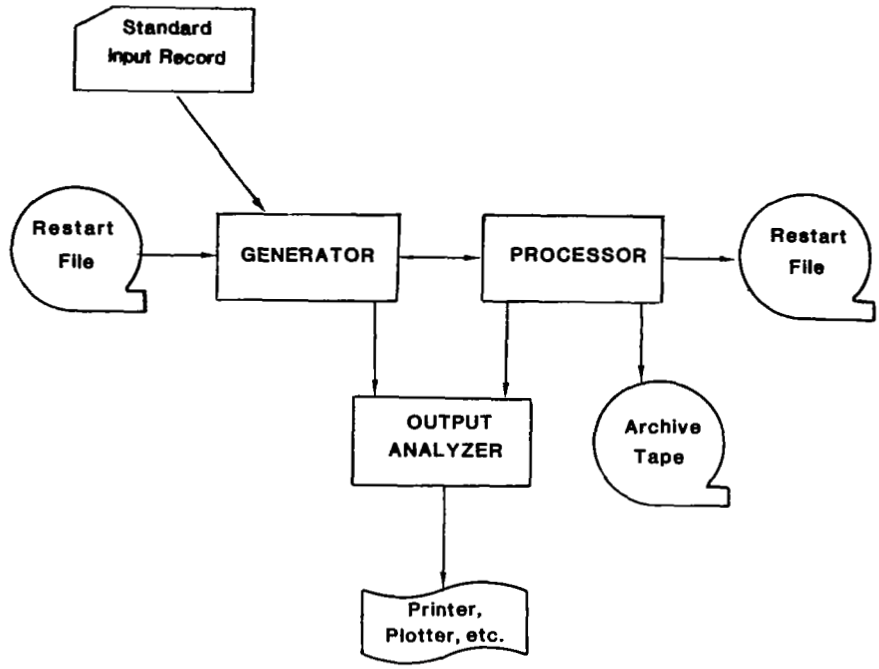

Figure 6.- Phase group flowchart.

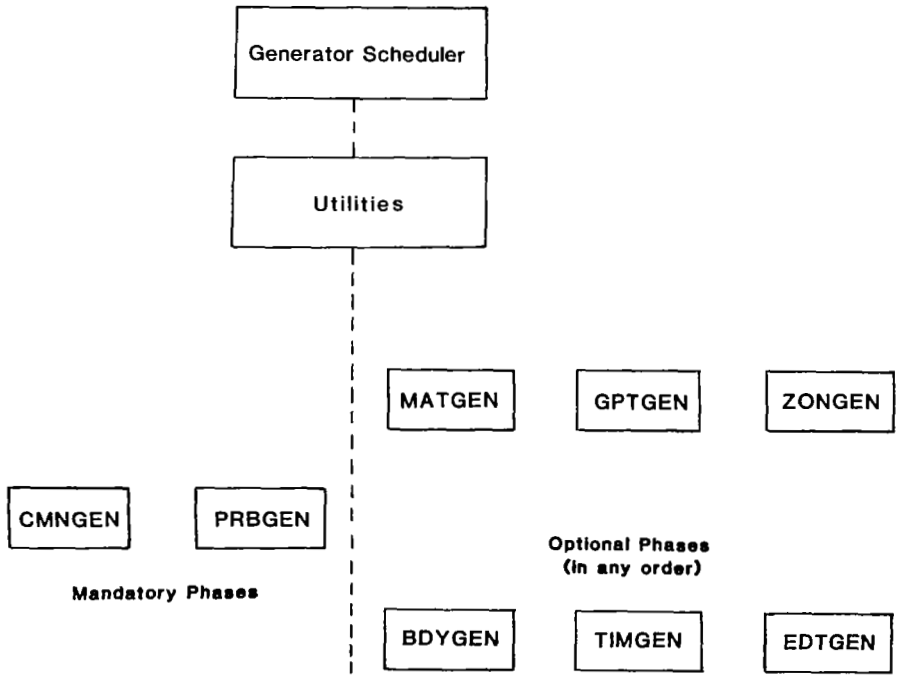

Figure 7.- GENERATOR phase group flowchart.

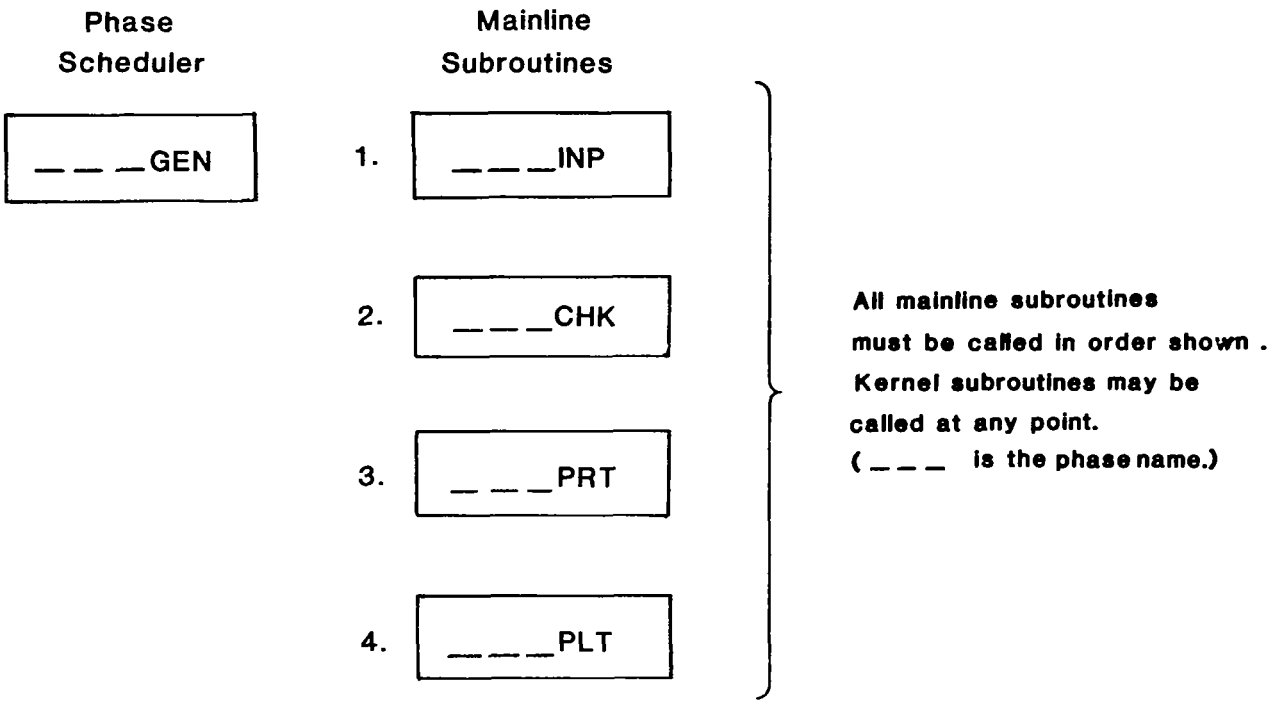

Figure 8.- Typical GENERATOR phase structure.

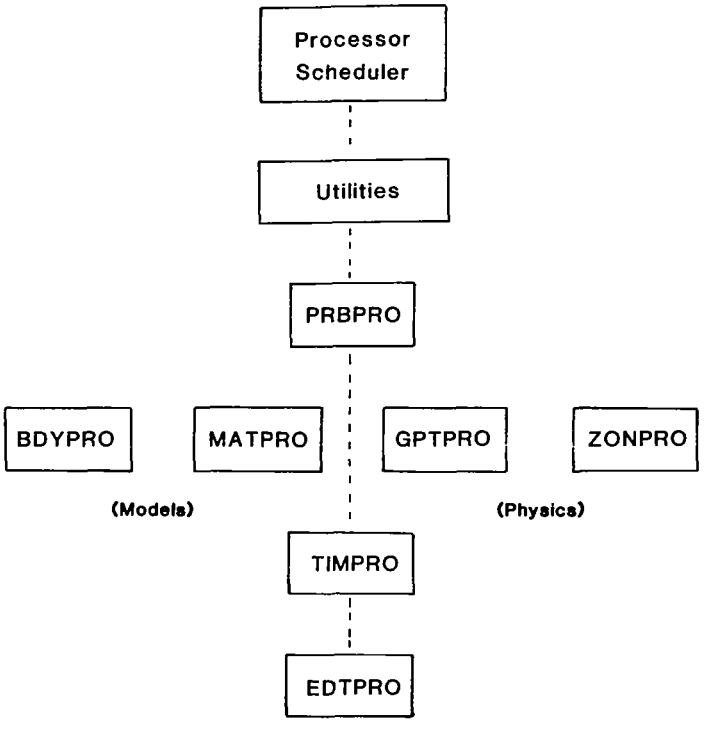

Figure 9.- PROCESSOR phase group flowchart.

SELF-ADAPTIVE INCREMENTAL NEWTON-RAPHSON ALGORITHMS*

Joseph Padovan
University of Akron
Akron, Ohio 44325

SUMMARY

Multilevel self-adaptive Newton-Raphson type strategies are developed to improve the solution efficiency of nonlinear finite element simulations of statically loaded structures. The overall strategy involves three basic levels. The first level involves preliminary solution "tunneling" via primative operators. Secondly, the solution is constantly monitored via so-called quality/convergence/nonlinearity tests. Lastly, the third level involves self-adaptive algorithmic update procedures aimed at improving the convergence characteristics of the Newton-Raphson strategy. Numerical experiments are included to illustrate the results of the procedure.

INTRODUCTION

Finite element (FE) or difference simulations of continuum problems generally lead to nonlinear modelling equations [1,2]. Generally, such simulations must be solved by various techniques which are inherently iterative in nature. For instance, such methodologies as direct numerical integration, Newton-Raphson (NR), and modified Newton-Raphson (MNR), as well as the incremental versions of such procedures (INR, IMNR) have all been employed [2]. Since the types of nonlinearity exhibited by continuum problems are both diverse and complex, the question of the best choice of an appropriate solution algorithm inevitably arises. Note, while many alternatives are available, generally the various solution procedures may have special advantages for certain classes of problems but may exhibit poor convergence for other situations.

In this context, the ideal general purpose (GP) nonlinear FE code should have numerous algorithmic options augmented with a degree of artificial intelligence. Namely, the problem solving capability should involve a heuristically guided trial and error search in the space of possible solution via an automatically structured algorithm. Unfortunately, because of the inherent difficulties associated with code architecture and kinematic, kinetic, constitutive and boundary condition formulations, generally only one algorithmic option is usually available in GP codes. In this context, because of its wide

* This work has been partially supported by the ONR under Grant N00014-78-C-0691 and by NASA under Grant NA63-54.

applicability, most GP nonlinear FE codes employ some variant of either the straight or modified INR algorithmic procedures.

Note, while nonlinear codes present the user with far reaching capabilities, without a priori physical insight, expensive parametric studies are oftentimes necessary to insure adequate solution convergence. For instance, unless the proper load increment is employed, either poor convergence or out of balance loads are generally encountered. Incorporating heuristic programming could eliminate some of the expensive and time consuming parametric studies that are now required to determine the proper incrementation necessary for reasonable convergence.

In view of the shortcomings of the current generation of solution algorithms, this paper will consider the development of self-adaptive NR strategies for the solution of nonlinear FE or difference simulations of statically loaded structures. The main thrust will be to consider strategies which for the most part are compatible with currently available GP codes. The overall development will be considered in three main levels. The first will involve the use of INR operators to "tunnel" into the solution space in the usual manner. The second level will involve the constant monitoring of the different stages of solution via various quality/convergence/nonlinearity tests. Finally, the last level is an outgrowth of the findings of the second; namely, if one or more of the quality/convergence/nonlinearity tests are violated, various scenarios are then triggered to modify the INR strategy.

Based on the foregoing, the paper will outline in detail the multilevel static solution strategy, the development of the quality/convergence/nonlinearity tests as well as overview the various self-adaptive iterative update procedures. The analytical considerations will be complemented by several numerical experiments which outline the various aspects of the quality/convergence/nonlinearity tests and which demonstrate the self-adaptive strategy.

MULTILEVEL SOLUTION STRATEGY:

OVERVIEW

As noted earlier, unless the proper load incrementation is employed, either poor convergence or out of balance loads are generally encountered. Such anomalous behavior is generic to all nonlinear codes employing non-self-adaptive INR algorithms. In this context, the main thrust of this work is to establish a three level iterative solution strategy involving:

i) Level 1; Preliminary solution development via the primative but computationally efficient IMNR algorithm;

ii) Level 2; Solution monitoring via quality/convergence/nonlinearity tests and;

iii) Level 3; Self-adaptive update procedures to modify the primative operator.

Note here computational efficiency is meant to be a measure of the amount of time spent during a cycle of iteration not the overall process.

The main purpose of the first level of the overall strategy is essentially twofold. The first is to generate the most efficient solution if the requisite quality/convergence/nonlinearity criteria are satisfied. If not, the information generated by the IMNR "tunneling" of the solution space can, through the second level tests, trigger the proper third level action.

In terms of the foregoing, it follows that the second level is essentially threefold in nature. The quality check involves monitoring: the rate of convergence; monotonicity; positive, negative and semi-definiteness; etc. The convergence tests check for outright solution failure, and lastly, the nonlinearity tests ascertain the "degree" of nonlinearity excited.

In the third level, the foregoing information is used to trigger various self-adaptive modifications of the IMNR iterative strategy. Namely:

i) Global stiffness reformation;

ii) Preferential local reformation and;

iii) Load increment adjustment.

Such algorithmic adjustments form the heart of the third level of the overall strategy.

INR FAMILY OF STRATEGIES

The overall family of INR strategies can essentially be established by introducing increasingly severe restrictions to the straight methodology. Specifically, starting with the virtual work theorem depicted by [1]

$$\int_R \delta\underset{\sim}{\varepsilon}^T \underset{\sim}{S}\, dv = \underset{\sim}{Y}^T \underset{\sim}{F} \tag{1}$$

the typical FE shape function formulation yields the following nonlinear large deformation field equations [1]

$$\int_R [B^*]^T \underset{\sim}{S}\, dv = \underset{\sim}{F} \tag{2}$$

where

$$\delta\underset{\sim}{\varepsilon}^T \equiv \frac{1}{2}\left(\delta u_{i,j} + \delta u_{j,i} + u_{\ell,i}\delta u_{\ell,j} + u_{\ell,j}\delta u_{\ell,i}\right) \tag{3}$$

$$\underset{\sim}{S}^T = (S_{11}, S_{22}, S_{33}, S_{12}, S_{23}, S_{31}) \tag{4}$$

such that $\underset{\sim}{\varepsilon}$, $\underset{\sim}{S}$, $\underset{\sim}{Y}$ and $\underset{\sim}{F}$ are, respectively, the strain tensor in vector form, the second Piola Kirchhoff pseudo stress tensor, the nodal displacement vector, and lastly, the nodal force vector.

To solve (2), the Taylor expansion theorem can be used to establish the following tangent stiffness formulation, namely

$$[K_t(Y^{\ell}_{i-1})]\ \Delta Y^{\ell}_{i} = \Delta F_i \tag{5}$$

where ΔY^{ℓ}_{i} denotes the i^{th} nodal displacement iterate associated with the ℓ^{th} load increment. The nodal displacement, tangent stiffness and load imbalance are defined by

$$Y^{\ell}_{i-1} = \sum_{k=1}^{\ell-1} \sum_{j=1}^{I_k} \Delta Y^{k}_{j} + \sum_{j=1}^{i-1} \Delta Y^{\ell}_{j} \tag{6}$$

$$[K_t(Y^{\ell}_{i-1})] = \int_R \left\{ [G]^T [\sigma(Y_{i-1})][G] + [B^*(Y^{\ell}_{i-1})]^T [D_t(Y^{\ell}_{i-1})][B^*(Y^{\ell}_{i-1})] \right\} dv \tag{7}$$

$$\Delta F^{\ell}_{i} = F^{\ell} - \int_R [B^*(Y^{\ell}_{i-1})]^T \sigma\ (Y^{\ell}_{i-}\ )\ dv \tag{8}$$

such that I_k, $[\sigma(Y_{i-1})]$, $[D_t(Y_{i-1})]$ and F^{ℓ} respectively denote the number of iterations required of k^{th} load step, the initial stress matrix, the tangent material stiffness and the total nodal load after ℓ increments. For the straight INR approach, $[K_t]$ is continuously reformed and inverted. This is obviously quite expensive. In this context, the following versions of the INR algorithm can be established for a specific load increment solution cycle, namely:

i) Straight INR with constant reformation of tangent stiffness matrix during iteration;

ii) Intermittent global reformation during iteration;

iii) Preferential local reformation during iteration;

iv) BFGS type [3] reformation during iteration;

v) Classical modified INR procedure wherein stiffness is reformed only at beginning of load step;

vi) No reformation, just iteration;

vii) Reformation with no iteration, etc.

As will be seen later, various versions of the foregoing INR family of algorithm are incorporated in the self-adaptive strategy. This will obviously lead to a hierarchy with varying degrees of computation power/efficiency.

QUALITY/CONVERGENCE/NONLINEARITY TESTS

The quality/convergence/nonlinearity tests are the core of the multi-level strategy. Such tests are themselves organized into three main categories, namely:

i) Classical norm type convergence tests;

ii) Quality of convergence tests and;

iii) Degree of nonlinearity tests.

The first group of tests are essentially of the normed type pass or fail variety as typified by:

a) The out of balance norm test;

$$\| \Delta F^{\ell}_{\sim i} \| / \| \Delta F^{\ell}_{\sim i-1} \| < \text{tol} \tag{9}$$

b) The global displacement norm test;

$$\| Y^{\ell}_{i} \| / \| Y^{\ell}_{i-1} \| < \text{tol} \tag{10}$$

The main intent of such tests is essentially to monitor the success or failure of the iterative process. Note, while such tests are efficient and well adapted to this purpose, they cannot be used effectively to forecast potential difficulties until outright failure occurs.

In this context, what is required are so-called quality checks which enable a constant monitoring of the solution so as to determine whether the direction of convergence is proper. This is the purpose of the second stage of checking. Namely, the quality checks test whether the iterative process possesses the requisite: rate; monotonicity; positive, negative and semi definiteness; etc. Once determined, such information is used to trigger the various modifications of the primative first level IMNR strategy.

Since the paper is mainly concerned with static loading problems, various statements concerning the quality of solution convergence can be made at the outset. For instance, since most static loading is applied in a monotone fashion, it is expected that unless there is overshoot, successive iterated solutions should behave as a monotone, positive, negative or semi definite sequence. Behavior to the contrary obviously represents either overshoot or potential divergence.

Since it is difficult to ascertain the monotonicity and definiteness from either of the normed or vectorial versions of the nodal displacements and forces, alternative field measures must be employed. In this direction, the local (element) and global strain energy stored can serve in such a capacity. This follows from the fact that for monotone loading situations, successive

iterations lead to a monotone positive definite sequence of energy iterates for softening structure. In the case of hardening situations, successive iterates may be nonmonotone for at least the first two iterates. Thereafter, the energy iterates tend to be monotone and negative definite. This process is clearly seen by the normed analogy of the iterative process depicted in Figures 1 and 2.

The incremental iterate energy stored during a given iteration step is essentially the shaded area illustrated in Figure 1. Realizing that the ordinate values of the true solution curve are given by (1), it follows that the incremental energy stored during the k^{th} iteration step of the ℓ^{th} load increment can be approximated by the following inner product, that is

$$E^{\ell}_{k+1} = \frac{1}{2} (\underset{\sim}{F}^{\ell}_{k}+\underset{\sim}{F}^{\ell}_{k+1})^{T} \Delta\underset{\sim}{Y}^{\ell}_{k+1} = \frac{1}{2} \int_{R} ([B^{*}(\underset{\sim}{Y}^{\ell}_{k})]^{T} \underset{\sim}{S}(\underset{\sim}{Y}^{\ell}_{k}) +$$

$$[B^{*}(\underset{\sim}{Y}^{\ell}_{k+1})]^{T} \underset{\sim}{S} (\underset{\sim}{Y}^{\ell}_{k+1}))^{T} \, dv \, \Delta\underset{\sim}{Y}^{\ell}_{k+1} \tag{11}$$

Assuming that a total of K^{ℓ} iteration steps are associated with the ℓ^{th} loadstep, then the following expression can be developed for the energy stored, namely:

$$E^{\ell} = \sum_{k=1}^{K^{\ell}-1} E^{\ell}_{k} = \frac{1}{2} \sum_{k=1}^{K^{\ell}-1} (\underset{\sim}{F}^{\ell}_{k} + \underset{\sim}{F}^{\ell}_{k+1})^{T} \Delta\underset{\sim}{Y}^{\ell}_{k+1}$$

$$= \frac{1}{2} \sum_{k=1}^{K^{\ell}-1} \int_{R} ([B^{*}(\underset{\sim}{Y}^{\ell}_{k})]^{T} \underset{\sim}{S}(\underset{\sim}{Y}^{\ell}_{k}) + [B^{*}(\underset{\sim}{Y}^{\ell}_{k+1})]^{T}\underset{\sim}{S}(\underset{\sim}{Y}^{\ell}_{k+1}))^{T} dv \Delta\underset{\sim}{Y}^{\ell}_{k+1} \tag{12}$$

Note (12) is essentially a trapezoidal type integration approximation for the area under the hyper-curve defining the solution of the ℓ^{th} loadstep. Now, summing (12) over the entire set of L loadsteps associated with a given problem yields the requisite overall strain energy stored, namely:

$$E_{total} = \frac{1}{2} \sum_{\ell=1}^{L} \sum_{k=1}^{K^{\ell}-1} (\underset{\sim}{F}^{\ell}_{k} + \underset{\sim}{F}^{\ell}_{k+1})^{T} \Delta\underset{\sim}{Y}^{\ell}_{k+1} \tag{13}$$

To obtain the strain energies for say the e^{th} element, (13) must be interpreted from a local point of view. Namely, the requisite partitions of $\underset{\sim}{F}_{k}^{e}$ and $\Delta\underset{\sim}{Y}_{k}^{e}$ must be employed in a partitioned version of (13), that is

$$E^{e}_{total} = \frac{1}{2} \sum_{\ell=1}^{L} \sum_{k=1}^{K^{\ell}-1} (\underset{\sim}{F}^{\ell e}_{k} + \underset{\sim}{F}^{\ell e}_{k+1}) \Delta\underset{\sim}{Y}^{\ell e}_{k+1} \tag{14}$$

where here $\Delta\underset{\sim}{Y}^{\ell e}$ and $\underset{\sim}{F}^{\ell e}_{k}$, are respectively the local and element nodal displace-

ments and forces. Note, due to the form of (14), any form of tangent stiffness type of constitutive law can be accomodated.

In terms of the iteration process associated with softening media, it follows that for convergent situations

$$E_1^{\ell} > E_2^{\ell} > \ldots > E_k^{\ell} > E_{k+1}^{\ell} \ldots > 0 \tag{15}$$

that is, successive iterates are monotone and positive definite. Hence, for softening media, a check of successive iterates for monotone decreasing positive definiteness will establish a measure of the quality of convergence. For the hardening case, the E_k^{ℓ} sequence associated with the convergent solution process takes the form:

$$E_2^{\ell} < E_3^{\ell} < \ldots < E_k^{\ell} < E_{k+1}^{\ell} \ldots < 0 < E_1^{\ell} \tag{16}$$

As can be seen, for k>1, the sequence E_k^{ℓ} is monotone increasing but negative definite. In this context, similar to the softening case, a check of the monotone increasing negative definiteness of successive iterates is used as one of the measures of the quality of convergence.

A last but very important way of predicting potential solution difficulties can be achieved by monitoring the degree of nonlinearity excited as the deformation process continues. This can be achieved by selectively checking the changes of curvature of the global and local strain energy space. Such behavior can be ascertained using difference operators to evaluate either the slope, rate of change of slope, or more elaborately, the radius of curvature of the energy space as either a function of the loading parameter or the nodal displacements. An alternative approach would be to locally spline fit the energy-loading parameter space. In this way, the current curvature/slope can be obtained either on a local element or global basis. Such information can be used to initiate changes in load step size as well as to control local and global stiffness reformation.

The importance of such tests follows from the fact that although FE simulations of structures composed of general media undergoing large deflections are inherently nonlinear, the degree of nonlinearity excited varies from point to point as well as from load increment to load increment. As it is possible that large portions of the structure may exhibit basically linear behavior, many general purpose codes allow the user to partition the overall structure into its linear and nonlinear groups. Although this certainly adds to the efficiency of the code, generally such information is not known a priori unless extensive parametric studies have already been performed. In this context, the nonlinearity check will enable the automatic partitioning of the structure by allowing for preferential reformation of the tangent stiffness depending on the amount of local nonlinearity excited.

ADAPTIVE STRATEGY

In the context of the inherent features of the INR family of algorithms, the adaptive strategy incorporates the following procedural options namely:

i) Tangent stiffness reformation and;

ii) Load increment adjustment.

Each of these options in turn involves several different levels. For instance, stiffness reformation can be considered in several stages, that is:

i) Global reformation;

ii) Preferential local reformation or;

iii) BFGS [3] reformation.

The adaptive incremental load can also be achieved in several ways namely:

i) Increment expansion;

ii) Increment contraction or;

iii) Corrective incrementation.

As noted earlier, the initiation of either option is dependent on three basic criteria, that is:

a) Quality of convergence;

b) Outright failure to converge or;

c) The degree of nonlinearity excited.

While the reformation option is triggered by the second level tests, the specific adaption triggered is primarily dependent on the degree of nonlinearity excited. Hence, for mildly nonlinear (elastic) situations, the BFGS reformation process is employed. In the case where significant local or global nonlinearity is excited, then either global or preferential reformation is initiated.

As can be seen from the proceeding categories, various types of load incrementation are possible. The overall strategy is a combination of such options. Specifically, when significant solution degradation is monitored by the level two tests, then corrective incrementation is initiated. Namely, negative load incrementation is employed to enable the retracing of a portion of load history wherein a lower order algorithmic strategy yielded poorly converged results.

To strike a balance between solution convergence and economy, the overall

adaptive strategy is centered about a primative version of the INR algorithm namely the IMNR. Depending on the results of the quality/convergence/nonlinearity tests, the level of the IMNR is either upgraded or lowered by modifying the pattern of stiffness reformation and incrementation. Note, since the main incentive is to achieve a successful solution at least cost, the hierarchy is ordered to first implement increment adjustment and then reformation. As a further move to achieve economy, the global reformation process typically employed at the start of an IMNR increment can be established preferentially depending on the curvature tolerance associated with the global and local nonlinearity checks.

Since space is limited, a full description of the various detailed hierachies must be left to future publications. In this context, for the present purposes, Figure 3 gives a good overview of all the possible flows of control associated with the three-level strategy. As can be seen from this figure, contingent upon the various "flags" generated in the level two tests, the condition code check routine will initiate the actual modification of the INR strategy along the lines outlined in the proceeding discussion.

DISCUSSION

Interestingly, while such factors as geometry, material properties, boundary conditions, etc., all have some effect on the choice of load increment size, once an excessive value has been chosen, typically similar types of solution degradation are encountered when only the primative non-self-adaptive algorithm is used. Specifically, three basic types of solution pathology tend to occur. These can be categorized by:

i) Immediate and strong nonmonotonicity;

ii) Moderate but progressively increasing nonmonotonicity and nonpositive definiteness and;

iii) Mild monotonicity with either very gradual increases or decreases in solution oscillation.

Note, such behavior can be excited either in the first or successive load steps. Figures 4 and 5 give examples of such behavior. While the results illustrated pertain to a rubber sheet, similar results were obtained for elastic/plastic media as well as for different geometries and boundary conditions.

The solution failure depicted in Figure 5 is typical of those that usually arise. Specifically, as can be seen, for the given load increment excellent convergence is obtained in the first step. In the second, a mild form of nonmonotonicity and nonpositive definiteness is encountered. Finally, in the third step, strong and progressively increasing nonpositive definiteness is encountered. Solution failure is finally initiated by out of balance loads. This scenario is typical of excessive load incrementation. Note, as can be seen from these results, the onset of such behavior is signalled by the initiation of nonmonotonicity or incorrect definiteness. By studying the behavior

of local element energies, additional insights are obtained. For the problems illustrated in Figures 4 and 5, the solution degradation is initially localized but gradually spreads to the entire structure as the iteration process continues. Employing the self-adaptive strategy to the foregoing problems caused the second level monotonicity tests to trigger automatic increment adjustment and preferential stiffness reformation. This led to the generation of the correct solution. The overall strategy was tested on several nonlinear problems which exhibited pathological behavior for given load increment choices. The types of problems considered combined varying degrees of kinematic, kinetic and material nonlinearity. In each case barring possible bifurcations, the level two tests were able to automatically initiate the requisite corrective self adaptions to enable successful solutions. The main problem encountered with the concept of self-adaptive strategies arises from the fact that some engineering insight must be practiced in order to cut down overall running times. Otherwise, excessive execution times are encountered as the adaptive strategy shifts gears to adjust for improper incrementation.

REFERENCES

1. Zienkiewicz, O. C., "The Finite Element Method", McGraw Hill Co. New York, 1978.

2. Chang, T. Y. and Padovan, J., "General Purpose Finite Element Programs," Structural Mechanics Software Series, Vol. III, Nicholas Parrone and Walter D. Pilkey, eds., Univ. Press of Va., 1980.

3. Strang, G., "Numerical Computations in Nonlinear Mechanics", ASME Paper No. 79-PVP-114.

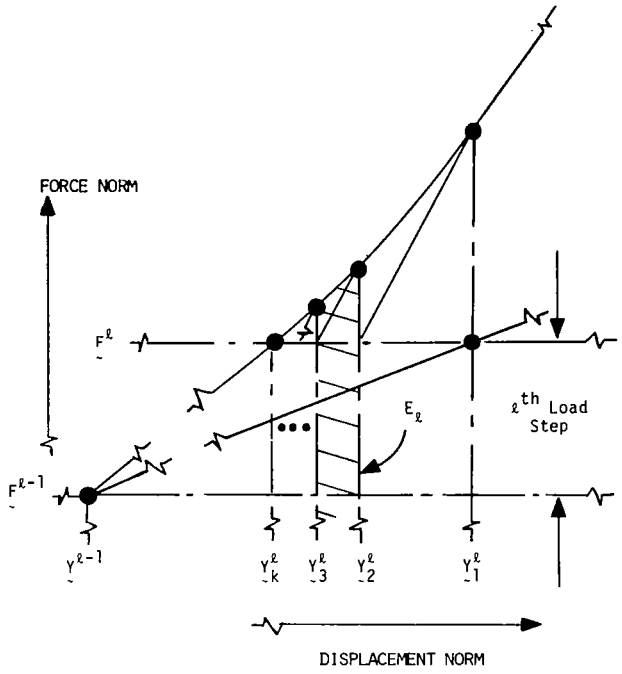

Figure 1.- Iteration process for hardening problem.

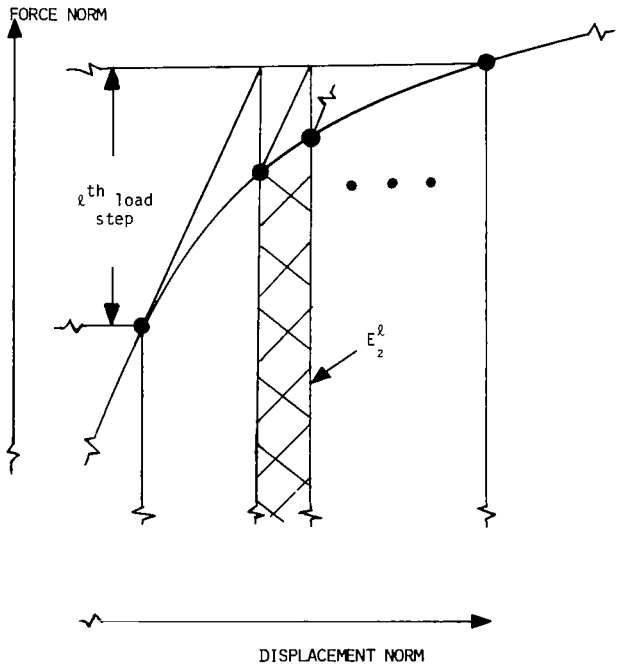

Figure 2.- Iteration process for softening problem.

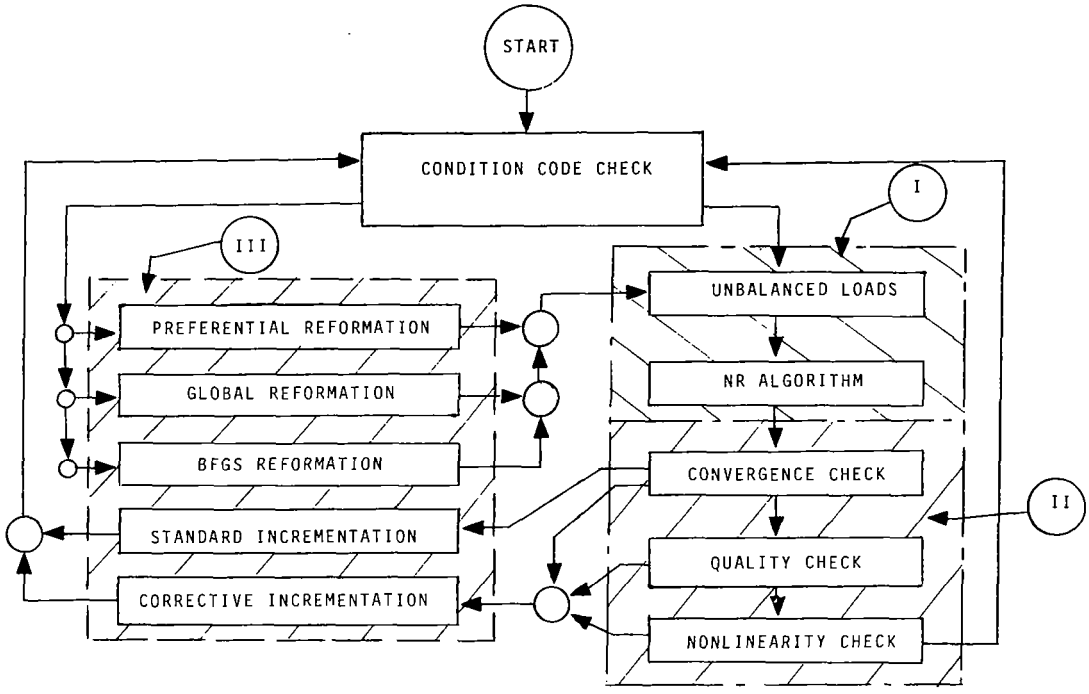

Figure 3.- Overall flow of control of three-level self-adaptive strategy.

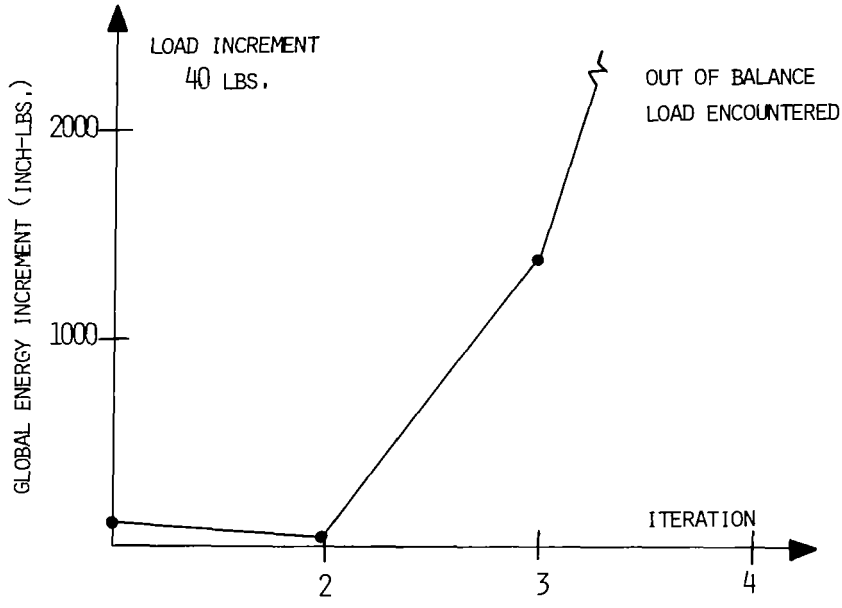

Figure 4.- Global energy increment of rubber sheet (1st load step).

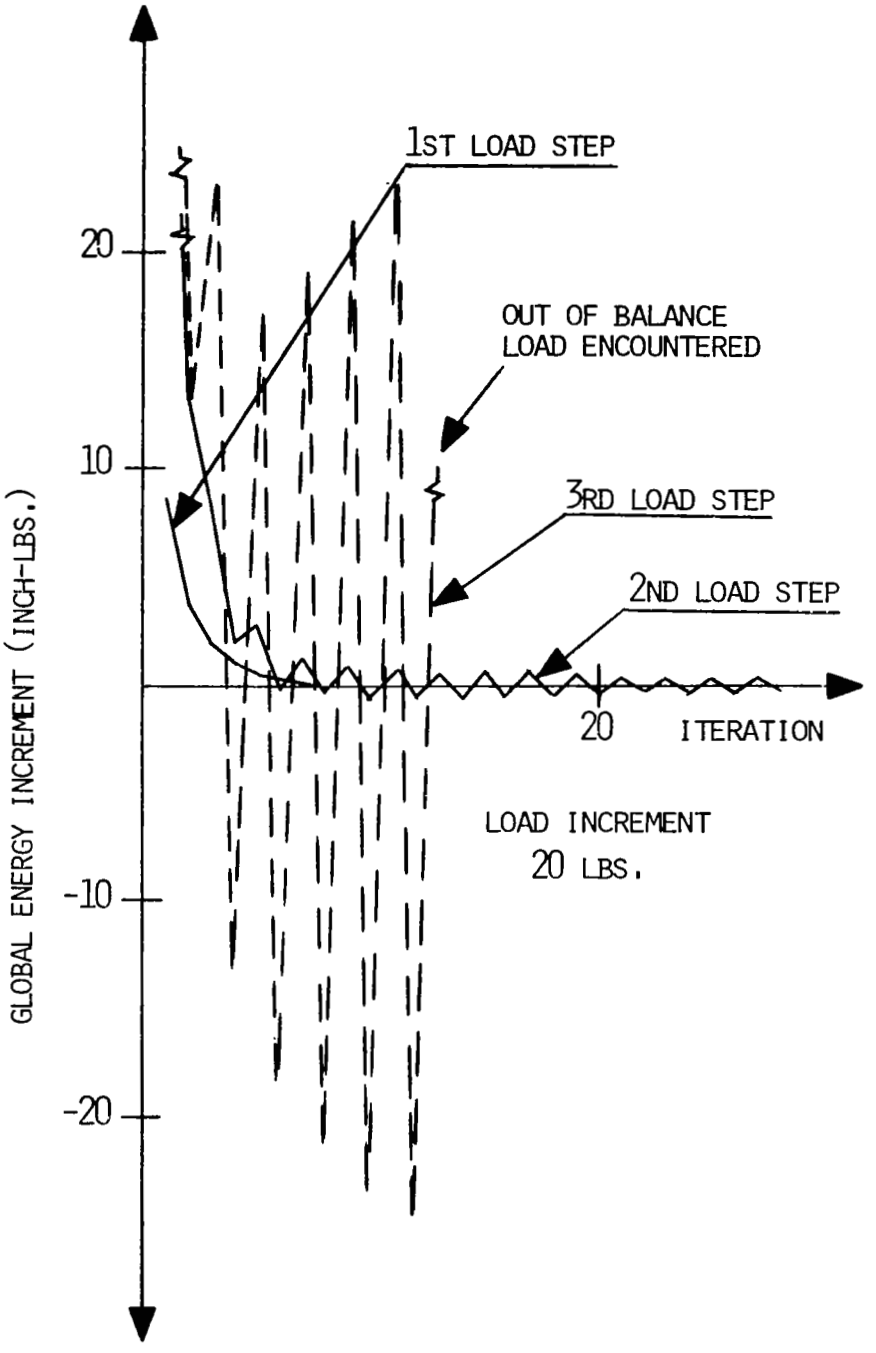

Figure 5.- Global energy increment of rubber sheet (1st, 2nd, 3rd load steps).

STUDY OF SOLUTION PROCEDURES FOR NONLINEAR STRUCTURAL EQUATIONS

Cline T. Young II
Mechanical and Aerospace Engineering
Oklahoma State University

Rembert F. Jones, Jr.
David Taylor Naval Ship R & D Center

SUMMARY

A method for the reduction of the cost of solution of large nonlinear structural equations was developed. Verification was made using the MARC-STRUC structure finite element program with test cases involving single and multiple degrees-of-freedom for static geometric nonlinearities. The method developed was designed to exist within the envelope of accuracy and convergence characteristic of the particular finite element methodology used.

INTRODUCTION

At present the finite element codes in conjunction with the large, high-speed computers available are capable of producing reasonable solutions to practically all static problems conceivable in structural analysis. In addition, well-behaved problems such as those involving small elastic deformations are solved relatively inexpensively and accurately. Computational difficulties do not arise until the stiffness of the structure becomes a function of displacement and/or displacement history. An opinion widely held is that when this does occur an implicit solution scheme is necessary for accuracy. All implicit schemes require an iterative solution where there is an attempt to reduce some error term to zero at each iteration. Therefore, a nonlinear problem is more expensive to solve and can become astronomically so depending upon the degree of nonlinearity and the convergence criteria used.

In the solution of nonlinear structural equations the reformulation of the stiffness matrix is a first order contribution to the cost. The first logical step in attempting to reduce the cost would be to seek a less expensive way to update the stiffness matrix. This of course has been done with some success and is apparently still being researched. Looking at only the most recent developments or evaluations we see that Mondkar and Powell [1] have used the constant alpha technique to try updating the stiffness matrix for the modified Newton-Raphson approach. Matthies and Strang [2,3] have taken similar approaches born from a paper by Dennis and Moré [4] on Quasi-Newton methods. The basic premise was that the stiffness matrix could be updated without going through the full process of reformulation and decomposition or inversion. The most popular approach was to update the stiff-

ness matrix by a matrix of rank two. This is known as the BFGS (Broyden-Fletcher-Goldfarb-Shanno) update. Crisfield [5] used a method similar to a BFGS update of rank one. All of these papers show conclusive evidence of cost reduction for certain problems. The last by Crisfield is closest in form to the method developed here.

A second logical step is to reduce the number of iterations required to satisfy the convergence criteria. This can be done by determining an estimated displacement as accurately as possible. The development which follows shows how to do this. All forces and loads are of an incremental nature.

DEVELOPMENT

In general, the iterative methods of solution using the stiffness formulation will by some logical means calculate a generalized displacement for a given generalized load. Returning then to the elemental level, the elemental stiffness matrices are altered to reflect this change in shape and the total resistance of the structure to the applied load is determined. If the structure is to be considered in equilibrium, the applied load must be exactly balanced by the resulting resistance of the structure. Any imbalance is termed a residual force and must be considered as an error. An attempt is made to reduce this error by altering the estimated displacement. The rate of convergence depends on the manner of estimated displacement selection.

The vast majority of implicit schemes available utilize only the most recent residual and thereby ignore any possible trend determination. Felippa [6] recognized this and proposed a viable method for determining the displacement that would yield the least residual within specified limitations. This approach required the determination of a weighting matrix that was dependent upon the elements chosen and the applied loads. The development in this paper is independent of the physical characteristics of the elements.

A key element in the success of the approach developed is the finite element method used. As mentioned before the MARC-STRUC structure program was used but the variational formulation of the structural equations was performed according to the method of Jones [7]. It is most important to have the most accurate method possible for the determination of the residuals.

Considering the solution form, in Figure 1 a graph of force versus displacement is shown. The curve represents the calculated resistance of the structure. The original stiffness matrix, $\tilde{K}_o$, assumes linearly elastic deformation and yields the displacement, $\bar{u}_o$, and the residual, $\bar{R}_o$, for the applied load, $\bar{F}$. The displacement, $\bar{u}_o$, and residual, $\bar{R}_o$, are then used in a Quasi-Newton fashion to update the stiffness matrix to $\bar{K}_1$ and a new displacement, $\bar{u}_1$, and consequently a new residual, $\bar{R}_1$, are calculated. Highly accurate answers may result, but they are clearly expensive to obtain.

The extrapolation method presented in this paper is clearly exemplified by the triangle, ACE, shown in Figure 2. The method used was identical to the direct iteration method (shown in Figure 1 earlier) up to and through the

calculation of $\bar{u}_o$, $\bar{R}_o$ and $\bar{u}_1$, $\bar{R}_1$. It was the determination of the new estimated displacement, $\bar{u}_2$, that was performed differently. In a one dimensional sense the residuals $\bar{R}_o$, $\bar{R}_1$ and the distance between them, $\bar{d}$, were used to calculate a scalar, ω, that predicted the displacement at which equilibrium supposedly existed under the load, $\bar{F}$. Of course, this was not the equilibrium position and a new residual, $\bar{R}_2$, was determined. The residuals, $\bar{R}_1$, $\bar{R}_2$, and the distance between them, $\omega\bar{d} - \bar{d}$, were then used to predict a new equilibrium position. The process continued until convergence was satisfied.

A major difficulty encountered was the determination of the scalar, ω. In a one dimensional case it was easy enough to see that

$$\omega = \frac{\bar{R}_o}{\bar{R}_o - \bar{R}_1} \tag{1}$$

However, since in general the vectors $\bar{R}_o$, $\bar{R}_1$ and $\bar{d}$ are heterogeneous in their components' units, a division as mentioned above is impossible even when using vector lengths. The solution to this difficulty came about by considering the units of work. In fact, this extrapolation process may be symbolically thought of as minimizing the work done by the residuals. In this light it was then decided that equating the area of the trapezoid, ABDE, plus the area of the triangle, BCD, to the area of the triangle, ACE, would result in an equation with only one unknown. Simplifying and rearranging, the following was obtained.

$$\omega = \frac{\bar{R}_o \cdot \bar{d}}{(\bar{R}_o - \bar{R}_1) \cdot \bar{d}} \tag{2}$$

At this point it was decided to implement the theory and test for a one degree-of-freedom case and follow that with a more complex case.

VERIFICATION

In an attempt to determine the validity of the aforementioned extrapolation method it was determined that a one dimensional buckling problem would be appropriate as a first test case. The bar-spring problem of Jones was selected.

Bar-Spring Problem

In Figure 3 the dimensions used on the problem may clearly be seen. The length of the spring was unimportant as long as nonlinear effects did not enter the calculations for the spring's deflection. The bar was modeled so as to allow only a change in length and no bending deformation, hence the absence of an EI term. A load was applied at the end of the bar and spring in the direction of deformation to render the problem one of a purely single dimensional

case. The buckling load was at 2.7 kg. (6 lb.) with the results tabularized in Table I. The exact deformation was calculated and plotted in Figure 4 to show the high degree of nonlinearity of the problem.

In analyzing the results (see Table I) it was decided that a comparison of the values calculated against the exact values as well as a comparison of the number of iterations required for each method would be of use. The raised numbers beside the calculated displacements in Table I represent the number of iterations required above the original estimate to reduce the quotient of the calculated displacement and the estimated displacement to the tolerance indicated at the column heading.

It should be noted that at the buckling load the tolerance required to obtain two significant digits accuracy, 1.001, led to a 5 vs. 26 advantage in iterations for the new method. However, the new method was edged by the old in the post-buckled region by a consistent 4 vs. 7 margin. The reason for this was apparently that the linear extrapolation did not follow the changing stiffness of the structure very well. If so, a better approximation would be obtained with a parabolic extrapolation.

On the whole this extrapolation showed promise in this case but not of a clearly decisive nature. Therefore, the motivation for a more complex example was established.

Ring Buckling Problem

This problem was to determine the deflection of a ring under a uniformly loaded external pressure of varying values. The ring was modeled through 90 degrees as shown in Figure 5. The 90 degree arch was broken into two substructure. The degrees of freedom per node were

1. Z
2. R
3. dZ/ds
4. dR/ds

with the rotations positive as shown by Θ in Figure 5. The ring was modeled with a modulus of elasticity of 2.1×10^6 kg/cm^2 (30×10^6 psi) and a radius of 51 cm (20 in.). Finally, a kicker force was applied at node 1 of substructure 1 in the negative R direction with a magnitude of 1.5×10^{-6} kg. (3.4×10^{-6} lb). Obviously, this was simply to force the ring into a buckled mode without altering the deflections due to the pressure loading.

As there was no exact solution other than the known collapse load, the tolerance chosen, 1.001, was that which gave two significant digits accuracy for the bar-spring problem. The results obtained are shown in Table II. The point at which the structure would "collapse" was 4.22 kg/cm^2 (60 psi). As can be seen, the results were quite remarkable as the structure became softer. At 4.18 kg/cm^2 (59.5 psi) the number of iterations reached by the old method were not enough yet to satisfy the tolerance requirement of 1.001. The authors suspect that another 50 to 100 iterations would have been required.

CONCLUDING REMARKS

The problem discussed in this paper was the cost of solution of large nonlinear structural equations. This difficulty has been and is being researched; however, the direction of most present research is apparently concerned with the second partial of the strain energy expression (stiffness matrix). This paper implies and subsequent research by the authors supports the supposition that the first partial of the strain energy expression (resisting force) is not being fully utilized in the determination of the new estimated displacement needed for implicit methods. It may well be determined that updating and/or reformulation of the stiffness matrix is occurring far too often in present solution techniques.

REFERENCES

1. Mondkar D. P. and G. H. Powell, "Evaluation of Solution Schemes for Nonlinear Structures." Computers & Structures, Vol. 9, 1978, pp. 223-236.

2. Matthies, H. and G. Strang, "The Solution of Nonlinear Finite Element Equations." International Journal for Numerical Methods in Engineering, Vol. 14, pp. 1613-1626, Nov., 1979.

3. Strang, G. and H. Matthies, "Numerical Computations in Nonlinear Mechanics." NSF Report, MCS 78-12363.

4. Dennis, J. E. and J. J. More', "Quasi-Newton Methods, Motivation and Theory." SIAM Review, Vol. 19, pp. 46-89, 1977.

5. Crisfield, M. A., "A Faster Modified Newton-Raphson Iteration." Computer Methods in Applied Mechanics and Engineering, Vol. 20, pp. 267-278, 1979.

6. Felippa, C. A., "Procedures for Computer Analysis of Large Nonlinear Structural Systems." Large Engineering Systems, ed. by A. Wexler, Pergamon Press, London, pp. 60-101, 1976.

7. Jones, R. F., "Incremental Analysis of Nonlinear Structural Mechanics Problems with Applications to General Shell Structures." Naval Ship Research and Development Center Report 4142, 1973.

TABLE 1

BAR-SPRING PROBLEM

Load kg (lb)	Method	Exact (cm)	1.1	1.01	1.001	1.0001	1.00001
1.4	Old	0.59781	0.5915_{1}^{1}	0.5964_{3}^{2}	0.5978_{5}^{4}	0.5978^{6}	0.5978^{7}
(3.0	New		0.5915^{1}	0.5964^{3}	0.5978^{5}	0.5978^{6}	0.5978^{7}
2.7	Old	2.5400	2.0177_{2}^{3}	2.4545_{4}^{13}	2.5320_{5}^{26}	2.5392^{39}	2.5400^{51}
(6.0)	New		2.2329^{2}	2.5018^{4}	2.5373^{5}	2.5400^{6}	2.5400^{6}
4.1	Old	4.4821	4.4933_{1}^{1}	4.4806_{1}^{1}	4.4821_{1}^{1}	4.4821^{1}	4.4821_{3}^{1}
(9.0)	New		4.4788^{1}	4.4816^{1}	4.4821^{1}	4.4821^{1}	4.4821^{3}
5.4	Old	5.0800	5.0792_{3}^{2}	5.0800_{5}^{3}	5.0800_{7}^{4}	5.0800_{8}^{4}	5.0800_{9}^{5}
(12.0)	New		5.0828^{3}	5.0803^{5}	5.0800^{7}	5.0800^{8}	5.0800^{9}
6.8	Old	5.4907	5.4943_{1}^{1}	5.4907_{5}^{3}	5.4907_{7}^{4}	5.4907_{9}^{6}	5.4907_{10}^{6}
(15.0)	New		5.4948^{1}	5.4910^{5}	5.4907^{7}	5.4907^{9}	5.4907^{10}
8.2	Old	5.8143	5.8176_{1}^{1}	5.8146_{5}^{3}	5.8143_{7}^{4}	5.8143_{9}^{6}	5.8143_{11}^{7}
(18.0)	New		5.8176^{1}	5.8148^{5}	5.8146^{7}	5.8143^{9}	5.8143^{11}

*Buckling Load

Note: When the number of iterations is less than (2), there is NO difference between the new and old methods.

TABLE II

RING PROBLEM (1.001)

Load kg/cm^2 (psi)	Method	Iterations	Substructure 1 (cm) Node 1 D.O.F. 2	Substructure 2 (cm) Node 1 D.O.F. 2
.5	Old	2	-.78547 E-03	-.41397 E-03
(7)	New	4	-.78555 E-03	-.41397 E-03
1.5	Old	5	-.25537 E-02	-.10468 E-02
(21)	New	4	-.25545 E-02	-.10459 E-02
2.5	Old	9	-.49439 E-02	-.10607 E-02
(35)	New	4	-.49472 E-02	-.10576 E-02
3.5	Old	23	-.10230 E-01	.18172 E-02
(49)	New	3	-.10237 E-01	.18243 E-02
3.9	Old	54	-.22451 E-01	.12827 E-01
(56)	New	3	-.22597 E-01	.12972 E-01
4.2	Old	149*	-.88354 E-01*	.77978 E-01*
(59.5)	New	4	-.95669 E-01	.85268 E-01

*Maximum number of iterations allowed.
Convergence not yet satisfied.

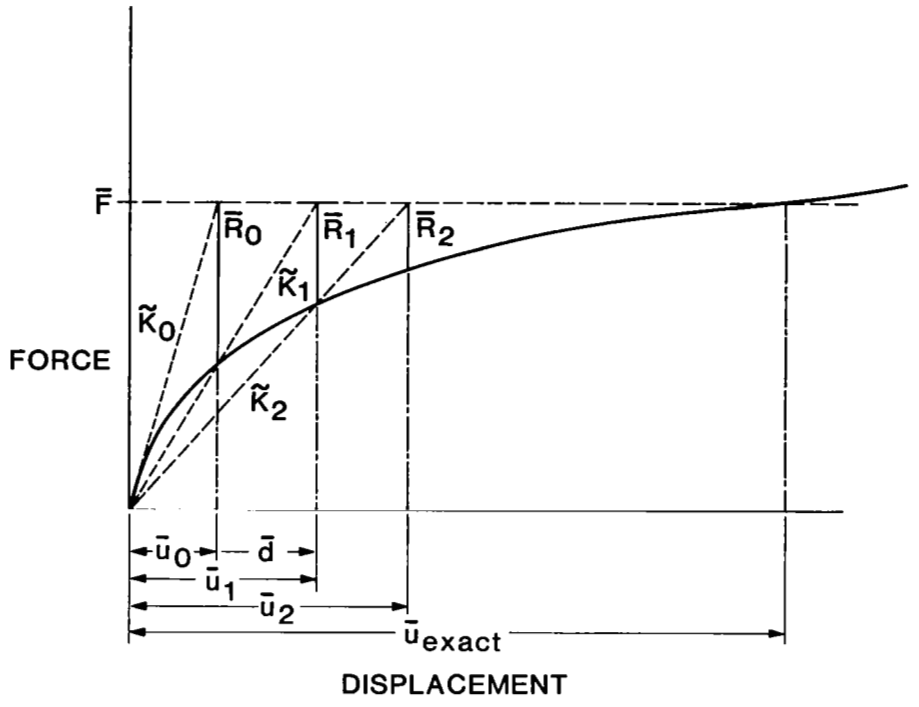

Figure 1.- Direct iteration method.

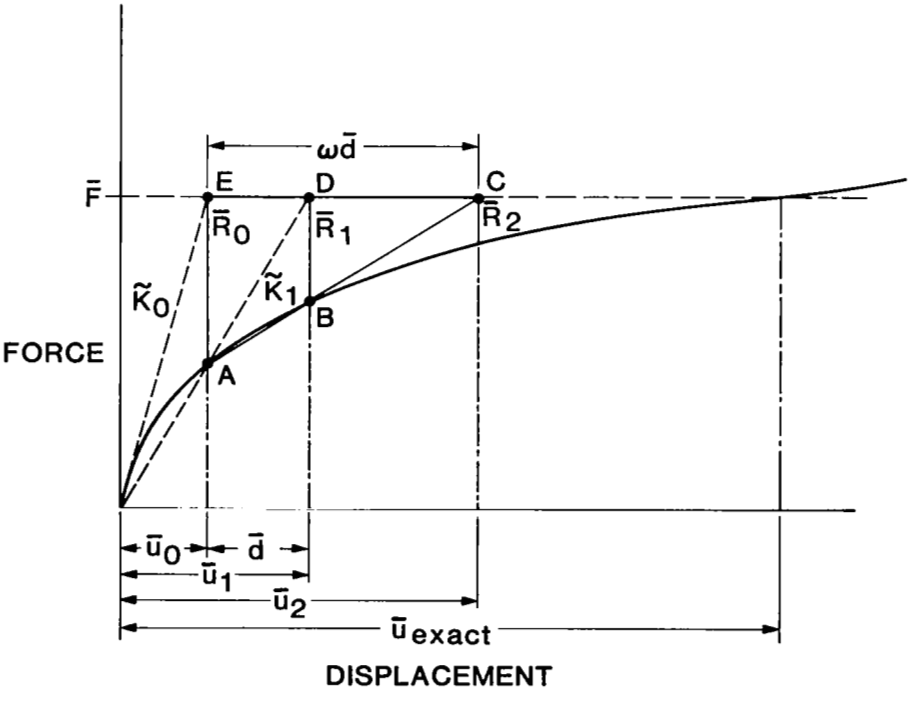

Figure 2.- Direct iteration method with extrapolation modification.

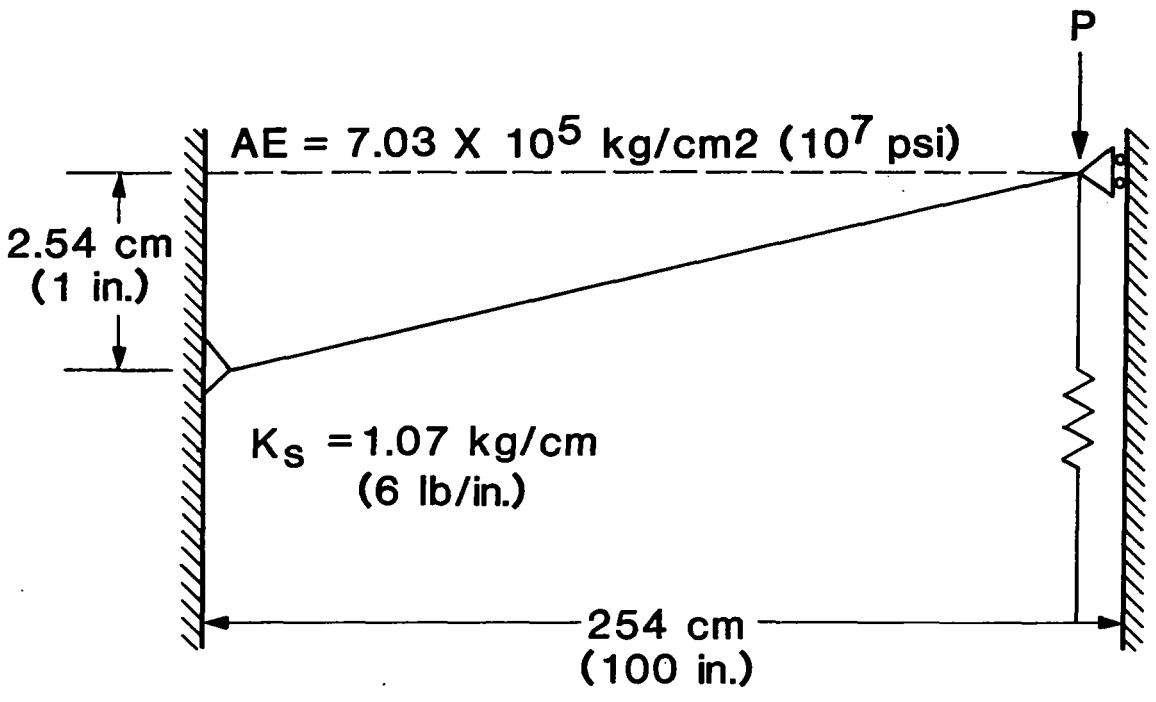

Figure 3.- Bar-spring problem.

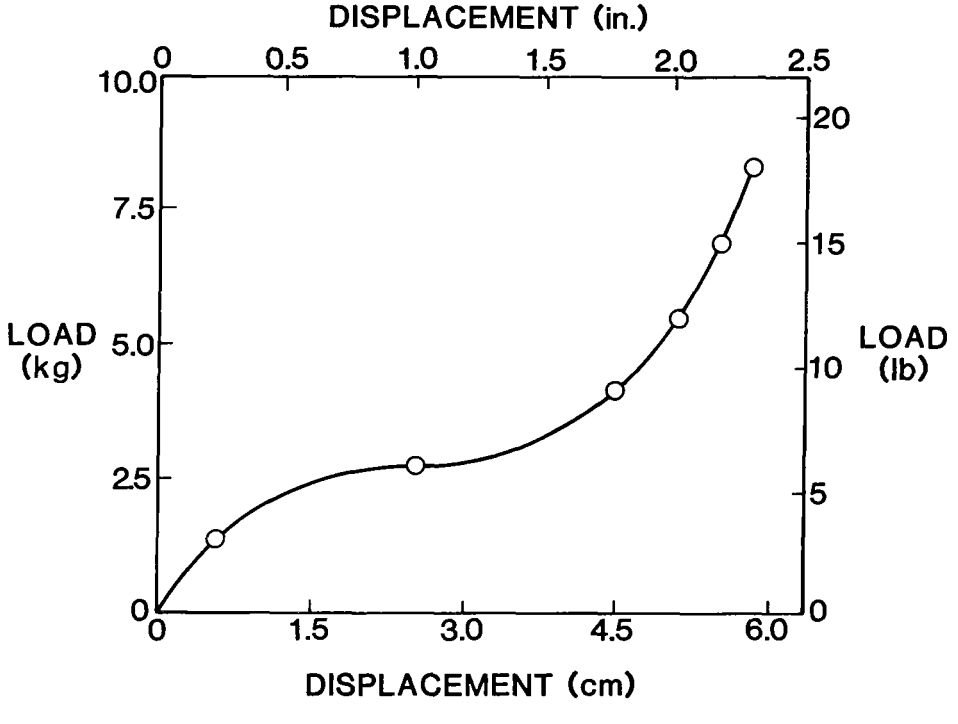

Figure 4.- Exact solution to bar-spring problem.

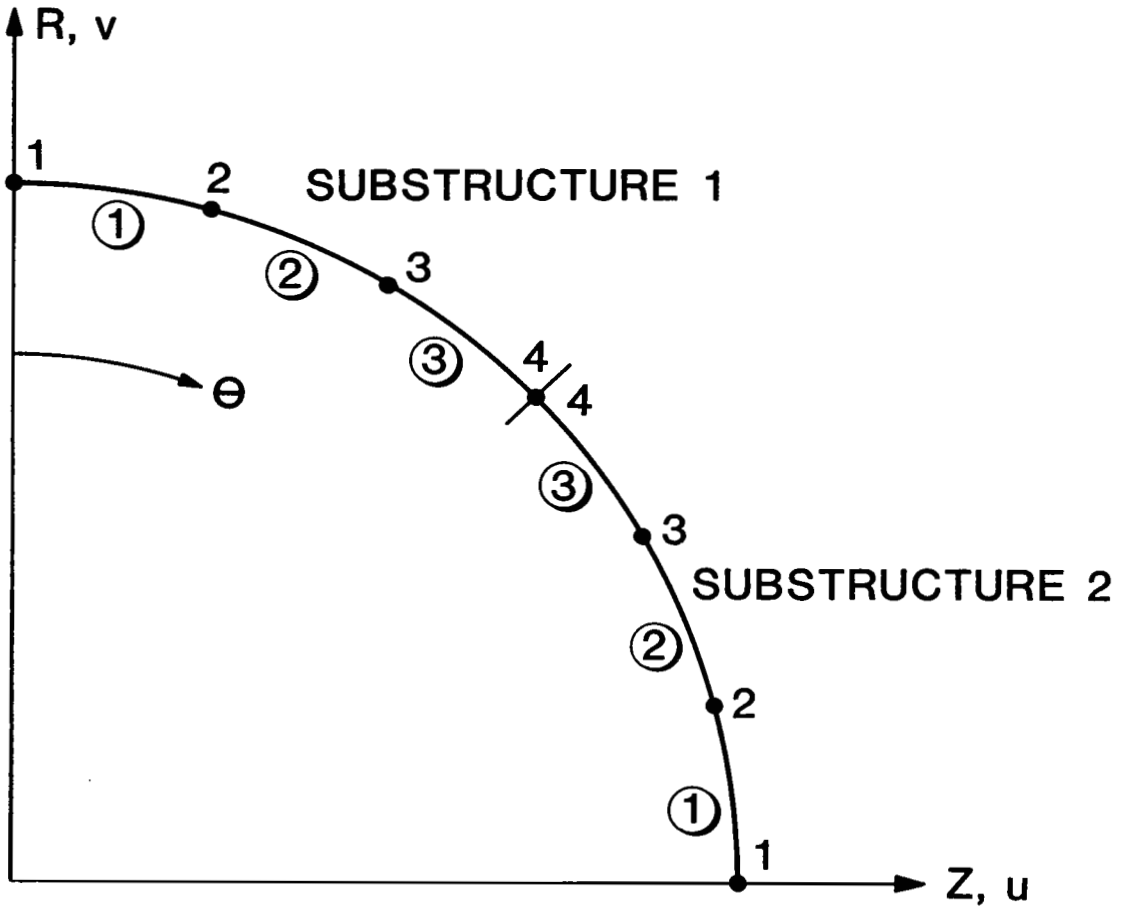

Figure 5.- Ring problem.

RESPONSE OF NONLINEAR PANELS TO RANDOM LOADS*

Chuh Mei
Old Dominion University

SUMMARY

Lightweight aircraft structures exposed to a high intensity noise environment can fatigue fail prematurely if adequate consideration is not given to the problem. Design methods and design criteria for sonic fatigue prevention have been developed based on analytical and experimental techniques. Most of the analytical work was based upon small deflection or linear structural theory which did not agree with the experimental results. A large deflection geometrical nonlinearity was incorporated into the analysis methods for determining the structural response to high intensity noise. The Karman-Herrmann large deflection equations with a single-mode Galerkin approximation, and the method of equivalent linearization were used to predict mean-square amplitude, mean-square stresses, and nonlinear frequency at various acoustic loadings for rectangular panels. Both simply supported and clamped support conditions with immovable or movable inplane edges are considered. Comparisons with experimental results are presented.

INTRODUCTION

Vibrations caused by acoustic pressure can frequently disturb the operating conditions of various instruments and systems, and sonic fatigue failures which occurred in aircraft structural components cause large maintenance and inspection burdens. The development of sonic fatigue data and design techniques were initiated to prevent sonic fatigue failures. Design methods and design criteria for many types of aircraft structures have been developed under Air Force sponsorship and by the industry in the past twenty years. Reference 1 has a complete list of the reports describing these efforts. This research led to sonic fatigue design criteria and design charts which are widely used during the design of an aircraft. Although current analytical sonic fatigue design methods are essentially based on small deflection or linear structural theory (see ref. 1, page 209), many documented tests (refs. 2 - 6) on various aircraft panels have indicated that high noise levels in excess of 110 decibels (dB) produce nonlinear behavior with large amplitudes of one to two times the

*This work was supported by the Air Force Office of Scientific Research (AFSC), United States Air Force, under contract F49620-79-C00169.

panel thickness in such structural panels. The neglect of such large deflection geometrical nonlinearity in analysis and design formulations has been identified as one of the major causes for poor agreement between experimental data and analytical results. The evidence of those researchers was summarized in reference 7, where a comprehensive review of existing analytical methods on random excitations of nonlinear systems was also given.

In this paper, the Karman-Herrmann large deflection equations for rectangular plates (ref. 8) are employed. Using a single-mode Galerkin's approximation, the dynamic equations reduce to a nonlinear differential equation with time as the independent variable. The method of equivalent linearization (refs. 9 - 11) is then applied to reduce the nonlinear equation to an equivalent linear one. Mean-square displacements, mean-square stresses, and nonlinear frequencies at various acoustic loadings are obtained for rectangular panels of different aspect ratios and damping factors. Both simply supported and clamped boundary conditions with immovable or movable inplane edges are considered. Comparisons with experimental results are also presented.

SYMBOLS

a,b	Panel length and width
A,B	Panel dimension parameters, $2\pi/a$ and $2\pi/b$
C_1,C_2	Constants
D	Bending rigidity
err	Error of linearization
E	Young's modulus
f	Equivalent linear frequency in Hz
F	Stress function
h	Panel thickness
$H(\omega)$	Frequency response function
L	Spectrum level
m	Mass coefficient
N	Membrane stress resultant
$\overline{N}$	Constant
p	Pressure loading
q	Generalized or modal displacement
r	Aspect ratio, a/b
$S(\omega)$	Spectral density function of excitation pressure p(t)
t	Time
u,v	Displacement of midplane
w	Transverse deflection
x,y,z	Coordinates
β	Nonlinearity coefficient
β^*	Nondimensional nonlinearity coefficient
ζ	Ratio of damping to critical damping
λ	Nondimensional frequency parameter
ν	Poisson's ratio
ρ	Panel mass density
σ,τ	Normal and shear stresses

ω Radian frequency
Ω Equivalent linear or nonlinear radian frequency

Subscripts:

b Bending
c Complementary solution or critical
m Membrane
max Maximum
o Linear
p Particular solution

FORMULATION AND SOLUTION PROCEDURE

Governing Equations

Assuming that the effect of both the inplane and rotatory inertia forces can be neglected, the dynamic von Karman equations of a rectangular isotropic plate undergoing moderately large deflections are (refs. 8, 12):

$$L(w,F) = D\nabla^4 w + \rho h w_{,tt} - h\,(F_{,yy}\,w_{,xx} + F_{,xx}\,w_{,yy} - 2F_{,xy}\,w_{,xy}) - p(t) = 0 \tag{1}$$

$$\nabla^4 F = E\,(w^2_{,xy} - w_{,xx}\,w_{,yy}) \tag{2}$$

where w is the transverse deflection of the plate, h is the panel thickness, ρ is the mass density of the panel material, $D = Eh^3/12(1-\nu^2)$ is the flexural rigidity, E is Young's modulus, ν is Poisson's ratio, p(t) is the exciting pressure, and a comma preceding a subscript(s) indicates partial differentiation (s). The stress function F is defined by

$$\sigma_x = F_{,yy}$$
$$\sigma_y = F_{,xx} \tag{3}$$
$$\tau_{xy} = -F_{,xy}$$

where σ_x, σ_y, and τ_{xy} are membrane stresses.

Simply Supported Panels. For a rectangular plate simply supported along all four edges as shown in Figure 1, Chu and Herrmann (ref. 8), and Lin (ref. 13) have considered that if the fundamental mode is predominant, the motion of the panel can be represented adequately as

$$w = q(t)\,h \cos(\pi x/a) \cos(\pi y/b) \tag{4}$$

where q(t) is a function of time only. The maximum value of q(t) coincides with

the maximum deflection w_{max} divided by panel thickness h. The expression w satisfies the boundary conditions for simple supports

$$\begin{aligned} w &= w_{,xx} + \nu\, w_{,yy} = 0, \text{ on } x = \pm\, a/2 \\ w &= w_{,yy} + \nu\, w_{,xx} = 0, \text{ on } y = \pm\, b/2 \end{aligned} \tag{5}$$

Substituting the expression for w in Eq. (2) and solving for a particular solution F_p yields

$$F_p = -\frac{1}{32}\, q^2 h^2 E r^2 \left(\cos\frac{2\pi x}{a} + \frac{1}{r^4}\cos\frac{2\pi y}{b}\right) \tag{6}$$

where r = a/b. The complementary solution to equation (2) is taken in the form

$$F_c = \bar{N}_x \frac{y^2}{2} + \bar{N}_y \frac{x^2}{2} \tag{7}$$

where the constants $\bar{N}_x$ and $\bar{N}_y$ contribute to the membrane stresses σ_x and σ_y and are to be determined from the inplane boundary, immovable or movable, conditions.

For the immovable edges case, the conditions of zero inplane normal displacement at all four edges are satisfied in an averaged manner as

$$\begin{aligned} \iint \frac{\partial u}{\partial x}\, dxdy &= \iint \left[\frac{1}{E}\left(F_{,yy} - \nu F_{,xx}\right) - \tfrac{1}{2}\, w^2{}_{,x}\right] dxdy, \text{ on } x = \pm\, a/2 \\ \iint \frac{\partial v}{\partial y}\, dydx &= \iint \left[\frac{1}{E}\left(F_{,xx} - \nu F_{,yy}\right) - \tfrac{1}{2}\, w^2{}_{,y}\right] dydx, \text{ on } y = \pm\, b/2 \end{aligned} \tag{8}$$

where u and v are inplane displacements. For the movable edges case, the edges are free to move as a rigid body with the average inplane stress equal to zero. The inplane boundary conditions are

$$\left.\begin{aligned} N_x &= h\int_{-b/2}^{b/2} F_{,yy}\, dy = 0 \\ u &= \text{constant} \end{aligned}\right\}, \qquad \text{on } x = \pm\, a/2 \tag{9}$$

$$\left.\begin{aligned} N_y &= h\int_{-a/2}^{a/2} F_{,yy}\, dx = 0 \\ v &= \text{constant} \end{aligned}\right\}, \qquad \text{on } y = \pm\, b/2$$

where N_x and N_y are membrane stress resultants per unit length in plate. By

making use of these inplane edge boundary conditions, equations (8) and (9), it easily can be shown that for the immovable edges

$$\bar{N}_x = \frac{q^2h^2E\pi^2}{8a^2(1-\nu^2)}(1 + \nu r^2)$$

$$\bar{N}_y = \frac{q^2h^2E\pi^2}{8a^2(1-\nu^2)}(r^2 + \nu) \tag{10}$$

and for the movable edges

$$\bar{N}_x = \bar{N}_y = 0 \tag{11}$$

the complete stress function is then given by $F = F_p + F_c$.

With the assumed w given by equation (4) and stress function given by equations (6) and (7), equation (1) is satisfied by applying Galerkin's method

$$\int_{-a/2}^{a/2} \int_{-b/2}^{b/2} L(w,F)\ w\ dxdy = 0 \tag{12}$$

from which yields the modal equation of the form

$$\ddot{q} + \omega_o^2\, q + \beta q^3 = \frac{p(t)}{m} \tag{13}$$

and

$$\omega_o^2 = \lambda_o^2 \frac{D}{\rho h b^4},\quad \lambda_o^2 = \pi^4 \left(1 + \frac{1}{r^2}\right)^2$$

$$m = \pi^2 \rho h^2/16 \tag{14}$$

$$\beta = \beta_p + \beta_c = (\beta_p^* + \beta_c^*) \frac{D}{\rho h b^4}$$

with

$$\beta_p^* = \frac{3\pi^4}{4r^4}(1 + r^4)(1 - \nu^2)$$

$$\beta_c^* = \frac{3\pi^4}{2r^4}(1 + 2\nu r^2 + r^4)$$

where ω_o is linear radian frequency, m is mass coefficient, and β is nonlinearity coefficient. The linear frequency λ_o, nonlinearity coefficients β_p^* and β_c^*, and aspect ratio r are all nondimensional parameters.

Clamped Panels. Yamaki (ref. 14) considered the predominant mode

$$w = \frac{q(t)h}{4}\left(1 + \cos\frac{2\pi x}{a}\right)\left(1 + \cos\frac{2\pi y}{b}\right) \tag{15}$$

which satisfies the clamped support conditions

$$\begin{aligned} w = w_{,x} &= 0, \qquad \text{on } x = \pm a/2 \\ w = w_{,y} &= 0, \qquad \text{on } y = \pm b/2 \end{aligned} \tag{16}$$

By introducing equation (15) in equation (2) and solving it, the particular stress function is

$$\begin{aligned} F_p = -\frac{1}{32} q^2 h^2 E r^2 \Big[&\cos Ax + \frac{1}{r^4}\cos By + \frac{1}{16}\cos 2Ax \\ &+ \frac{2}{(1+r^2)^2}\cos Ax \cos By + \frac{1}{16r^4}\cos 2By \\ &+ \frac{1}{(4+r^2)^2}\cos 2Ax \cos By + \frac{1}{(1+4r^2)^2}\cos Ax \cos 2By \Big] \end{aligned} \tag{17}$$

where $A = 2\pi/a$ and $B = 2\pi/b$. The complementary stress function is assumed as the form appearing in equation (7). Upon enforcing the inplane edge conditions, equations (8) and (9), it can be shown that for the immovable edges

$$\begin{aligned} \bar{N}_x &= \frac{3q^2h^2E\pi^2}{32\,a^2(1-\nu^2)}(1 + \nu r^2) \\ \bar{N}_y &= \frac{3q^2h^2E\pi^2}{32\,a^2(1-\nu^2)}(r^2 + \nu) \end{aligned} \tag{18}$$

and for the movable edges

$$\bar{N}_x = \bar{N}_y = 0 \tag{19}$$

the complete stress function is given by $F = F_p + F_c$. Introducing these expressions for w and F in equation (1) and applying Galerkin's procedure yields the equation

$$\ddot{q} + \omega_o^2 q + \beta q^3 = \frac{p(t)}{m} \tag{13}$$

where

$$\omega_o^2 = \lambda_o^2 \frac{D}{\rho h b^4}, \qquad \lambda_o^2 = \frac{16\pi^4}{9r^4}(3 + 2r^2 + 3r^4)$$

$$m = 9\,\rho h^2/16 \tag{20}$$

$$\beta = \beta_p + \beta_c = (\beta_p^* + \beta_c^*)\frac{D}{\rho h b^4}$$

and

$$\beta_p^* = \frac{4}{3}\pi^4(1-\nu^2)\left[1 + \frac{1}{r^4} + \frac{1}{16} + \frac{2}{(1 + r^2)^2} + \frac{1}{16r^4}\right.$$

$$\left. + \frac{1}{2(4 + r^2)^2} + \frac{1}{2(1 + 4r^2)^2}\right] \tag{21}$$

$$\beta_c^* = \frac{3\pi^4}{2r^4}(1 + 2\nu r^2 + r^4)$$

Equation (13) represents the undamped, large-amplitude vibration of a rectangular panel with simply supported or damped edges.

The methods commonly used for determining the damping coefficient are the bandwidth method in which half-power widths are measured at modal resonances, and the decay rate method in which the logarithmic decrement of decaying modal response traces is measured. The values of damping ratio ζ range from 0.005 to 0.05 for the common type of panel construction used in aircraft structures. Once the damping coefficient is determined from experiments or from existing data of similar construction, the modal equation, equation (13), now reads

$$\ddot{q} + 2\zeta\omega_o\dot{q} + \omega_o^2 q + \beta q^3 = \frac{p(t)}{m} \tag{22}$$

The method of equivalent linearization is then employed to determine an approximate root-mean-square (RMS) displacement from equation (22).

Method of Equivalent Linearization

The basic idea of the equivalent linearization (refs. 9 - 11) is to replace the original nonlinear equation, equation (22), with an equation of the form

$$\ddot{q} + 2\zeta\omega_o\dot{q} + \Omega^2 q + \text{err}\,(q) = \frac{p(t)}{m} \tag{23}$$

where Ω is an equivalent linear or nonlinear frequency, and err is the error of linearization. An equivalent linear equation is obtained by omitting this error term, then equation (23) is linear and it can be readily solved. The error of linearization is

$$\text{err} = (\omega_o^2 - \Omega^2)\, q + \beta q^3 \tag{24}$$

which is the difference between equation (22) and equation (23). The smaller that the error is, the smaller the error in neglecting it, and the better approximate solution to equation (22) will be obtained. To this end, the equivalent linear frequency square Ω^2 in the linearized equation is chosen in such a way that the mean-square error err^2 is minimized, that is

$$\frac{\partial(\text{err}^2)}{\partial(\Omega^2)} = 0 \tag{25}$$

If the acoustic pressure excitation p(t) is stationary Gaussian and ergodic, then the response q computed from the linearized equation, equation (23), must also be Gaussian. Substituting equation (24) into equation (25) yields (refs. 9, 13)

$$\Omega^2 = \omega_o^2 + 3\beta\overline{q^2} \tag{26}$$

where $\overline{q^2}$ is the maximum mean-square deflection of the panel. Dividing both sides of equation (26) by $D/\rho h b^4$ yields

$$\lambda^2 = \lambda_o^2 + 3\beta^*\overline{q^2} \tag{27}$$

where λ^2 is a nondimensional equivalent linear or nonlinear frequency parameter.

An approximate solution of equation (23) is obtained by dropping the error term; the mean-square response of amplitude is

$$\overline{q^2} = \int_0^\infty S(\omega)\,|H(\omega)|^2\, d\omega \tag{28}$$

where $S(\omega)$ is the spectral density function of the excitation pressure $\dot{p}(t)$, and the frequency response function $H(\omega)$ is given by

$$H(\omega) = \frac{1}{m(\Omega^2 - \omega^2 + 2i\zeta\omega_o\omega)} \tag{29}$$

For lightly damped ($\zeta \leq 0.05$) structures, the response curves will be highly peaked at Ω. The integration of equation (28) can be greatly simplified if the forcing spectral density function $S(\omega)$ can be considered to be constant in the frequency band surrounding the nonlinear resonance peak Ω, so that

$$\overline{q^2} \simeq \frac{\pi S(\Omega)}{4m^2\zeta\omega_o\Omega^2} \tag{30}$$

In practice, the spectral density function is generally given in terms of the frequency f in Hertz. To convert the previous result one must substitute

$$\Omega = 2\pi f \tag{31}$$

and $S(\Omega) = S(f)/2\pi$

into equation (30); the mean-square peak deflection is simply

$$\overline{q^2} = \begin{cases} \dfrac{32\ S_f}{\pi^4\zeta\lambda_o\lambda^2}, & \text{for simply supported panels} \\ \dfrac{32\ S_f}{81\zeta\lambda_o\lambda^2}, & \text{for clamped panels} \end{cases} \tag{32}$$

The pressure spectral density function $S(f)/2\pi$ has the units $(Pa)^2/Hz$ or $(psi)^2/Hz$, and S_f is a nondimensional forcing excitation spectral density parameter defined as

$$S_f = \frac{S(f)}{\rho^2h^4(D/\rho hb^4)^{3/2}} \tag{33}$$

The linear frequency parameters λ_o in equations (32) are given in equation (14) and equation (20) for simply supported and clamped panels, respectively, and the equivalent frequency parameters λ^2 can be determined through equation (27).

Solution Procedure

The mean-square response $\overline{q^2}$ in equation (30) (or equation 32) is determined at the equivalent linear frequency Ω (or λ) which is in turn related to $\overline{q^2}$ through equation (26) (or equation 27). To determine the mean-square deflection, an iterative procedure is introduced. One can estimate the initial mean-square deflection $\overline{q_o^2}$ using linear frequency ω_o through equation (30) as

$$\overline{q_o^2} = \frac{\pi S(\omega_o)}{4m^2\zeta\omega_o^3} \tag{34}$$

This initial estimate of $\overline{q_o^2}$ is simply the mean-square response based on linear theory. This initial estimate of $\overline{q_o^2}$ can now be used to obtain refined estimate

of Ω_1 through equation (26), $\Omega_1^2 = \omega_o^2 + 3\beta\,\overline{q_o^2}$, then $\overline{q_1^2}$ is obtained through equation (30) as

$$\overline{q_1^2} = \frac{\pi S(\Omega_1)}{4m^2\zeta\omega_o\Omega_1^2} \tag{35}$$

As the iterative process converges on the n-th cycle, the relation

$$\overline{q_n^2} = \frac{\pi S(\Omega_n)}{4m^2\zeta\omega_o\Omega_n^2} \simeq \overline{q_n^2} - 1 \tag{36}$$

becomes satisfied. In the numerical results presented in the following section, convergence is considered achieved whenever the difference of the RMS displacements satisfied the relation

$$\left| \frac{\sqrt{\overline{q_n^2}} - \sqrt{\overline{q_n^2} - 1}}{\sqrt{\overline{q_n^2}}} \right| \leq 10^{-3} \tag{37}$$

Stress Response

Once the RMS displacement is determined, the bending stresses on the surface of the panel can be determined from

$$\sigma_{xb} = -\frac{6D}{h^2}(w_{,xx} + \nu w_{,yy})$$

$$\sigma_{yb} = -\frac{6D}{h^2}(w_{,yy} + \nu w_{,xx}) \tag{38}$$

From equations (3) and (38), and using equations (4), (6), (7) and (10), the expressions for the nondimensional stresses on the surface of a simply supported panel with immovable edges are given by

$$\frac{\sigma_x b^2}{Eh^2} = (\sigma_{xb} + \sigma_{xm})\frac{b^2}{Eh^2} = \left[\frac{\pi^2}{2(1-\nu^2)}\left(\frac{1}{r^2} + \nu\right)\cos\frac{\pi x}{a}\cos\frac{\pi y}{b}\right] q$$

$$+ \left(\frac{\pi^2}{8r^2}\cos\frac{2\pi y}{b}\right)q^2 + \left[\frac{\pi^2(1 + \nu r^2)}{8r^2(1-\nu^2)}\right]q^2$$

$$\frac{\sigma_y b^2}{Eh^2} = (\sigma_{yb} + \sigma_{ym}) \frac{b^2}{Eh^2} = \left[\frac{\pi^2}{2(1-\nu^2)} \left(1 + \frac{\nu}{r^2}\right) \cos\frac{\pi x}{a} \cos\frac{\pi y}{b}\right] q$$

$$+ \left(\frac{\pi^2}{8} \cos\frac{2\pi x}{a}\right) q^2 + \left[\frac{\pi^2 (r^2+\nu)}{8r^2(1-\nu^2)}\right] q^2 \qquad (39)$$

For movable inplane edges, the last term in equation (39) vanishes. Similarly, from equations (3) and (38), and using equations (7), (15), (17), and (18), the expressions for the nondimensional tensile stresses on the surface of a clamped panel with immovable edges are

$$\frac{\sigma_x b^2}{Eh^2} = \frac{\pi^2}{2(1-\nu^2)} \left[\frac{1}{r^2} \cos Ax(1+\cos By) + \nu(1+\cos Ax) \cos By\right] q$$

$$+ \frac{\pi^2 r^2}{8}\left[\frac{1}{r^4} \cos By + \frac{2}{(1+r^2)^2} \cos Ax \cos By + \frac{1}{4r^4} \cos 2By\right.$$

$$\left. + \frac{1}{(4+r^2)^2} \cos 2Ax \cos By + \frac{4}{(1+4r^2)} \cos Ax \cos 2By\right] q^2$$

$$+ \left[\frac{3\pi^2 (1+\nu r^2)}{32r^2(1-\nu^2)}\right] q^2 \qquad (40)$$

$$\frac{\sigma_y b^2}{Eh^2} = \frac{\pi^2}{2(1-\nu^2)} \left[(1+\cos Ax) \cos By + \frac{\nu}{r^2} \cos Ax(1+\cos By)\right] q$$

$$+ \frac{\pi^2}{8} \left[\cos Ax + \frac{1}{4} \cos 2Ax + \frac{2}{(1+r^2)^2} \cos Ax \cos By\right.$$

$$\left. + \frac{4}{(4+r^2)^2} \cos 2Ax \cos By + \frac{1}{(1+4r^2)^2} \cos Ax \cos 2By\right] q^2$$

$$+ \left[\frac{3\pi^2 (r^2+\nu)}{32r^2(1-\nu^2)}\right] q^2$$

where $A = 2\pi/a$ and $B = 2\pi/b$. For movable edges, the last term in equation (40) vanishes.

Examining equations (39) and (40), a general expression is obtained for the stress at any point in the structure as

$$\sigma = C_1 q + C_2 q^2 \tag{41}$$

where C_1 and C_2 are constants. The constants can be determined from material properties, dimensions of the panel, and the location and direction at which the stress is to be measured. The mean-square stress is then related to the mean-square modal amplitude in a general expression as

$$\overline{\sigma^2} = C_1^2 \overline{q^2} + 3 C_2^2 (\overline{q^2})^2 \tag{42}$$

Once the mean-square deflection $\overline{q^2}$ is determined, equations (36) and (37), the mean-square stress can then be obtained from equation (42).

RESULTS AND DISCUSSION

Because of the complications in analysis of the many coupled modes, only one-mode approximation is used in the formulation. The assumption for fundamental mode predominacy is admittedly overly simplified; the conditions under which this is a valid approximation remain to be investigated. However, a simple model sometimes helps to give basic understanding of the problem.

Using the present formulation, response of nonlinear rectangular panels with all edges simply supported and all edges clamped subjected to broadband random acoustic excitation are studied. Both immovable and movable inplane edges are considered. In the results presented, the spectral density function of the excitation pressure S(f) is considered flat within a certain region near the equivalent linear frequency f and a value of Poisson's ratio of 0.3 is used in all computations, unless otherwise mentioned. Mean-square amplitudes and mean-square nondimensional stresses for panels of various aspect ratios and damping ratios are determined and presented in graphical form. These graphs can be used as guides for preliminary design of aircraft panels. The maximum mean-square deflection can be reasonably obtained from these figures; however, multiple modes had to be considered for accurate determination of mean-square stresses. This has been demonstrated by Seide in reference 15 for a simple beam subjected to uniform pressure excitation and in reference 16 for large deflections of prestressed simply supported rectangular plates under static uniform pressure. Comparison with experiment is also given. It is demonstrated that the present formulation gives remarkable improvement in predicating RMS responses as compared with using the linear theory.

Analytical Results

Figure 2 shows the maximum mean-square nondimensional deflection versus nondimensional spectral density parameter of acoustic pressure excitation for rectangular panels of aspect ratios r = 1, 2, and 4, and a damping ratio 0.02. It is clear from the figure that an increase of r will "close" the curve.

This occurs because as r increases, the panel becomes less stiff, and the mean-square deflection has to be finite. It can also be seen from the figure that the mean-square deflection of the movable inplane edges case is approximately twice as that of the immovable edges.

The maximum mean-square nondimensional stress (bending plus membrane stress, at the center of the panel and in the y-direction) is given in Figure 3 as a function of excitation spectral density parameter for simply supported rectangular panels of various aspect ratios and a damping factor 0.02. Results showed that the difference of maximum mean-square stresses between immovable and movable edges is small as compared with the difference of mean-square deflections between the two edge conditions.

Figure 4 shows the mean-square deflection versus forcing spectral density parameter for simply supported square panels of different damping ratios. The corresponding maximum mean-square stress (bending plus membrane stress, at the center of panel) is shown in Figure 5. As it can be seen from the figure that the precise determination of damping ratio from experiment is important, e.g., stress increases by 25-30 percent as ζ is decreased from 0.015 to 0.01 (for S_f between 5000 to 20000).

Plots of the equivalent linear or nonlinear frequency parameter λ^2 versus mean-square modal amplitude for simply supported rectangular panels of aspect ratios r = 1, 2, and 4 are shown in Figure 6. The lowest value of λ^2 corresponds to the linear case.

In Figure 7, the mean-square deflection is given as a function of excitation spectral density parameter for rectangular panels of aspect ratios r = 1, 2, and 4 and a damping ratio 0.02. The maximum mean-square deflection of the clamped panels is somewhat much less than that of the simply supported. The corresponding maximum mean-square nondimensional stress (bending plus membrane stress, in the y-direction and at the center of the long edge) versus spectral density parameter is shown in Figure 8.

Figure 9 shows the mean-square modal amplitude versus spectral density parameter of excitation for a square panel of different damping ratios. In Figure 10, the equivalent linear frequency parameter is given as a function of mean-square deflection for clamped rectangular panels of aspect ratios r = 1, 2, and 4.

Comparison with Experimental Results

The experimental measurements on skin-stringer panels exposed to random pressure loads reported in references 3 and 4 are used to demonstrate the improvement in predicting panel responses by using the present formulation. The structure was a skin-stringer, 3-bay panel as shown in Figure 11. The panels were constructed of 7075-T6 aluminum alloy. Details of the test facility, noise sources, test fixture, and test results are given in reference 3. The important properties of the panel are

Length	$a = 68.58$ cm (27 in.)
Width between the rivet lines	$b = 16.84$ cm (6.63 in.)
Thickness	$h = 0.81$ mm (0.032 in.)
Damping ratio	$\zeta = 0.0227$
Poisson's ratio	$\nu = 0.33$
Young's modulus	$E = 66.19 \times 10^3$ MPa (9.6×10^6 psi)
Weight density	$\rho = 7.164$ kg/m^3 (0.1 lb/in.^{3})

The tests were conducted with an overall sound pressure level (SPL) of 157 dB, with a range of $\pm$ 1.5 dB which corresponds to an average spectrum level of 125.26 dB (see Table IV of ref. 3 or Table 8 of ref. 17). The central bay of the 3-bay test panels is simulated by a flat rectangular plate. The linear frequencies for both simply supported (equation (14)) and clamped (equation (20)) support conditions are calculated and shown in Table 1. Test measurements and finite element solution are also given for comparison. Table 1 also shows the equivalent linear or nonlinear frequencies at overall SPL 157 dB.

Table 1. Frequency Comparison

	Natural frequency f_o	Equivalent linear frequency f_{157}
Simply supported - Immovable edges	71	321
- Movable edges	71	240
Clamped - Immovable edges	159	311
- Movable edges	159	264
Finite element (ref. 4)	155	N/A
Experiment (ref. 3)	126, 129	N/A

Frequency at high intensity noise level was not reported in reference 3. From the results shown in Table 1, it is clear that the central bay of the test panels did not respond to the acoustic excitation as though it were fully clamped on all four edges. This was also demonstrated in Figures 12 and 17 of reference 3 in the sense that the highest measured RMS strains did not occur at the center of the long edges. The central bay of the test panels actually behaved somewhat between fully simply supported and fully clamped support conditions.

The acoustic pressure spectral density S(f) is related to the spectrum level L as

$$S(f) = \begin{cases} 8.41 \times 10^{(L/10 - 18)} & (psi)^2/Hz \\ 4 \times 10^{(L/10 - 8)} & (dynes/cm^2)^2/Hz \end{cases} \quad (47)$$

A spatially uniform white noise pressure loading with spectral density of $S(f) = 2.824 \times 10^{-5}$ $(psi)^2/Hz$ (or nondimensional spectral density parameter $S_f = 5100$), which corresponds to an average spectrum level L = 125.26 dB, is used in the computations. The RMS stresses (equation (42)) at the center of the long edges for simply supported (equation (39)) and clamped (equation (40)) boundary conditions are calculated and given in Table 2.

Table 2. Stress Comparison

(RMS stress, kpsi at overall SPL 157 dB)

	$\sqrt{\overline{\sigma_x^2}}$		$\sqrt{\overline{\sigma_y^2}}$	
	Linear Theory	Nonlinear Theory	Linear Theory	Nonlinear Theory
Simply-Supported	0.0	0.58(Im.) 0.17(Movable)	0.0	3.28(Im.) 2.74(Movable)
Clamped	2.17	1.12(Im.) 1.32(Movable)	6.57	3.84(Im.) 4.24(Movable)
Finite Element (ref. 4)	2.4	NA	7.7	NA
Experiment (refs. 3, 4)				
Panel A		0.63		2.2
Panel B		0.94		2.9
Panel C		0.78		2.5
Panel D		1.1		-
Panel E		0.84		2.2
Average A-E		0.87		2.5

Table 3 shows the RMS deflections using the present formulation. The measured and finite element RMS stresses and RMS deflections in reference 4 are also given in the tables for comparison. It demonstrates that a better correlation between theory and experiment can be achieved when large deflection geometrical nonlinearity effect is included in the formulation.

Table 3. Deflection Comparison

$\sqrt{\overline{(w_{max}/h)^2}}$

	Linear Theory	Nonlinear Theory
Simply Supported	8.0	1.8 (Immovable) 2.4 (Movable)
Clamped	2.7	1.4 (Immovable) 1.6 (Movable)
Finite Element (ref. 4)	3.1	NA
Measured (refs. 3, 4)	-	2.0

CONCLUDING REMARKS

An analytical method for predicating response of rectangular nonlinear structural panels subjected to broadband random acoustic excitation is presented. The formulation is based on the Karman-Herrmann large deflection plate equations, a single-mode Galerkin approximation, the equivalent linearization method, and an iterative procedure. Both simply supported and clamped support conditions with immovable or movable inplane edges are considered. Panel mean-square deflection, maximum mean-square stress, and equivalent linear frequency at given excitation pressure spectral density can be determined, and they are presented in graphical form. These graphs can be used as guides for preliminary design of aircraft panels under high noise environment. Results obtained agree well with the experiment. It is suggested that further research be carried out with special attention to employ multiple modes in the formulation for accurate determination of mean-square stresses, and additional test data on simple panels are needed for an adequate quantitative comparison.

REFERENCES

1. Rudder, F. F., Jr. and Plumblee, H. E., Jr., "Sonic Fatigue Design Guide for Military Aircraft", AFFDL-TR-74-112, W-PAFB, OH, May 1975.

2. Fitch, G. E. et al, "Establishment of the Approach to and Development of Interim Design Criteria for Sonic Fatigue", ASD-TDR-62-26, W-PAFB, OH, June 1962.

3. Van der Heyde, R. C. W. and Smith, D. L., "Sonic Fatigue Resistance of Skin-Stringer Panels", AFFDL-TM-75-149-FYA, W-PAFB, OH, April 1974.

4. Jacobs, L. D. and Lagerquist, D. R., "Finite Element Analysis of Complex Panel to Random Loads," AFFDL-TR-68-44, W-PAFB, OH, October 1968.

5. Jacobson, M. J., "Advanced Composite Joints: Design and Acoustic Fatigue Characteristics," AFFDL-TR-71-126, W-PAFB, OH, April 1972.

6. Jacobson, M. J., "Sonic Fatigue Design Data for Bonded Aluminum Aircraft Structures," AFFDL-TR-77-45, W-PAFB, OH, June 1977.

7. Mei, C., "Large Amplitude Response of Complex Structures Due to High Intensity Noise," AFFDL-TR-79-3028, W-PAFB, OH, April 1979.

8. Chu, H. N. and Herrmann, G., "Influence of Large Amplitudes on Free Flexural Vibrations of Rectangular Elastic Plates," J. of Applied Mechanics, Vol. 23, December 1956, pp. 532-540.

9. Caughey, T. K., "Equivalent Linearization Techniques," JASA, Vol. 35, November 1963, pp. 1706-1711.

10. Caughey, T. K., "Nonlinear Theory of Random Vibrations," in Advances in Applied Mechanics, Vol. 11, Yih, C. S., ed., Academic Press, 1971, pp. 209-253.

11. Spanos, P. T. D. and Iwan, W. D., "On the Existence and Uniqueness of Solutions Generated by Equivalent Linearization," Int. J. of Non-Linear Mechanics, Vol. 13, 1978, pp. 71-78.

12. Timoshenko, S. and Woinowsky-Krieger, S., Theory of Plates and Shells, McGraw-Hill, 1959, pp. 415-428.

13. Lin, Y. K., "Response of a Nonlinear Flat Panel to Periodic and Randomly-Varying Loadings," J. Aero. Sci., September 1962, pp. 1029-1033, p. 1066.

14. Yamaki, N., "Influence of Large Amplitudes on Flexural Vibrations of Elastic Plates," Z. Angew. Math. Mech., Vol. 41, 1961, pp. 501-510.

15. Seide, P., "Nonlinear Stresses and Deflections of Beams Subjected to Random Time Dependent Uniform Pressure," ASME Paper No. 75-DET-23, 1975.

16. Seide, P., "Large Deflections of Prestressed Simply Supported Rectangular Plates under Uniform Pressure," Int. J. Non-Linear Mechanics, Vol. 13, 1978, pp. 145-156.

17. Van der Heyde, R. C. W. and Wolfe, N. D., "Comparison of the Sonic Fatigue Characteristics of Four Structural Designs," AFFDL-TR-76-66, W-PAFB, OH, September 1976.

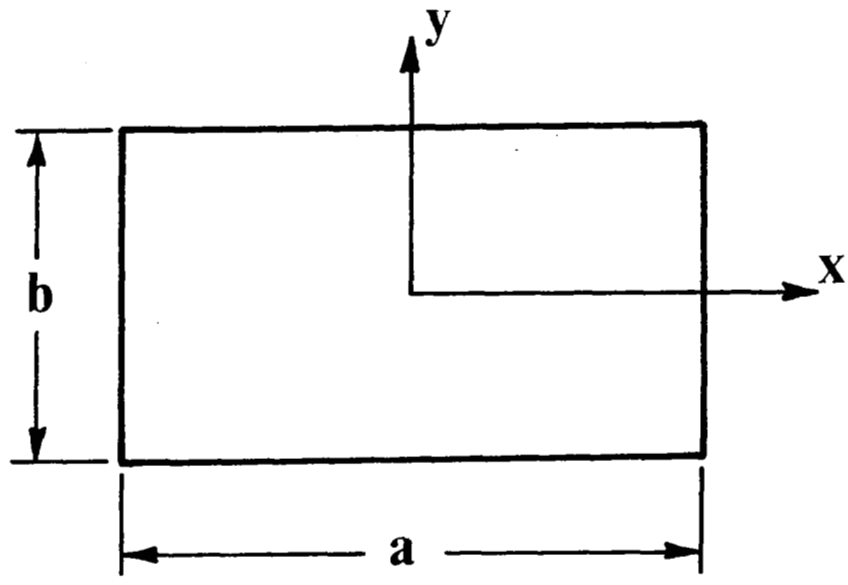

Figure 1. Geometry and coordinates.

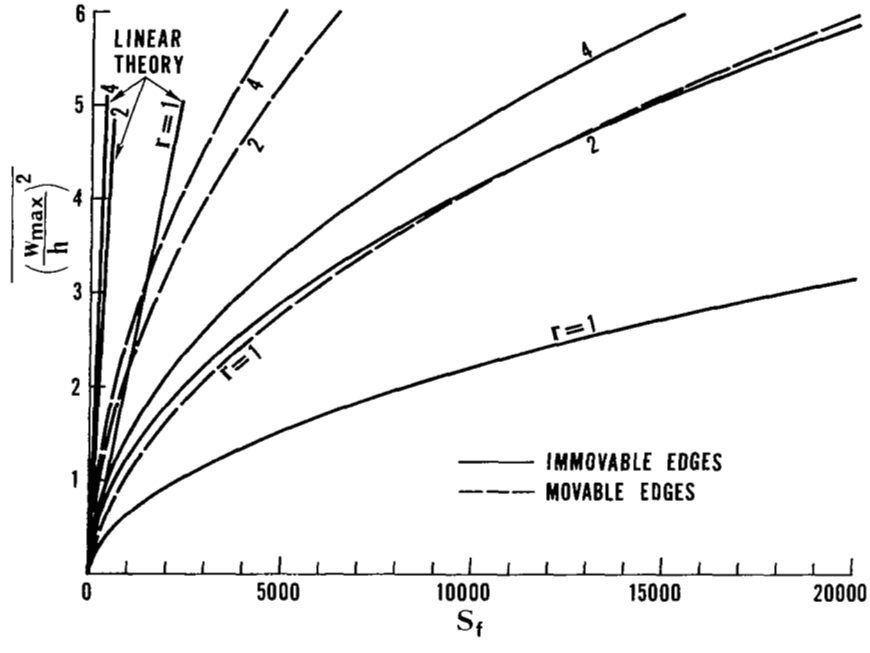

Figure 2. Mean-square deflection versus spectral density parameter of excitation for simply supported panels, $\zeta = 0.02$.

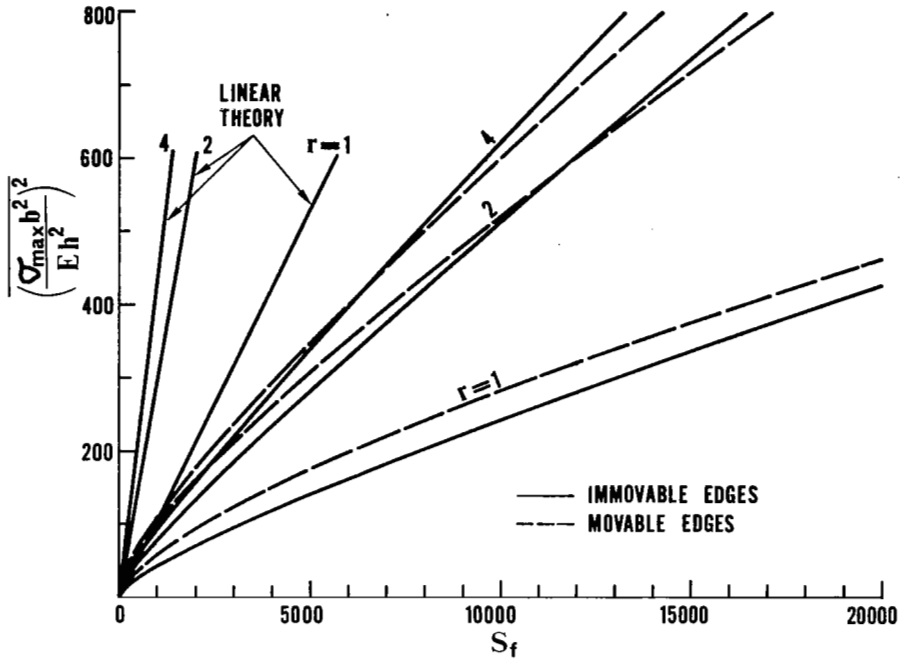

Figure 3. Maximum mean-square stress versus spectral density parameter of excitation for simply supported panels, $\zeta = 0.02$.

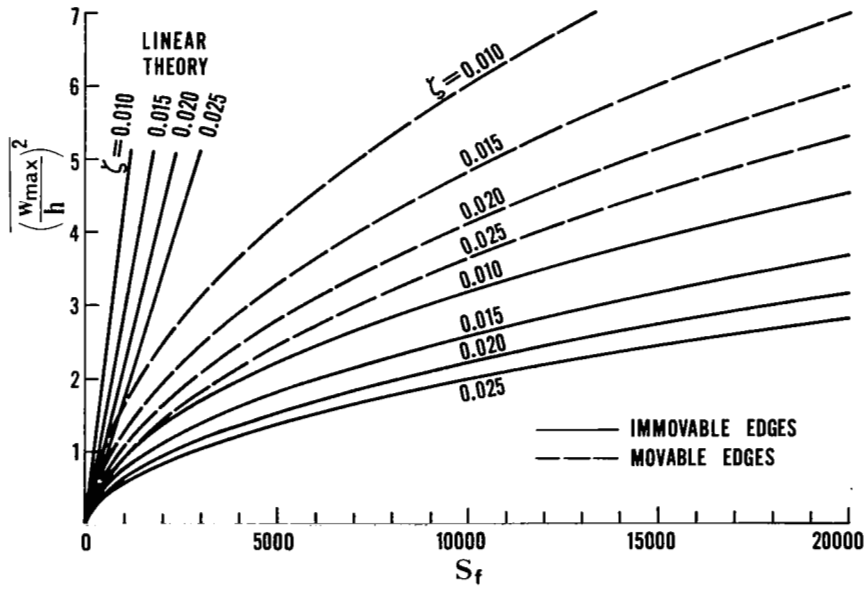

Figure 4. Effect of damping on mean-square deflection for a simply supported square panel.

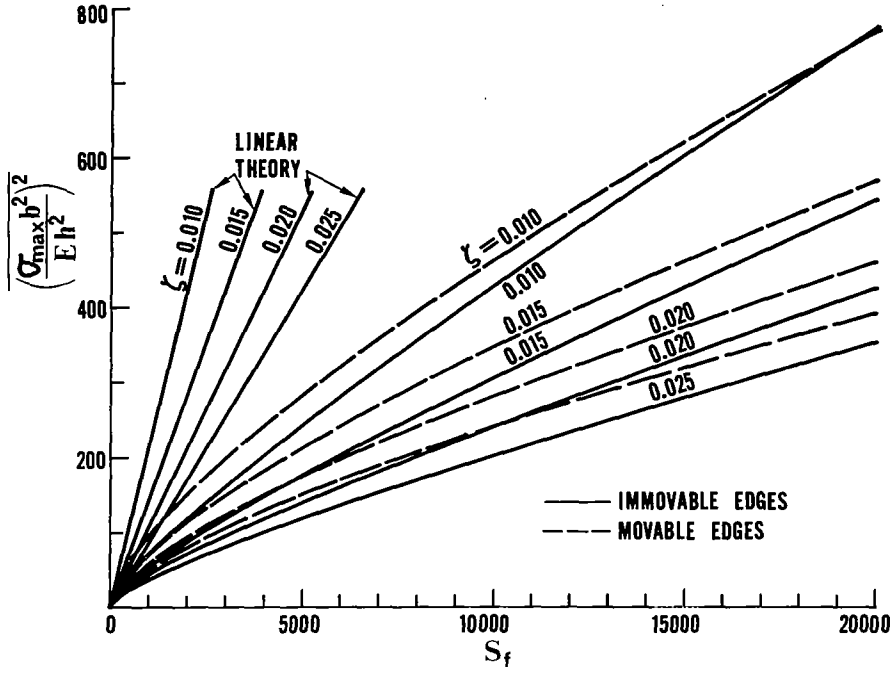

Figure 5. Effects of damping on maximum mean-square stress for a simply supported square panel.

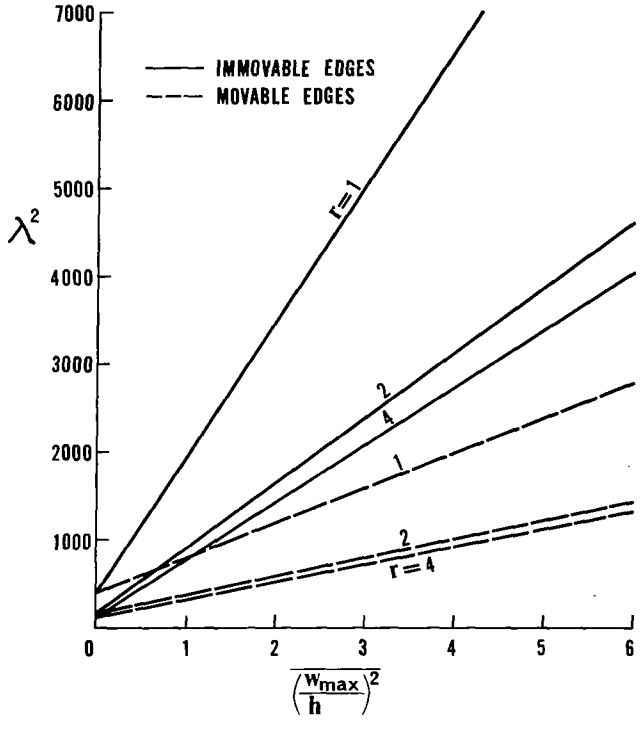

Figure 6. Frequency parameter versus mean-square deflection for simply supported panels.

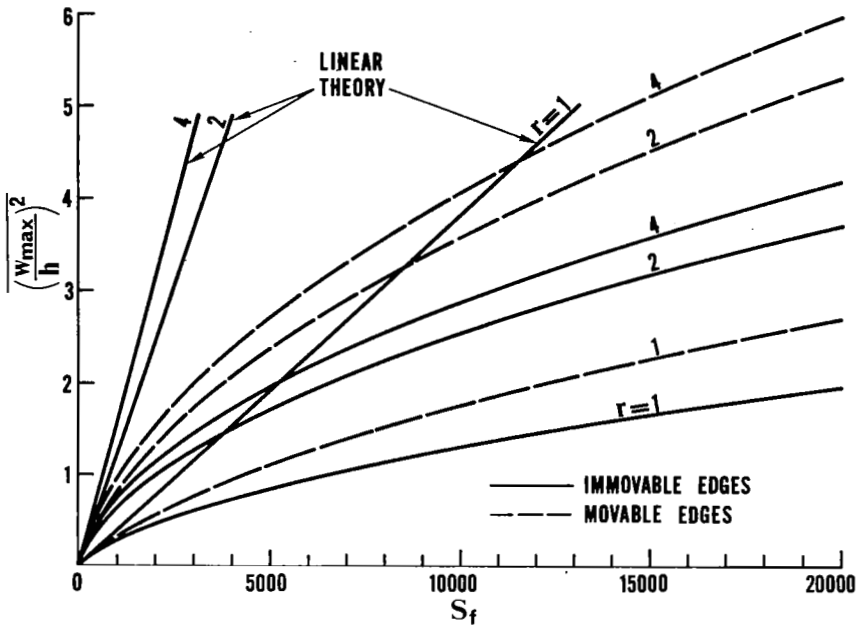

Figure 7. Mean-square deflection versus spectral density parameter of excitation for clamped panels, $\zeta = 0.02$.

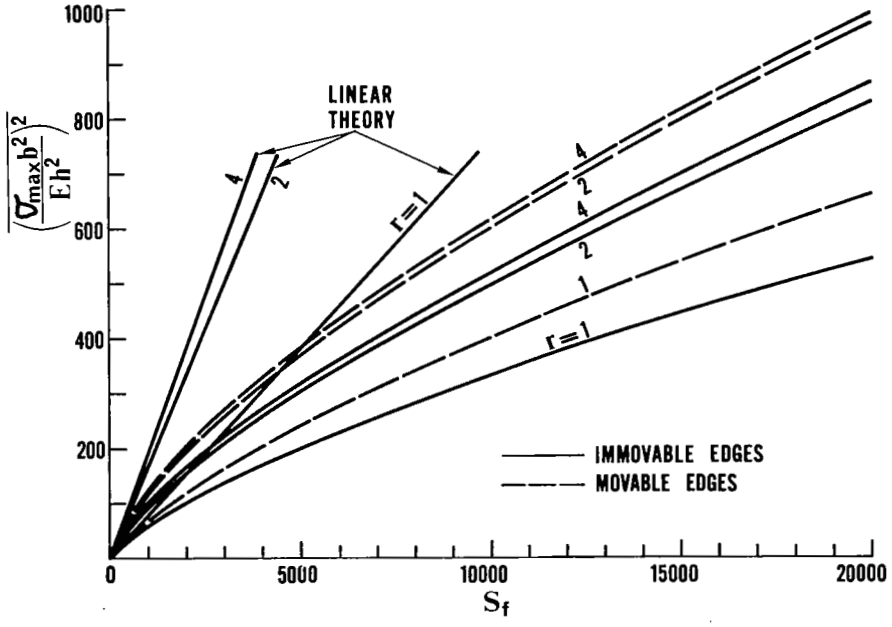

Figure 8. Maximum mean-square stress versus spectral density parameter of excitation for clamped panels, $\zeta = 0.02$.

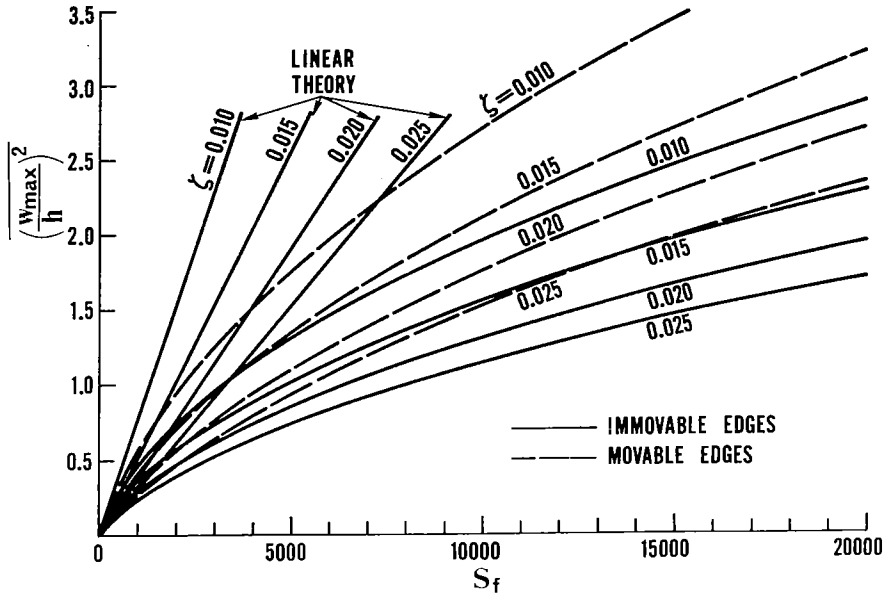

Figure 9. Effects of damping on mean-square deflection for a clamped square panel.

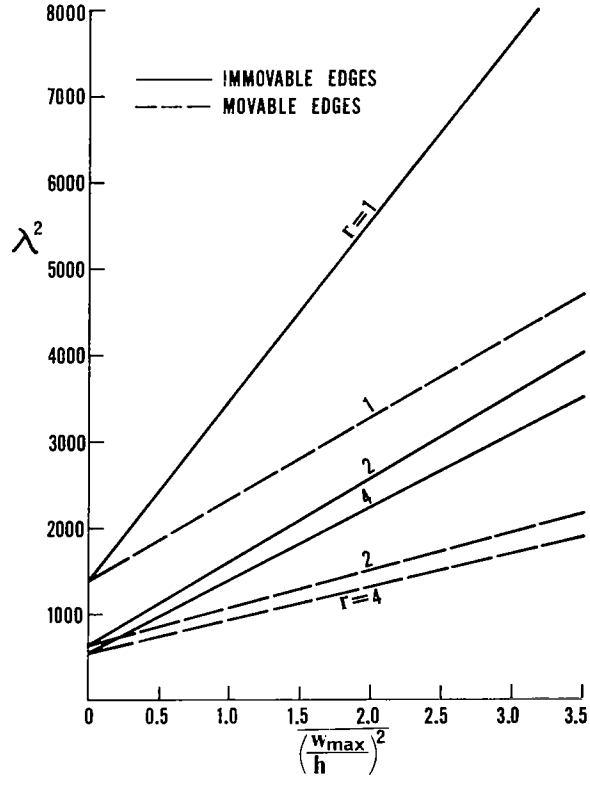

Figure 10. Frequency parameter versus mean-square deflection for clamped panels.

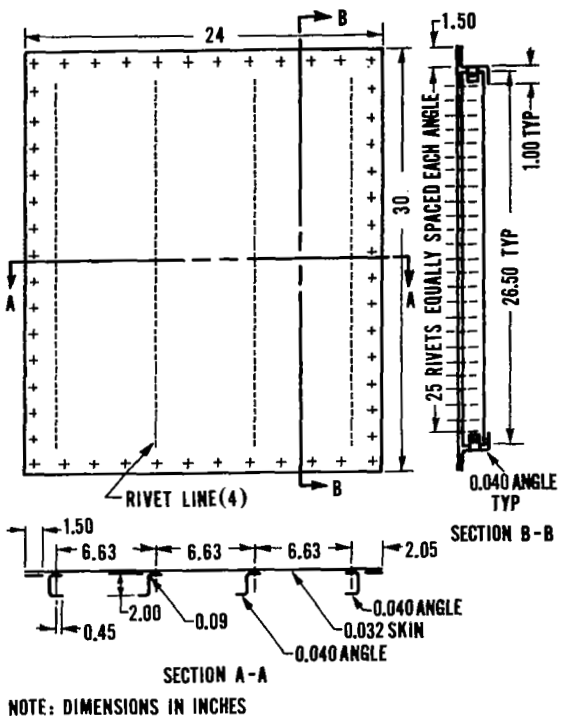

Figure 11. Skin-stringer panel (after Van der Heyde and Smith, ref. 3).

POST-BUCKLING BEHAVIOR OF A BEAM-COLUMN ON A NONLINEAR ELASTIC FOUNDATION WITH A GAP[1]

Edward N. Kuznetsov
Battelle Columbus Laboratories

Thomas G. Johns
Battelle Houston Operations

SUMMARY

The subject of this paper is the structural behavior of an elastic beam-column placed with a gap between two nonlinearly elastic layers each resting on a rigid foundation. The beam-column is laterally supported at both ends and subjected to a uniform transverse load and axial compression. Its slenderness is such that the axial compressive force exceeds the amount that would be necessary to buckle it as a simply supported column. The elastic layers are represented by an elastic foundation with a strongly nonlinear specific reaction taken as a rapidly increasing function of the layer compression. The analytical model developed simulates the entire pattern of the deflection and stress state including layer and end support reactions, under gradually increasing axial force.

INTRODUCTION

There are many cases when a primary buckling mode occurring at the onset of buckling cannot develop freely (References 1-2) because of changing constraint or support conditions. Such is, in particular, the case of a column with lateral supports arranged with gaps, etc. In this case, the post-buckling deflection is constrained laterally and the axial force can be increased by far in excess of its first critical value. As a result, the structural behavior is characterized by a sequence of alternating gradual changes in the deformed configuration and rather abrupt jumps from one equilibrium configuration to another. A similar behavior pattern was observed (Reference 3) for a compressed plate.

The subject of this paper is an elastic beam-column placed with a gap between two nonlinearly elastic layers each resting on a rigid foundation (Figure 1). The beam-column is laterally supported at both ends and subjected

[1] This study was sponsored by the American Gas Association Pipeline Research Committee.

to a uniform transverse load and axial compression. The elastic layers have a strongly nonlinear specific reaction taken as a rapidly increasing function of the layer compression. The problem consists in the analytical evaluation of the stress state and deflection under gradually increasing axial compression.

The deflection of the beam-column in consideration is small enough to justify the use of the conventional linearized expression for the curvature. However, there are two other sources of nonlinearity (nonlinearly elastic layers and the presence of a gap) which were fully accounted for. Note, that the presence of a transverse load makes the problem nonhomogeneous so that it is not a bifurcation problem.

ANALYTICAL FORMULATION AND SOLUTION METHOD

Under the above assumptions, vertical equilibrium of the beam-column requires that

$$F(Y) \cong EIY(x)^{IV} + PY(x)^{II} + Q(Y(x)) - G = 0 \qquad (1)$$

Here Y is the elastic deflection of the beam-column, EI is its flexural rigidity, P is the axial compression force, Q(Y) is the foundation reaction per unit length as a function of Y, G is the distributed transverse load (assumed uniform and constant), x' is the column longitudinal axis and prime denotes differentiation with respect to x.

The elastic foundation reaction is taken in the following form:

$$Q(Y) = \begin{cases} 0 & |Y| \leq c \\ (\text{sgn } Y)\ k\ (|Y| - c)^n & |Y| > c \end{cases} \qquad (2)$$

where k and n are given constants and c is the gap size. Thus, the foundation reaction is proportional to a power of the beam-column penetration into the elastic layer.

The self-correcting finite increment method (Reference 4) will now be applied for solving Equation (1). To this end the compression force P is given an infinitesimal increment p which results in some infinitesimal variation y(x) of deflection Y(x):

$$F(Y+y) \equiv EI(Y+y)^{IV} + (P+p)(Y+y)^{II} + Q(Y+y) - G = 0. \qquad (3)$$

Specializing Q(Y) in accordance with Equation (2) yields

$$F(Y) + EIy^{IV} + Py^{II} + pY^{II} + \begin{Bmatrix} 0 \\ kn(Y-c)^{n-1}y \end{Bmatrix} - G = 0. \qquad (4)$$

The operation performed is known as Frechet differentiation. It resulted in a linearized equation in unknown variation y(x) and is rigorous for infinitesimal increments only. The equation is extrapolated to small but finite increments which permits its use in a step-by-step solution procedure. A solution obtained at each step is an approximate one. Therefore, employing it as a starting point for the next step introduces some error in addition to that resulting from the next step itself. This is partially offset by a correction which consists in retaining the first term in Equation (4). For an exact Y(x), this term, according to Equation (1) would be an identical zero. Since in reality the solution obtained after the m-th step,

$$Y^m(x) = Y^{m-1}(x) + y^m(x), \tag{5}$$

is approximate, it does not turn F(Y) into zero. Retaining this term in Equation (4) compensates for the error of a current step solution thus preventing both systematic and occasional errors from passing to the next step and accumulation.

The solution of linearized Equation (4) is sought in the form of a linear combination of several approximating functions satisfying the boundary conditions of the problem:

$$y(x = \sum_{i=1}^{N} y_i \sin\frac{(2i-1)\pi x}{2\ell} \tag{6}$$

where ℓ is the beam half-length (Figure 2). As is readily seen, only symmetric configurations of the beam are taken into consideration. This was done because the particular case of interest is characterized by a relatively big transverse load, which precludes the antisymmetric configurations from occurrence at the early stages of post-buckling deformation. (The uniform transverse load would perform zero mechanical work over antisymmetric displacements).

The Galerkin method is now applied. It requires substituting the above y(x) into Equation (4), multiplying it by one of the approximating functions and integrating the product over the beam length. This results in a system of N linear algebraic equations in unknown parameters y_i with coefficients

$$a_{ii} = (D_i EI - P)D_i \frac{\ell}{2} + \int_0^{\ell} S(x) \sin^2 \frac{(2i-1)\pi x}{2\ell}\, dx \tag{7}$$

$$a_{ij} = \int_0^{\ell} S(x) \sin\frac{(2i-1)\pi x}{2\ell} \sin\frac{(2j-1)\pi x}{2\ell}\, dx$$

and free terms

$$a_{io} = -D_i Y_i p\frac{\ell}{2} + \int_0^{\ell} F(x) \sin\frac{(2i-1)\pi x}{2\ell} \tag{8}$$

where

$$D_i = [(2i-])\pi/2\ell]^2$$

$$S(x) = kn[Y(x)-c]^{n-1}$$

$$F(x) = \sum_{i=1}^{N} (D_i EI-P)\ D_i Y_i \sin \frac{(2i-1)\pi x}{2\ell} + Q\ [Y(x)]-G \qquad (9)$$

and

$$Y_i \equiv Y_i^{m-1} \qquad (10)$$

Obviously, making the axial force increments smaller improves the accuracy of the solution, but increases the number of solution steps. A reasonable compromise was achieved by arranging intermediate iterations in which Equation (4) was solved without incrementing the axial force (i.e., setting p = 0). In these iterations, the pattern of the beam interaction with the elastic layers is refined for the fixed magnitude of the axial force. Only after some assigned level of accuracy is reached, the axial force is given its next increment.

The specificity of the problem in consideration is that more than one equilibrium configuration may correspond to a given axial force. To determine whether other equilibrium configurations exist in the vicinity of the original one, the following approach is employed. Upon achieving the convergence of the internal iterations for a fixed value of the axial force, the system is perturbed by giving the deflection some random distortion and internal iterations are performed once again. This may result in overcoming the energy barriers separating the possible equilibrium configurations and increases the likelihood of solution convergence to the most stable configuration.

The perturbation is physically meaningful: it reflects imperfections in material properties, system geometry, load application and many other factors not accounted for explicitly. The magnitude of the distortion presumably correlates with the mentioned imperfections.

A computer program implementing the above features was written and applied to the analysis of a precompressed cryogenic pipeline.

NUMERICAL RESULTS AND DISCUSSION

The concept of preshortening a cryogenic pipeline by compression is intended to reduce or eliminate the need for thermal expansion/contraction devices. The concept involves the compression of one pipe (inner, conveying pipe) within another (casing pipe). The pipes are separated by thermal insulation and an air gap (clearance) exists between the insulation and the inner or the outer pipe. The magnitude of the compressive force is limited by the amount that can be tolerated in the inner pipe without its local inelastic buckling as a cylindrical shell (Reference 5). Under this force,

the column buckling behavior of the pipe was investigated to determine the effect of design variables such as the gap size, pipe length, insulation elastic properties, etc., upon the maximum stresses, lateral reactions, and amount of absorbed compressed length.

The following, rather typical data were used in one of the numerical examples:

- pipe length - 100 m (328 ft)
- pipe outer diameter - 46.7 cm (18 inches)
- wall thickness - 0.9525 cm (3/8 inch)
- clearance - 2.54 cm (1 inch)
- permissible stress - 320 MPa (46 ksi).

Figure 3 shows the evolution of the elastic deflection of the pipe as the compression force grows. Diagram 3a is the sagged configuration of the pipe resting on the elastic layer almost uniformly compressed. As the axial force is increased, the pipe bends and develops progressively increasing waviness (3b and c) till the end segment "snaps through" (3d). At this moment the pipe assumes another equilibrium configuration which continues its evolution in further loading (3e).

The results of numerical experiments confirmed the role of systematic perturbations applied during the analysis in order to obtain equilibrium states with lower total energy. In all cases the self-correcting finite increment method provided a rapid convergence of the computation process.

From the viewpoint of the precompression concept it was important to establish the role of the gap between the pipe and insulation. Conceivably, a wider gap could even be an advantage since it would provide more room with which to absorb the "excess" pipe length. A parametric study showed, however, an adverse effect of the gap on the relative compression of the pipe: the wider the gap, the greater the portion of the material strength spent on bending stress. Interestingly, the maximum stress (composed of the axial and bending stresses) does not grow monotonically with the compression force.

The performed study also revealed the role of the pipe length. As shown in Figure 4, the amount of compression that can be absorbed without exceeding the permissible stress increases for shorter lengths of pipe. The limiting case is the pipe length at which overall buckling does not occur at all.

REFERENCES

1. Thompson, J.M.T. and Hunt, G. W., "A General Theory of Elastic Stability," Wiley, London, 1973.

2. Budiansky, B., "Theory of Buckling and Post-Buckling Behavior of Elastic Structures," Advances Appl. Mech., Vol. 14, Academic Press, 1974.

3. Nakamura, T. and Uctani, K., Int. J. Mech. Sci., Vol. 21, No. 5, 1979.

4. Mescall, J., "Numerical Solutions of Nonlinear Equations for Shells of Revolution," AIAA Journal, Vol. 4, No. 11, 1966.

5. Volmir, A. S., "Stability of Elastic Systems," Moscow, 1963. (WPAFB Translation AD 628508, 1966).

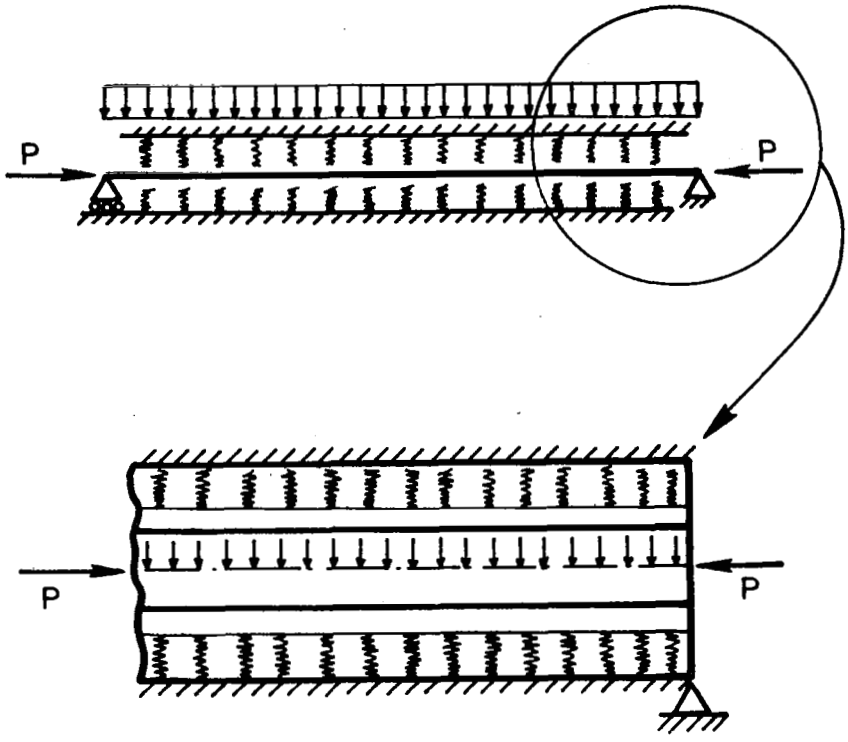

Figure 1.- Beam-column between two layers of elastic foundation with gap.

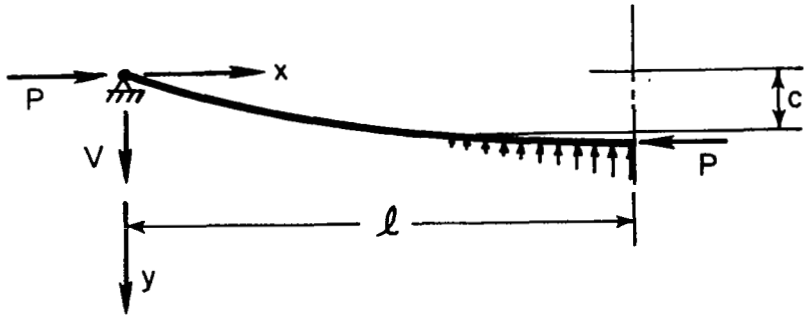

Figure 2.- Buckled column segment with partial contact with foundation.

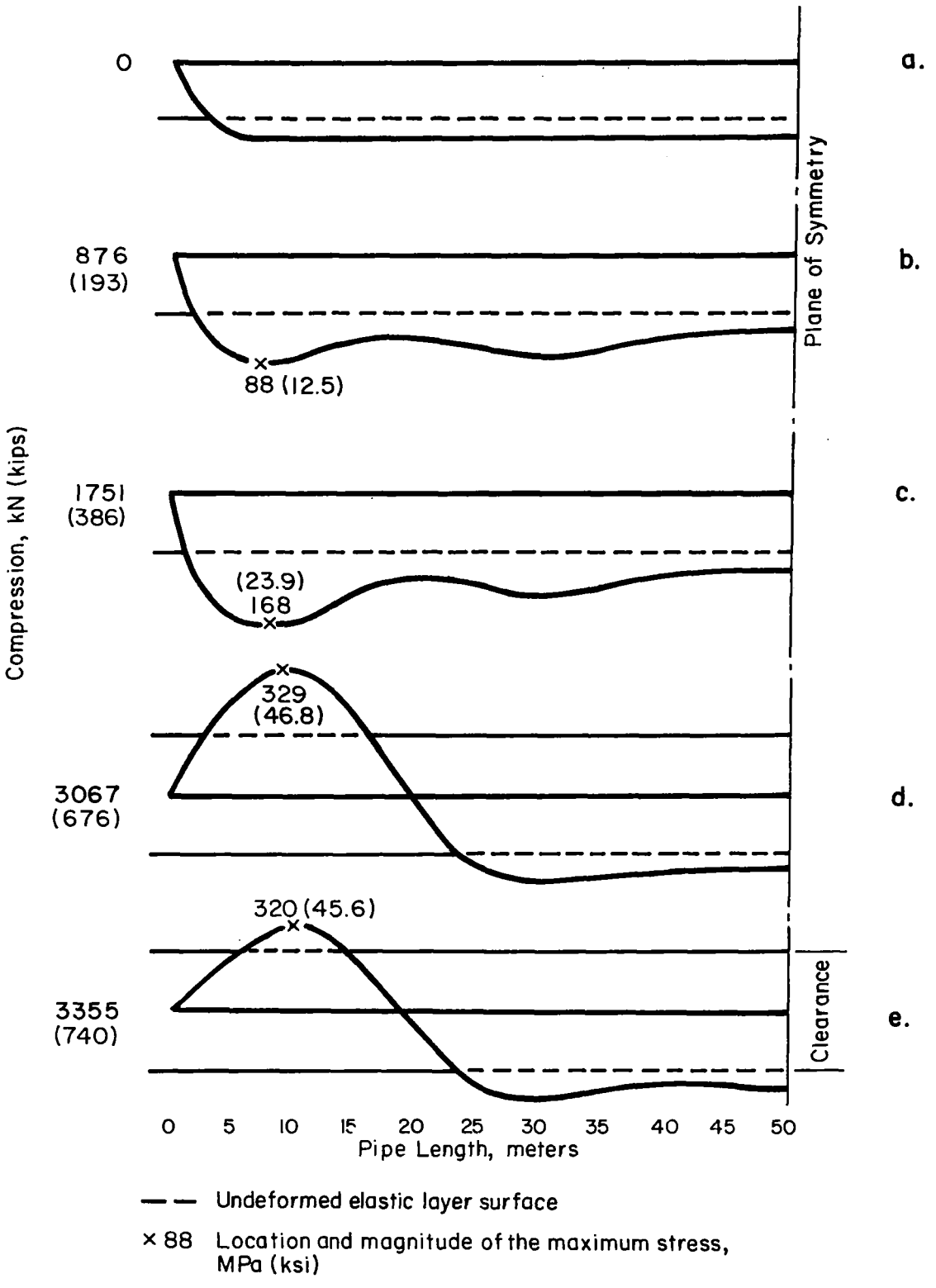

Figure 3.- Development of elastic deflected shape with increasing axial load.

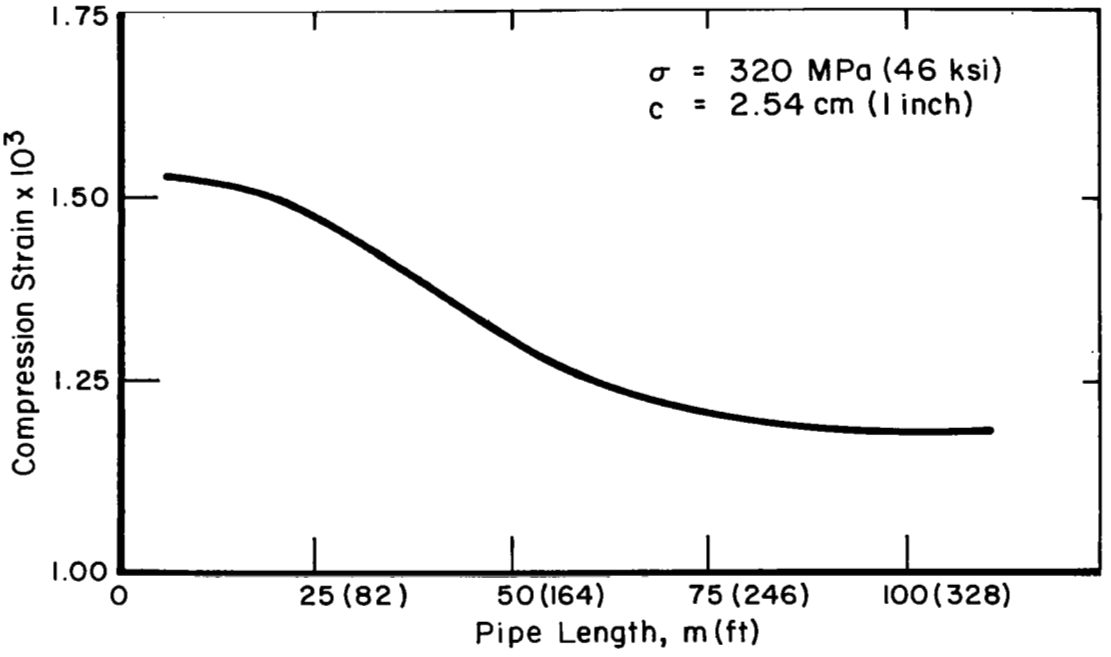

Figure 4.- Amount of compression that can be absorbed without exceeding the allowable stress versus pipe length.

STRAIGHTENING OF A WAVY STRIP - AN ELASTIC-PLASTIC CONTACT PROBLEM INCLUDING SNAP-THROUGH

Dieter F. Fischer and Franz G. Rammerstorfer
VOEST-ALPINE AG, FAT, Linz, Austria

SUMMARY

This paper deals with calculating the non-linear behaviour of a wave-like deformed metal strip during the levelling process. Elastic-plastic material behaviour as well as nonlinearities due to large deformations are considered. The considered problem leads to a combined stability and contact problem. It is shown that, despite of the initially concentrated loading, neglecting the change of loading conditions due to altered contact domains may lead to a significant error in the evaluation of the nonlinear behaviour and particularly to an underestimation of the stability limit load. The stability is examined by considering the load deflection path and the behaviour of a load-dependent current stiffness parameter in combination with the determinant of the current stiffness matrix.

INTRODUCTION

The stability of nonlinear structures is the goal of many recent papers. Especially the snap-through behaviour of initially curved slender bars has been analytically as well as numerically considered (e.g. ref. 1,2). But investigations in which the influence of contact between the loading and the loaded structures is considered are rather rare. Such a combined contact and stability problem will be treated in this paper. In order to show how the loading conditions influence the nonlinear behaviour and the stability limit in particular, let us draw our attention to the following simple example.

Figure 1 shows a shallow circular arch which is loaded once directly by a concentrated load and in a second case by a rigid horizontal plane plate moved towards the arch. The latter is treated as a contact problem. In both cases, symmetry with respect to the vertical axis is assumed for simplicity.

Applying the algorithm which is described later we get results shown in figure 2. In figure 2 the load displacement path, $P(w)$, the dependence of the normalized determinant of the current stiffness matrix, $\det_n \underline{K}(P)$, and of the current stiffness parameter (ref. 3,4), $CS(P)$, on the applied load, P, is described. In both cases, distinct snap-through behaviour can be observed by considering the final tangent of the $\det_n \underline{K}(P)$ curve which crosses the P-axis perpendicularly (ref. 5). Also the vanishing current stiffness parameter, CS, indicates snap-through. However in the case b (load application by a rigid plate) a significantly higher stability limit than in case a was found. Thus,

it is important to recognize the altering loading conditions even if the load is applied at a single point in the initial state (i.e. at a very low load level). The problem being dealt with in the following chapters is a typical stability and contact problem.

DESCRIPTION OF THE WAVED STRIP PROBLEM

The behaviour of an infinite strip with periodic wave-like initial out-of-plane deformations is investigated during a straightening process. Periodic out-of-plane deformations at the boundaries (fig. 3) or in the middle domain of the strip sometimes appear in metal sheets as a consequence of the rolling process. The straightening is based on plastic deformations caused by moving the strip through a leveller in which it is bent by rollers in a repeated manner. In some cases, a snap-through of the waves can be observed which renders an unsuccessful result of the levelling process. In order to find proper conditions for avoiding snap-through, a procedure for calculating the non-linear elastic-plastic stability problem was developed. The deformations during levelling are caused by rather stiff rollers. A contact problem has to be solved simultaneously with the stability problem in order to account for the stiffening effect due to expanded contact.

To approach the real behaviour of the waved strip during the levelling process by mathematical investigation, the complicated transient problem is simplified to a static consideration: The nonlinear behaviour of the shaded area of the strip in figure 3 under a downward moving rigid roller is calculated with the aid of the finite element method.

THE MATHEMATICAL MODEL

The following data were taken from an example in which instabilities in the practical levelling process were observed: B = 3500 mm, L = 1000 mm, S = 20 mm, t = 10 mm. The material is assumed to be elastic-plastic with linear strain hardening. The following material properties correspond to experimentally derived values at a temperature of 600 ^{o}C (the strip temperature during the levelling process): E = 180000 N/mm^2 (Youngs' modulus), ν = 0.3 (Poisson's ratio), σ_y = 130 N/mm^2 (initial yield stress), E_T = 5000 N/mm^2 (strain hardening modulus). The shaded area in figure 3 under consideration represents a doubly curved shallow shell which is modeled using ADINA shell elements (ref. 6). These elements allow for nonlinear material behaviour as well as geometric nonlinearities using the total Lagrangian formulation. Figure 4 shows the finite element model.

The midsurface of the shell is approximated by

$$z(x,y) = S \frac{4y^2}{B^2} \sin \frac{(L-2x)\pi}{2L} . \qquad (1)$$

As shown in reference 7 the contact conditions can be verified with the aid of contact elements. These contact elements are simple truss elements

which have a certain nonlinear elastic material behaviour (figure 5).

The contact elements give only contributions to the global current stiffness matrix if the shell nodes to which they are attached belong to the contact area. They allow only transmission of compression forces corresponding to the contact pressure. Before a shell node becomes a contact point, the gap between the rigid roller and the shell surface must be closed. This is accounted for in the location-dependent activating strain, $\varepsilon_{gap}(y)$:

$$\varepsilon_{gap}(y) = - \frac{S - z(x=0,y)}{S + h - z(x=0,y)} \qquad (2)$$

The values of the tangent moduli, E_1, E_2, the stresses, σ_1^* and σ_2^*, the fictitious length, h, and the cross section area, A, of the contact elements must be properly chosen. This means that the contact elements should be stiff enough to prevent the roller from penetrating in the shell and, that the properties must not lead to a numerical instability of the incremental-iterative algorithms described below. The following values appear in the presented analysis: $E_1 = 1000\ N/mm^2$, $E_2 = 7500\ N/mm^2$, $\sigma_1^* = -5\ N/mm^2$, $\sigma_2^* = -20\ N/mm^2$, $h = 80\ mm$, $A = 1000\ mm^2$. These values render a well-conditioned system of equations. If one would like to regard the local compressibility of the roller, a certain choice of the σ-ε-behaviour of the contact elements would make it possible. Furthermore, bending deformations of the roller could be considered, if beam elements would represent the axis of the roller instead of the rigid line $\overline{BC}$ (figure 4). Both effects, local compressibility and bending of the roller, are negligible in the investigated example.

In order to represent the periodicity of the structure, the boundary conditions of the finite element model are introduced as shown in figure 4. The waved strip will elongate globally due to the levelling process. For the x-displacement at the boundary $x = L/2$ the following restriction is valid: $u_x(x=L/2,y) = u_x(x=L/2,y=0)$.

DESCRIPTION OF THE ALGORITHMS

The analysis is performed in an incremental-iterative manner, using the tangent stiffness matrix concept and the BFGS iteration procedure as described elsewhere, e.g. in references 8,9. Let us concentrate our attention to the stability algorithms. Algorithms which treat nonlinear stability problems as a sequence of eigenvalue problems are described in recent papers (e.g. ref. 10 - 12). Let us now use the normalized determinant of the current tangent stiffness matrix, $\det_n \underline{K}$, and the current stiffness parameter, CS, recently introduced by Bergan (ref. 3,4) as indicators for the stability behaviour of the structure during the lowering of the rigid roller. It is a well-known fact that at the stability limit, $\lambda \rightarrow \lambda_{crit}$ (λ... load amplifier, λ_{crit}... critical load amplifier), the determinant of the tangent stiffness matrix vanishes:

$$\lim_{\lambda \rightarrow \lambda_{crit}} \det \underline{K}(\lambda) = 0. \qquad (3)$$

This criterion holds for both buckling as well as snap-through because it is based on the existence of a nontrival solution $\underline{\delta_u}$ of the equation

$$\underline{K}(\lambda_{crit}) \cdot \underline{\delta_u} = \vec{0}, \tag{4}$$

valid at the bifurcation point and at the snap-through point.

One can distinguish between buckling and snap-through by considering how the determinant approaches zero (ref. 5,10): In the buckling case

$$\lim_{\lambda \to \lambda_{crit}} \frac{\partial \det K}{\partial \lambda} = (-\infty, 0) \tag{5}$$

holds. If the determinant behaves according to

$$\lim_{\lambda \to \lambda_{crit}} \frac{\partial \det K}{\partial \lambda} = -\infty \tag{6}$$

snap-through is indicated.

The Gauss elimination procedure which is implemented in ADINA (ref. 6) is used in combination with the LDL^T fractorization (ref. 13) to solve the finite element equation system during the incremental-iterative analysis. Thus, it is almost no effort to calculate the determinant of the nxn stiffness matrix using the following relations:

$$\underline{K} = \underline{L}\,\underline{D}\,\underline{L}^T, \tag{7}$$

$\underline{L}$ is a lower unit triangular matrix and $\underline{D}$ is a diagonal matrix. Hence,

$$\det \underline{K} = \det \underline{D} = \prod_{i=1}^{n} D_{ii}. \tag{8}$$

This det $\underline{K}$ is normalized so that $\det_n \underline{K}(\lambda=0) = 1$. At each load level at which a further contact element is activated, the current global stiffness matrix increases suddenly due to the added contribution of the activated contact element. In order to avoid discontinuities in the $\det_n \underline{K}(\lambda)$ curve the current $\det_n$ values are smoothened by a further normalizing procedure which levels the $\det_n$ value just after a jump to that which appeared immediately before it. It might be proper to delete all contributions related to the contact elements from the current stiffness matrix if $\det_n \underline{K}(\lambda)$ is calculated. This would represent the determinant behaviour of the shell itself and the contact would only contribute to the load vector on the right-hand side of the incremental finite element equations.

The current stiffness parameter, ${}^{i}CS$, has the following meaning (i denotes the increment number): It represents the current stiffness of the structure as being a relation between a load increment and the corresponding displacement increment. Assuming proportional loading one can express

$${}^{i}\underline{R} = {}^{i}\lambda \underline{R}_{ref}. \tag{9}$$

${}^{i}\underline{R}$ denotes the external load vector at load level ${}^{i}\lambda$, $\underline{R}_{ref}$ is the constant reference load vector. Relating the current stiffness to the initial stiffness

(with ${}^{1}\lambda \ll 1$) ${}^{i}CS$ can be defined as

$$ {}^{i}CS = \frac{({}^{i}\lambda - {}^{i-1}\lambda)/\|{}^{i}\underline{u} - {}^{i-1}\underline{u}\|}{{}^{1}\lambda/\|{}^{1}\underline{u}\|} \tag{10} $$

using the Euclidean norm of the incremental displacement vector to scale the relations.

The combination of the determinant analysis and the current stiffness parameter calculation offers a good tool to predict the stability limit, λ_{crit}, as well as the instability mechanism (i.e. buckling or snap-through) as shown in reference 14.

DISCUSSION OF THE RESULTS

Figure 6 shows the load displacement path of the initial contact point (node A in figure 4), the normalized determinant of the stiffness matrix, $\det_n \underline{K}(\lambda)$, and the current stiffness parameter, $CS(\lambda)$. The results of the analysis of the same shell loaded by a concentrated load in A are also presented in figure 6 as a comparison. The following facts can be observed: In both cases a stability limit is reached and snap-through of the wave takes place. The shell loaded by the roller behaves significantly stiffer than the point-loaded shell. This is caused by the altering loading conditions due to the increasing contact domain as explained above. In the concentrated load approach, a horizontal tangent of the load displacement path is reached before considerable plastification takes place. In the contact solution, plastic domains appear in the vicinity of the contact area long before a significant stiffness loss (i.e. a rapid decrease of CS) can be observed.

In figure 7 the deformed state of the shell immediately before snap-through is shown. One can see that the contact domain between roller and strip is considerable. Furthermore, it is interesting to notice that the initial contact point A belongs no longer to the contact area.

CONCLUSION

From these considerations one can conclude that neglecting the change of loading conditions due to deformation dependent contact conditions may lead to an unnegligible error even if initially concentrated load conditions are justified.

REFERENCES

1. Pisanti, A.: Geometrically Nonlinear Behaviour of Initially Curved Plane Slender Bars and Frames. Inenieur-Archiv, Vol. 46, pp. 235 - 244, 1977.

2. Noor, A.K., Greene, W.H. and Hartley, S.J.: Nonlinear Finite Element Analysis of Curved Beams. Computer Methods Appl. Mech. Eng., Vol. 12, pp. 289 - 307, 1977.

3. Bergan, P.G., Horrigmoe, G., Kråkeland, B. and Søreide, T.H.: Solution Techniques for Non-Linear Finite Element Problems. Int. J. Numer. Methods Eng., Vol. 12, pp. 1677 - 1696, 1978.

4. Bergan, P.G.: Solution Algorithms for Nonlinear Structural Problems. Proc. Int. Conf. Eng. Appl. FEM, Høvik, Norway, 1979.

5. Gallagher, R.H. and Mau, S.: A Method of Limit Point Calculation in Finite Element Structural Analysis, NASA CR-2115, 1972.

6. Bathe, K.-J.: ADINA, A Finite Element Program for Automatic Dynamic Incremental Nonlinear Analysis, M.I.T. Report 82448-1, Acoustics and Vibration Laboratory, Mechanical Engineering Department, Mass. Inst. Techn., 1975 (Rev. 1978).

7. Rammerstorfer, F.G., Fischer, D. and Zitz, A.: Rock Bursting - A Nonlinear Dynamic Contact Problem, Num. Methods in Geomechanics, W. Wittke, A.A. Balkema, Rotterdam, 1979.

8. Bathe, K.-J., Bolourchi, S., Ramaswamy, S. and Snyder, M.D.: Some Computational Capabilities for Nonlinear Finite Element Analysis. Nucl. Eng. Design, Vol. 46, pp. 429 - 455, 1978.

9. Matthies, H. and Strang, G.: The Solution of Nonlinear Finite Element Equations, Int. J. Numer. Methods Eng., Vol. 14, pp. 1613 - 1626, 1979.

10. Ramm, E.: Geometrisch nichtlineare Elastostatik und finite Elemente, Habilitationsschrift, Univ. Stuttgart, 1975.

11. Brendel, B.: Geometrisch nichtlineare Elastostabilität, Bericht Nr. 79-1, Inst. f. Baustatik d. Univ. Stuttgart, 1979.

12. Brendel, B., Ramm, E., Fischer, D. and Rammerstorfer, F.G.: Linear and Nonlinear Stability Analysis of Thin Cylindrical Shells Under Wind Loads. To be published in J. Struct. Mech., Vol. 9, 1981.

13. Bathe, K.-J. and Wilson, E.L.: Numerical Methods in Finite Element Analysis, Prentice-Hall, Inc., Englewood Cliffs, New Jersey, 1976.

14. Rammerstorfer, F.G. and Fischer, D.F.: Nonlinear Elastic-Plastic Stability and Contact Problems Concerning the Straightening of a Wave-Like Deformed Strip Plate. Proc. 1st Int. Conf. Num. Methods for Non-Linear Problems, Swansea, Pineridge Press, 1980.

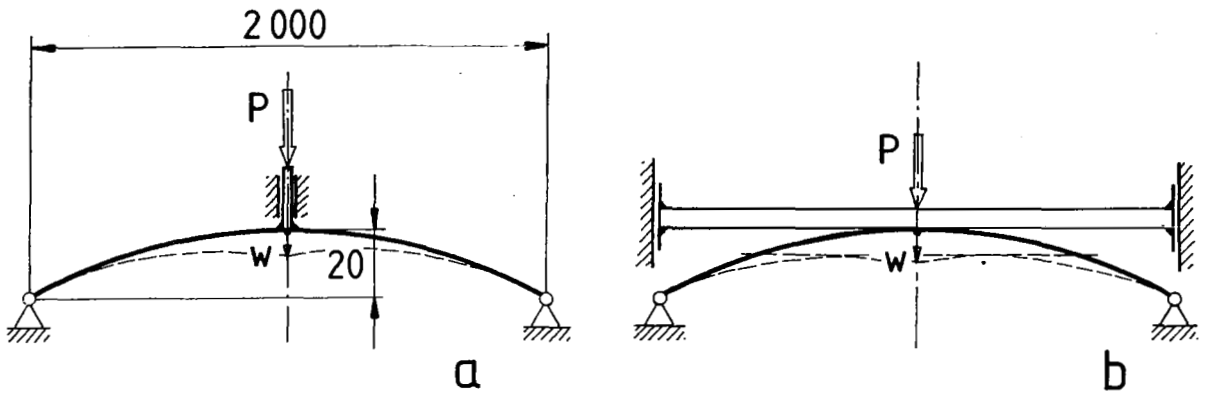

$EJ = 2.5 \times 10^{8}\ Nmm^{2}$

$EA = 3.0 \times 10^{7}\ N$

Figure 1.- The circular arch loaded by concentrated load directly (a) or via rigid plate (b).

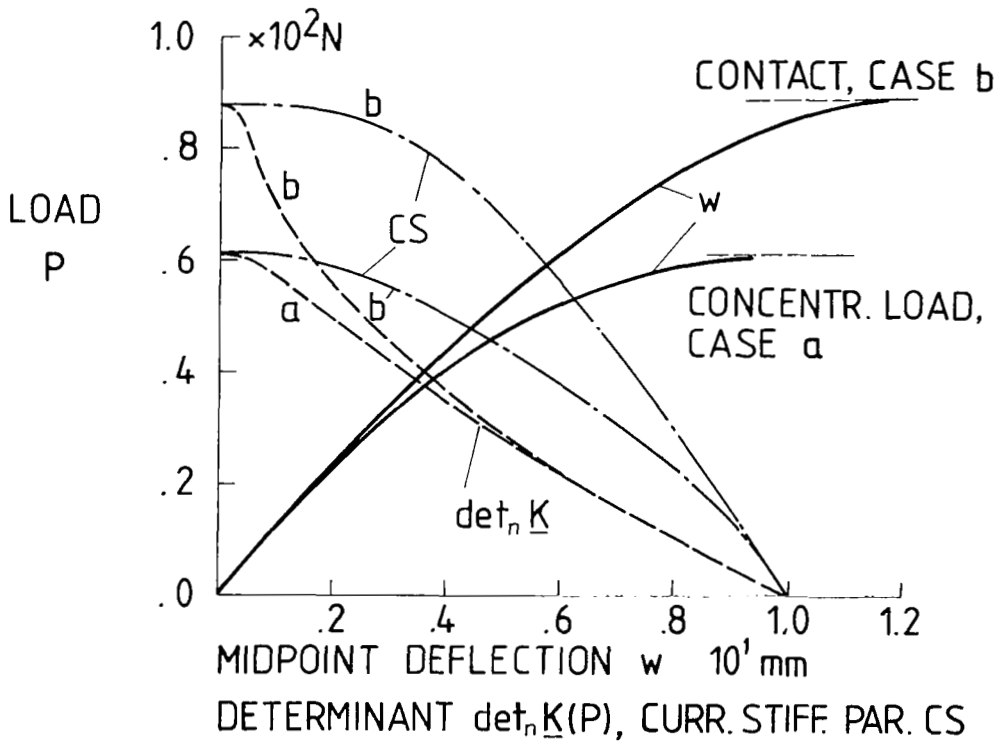

Figure 2.- Load displacement behaviour, normalized determinant of the current stiffness matrix and current stiffness parameter for the two different loading conditions.

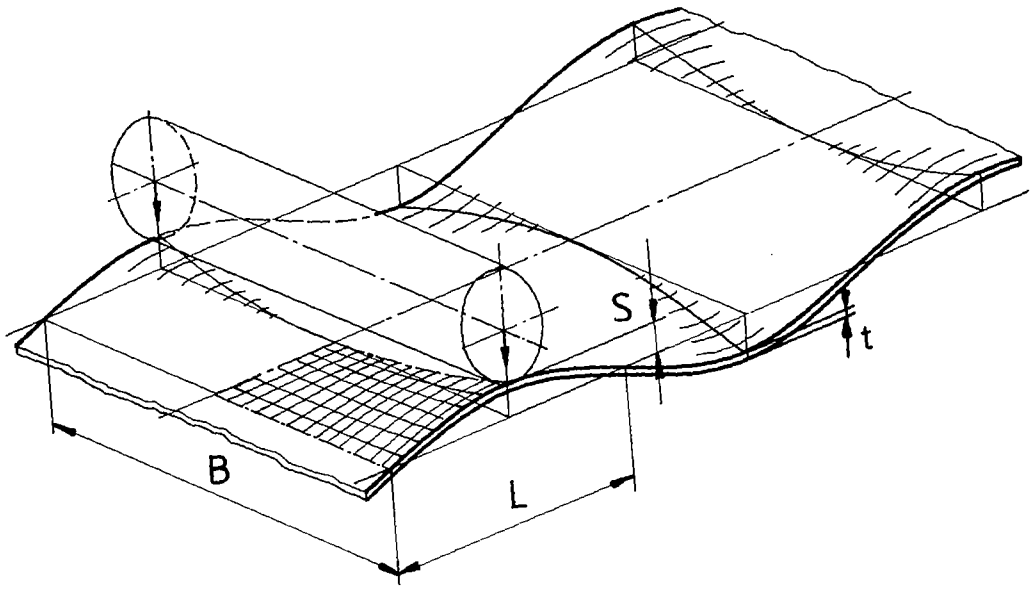

Figure 3.- The waved strip.

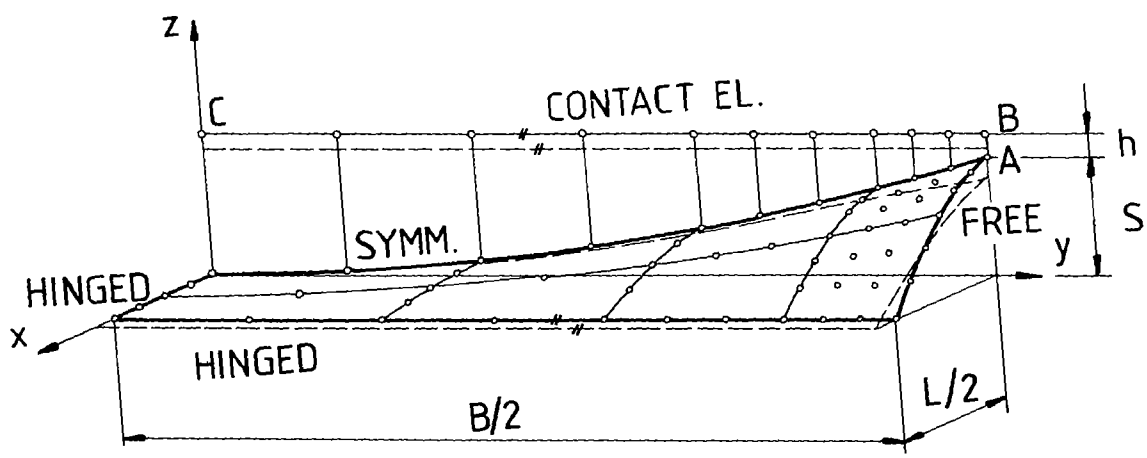

Figure 4.- The finite element model.

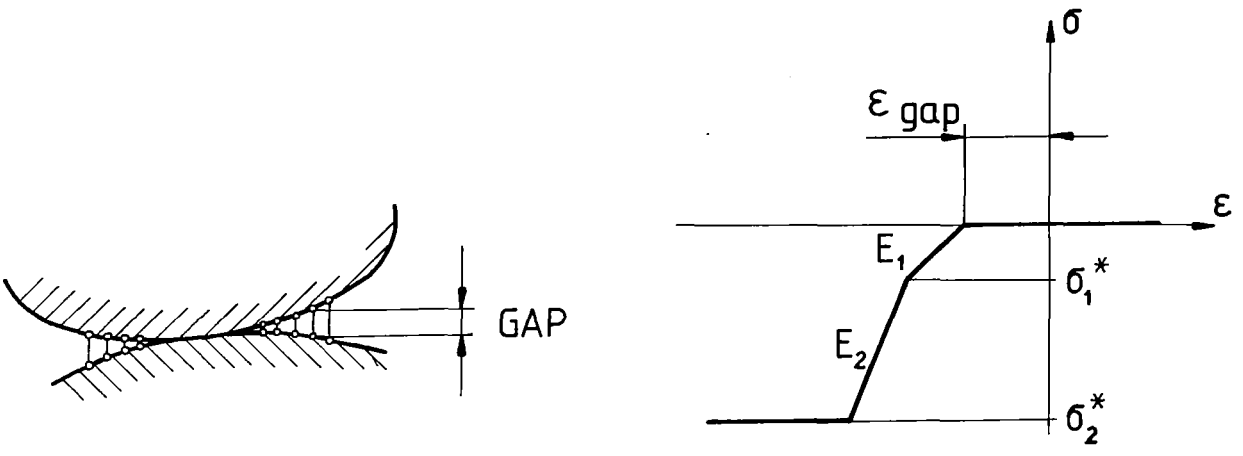

Figure 5.- Schematic sketch of the contact element material behaviour.

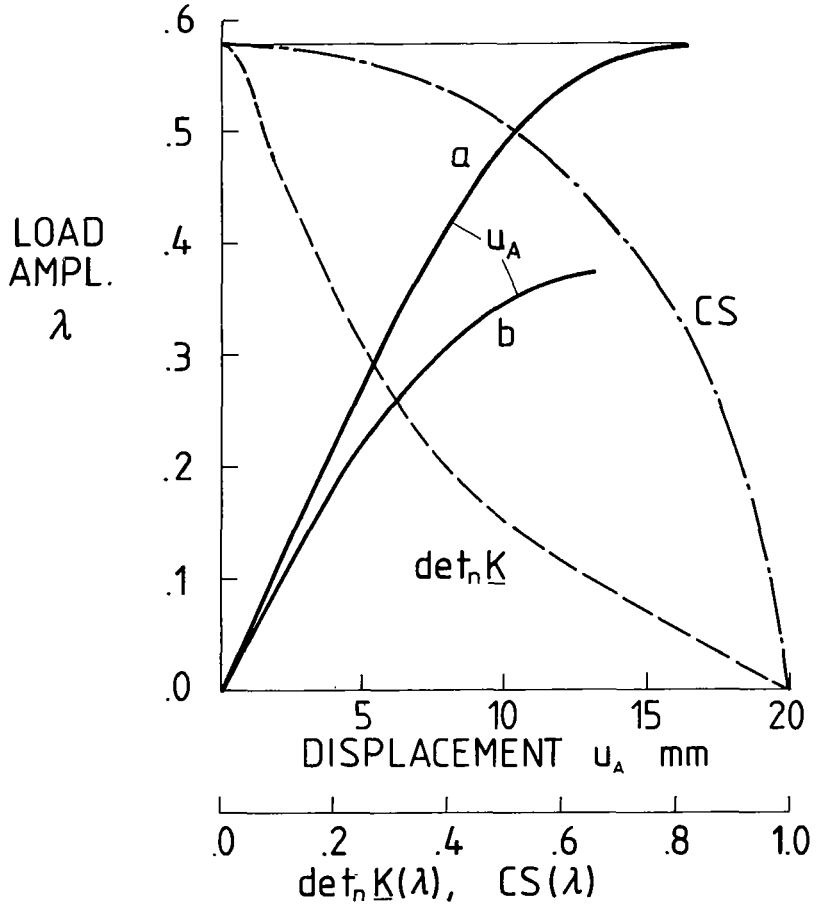

Figure 6.- Results of the analysis of the wavy strip plate obtained by (a) solving the contact problem and (b) concentrated load approach.

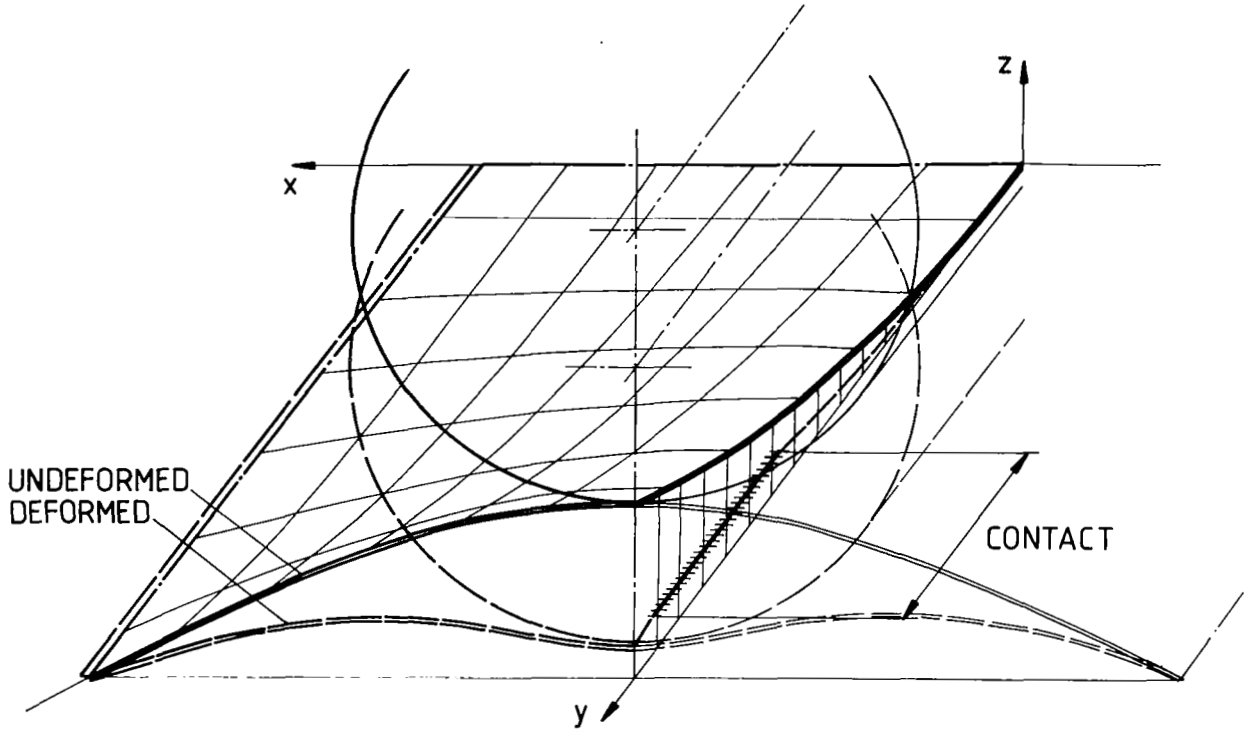

Figure 7.- Undeformed shell and configuration immediately before snap-through.

A PROPOSED GENERALIZED CONSTITUTIVE EQUATION FOR NONLINEAR PARA-ISOTROPIC MATERIALS*

K.K. Hu, S.E. Swartz and C.J. Huang
Department of Civil Engineering
Kansas State University
Manhattan, Kansas

INTRODUCTION

With the advent of finite element models of varying complexity the focus of solutions to problems in solid mechanics has shifted very strongly into the direction of more accurate material description. This is especially true for materials for which strength characteristics vary widely with state of stress. In particular, concrete which is non-isotropic at any level of deformation and is also non-linear in terms of stress-strain relationships has been singled out for intensive study. This includes work on constitutive relations (refs. 1 to 5), and failure (refs. 3,4, and 6 to 15).

Related developments in failure theories are those included in references 16 to 25.

This list is by no means exhaustive but formed a background basis which led to the model proposed in this paper. In particular, the developments in the areas of maximum deformation theory and the Von Mises-Hencky theory provided motivation for the concept used here (ref. 26).

FAILURE SURFACE

The proposed generalized constitutive equation is an extension of the work of Hu and Swartz (26) on the study of the failure of materials so that for any kind of material in any state of stress its mechanical behavior can be characterized by a single functional. According to the theory, a material failure initiates when the state of stress at a point is such that the following functional reaches a threshold value F_o:

$$F(\vec{\sigma}) = \frac{\alpha J_2}{2[\sigma_f^c \sigma_f^t - (\sigma_f^c - \sigma_f^t) J_1]} + (1-\alpha) \frac{[\frac{\sigma_1}{E(\sigma_1)} - \mu(\frac{\sigma_2}{E(\sigma_2)} + \frac{\sigma_3}{E(\sigma_3)})](\sigma_f^c + \sigma_f^t)}{\varepsilon_f^t(\sigma_f^c + J_1) + \mu\varepsilon_f^c(\sigma_f^t - J_1)} \quad (1)$$

* This research reported herein was supported in part by the National Science Foundation, Grant No. ENG 78-07829.

In this equation

α = a material related scalar factor which is determined by experimental data.

$$J_1 = \sigma_1 + \sigma_2 + \sigma_3.$$

$$J_2 = (\sigma_1 - \sigma_2)^2 + (\sigma_2 - \sigma_3)^2 + (\sigma_3 - \sigma_1)^2.$$

σ_1, σ_2, σ_3 = the components of principal stresses, tensile stress has positive value. A vector of principal stresses is expressed by $\vec{\sigma}$.

σ_f^t, σ_f^c = the absolute value of the ultimate stresses of the material under uniaxial tension and compression, respectively.

ε_f^t, ε_f^c = the absolute values of strain component in the direction of uniaxial force when stress reaches the corresponding ultimate value.

$E(\sigma)$ = the secant modulus of elasticity of the material subjected to uniaxial stress (tension or compression as appropriate).

μ = the Poisson's ratio of the material (related to stress level).

CONSTITUTIVE EQUATIONS

Non-linear response will take place when the increment of the functional is in an increasing manner and its value is beyond some threshold level (possibly zero). The material will be fractured at points where the state of stress reaches the surface of failure, i.e., $F(\vec{\sigma}) = 1$.

Between the initial state to fracture, the response is assumed to be characterized by Drucker's (17) theorem of orthogonality with the use of the functional proposed by the generalized failure theory, eqn. (1). That is, if the increment of principal strain components is decomposed into linear and non-linear increments,

$$\{d\varepsilon\} = \{d\varepsilon^e\} + \{d\varepsilon^p\}, \tag{2}$$

the non-linear part is characterized by

$$\{d\varepsilon^p\} = G(\vec{\sigma})\{g(\vec{\sigma})\}\, dF. \tag{3}$$

where

$G(\vec{\sigma})$ = a scalar function of stresses,

$\{g(\vec{\sigma})\}$ = a unit vector of the gradient of the functional at the point of interest.

Note that G values (under uniaxial loading) can be determined by some stress-

strain relationship. In the general case, especially for those materials like glass or concrete, the G function in uniaxial tension differs from that of uniaxial compression remarkably. Therefore a weighted average is proposed. According to this, the relationship between the vectors and principal strain increment and the principal stress increment is proposed to be characterized by the following generalized constitutive equation:

$$\{d\varepsilon\} = \left[\frac{1}{E} \begin{pmatrix} 1 & -\mu & -\mu \\ -\mu & 1 & -\mu \\ -\mu & -\mu & 1 \end{pmatrix} + G(\vec{\sigma}) \{g(\vec{\sigma})\} \lfloor \nabla F(\vec{\sigma}) \rfloor \right] \{d\sigma\} \tag{4}$$

In this E = the modulus of elasticity of the material, $\lfloor \nabla F \rfloor$ = the row vector of the gradient of the functional at the point of interest, and the function $G(\vec{\sigma})$ is calculated by

$$G(\vec{\sigma}) = \sqrt{\frac{\left[\sum_{i=1}^{3} (G_i(\sigma_i)\sigma_i)^2 \right]}{\sum_{i=1}^{3} \sigma_i^2}} \; H(F-F_o) \; H(\Delta F) \tag{5}$$

which is a weighted average according to the values of the corresponding principal stress components. $G_i(\sigma_i)$ depends on the value of the i-th uniaxial principal stress and is calculated according to

$$G_i(\sigma_i) = G^+[F(\sigma_i)] \; H(\sigma_i) + G^-[F(\sigma_i)] \; H(-\sigma_i). \tag{6}$$

In this formula, H is a unit step function. Let $\Delta\varepsilon_i^p = \varepsilon_i^p(\sigma_i + \Delta\sigma_i) - \varepsilon^p(\sigma_i)$, $\Delta F = F(\sigma_i + \Delta\sigma_i) - F(\sigma_i)$.
Then,

$$G^+[F(\sigma_i)] = \lim_{\Delta F \to 0} \frac{1}{\Delta F} \left| \frac{\Delta\varepsilon_i^p}{g_i} \right| , \quad \sigma_i \geq 0, \tag{7a}$$

$$G^-[F(\sigma_i)] = \lim_{\Delta F \to 0} \frac{1}{\Delta F} \left| \frac{\Delta\varepsilon_i^p}{g_i} \right| , \quad \sigma_i \leq 0, \tag{7b}$$

where g_i is the i-th component of the unit vector $\{g\}$.

If $\sigma_f^c = \sigma_f^t$, $\varepsilon_f^t = \varepsilon_f^c$ and $\alpha = 1$ is selected, the proposed failure theory agrees with the Von Mises' theory and the generalized constitutive equation reduces to the well known Prandtl-Reuss stress-strain relation (refs. 4,11).

NUMERICAL EXAMPLE

Applying the proposed theory to plain concrete for the purpose of illustration equ. (1) is modified to read

$$F = \frac{\alpha}{2}\frac{J_2}{\sigma_f^c\sigma_f^t - (\sigma_f^c-\sigma_f^t)J_1} + (1-\alpha)\frac{[\sigma_1+\mu(\sigma_2+\sigma_3)](\sigma_f^t+\sigma_f^c)}{\sigma_f^t\sigma_f^c(1+\mu) + (\sigma_f^t-\mu\sigma_f^c)J_1} \tag{8}$$

The implication used is an invariant modulus of elasticity and for concrete, so-called initial yield occurs at about $.45\ f_c'$.

Using test data for concrete (3) the level surfaces of the functional, the stress-strain curves of uniaxial tension and compression tests and the variations of $G^+[F(\sigma_i)]$ and $G^-[F(\sigma_i)]$ are shown in Figs. 1-3. The best value of α for concrete is 0.46 which has been used in these curves.

Note in Fig. 1 the shape of the curve in the tension-compression zone follows very closely the shape of the experimental curve obtained by Kupfer, Hilsdorf and Rusch (3). The stress-strain curves presented in Figs. 2 and 3 were obtained using testing equipment described in Ref. 27. Using these data, Equations 8 for F and 7a and 7b for G^+ and G^- were evaluated numerically to obtain the curves displayed.

CONCLUSIONS

A proposed constitutive model for non-linear materials has been presented. The primary virtues of the model are its logical combination of distortion states, inherent simplicity and generality.

Results presented for the model applied to concrete show good agreement with published experimental data for failure. The model can be readily incorporated into existing computer codes provided sufficient experimental supportive data are available.

As reported elsewhere (10), for instance, the experimentally obtained parameter α for cast iron is around 0.93.

The proposed constitive equation is presently being utilized in the development of a finite element code for determination of unstable crack growth and stress intensity in concrete beams.

REFERENCES

1. Andenes, Einar, "Response of Mortar to Biaxial Compression, "Thesis presented to the Faculty of the Graduate School, University of Colorado, in partial fulfillment of the requirements for the degree of Masters of Science, Boulder, Colorado, 1974.

2. Chen, A. C. T., and Chen, W. F., "Constitutive Relations for Concrete." J. ASCE 101, EM 4, 1975, pp. 465-481.

3. Kupfer, Helmut; Hilsdorf, Hubert K., and Rusch, Hubert, "Behavior of Concrete Under Biaxial Stresses," J. American Concrete Inst., Vol. 66, No. 8, Aug. 1969, pp. 656-666.

4. Palaniswamy, R., and Shah, S. P., "Fracture and Stress-Strain Relationship of Concrete Under Triaxial Compression," J. Struct. Div., ASCE 100, 1974, pp. 901-916.

5. William, K. J., and Warnke, E. P., Constitutive Model for the Triaxial Behaviour of Concrete, IABSE Proc., Seminar Concrete Structures Subjected to Triaxial Stress, LLL-1, ISMES, Bergamo, 1974.

6. Bresler, B., and Pister, K. S., "Failure of Plain Concrete Under Combined Stresses." Trans. ASCE, Vol. 122, 1957, pp. 1049-1059; Discussion, pp. 1060-1068.

7. Hannant, D. J., and Frederick, C. O., "Failure Criteria for Concrete in Compression." Mag. Concrete Res., Vol. 20, 1968, pp. 137-144.

8. Iyengar, K. T., Sundara, Raja, Chandrashekhara, K., and Krishnaswamy, K. T., "Strength of Concrete Under Biaxial Compression," J. American Concrete Inst., Vol. 62, No. 2, Feb. 1965, pp. 239-249.

9. McHenry, D., and Karni, J., "Strength of Concrete Under Combined Tensile and Compressive Stress," J. American Concrete Inst., Vol 54, No. 10, Apr. 1958, pp. 829-840.

10. Newman, K., and Newman, J. B., "Failure Theories and Design Criteria for Plain Concrete." Structure, Solid Mechanics and Engineering Design - Proceedings of the 1969 Civil Engineering Materials Conference, edited by M. Te'eni, Vol. 2, pp. 963-995.

11. Reimann, H., "Kritische Spannungszustande des Betons bei mehrachsiger," ruhender Kurzzeitbelastung, Deutscher Ausschuß fur Stahlbeton 175, Berlin, 1965, pp. 35-63.

12. Saucier, K. L., "Equipment and Test Procedure for Determining Multiaxial Tensil and Combined Tensil-Compressive Strength of Concrete," Technical Report C-74-1, U.S. Army Engineer Waterways Experiment Station, Vicksburg, Miss., March 1974.

13. Vile, G. W. D., "Strength of Concrete Under Short-Time Static Biaxial Stress," International Converence on the Structure of Concrete, Paper F2, Sept. 1965.

14. Wastlund, G., "New Evidence Regarding the Basic Strength Properties of Concrete," Betong, Stockholm, Vol. 3, 1937.

15. Weigler, H., and Becker, G., "Untersuchungen uber das Bruch-und Verformungsverhalten von Beton bei Zweiachsiger Beanspruchung," Deutscher Ausschuss fur Stahlbeton, V. 157, Berling, 1963.

16. Argyris, J. H., Faust, G., and William, K. J.Limit Load Analysis of Thick-Walled Concrete Structures - A Finite Element Approach to Fracture, ISD-Report No. 166, University of Stuttgart (1975), also in Comp. Meth. Appl. Mech. Eng., Vol. 8, No. 2, 1976, pp. 215-243.

17. Drucker, D. C., "A More Fundamental Approach to Plastic Stress-Strain Solution", Proceedings, 1st U.S. National Congress Applied Mechanics, ASME, New York, 1951, pp. 487-491.

18. Cornet, I., and Grassi, R. C., "Study of Theories of Fracture Under Combined Stresses." J. Basic Eng., Vol. 83, No. 1, 1961, pp. 39-44.

19. Eisenstadt, M. M., Introduction to Machanical Properties of Materials, MacMillan and Co., New York, 1971.

20. Grassi, R. C., and Cornet, I., "Fracture of Gray Cast Iron Tubes Under Biaxial Stresses." J. Appl. Mech., Vol. 16, No. 2, 1949, pp. 178-182.

21. Mair, W. M., "Fracture Criteria for Cast Iron Under Biaxial Stress." N.E.L. report No. 261. National Engineering Laboratory, East Kilbride, Glasgow, 1966.

22. Murphy, Glenn, Advanced Mechanics of Materials, 1st Edition, p. 83, McGraw-Hill Book Co., New York, 1946.

23. Nadai, A., Theory of Flow and Fracture of Solids, 2nd ed., McGraw-Hill Book Co., New York, 1950.

24. Prandtl, L., "Spannungsverteilung in plastischen Koerpern," Proceedings of the 1st International Congress on Applied Mechanics, Delft, Technische Roekhandel on Druckerij, J. Waltman, Jr., 1925, pp. 43-54.

25. Reuss, E., "Beruecksichtigung der elastischen Formaenderungen in der Plastizitaetstheorie," Z. Angew. Math. Mech., 10, 1930, pp. 266-274.

26. Hu, K. K., and Swartz, Stuart E., "A Proposed Generalized Material Failure Theory," Proceedings of the 15th Midwestern Mechanics Conference, University of Illinois at Chicago Circle, Chicago, Illinois, March 23-25, 1977, pp. 144-147.

27. Swartz, S. E., Hu, K. K., Huang, J., and Jones, G. L., "An Apparatus for Tensile Testing of Concrete", Experimental Mechanics, Vol. 19, No. 3, March 1979.

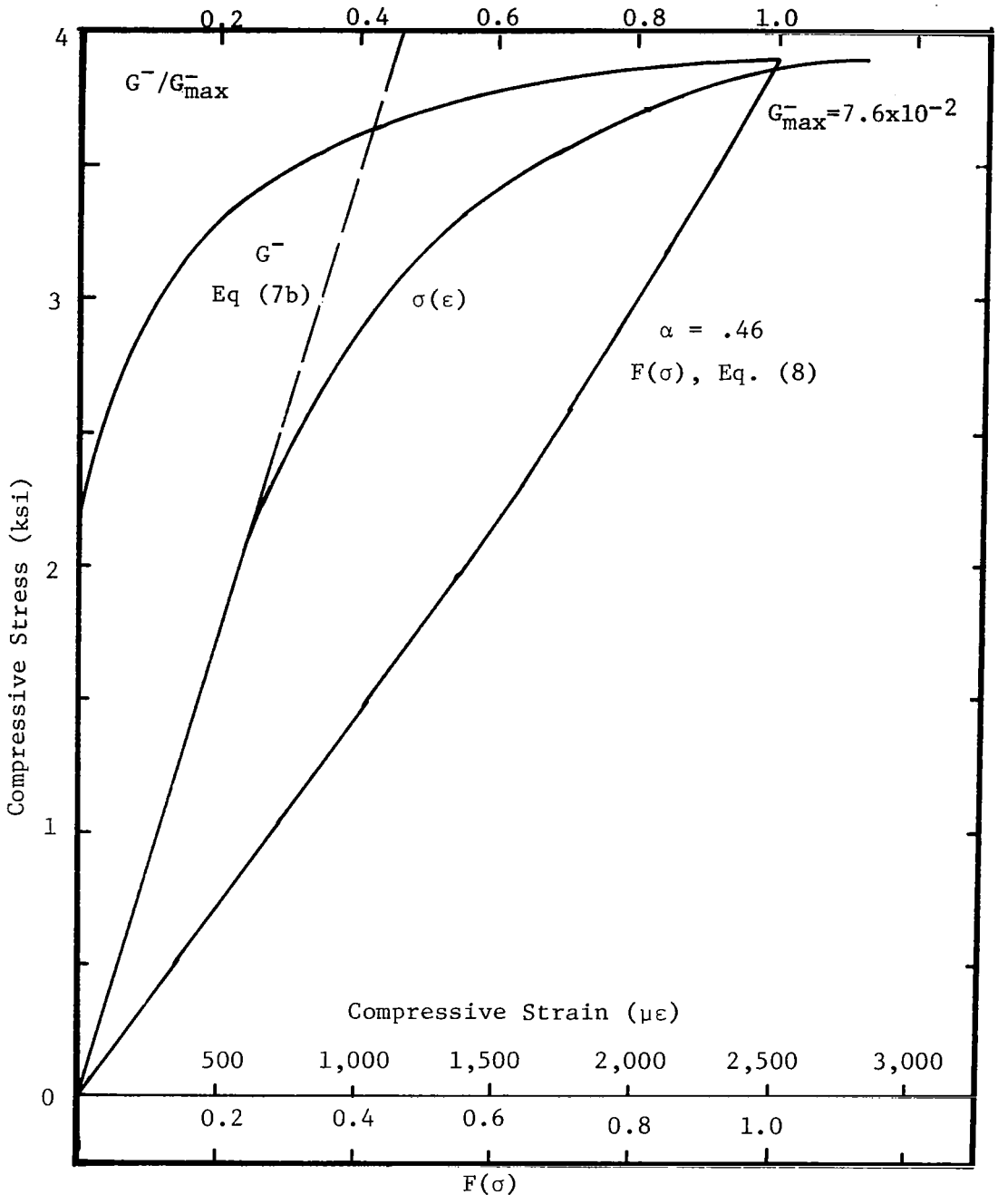

Figure 3.- Data of uniaxial compressive test of concrete.

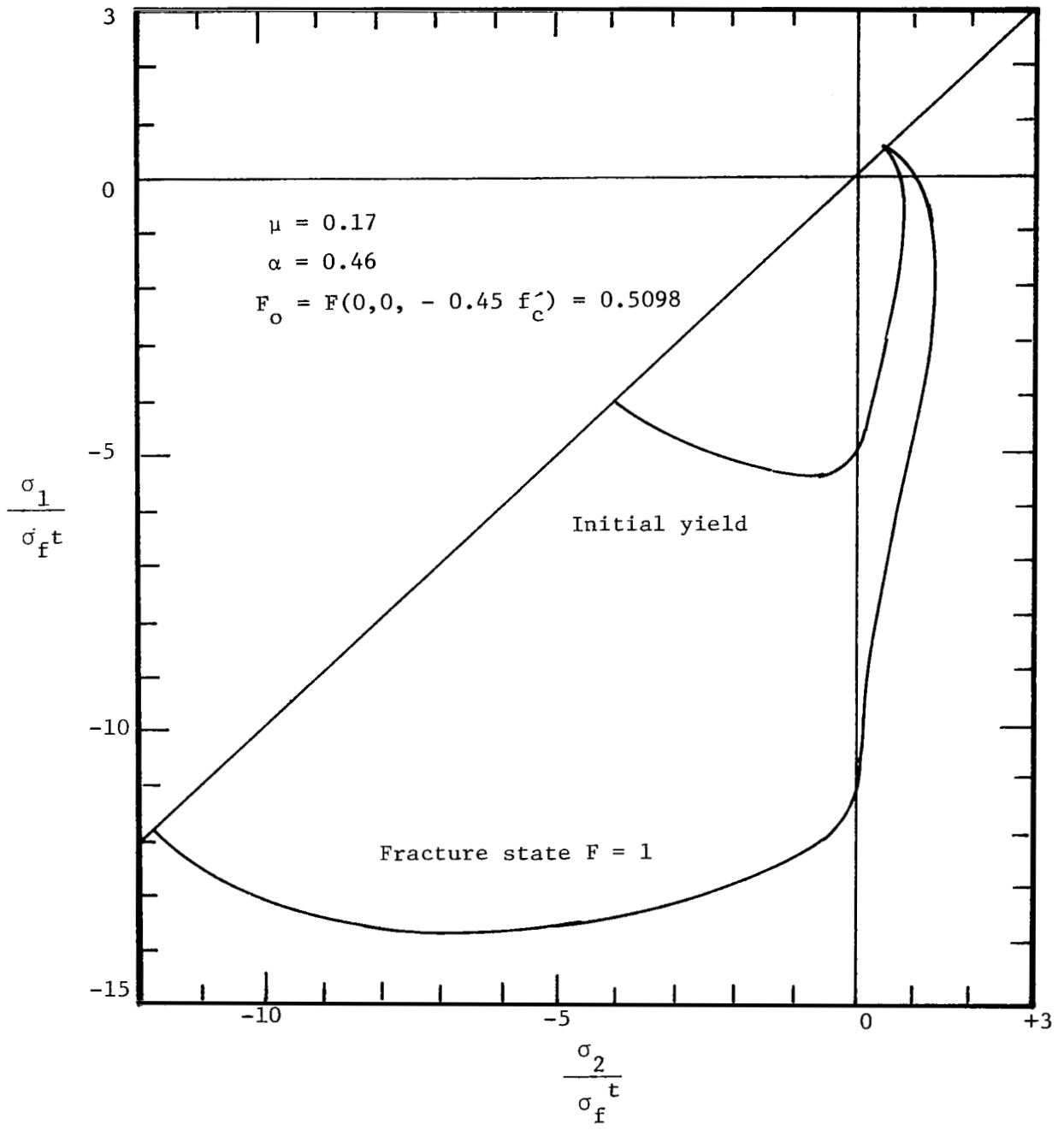

Figure 1.- Yield and fracture surfaces of concrete.

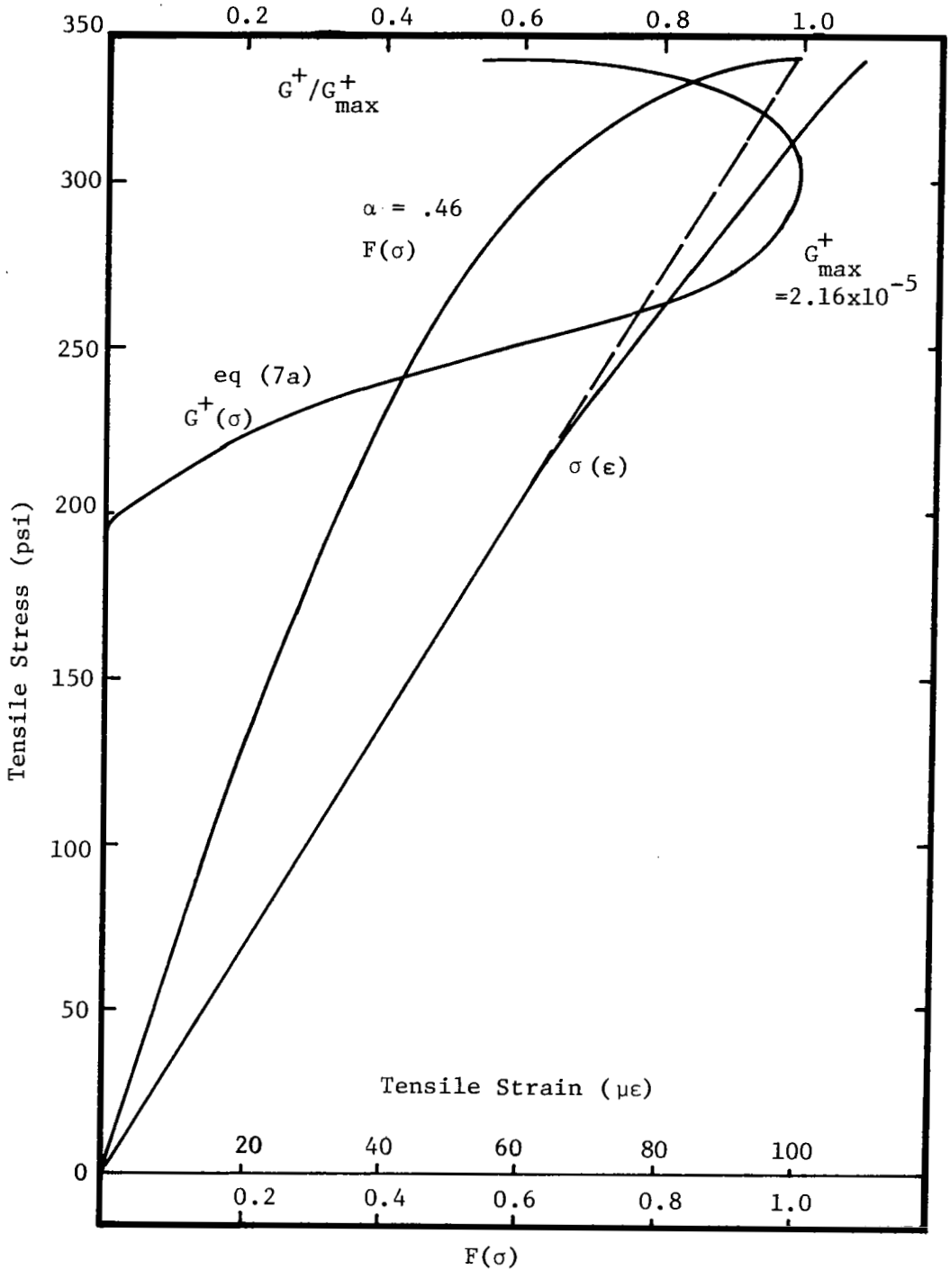

Figure 2.- Data of uniaxial tensile test of concrete.

FINITE ELEMENT ANALYSIS OF HYPERELASTIC STRUCTURES

Farhad Tabaddor
B.F.Goodrich
Akron, Ohio

SUMMARY

Most hyperelastic materials are treated as incompressible or nearly incompressible in analytical approach. The use of the penalty function, to account for near incompressibility is discussed and compared to that of Lagrange multiplier. A scheme to use Lagrange multiplier, without having to treat it as unknown, is also presented.

INTRODUCTION

The finite element analysis of hyperelastic materials involves large displacements and nonlinear material description. These materials are often considered as incompressible or nearly incompressible in theoretical developments. The incompressibility condition leads to certain simplifications in the analysis for exact solutions. Such is not, however, the case in finite element applications.

In the variational formulation of the finite element problems of incompressible media, the incompressibility condition is introduced through the use of Lagrange multiplier (1,2). This multiplier is an additional unknown scalar function which can be accommodated in the discrete model by displacement shape functions or by similar methods. The procedure results in an increase in the number of unknowns.

The incompressibility condition, aside from being inconvenient in finite element analysis, is an approximation for rubberlike materials. Such approximation becomes increasingly less accurate as the percentage of carbon black increases in the rubber compound (3). The exact enforcement of incompressibility is therefore not actually required.

In this work the near incompressibility is accounted for by use of the penalty function (4) in the expression for the strain energy function. The constitutive equations are then obtained in incremental form. This is most suitable for a nonlinear finite element. The incompressibility is shown to be closely satisfied for large penalty numbers. The

constitutive relations with penalty number are compared with the exact solution for the incompressible case. It is shown that for a given accuracy of the solution, the penalty number must vary in the course of finite element solution from element to element and from one increment to the next. Some numerical results are presented to illustrate these points. A simple scheme to use variable penalty number is also proposed. Finally the incremental form of constitutive equations for the case of incompressible material is derived from the strain energy function with the Lagrange multiplier. An alternative procedure is then proposed which does not require treatment of the Lagrange multiplier as unknown.

BASIC EQUATION

The strain energy function W for isotropic hyperelastic materials has the following form:

$$W = W(I_1, I_2, I_3) \tag{1}$$

Where I_1, I_2, and I_3 are the three invariants of Green-Lagrange strain tensor and are related to strain components, for the axisymmetric case, as follows:

$$I_1 = 3 + 2\,({}^t\gamma_{11} + {}^t\gamma_{22} + {}^t\gamma_{33}) \tag{2}$$

$$I_2 = 3 + 4\,({}^t\gamma_{11} + {}^t\gamma_{22} + {}^t\gamma_{33} + {}^t\gamma_{11}{}^t\gamma_{22} + {}^t\gamma_{11}{}^t\gamma_{33} + {}^t\gamma_{22}{}^t\gamma_{33} - {}^t\gamma_{12}{}^2) \tag{3}$$

$$I_3 = \left\{(2\,{}^t\gamma_{11} + 1)\,(2\,{}^t\gamma_{22} + 1) - 4\,{}^t\gamma_{12}{}^2\right\}(1 + 2\,{}^t\gamma_{33}) \tag{4}$$

${}^t\gamma_{11}$, ${}^t\gamma_{22}$ and ${}^t\gamma_{33}$ are the current values of strains. In this work, only the axisymmetric case is considered. The discussion, however, can be extended to the three-dimensional case without any difficulty. In the axisymmetric case, the strain invariants are related to current displacements by

$$ {}^{t}\gamma_{11} = \frac{\partial {}^{t}u_1}{\partial x_1} + \frac{1}{2}\left[\left(\frac{\partial {}^{t}u_1}{\partial x_1} \right)^2 + \left(\frac{\partial {}^{t}u_2}{\partial x_1} \right)^2 \right] \tag{5} $$

$$ {}^{t}\gamma_{22} = \frac{\partial {}^{t}u_2}{\partial x_2} + \frac{1}{2}\left[\left(\frac{\partial {}^{t}u_1}{\partial x_2} \right)^2 + \left(\frac{\partial {}^{t}u_2}{\partial x_2} \right)^2 \right] \tag{6} $$

$$ {}^{t}\gamma_{33} = \frac{{}^{t}u_1}{x_1} + \frac{1}{2}\left(\frac{u_1}{x_1} \right)^2 \tag{7} $$

$$ {}^{t}\gamma_{12} = \frac{1}{2}\left[\frac{\partial {}^{t}u_1}{\partial x_2} + \frac{\partial {}^{t}u_2}{\partial x_1} \right] + \frac{1}{2}\left[\frac{\partial {}^{t}u_1}{\partial x_1} \frac{\partial {}^{t}u_1}{\partial x_2} + \frac{\partial {}^{t}u_2}{\partial x_1} \frac{\partial {}^{t}u_2}{\partial x_2} \right] \tag{8} $$

x_2 is the axis of symmetry and x_1x_2 is the axisymmetric plane. The current displacements parallel to x_1 and x_2 axes are denoted by ${}^{t}u_1$ and ${}^{t}u_2$ respectively.

The second Piola-Kirchoff stress tensor components ${}^{t}\tau^{ij}$ at current time, can be obtained from the following relations

$$ {}^{t}\tau^{ij} = \frac{\partial W(I_1, I_2, I_3)}{\partial {}^{t}\gamma_{ij}} \qquad i,j = 1,2,3 \tag{9} $$

To obtain the incremental form of constitutive equations we define

$$ {}^{\tau}ij = {}^{t+\Delta t}\tau^{ij} - {}^{t}\tau^{ij} \qquad i,j = 1,2,3 \tag{10} $$

$$ \gamma_{ij} = {}^{t+\Delta t}\gamma_{ij} - {}^{t}\gamma_{ij} \qquad i,j = 1,2,3 \tag{11} $$

where τ^{ij} and γ_{ij} are incremental stress and strain components respectively. The incremental stress-strain relations may now be obtained from the preceding equations, after some algebraic manipulations, as

$$\tau^{ij} = C_{ijkl}\,\gamma_{kl} \qquad i,j,..= 1,2,3 \tag{12}$$

where

$$C_{ijkl} = \left(\frac{\partial^2 W}{\partial I_m\,\partial I_n}\right)\frac{\partial I_n}{\partial \gamma_{kl}}\;\frac{\partial I_m}{\partial \gamma_{ij}}$$

$$+ \frac{\partial W}{\partial I_m}\;\frac{\partial^2 I_m}{\partial \gamma_{kl}\,\partial \gamma_{ij}} \qquad i,j...= 1,2,3 \tag{13}$$

Repeated indices imply summation convention.

STRAIN ENERGY AND PENALTY FUNCTION

The strain energy function for nearly incompressible materials can be obtained by a series expansion of the strain energy function about (I_3-1) and retaining the leading terms

$$W = W_1(I_1,I_2) + W_2(I_2,I_1)\,(I_3-1)$$

$$+ W_3(I_1,I_2)\,(I_3-1)^2 + \ldots \tag{14}$$

We only consider the following special case

$$W = W_1(I_1,I_2) + H_1\,(I_3-1) + H_2\,(I_3-1)^2 \tag{15}$$

where H_1 and H_2 are constants. Many different strain energy functions have been proposed in the literature by further expansion of W_1 and

retaining the leading terms. A general form covering the proposed models is

$$W = \sum_{ij=0} C_{ij} (I_1-3)^i (I_2-3)^j + H_1(I_3-1) + H_2(I_3-1)^2 \qquad (16)$$

where C_{ij} are constants. The constant H_1 is not independent if the undeformed state is stress free, and should satisfy the following relation

$$H_1 = -(C_{10} + 2\,C_{01}) \qquad (17)$$

$$C_{00} = 0$$

We may now consider H_2 as a penalty number to handle the imcompressibility. The satisfaction of incompressibility requires H_2 to approach infinity. For practical purpose the incompressibility can be approximately satisfied by not too large values of H_2 . The incompressibility can, however, be satisfied more accurately as H_2 gets larger.

In finite element analysis, however, the large values of H_2 can lead to computational problems due to overriding stiffness associated with H_2 , as discussed in (4). A scheme to employ the variable H_2 , depending on the local deviations from ideal incompressibility, can therefore improve the solution as discussed later. On the other hand we can recover the classical approach by letting H_2 be zero and treating H_1 as the unknown Lagrange multiplier

$$W = \Sigma C_{ij} (I_1-3)^i (I_2-3)^j + \lambda(I_3-1) \qquad (18)$$

$$I_3 - 1 = 0$$

Unlike the penalty function, λ is then considered as an additional unknown and is equivalent to hydrostatic pressure.

ONE DIMENSIONAL STRESS-STRAIN RELATION

To compare the expressions (16) and (18) and to see the behaviour of the material with penalty number, we consider the case of one dimensional stress-strain relation. Let us consider an axisymmetric medium subject to the following uniform strain field:

$$\gamma_{11} = \bar{\gamma} = \text{constant}$$

$$\gamma_{22} = \gamma$$

$$\gamma_{33} = \bar{\gamma} \tag{19}$$

where γ and $\bar{\gamma}$ are constants. Let us further assume the simplest form of W_1 such that

$$W_1 = C_1 (I_1-3) + C_2 (I_2-3) \tag{20}$$

For strain energy function (18), the stress-strain relations are

$$\tau^{11} = 2C_1 + 4C_2 (1 + \gamma + \bar{\gamma}) + 2\lambda (1 + 2\gamma) (1 + 2\bar{\gamma})$$

$$\tau^{22} = 2C_1 + 4C_2 (1 + 2\bar{\gamma}) + 2\lambda (1 + 2\bar{\gamma})^2$$

$$\tau^{33} = 2C_1 + 4C_2 (1 + \gamma + \bar{\gamma}) + 2\lambda (1 + 2\gamma) (1 + 2\bar{\gamma})$$

$$\tau^{12} = 0 \tag{21}$$

$\bar{\gamma}$ is, however, not independent and is related to γ by

$$(1 + 2\gamma) (1 + 2\bar{\gamma})^2 - 1 = 0 \tag{22}$$

We choose λ, so that τ^{11} and τ^{33} are both zero to simulate the uniaxial loading. This choice would then lead to the following stress-strain relation

$$\tau^{22}_{inc} = \left[1 - (1 + 2\gamma)^{-3/2}\right] \left(2C_1 + 2\, C_2(1 + 2\gamma)^{-1/2}\right) \tag{23}$$

The Cauchy stress σ^{22} is then related to τ^{22} by

$$\sigma^{22} = (1 + 2\gamma)\, \tau^{22} \tag{24}$$

The one-dimensional stress-strain relation for the case of penalty number is now obtained from (16)

$$\tau^{11} = 2C_1 + 4C_2\,(1 + \gamma + \bar{\gamma}) + 2\,(1 + 2\gamma)\,(1 + 2\bar{\gamma})x \left[H_1 + 2H_2\,(I_3 - 1)\right]$$

$$\tau^{22} = 2C_1 + 4C_2\,(1 + 2\bar{\gamma}) + 2\,(1 + 2\bar{\gamma})^2 \left[H_1 + 2H_2\,(I_3 - 1)\right]$$

$$\tau^{33} = \tau^{11} \tag{25}$$

Following the same procedure, we arrive at the following one dimensional constitutive equation

$$\tau^{22} = \left(1 - \frac{(1 + 2\bar{\gamma})}{(1 + 2\gamma)}\right) \left(2C_1 + 2C_2\,(1 + 2\gamma)^{-1/2}\right) \tag{26}$$

where $\bar{\gamma}$ is now related to H_2 by

$$2H_2 \left[(1 + 2\bar{\gamma})^2 (1 + 2\gamma) - 1\right] =$$

$$\frac{4C_1 (\gamma + \bar{\gamma} + 2\gamma\bar{\gamma}) + 4C_2 (\gamma + \bar{\gamma} + 16\gamma\bar{\gamma})}{2 (1 + 2\gamma) (1 + 2\bar{\gamma})} \tag{27}$$

The above equation must be satisfied for all values of H_2. It can be seen that, for H_2 approaching the infinity, the above equation degenerates to

$$(1 + 2\bar{\gamma})^2 (1 + 2\gamma) - 1 = 0 \tag{28}$$

which is the expression of incompressibility condition. In this case equation (26) would become identical to equation (23).

IMCOMPRESSIBILITY AND PENALTY NUMBER

We consider the case where incompressibility is to be satisfied within some prescribed accuracy ε ; that is we require

$$(1 + 2\bar{\gamma})^2 (1 + 2\gamma) - 1 = \varepsilon \tag{29}$$

For numerical illustration, consider the case where

$$\frac{C_1}{C_2} = 4 \tag{30}$$

Combining equations (27) to (30), we arrive at the following relation

$$H\varepsilon = 6 - \frac{1}{x} - \frac{(x + 4)}{x^{1/2}} (1 + \varepsilon)^{1/2} \tag{31}$$

where

$$X = 1 + 2\gamma$$

$$H = \frac{2H_2}{C_2} \tag{32}$$

and $\varepsilon << 1$

For small values of ε , the relation (31) can be further simplified to

$$H\varepsilon = 6 - \frac{1}{x} - \frac{x + 4}{x^{1/2}} \tag{33}$$

The stress-strain relation of the equation (23) is plotted in Figure (1). The variation of $H\varepsilon$ as function of strain is plotted in Figure (2). It can be seen that as γ increases, H must also increase accordingly, to maintain the same accuracy ε on incompressibility condition. It can also be noted that higher values of H are required in compression than in tension. The relation (26) may now be written as follows:

$$\tau^{22}_{com} = \left[1 - \frac{(1+\varepsilon)^{1/2}}{(1 + 2\gamma)^{3/2}}\right] \left(4 + (1 + 2\gamma)^{-1/2}\right) \tag{34}$$

Comparing (34) and (23), it is observed that the stress for a nearly incompressible model is always less than that of an incompressible model, for the same strain. This difference, however, depends on the ε and approaches zero as ε approached zero, or H approaches infinity. The relative error, however, is

$$e = \frac{\tau^{22}_{inc} - \tau^{22}_{com}}{\tau^{22}_{inc}} = \frac{2\varepsilon}{(1 + 2\gamma)^{3/2} - 1} \tag{35}$$

For a fixed H, ε increases with γ but the relative error in the stress is governed by (35) which is less sensitive to a variation in H . Eliminating ε between (35) and (33), we obtain

$$He = \left(6 - \frac{1}{x} - \frac{(x+4)}{x+1/2}\right) \Big/ (x^{3/2}-1) \qquad (36)$$

The above equation relates the magnitude of H to level of strain for a prescribed error e. The equation (33) or (36) may serve as an approximate method of updating H, in a problem of combined stresses, for improved accuracy in incompressibility or stress calculation. Further work is, however, required to develop a more vigorious scheme in the general case.

INCREMENTAL FORM OF LAGRANGE MULTIPLIER

We now consider an alternative approach to incompressibility problems. Let us consider the following strain energy function

$$W = W_1(I_1, I_2) + \lambda (I_3-1)$$

$$I_3 - 1 = 0 \qquad (37)$$

where λ is the Lagrange multiplier. The second Piola-Kirchoff stresses can now be obtained as follow

$$t_\tau ij = \frac{\partial W}{\partial {}^t\gamma_{ij}} + {}^t\lambda \frac{\partial (I_3 - 1)}{\partial {}^t\gamma_{ij}} + (I_3 - 1) \frac{\partial {}^t\lambda}{\partial {}^t\gamma_{ij}} \qquad (38)$$

where ${}^t\lambda$ is the current value of λ. The incremental stress-strain relations may be obtained by a procedure similar to that used in the preceding pages. This would lead to

$$\tau^{ij} = \frac{\partial^2 W}{\partial {}^t\gamma_{ij}\, \partial {}^t\gamma_{kl}} \gamma_{kl} + {}^t\lambda \frac{\partial^2 (I_3 - 1)}{\partial {}^t\gamma_{ij}\, \partial {}^t\gamma_{kl}}$$

$$+ \lambda \frac{\partial (I_3 - 1)}{\partial {}^t\gamma_{ij}} \tag{39}$$

$$\lambda = {}^{t+\Delta t}\lambda - {}^t\lambda \tag{40}$$

where λ is the increment in the Lagrange multiplier between two consecutive steps in the incremental solution. The incremental form of incompressibility condition is

$$\frac{\partial I_3}{\partial {}^t\gamma_{ij}} \gamma_{ij} = 0 \tag{41}$$

multiplying both sides of (39) by γ_{ij}, and use of (41), leads to

$$\tau^{ij}\gamma_{ij} = \frac{\partial^2 W}{\partial {}^t\gamma_{ij}\, \partial {}^t\gamma_{kl}} \gamma_{kl}\, \gamma_{ij}$$

$$+ {}^t\lambda \left[\frac{\partial^2 (I_3 - 1)}{\partial {}^t\gamma_{ij}\, \partial {}^t\gamma_{kl}} \gamma_{kl}\, \gamma_{ij} \right] \tag{42}$$

or

$${}^t\lambda = \tau^{ij}\gamma_{ij} - C_{ijkl}\, \gamma_{ij}\, \gamma_{kl}$$

$$- \frac{\partial^2 (I_3 - 1)}{\partial {}^t\gamma_{ij}\, \partial {}^t\gamma_{kl}} \gamma_{kl}\, \gamma_{ij} \tag{43}$$

$$C_{ijkl} = \frac{\partial^2 W}{\partial {}^t\gamma_{ij}\, \partial {}^t\gamma_{kl}}$$

The following scheme may now be considered for the solution of incompressible materials without the need for introducing the unknown Lagrange multiplier. In the process of incremental solution, the last term in the right hand side of equation (39) is ignored. At the end of each increment, ${}^{t}\lambda$ can be updated from relation (43). There is, therefore, no need of treating ${}^{t}\lambda$ as an independent unknown. No numerical work, however, has been carried out with this alternative proposed scheme at this time.

REFERENCES

1. Herrmann, L.R., "Elasticity Equations for Incompressible and Nearly Incompressible Materials by a Variational Theorem", AIAA Jounal, Vol. 3, No. 10, pp, 1896-1900, Oct. 1965.

2. Oden, J.T., "Finite Elements of Nonlinear Continua", McGraw-Hill, Inc. 1972.

3. Tavazza, G. & Rimondi, G; " Stress and Strain Calculations of Rubber Goods", Proceeding of International Rubber Conference, Kiev USSR, 1978.

4. Zienkiewicz, O.C., "The Finite Element Method" Third Edition, McGraw-Hill Book Company 1977.

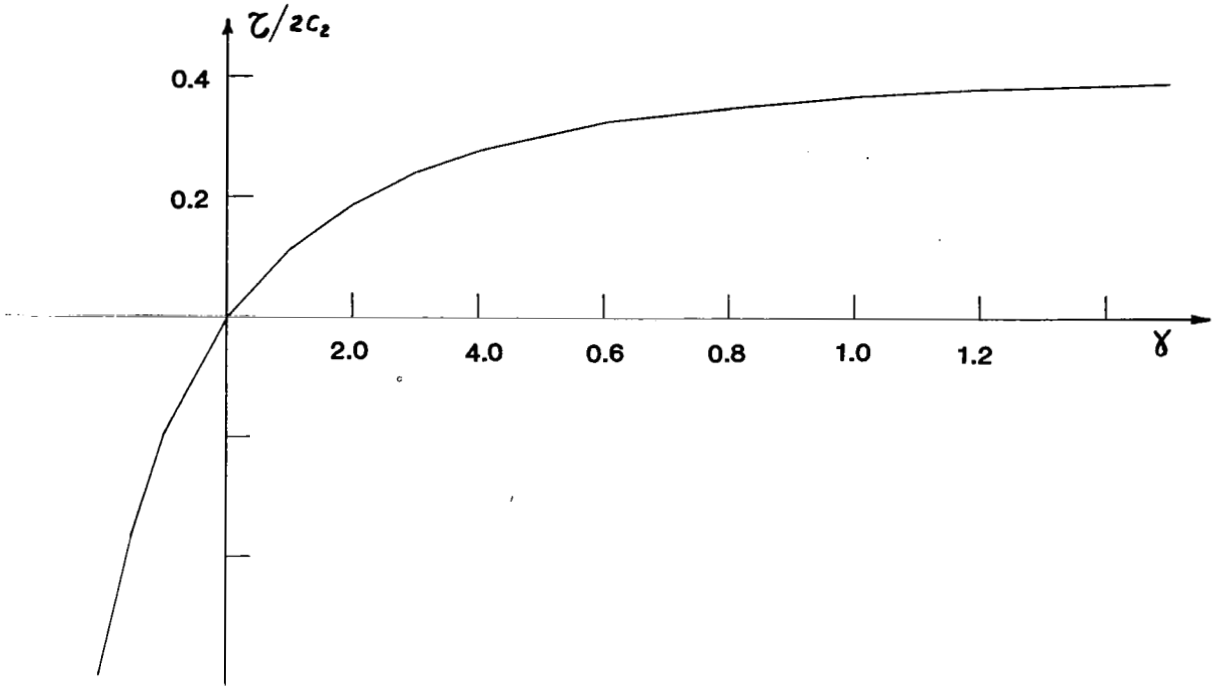

Figure 1.- One-dimensional stress-strain relation.

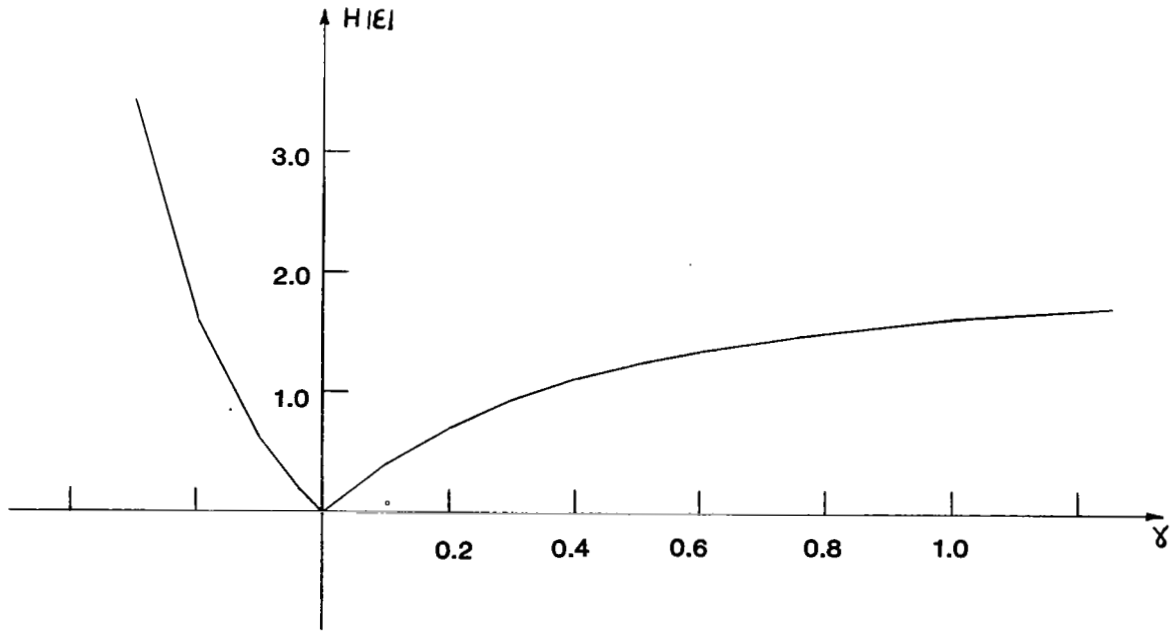

Figure 2.- Variation of Hε with strain.

SOLUTIONS OF CONTACT PROBLEMS BY THE ASSUMED STRESS HYBRID MODEL

Kenji Kubomura
System Development Corporation

Theodore H.H. Pian
Department of Aeronautics and Astronautics
Massachusetts Institute of Technology

SUMMARY

A method has been developed for contact problems which may be either frictional or frictionless and may involve extensive sliding between deformable bodies. It is based on an assumed stress hybrid approach and on an incremental variational principle for which the Euler's equations of the functional include the equilibrium and compatibility conditions at the contact surface. The tractions at an assumed contact surface are introduced as Lagrangian multipliers in the formulation. It has been concluded from the results of several example solutions that the extensive sliding contact between deformable bodies can be solved by the present method.

INTRODUCTION

The finite element method has been applied by many authors for solving solid mechanics problems which involve undetermined contact surfaces. They include the relatively simple Hertz contact problem for which there is no sliding between contact surfaces and the small displacement model can be used [1, 2]. They also include problems involving relative sliding either with friction or in frictionless conditions [3]. Existing solutions are based largely on the conventional assumed displacement finite element model.

The present paper is based on an assumed stress approach and on an incremental variational principle for which the Euler's equations of the functional include the equilibrium and compatibility conditions at the contact surface. An assumed contact surface is inserted between bodies in contact and is divided into elements. Contact tractions are independently assumed in terms of unknown values of such nodes of the contact elements. Thus, a finite element equation includes nodal displacements and nodal contact tractions as unknown. This paper is to present the variational principle and the corresponding finite element implementation for this problem.

SYMBOLS

X_i , $\underset{\sim}{X}$	Coordinates before deformation
U_i , $\underset{\sim}{U}$	Displacements defined within an element
U_i , $\underset{\sim}{\tilde{U}}$	Displacements defined along element boundaries
T_i , $\underset{\sim}{T}$	Tractions
$\tilde{T}_i$, $\underset{\sim}{\tilde{T}}$	Contact tractions
μ	Coefficient of friction
∂V	The whole boundary of the body
S_C	The contact surface
S_u	The portion of the boundary where displacements are prescribed
S_σ	The portion of the boundary where loads are applied.
V	Volume
e_{ij} , $\underset{\sim}{e}$	Strains
σ_{ij} , $\underset{\sim}{\sigma}$	Stresses
$(\ )_s$	Quantity tangential to the contact surface
$(\ )_n$	Quantity normal to the contact surface
$(\underset{\sim}{\ })$	Matrix
$(\ )_{ij}$, $(\ )_i$	Tensor
$(\bar{\ })$	Prescribed quantity
$\dot{(\ )}$	Rate of change of quantity
$(\ )^A$	Quantity pertinent to body A
$(\ )^B$	Quantity pertinent to body B
$(\ )^{A+B}$	Quantity pertinent to bodies A and B
$(\ )_N$	Quantity pertinent to element N
$\Delta(\ )$	Incremental quantity

GENERAL INCREMENTAL ASSUMED STRESS FORMULATION FOR CONTACT PROBLEM

The requirements for contact (the conditions of contact) are as follows:

(1) At the point of contact between two bodies tractions exerted on each other are the same in magnitude and are opposite in directions.

(2) The normal tractions are compressive and the tangential tractions counteract relative movement of the bodies.

(3) There should be no gap and no penetration of material points at the place of contact.

Consider two bodies A and B shown in Fig. 1 with volumes V^A and V^B, and boundary surfaces, ∂V^A and ∂V^B which are composed of portions, S_σ^A and S_σ^B, and S_u^A and S_u^B. These two bodies share a contact surface, S_C through which they interact. The previously mentioned conditions of contact in incremental form are

$$(T_n^A + \Delta T_n^A) + (T_n^B + \Delta T_n^B) = 0 \tag{1}$$

$$(T_s^A + \Delta T_s^A) + (T_s^B + \Delta T_s^B) = 0 \tag{2}$$

$$(T_s^A + \Delta T_s^A) \leq \pm \mu (T_n^A + \Delta T_n^A) \tag{3}$$

$$(T_s^B + \Delta T_s^B) \leq \pm \mu (T_n^B + \Delta T_n^B) \tag{4}$$

$$(U_n^A + \Delta U_n^A + X_n^A) - (U_n^B + \Delta U_n^B + X_n^B) = 0 \tag{5}$$

$$(U_s^A + \Delta U_s^A + X_s^A) - (U_s^B + \Delta U_s^B + X_s^B) = 0 \tag{6}$$

and the signs in Eqs. 3 and 4 are chosen such that tangential tractions on this surface act to restrain the relative movement of contacting points.

A finite element method which is based on a variational principle with relaxed continuity requirement at interelement boundaries is defined as a hybrid model [4]. Boland and Pian [5] have applied an incremental assumed stress hybrid method for large deflection analyses of thin elastic structures. The functional π_{mc} that has been derived in the reference [5] based on the Updated Lagrangian coordinate system is used as base for deriving the functional for the present problem.

The conditions of no gap and no overlapping on the place of contact are introduced into the functional by means of Lagrangian multipliers, $\tilde{T}_n + \Delta\tilde{T}_n$ and $\tilde{T}_s + \Delta\tilde{T}_s$. The functional π_{mc} becomes π^c_{mc}, i.e.

$$\pi^c_{mc} = \sum_N \Bigg[\Bigg[\int_{V_N} \Big[-B(\Delta\sigma_{ij}) - \frac{1}{2}(\sigma_{ij} + \Delta\sigma_{ij})\, \Delta U_{m,i}\, \Delta U_{m,j} \Big] dV + \int_{\partial V_N^{A+B}} \Delta T_i\, \Delta\tilde{U}_i\, dS$$

$$- \int_{S_{\sigma_N}^{A+B}} \Delta\bar{T}_i\, \Delta\tilde{U}_i\, dS - \int_{S_{C_N}^{A+B}} \Delta\tilde{T}_i\, (\Delta\tilde{U}_i^A - \Delta\tilde{U}_i^B)\, dS$$

$$+ \int_{\partial V_N^{A+B}} T_i\, \Delta\tilde{U}_i dS - \int_{S_{\sigma_N}^{A+B}} \bar{T}_i\, \Delta\tilde{U}_i dS - \int_{V_N^{A+B}} \Delta\sigma_{ij} \Big[e_{ij} - \frac{1}{2}(U_{i,j} + U_{j,i} - U_{m,i}\, U_{m,j}) \Big] dV$$

$$+ \int_{S_{C_N}} \tilde{T}_i (\Delta\tilde{U}_i^A - \Delta\tilde{U}_i^B)\, dS + \int_{S_{C_N}} \Delta\tilde{T}_i \Big[(\tilde{U}_i^A + X_i^A) - (\tilde{U}_i^B + X_i^B) \Big] dS \Bigg]\Bigg] \qquad (7)$$

The Euler's equations of π^c_{mc} are

$$e_{ij} + \Delta e_{ij} = \frac{1}{2}\left(U_{i,j} + U_{j,i} - U_{m,i}U_{m,j} + \Delta U_{i,j} + \Delta U_{j,i} + \Delta U_{m,i}\Delta U_{m,j}\right) \quad (8)$$

$$\text{in } V_N^{A+B}$$

$$T_i + \Delta T_i = \bar{T}_i + \Delta \bar{T}_i \qquad \text{on} \quad S_{\sigma_N}^{A+B} \quad (9)$$

$$\left(T_i + \Delta T_i\right)^a + \left(T_i + \Delta T_i\right)^b = 0 \qquad \text{on} \quad \partial V_N^{A+B} \quad (10)$$

On the contact surface S_{C_N}, in addition to Eqs. 5 and 6

$$\left(T_n^A + \Delta T_n^A\right) - \left(\tilde{T}_n + \Delta \tilde{T}_n\right) = 0 \quad (11)$$

$$\left(T_s^A + \Delta T_s^A\right) - \left(\tilde{T}_s + \Delta \tilde{T}_s\right) = 0 \quad (12)$$

$$\left(T_n^B + \Delta T_n^B\right) + \left(\tilde{T}_n + \Delta \tilde{T}_n\right) = 0 \quad (13)$$

$$\left(T_s^B + \Delta T_s^B\right) + \left(\tilde{T}_s + \Delta \tilde{T}_s\right) = 0 \quad (14)$$

Introducing frictional constraint on $\tilde{T}_s + \Delta \tilde{T}_s$ and $\tilde{T}_n + \Delta \tilde{T}_n$, such that

$$\tilde{T}_s + \Delta \tilde{T}_s \leq \pm \mu\left(\tilde{T}_n + \Delta \tilde{T}_n\right) \quad (15)$$

and rearranging Eqs. 11, 12, 13, 14 and 15, results in Eqs. 1, 2, 3, and 4. Thus, it has been proved that the conditions of contact are Eulers's equations of the functional π^c

These Euler equations are the strain displacement relations, the mechanical boundary condition, the stress equilibrium requirements along the interelement boundaries and the conditions of contact. Since they are only satisfied in an average sense within an increment they cannot be expected to satisfy these conditions in the usual sense. It is, therefore, necessary to consider a compatibility check, a stress equilibrium check, and a contact check.

It is seen that Eq. 7 already has all of these built-in checks. The 5-th and 6-th integral terms in the functional correspond to the equilibrium check and 7-th term to the compatibility check. Also, the compatibility and equilibrium checks of the contact surface (contact check) are easily identified, the equilibrium check being the 8-th integral term and the compatibility check, the 9-th term.

FINITE ELEMENT IMPLEMENTATION

Since the aim of the present work is to solve contact problems by the finite element method, expressions arising from nonlinearities, not due to contact, are excluded from equations. A technique for solving these equations, with only contact nonlinearities, will be discussed here.

Neglecting nonlinearities not due to contact, the assumed stress hybrid functional, π_{mc}^{c} takes the form

$$\pi_{mc}^{c} = \sum_{N} \left\{ \iint_{V_N} \frac{1}{2} {}_{\Delta}\tilde{\sigma}^{T} \cdot \tilde{S} \cdot {}_{\Delta}\tilde{\sigma} \, dV - \int_{\partial V_N} {}_{\Delta}\tilde{T}^{T} \cdot {}_{\Delta}\tilde{U} \, dS + \int_{S_{\sigma_N}} (\bar{\tilde{T}} + {}_{\Delta}\bar{\tilde{T}})^{T} \, {}_{\Delta}\tilde{U} dS \right.$$

$$- \int_{S_{\sigma_N}} \tilde{T}^{T} \cdot {}_{\Delta}\tilde{U} \, dS - \int_{S_{C_N}} (\tilde{\tilde{T}} + {}_{\Delta}\tilde{\tilde{T}})^{T} ({}_{\Delta}\tilde{U}^{A} - {}_{\Delta}\tilde{U}^{B}) dS$$

$$\left. - \int_{S_{C_N}} (\tilde{\tilde{T}} + {}_{\Delta}\tilde{\tilde{T}})^{T} \left[(\tilde{U}^{A} + \tilde{X}^{A}) - (\tilde{U}^{B} + \tilde{X}^{B}) \right] dS \right\} \qquad (16)$$

The stresses $\Delta\underset{\sim}{\sigma}$ are expressed in terms of a finite number of stress parameters, $\Delta\underset{\sim}{\beta}$ and the element boundary displacements interpolated in terms of the nodal displacements, $\underset{\sim}{q}$ and $\Delta\underset{\sim}{q}$. Also, coordinates are interpolated in terms of their nodal values. As a solid continuum is subdivided into elements, the contact surface is also discretized into finite number of elements referred to here as "contact elements" with "contact nodes." The contact traction $\bar{\underset{\sim}{T}} + \Delta\bar{\underset{\sim}{T}}$ is interpolated in terms of its nodal values, $\underset{\sim}{t}$.

Thus, interpolations of them are: $\Delta\underset{\sim}{\sigma} = \underset{\sim}{P} \cdot \Delta\underset{\sim}{\beta}$, $\Delta\bar{\underset{\sim}{T}} = \underset{\sim}{R} \cdot \Delta\underset{\sim}{\beta}$, $\tilde{\underset{\sim}{U}} = \underset{\sim}{L} \cdot \underset{\sim}{q}$, $\Delta\tilde{\underset{\sim}{U}} = \underset{\sim}{L} \cdot \Delta\underset{\sim}{q}$ and $\bar{\underset{\sim}{T}} + \Delta\bar{\underset{\sim}{T}} = \underset{\sim}{M} \cdot \underset{\sim}{t}$. Substituting these interpolations into Eq. 16, and defining the following matrices

$$\underset{\sim}{H}_N = \int_{V_N} \underset{\sim}{P}^T \cdot \underset{\sim}{S} \cdot \underset{\sim}{P} \, d\bar{V}, \quad \underset{\sim}{G}_N = \int_{\partial V_N} \underset{\sim}{R}^T \cdot \underset{\sim}{L} \, dS,$$

$$\Delta Q_N = \int_{S_{\sigma_N}} \underset{\sim}{L}^T \cdot \Delta\bar{\underset{\sim}{T}} \, dS, \quad \underset{\sim}{Q}^o_N = \int_{S_{\sigma_N}} \underset{\sim}{L}^T \cdot \bar{\underset{\sim}{T}} \, dS,$$

$$\underset{\sim}{R}^o_{E_N} = \int_{S_{C_N}} \underset{\sim}{L}^T \cdot \underset{\sim}{T} \, dS, \quad R^o_{C_N} = \int_{S_{C_N}} \underset{\sim}{M}^T \cdot \left[(\tilde{\underset{\sim}{U}}^A + \underset{\sim}{X}^A) - (\tilde{\underset{\sim}{U}}^B + \underset{\sim}{X}^B) \right] dS$$

$$\underset{\sim}{F}^A_N = \int_{S_{C_N}} \underset{\sim}{M} \cdot \underset{\sim}{L}^A \, dS, \quad F^B_N = \int_{S_{C_N}} \underset{\sim}{M} \cdot \underset{\sim}{L}^B \, dS$$

the functional, $\pi^c_{mc_N}$ becomes

$$\pi^c_{mc_N} = \frac{1}{2} \Delta\underset{\sim}{\beta}^T \cdot \underset{\sim}{H}_N \cdot \Delta\underset{\sim}{\beta} - \Delta\beta^T \cdot \underset{\sim}{G}_N \cdot \Delta\underset{\sim}{q} + \Delta\underset{\sim}{q}^T \cdot \Delta\underset{\sim}{Q}_N \qquad (17)$$

$$+ \Delta\underset{\sim}{q}^T \cdot \underset{\sim}{Q}^o_N - \Delta\underset{\sim}{q}^T \cdot \underset{\sim}{R}^o_{E_N} - \left(\Delta\underset{\sim}{q}^{A^T} \cdot \underset{\sim}{F}^A_N - \Delta\underset{\sim}{q}^{A^T} \underset{\sim}{F}^B_N \right) \cdot \underset{\sim}{t} - \underset{\sim}{t}^T \cdot \underset{\sim}{R}^o_{C_N}$$

in which $\underset{\sim}{Q}^{o}_{N}$ and $\underset{\sim}{R}^{o}_{E_N}$ result from stress equilibrium checks on S_{σ_n} and on the contact surface S_{C_N}, and $R^{o}_{C_N}$, from the initial mismatch checks on S_{C_N}.

Equation 17 contains three unknown vectors, the incremental stress parameters $\Delta\underset{\sim}{\beta}$, the incremental displacements $\Delta\underset{\sim}{q}$, and the contact stresses $\underset{\sim}{t}$. Whereas, the vector $\Delta\underset{\sim}{\beta}$ are independent on the element level, $\Delta\underset{\sim}{q}$ and $\underset{\sim}{t}$ are not. Thus, eliminating $\Delta\underset{\sim}{\beta}$ from Eq. 17, π^{c}_{mc} becomes

$$\pi^{c}_{mc} = -\frac{1}{2}\,\Delta\underset{\sim}{q}^{T}\cdot\underset{\sim}{G}_{N}\cdot\underset{\sim}{H}^{-1}_{N}\cdot\underset{\sim}{G}_{N}\cdot\Delta\underset{\sim}{q} + \Delta\underset{\sim}{q}^{T}\cdot\left(\Delta\underset{\sim}{Q}_{N} + \underset{\sim}{Q}^{o}_{N} - \underset{\sim}{R}^{o}_{E_N}\right)$$

$$-\left(\Delta\underset{\sim}{q}A^{T}\cdot\underset{\sim}{F}^{A}_{N} - \Delta\underset{\sim}{q}B^{T}\cdot F^{B}_{N}\right)\cdot\underset{\sim}{t} - \underset{\sim}{t}^{T}\cdot\underset{\sim}{R}^{o}_{C_N} \qquad (18)$$

Summing up over all elements and taking the variations of the functional with respect to $\Delta\underset{\sim}{q}$ and $\underset{\sim}{t}$, results in

$$\begin{bmatrix} \underset{\sim}{K} & \underset{\sim}{K}_{C} \\ \underset{\sim}{K}_{C}^{T} & \underset{\sim}{O} \end{bmatrix} \begin{Bmatrix} \Delta\underset{\sim}{q} \\ \underset{\sim}{t} \end{Bmatrix} = \begin{Bmatrix} \underset{\sim}{Q} \\ \underset{\sim}{R} \end{Bmatrix} \qquad (19)$$

where

$$\underset{\sim}{K} = \sum_{N}\underset{\sim}{G}^{T}_{N}\cdot\underset{\sim}{H}^{-1}_{N}\cdot\underset{\sim}{G}_{N}, \quad \underset{\sim}{Q} = \sum_{N}\left(\Delta\underset{\sim}{Q}_{N} + \underset{\sim}{Q}^{o}_{N} - \underset{\sim}{R}^{o}_{E_N}\right)$$

$$\underset{\sim}{K}_{C} = \begin{Bmatrix} \sum_{N}\underset{\sim}{F}^{A}_{N} \\ -\sum_{N}\underset{\sim}{F}^{B}_{N} \end{Bmatrix}, \quad \underset{\sim}{R} = \sum_{N}\underset{\sim}{R}^{o}_{C_N}$$

Equation 19 represents the total assembled finite element matrix equation.

TECHNIQUE OF ITERATIVE SOLUTION

Once the contacting bodies are adequately constrained such that the inverse of the global stiffness matrix, $\underset{\sim}{K}^{-1}$ in Eq. 19 can be calculated, it can be used throughout the iteration procedure. Thus, in locating the contact surface only $\underset{\sim}{K}_C$ needs to be recomputed in each iteration. The global stiffness matrix $\underset{\sim}{K}$ remains constant during this process. Even in the case of material and/or large deflection nonlinearities, it is possible to use a modified Newton-Raphson method, hence the global stiffness matrix $\underset{\sim}{K}$ may remain constant during this process.

For a two-dimensional problem, before each iteration, the contact surface is a line, fixed in the coordinate system, but not to the contacting bodies. Such line is assumed known in order to perform the necessary integrals. But if, before the iteration, one has assumed the location of the contact surface and the positions on it that the contacting nodes of the bodies will occupy, then it would appear that the displacement increment can be specified. This is not the case. Instead, the problem is solved for the displacement increments and if the contact surface found therefrom is not coincident with the one presupposed, a new contact surface location is calculated, and then an iteration can be followed.

It has been found that the length of the contact element which yields best results is the same as the length of the contacting side of boundary elements of the bodies. In order to facilitate programming, the nodes of the contact element are chosen to be coincident with those of one of the contacting bodies. As a result of variations in load, the place of contact changes; thus a vital part of the solution is to establish a procedure for calculating this change. A trial and error scheme is employed because it is virtually impossible to formulate a variational principle including unknown variables which locate the surface of contact.

The overall strategy for solving the contact problem is discussed here. First, an increment in the external load or prescribed displacement is applied. Second, a contact surface is assumed together with the points on it through which nodes of the bodies contact each other. Also, the types of contact (sliding or non-sliding) at each of the above-mentioned points are assumed. For the initial calculation of the first load increment, the above assumptions are made simply by inspection, and for the first iteration after each new load increment, the converged solution of the previous load step is used. Third, all the necessary matrices are calculated and assembled. At the i-th iteration of the N-th load step, incremental displacement, ${}^{i}\Delta U_k$ and contact tractions ${}^{i}(\tilde{T}_k + \Delta\tilde{T}_k)$ are solved from a finite element matrix equation. Fourth, knowing the total displacement ${}^{N-1}U_k$ at the end of the previous loading step N-1, the total displacements ${}^{N-1}U_k + {}^{i}\Delta U_k$ on the boundary, and contact tractions ${}^{i}(\tilde{T}_k + \Delta\tilde{T}_k)$ are checked to determine if they satisfy the conditions of contact. If they do not satisfy these conditions, the location of the assumed contact surface is modified and the procedure repeated until they do. Next, a convergence test is made, and if the solution is not convergent, the location of the

contact surface is further modified and the solution procedure repeated.

To determine if the solution satisfies the conditions of contact, the following assurances are made:

(1) That nodes of either body beyond the last contacting nodes from the previous iteration have not penetrated the other body.

(2) That tractions at the contacting nodes are compressive. These normal tractions can be calculated by three different methods; (a) from the stress coefficients, (b) from the equivalent nodal forces, and (c) from the contact tractions, $\tilde{T} + \Delta\tilde{T}$. Here the last method was used.

(3) That the relationship between normal and tangential contact tractions,

$$\left| \tilde{T}_s + \Delta\tilde{T}_s \right| \leq \mu \left| \tilde{T}_n + \Delta\tilde{T}_n \right|$$

is satisfied. Depending on which of the above checks, if any, is violated, one of the following procedures is employed to modify the assumed location of the contact surface.

(a) If (1) is violated, the contact surface may be extended to include the points at which penetration has occurred.

(b) If (2) is violated, the contact surface is reduced by excluding nodes at which the tractions are tensile.

(c) If (3) is violated, sliding is allowed to occur.

After the conditions of contact are satisfied, a test for convergence can be made by calculating the following quantity:

$$R = \left| \frac{{}^{i+1}\Delta U_k - {}^{i}\Delta U_k}{{}^{i+1}\Delta U_k} \right|$$

where ΔU_k is the displacement at the k-th degree of freedom. If R is less than a precribed quantity, say 0.01, the solution is considered as converged.

EXAMPLE SOLUTIONS

The finite element model and solution scheme are applied to problems of contact between a disk and a semi-infinite half-plane. The overall mesh pattern, the location of

the prescribed displacement and relevant dimensions are shown in Fig. 2-a, with the area immediately surrounding the contact surface shown in great detail in Fig. 2-b. The semi-infinite half-plane has been modeled by a finite one with overall dimensions much larger than those of the disk. The basic element used is four-node quadrilateral element derived by assuming seven β-parameters and linear displacement distribution along each edge. Five-node and six-node elements are also introduced in transition regions between coarser and finer meshes. Contact tractions along each contact element are approximated by linear interpolations.

Non-Sliding Contact

Problems are solved for the case with both applied loads and prescribed displacements at the top of the disk. In the problems, the ratio of Young's moduli are varied over a range from 1 to 10^{-4} and slightly different mesh patterns near the contact surface are used to accommodate node-to-node and node-to-internode contacts. Loads or displacements are applied by three increments until the length of contact surface becomes about 2.4 mm. For each increment, the converged solutions are reached with three or four iterations. For these solutions, the best results for contact tractions are obtained when calculated from equivalent nodal forces and are compared excellently with the Hertz solution in all cases.

Frictionless Contact With Extensive Sliding

The half disk and the semi-infinite half-plane are also used to demonstrate the capability of this formulation to solve extensive sliding contact problems. Since the contact between the two bodies is frictionless, the solution is independent of the path; thus a Hertz solution is again available for comparison. Solutions are obtained for prescribed displacements at the top of the disk by eight increments. Stress distributions on the plane of contact, for two prescribed displacements, are plotted in Fig. 3 where zero position represents the point of initial contact. It is seen that the solution agrees almost exactly with that of the Hertz solution. It is noted that the center of symmetry of the stress distribution moves to the left as the half-disk slides in that direction.

Frictional Contact With Extensive Sliding

The same problem is again solved here with friction between the disk and the half-plane as an added consideration. No solution to this problem, analytic or otherwise, can be found; thus, results arrived at here will be justified by comparison with the results of the previous section and by showing that they satisfy the conditions of contact.

The normal tractions at the contacting nodes between the disk and the half-plane for every 4th displacement increment are shown in Fig. 3 and are compared with those of the frictionless case. Because of friction, it can be seen that the displacement of the contact surface is retarded. That the normal tractions of the plane and disk are equal in magnitude and opposite in sign is also evident in the figure. This implies that the normal tractions satisfy a condition of contact. A condition of sliding contact requires the ratio between normal and tangential components of tractions to be constant and equal to the coefficient of

friction . They were approximately verified for all contacting nodes. Finally, the contacting surfaces of the disk and the plane are shown in Fig. 4 along with the locations of the nodes obtained in previous solutions. It can be seen that friction retards the movement of the contact surface, and as in the previous solution, through averaging over the entire contact surface, the contact condition of no separation or penetration is satisfied.

CONCLUSIONS

(1) An incremental variational principle and a corresponding finite element formulation have been made for contact problems based on an assumed stress hybrid method. An iterative scheme for the solution has been developed.

(2) Successful applications of the present method for plane elasticity problems have been demonstrated for

   (a) Non-sliding problems with node-to-node contact and with node-to-internode contact,

   (b) Frictionless contact with extensive sliding, and

   (c) Frictional contact with extensive sliding.

(3) The present method should be extended to problems involving material and/or geometrical nonlinearities in addition to contact nonlinearity.

REFERENCES

(1) Tsuta, T. and Yamaji, S., "Finite Element Analysis of Contact Problem", Theory and Practice in Finite Element Structure Analysis, University of Tokyo Press, 177-194 (1973).

(2) Wilson, E.A. and Parsons, B., "Finite Element Analysis of Elastic Contact Problems Using Differential Displacements", Int. J. Num. Meth. Engng., Vol. 2, 387-395 (1970).

(3) Chan, S.H. and Tuba, I.S., "A Finite Element Method for Contact Problems of Solid Bodies", Int. J. Mech. Sci., Vol. 13, 615-639, (1971).

(4) Pian, T.H.H., "Finite Element Methods by Variational Principle with Relaxed Continuity Requirement", Variational Methods in Engineering, Edited by C.A. Brebbia and H. Tottenham, Southhampton University Press, England, September, Session III, pp. 3.1-3.24, (1972).

(5) Boland, P.L. and Pian, T.H.H., "Large Deflection Analysis of Thin Elastic Structures by the Assumed Stress Hybrid Finite Element Method", Computers and Structures, Vol. 7, pp. 1-12, (1977).

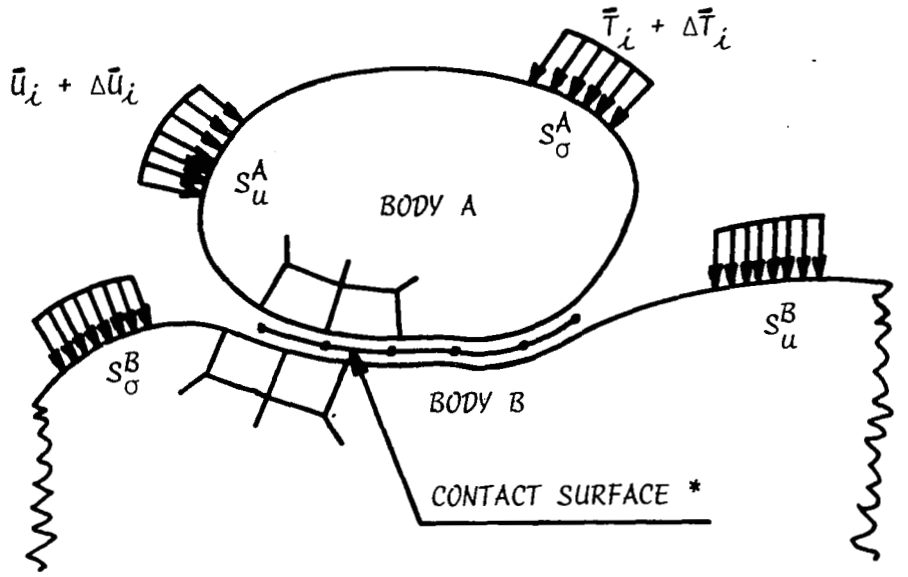

* BODY A AND BODY B INTERACT THROUGH THE CONTACT SURFACE.

Figure 1.- Contact surface.

($E = 21{,}000\ kg/mm^2$, $\nu = 0.3$)

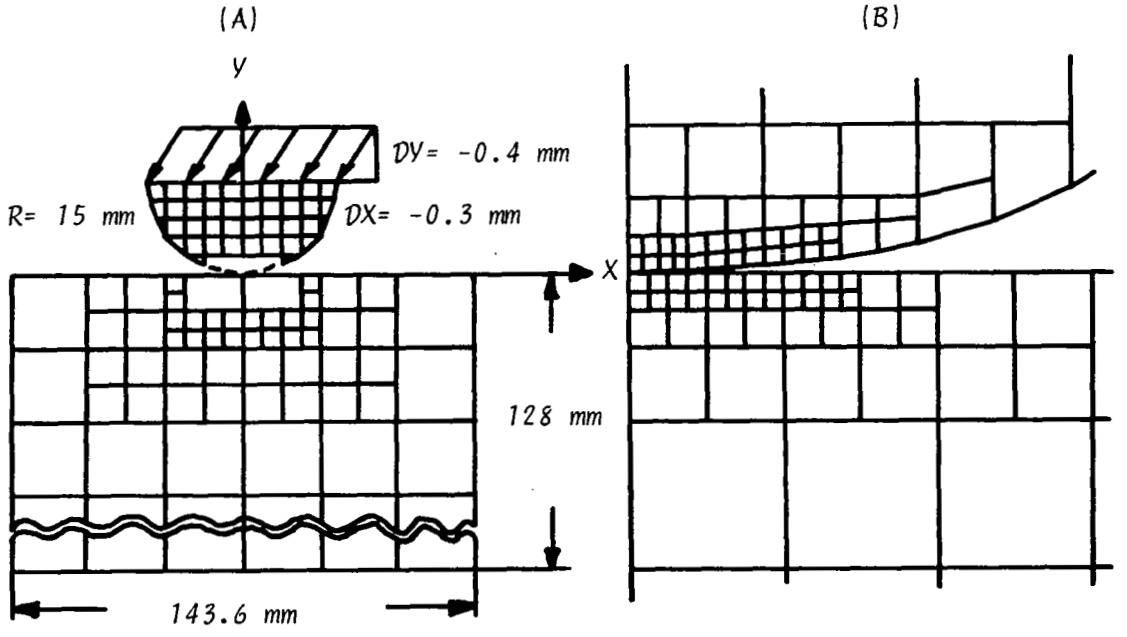

Figure 2.- Mesh pattern.

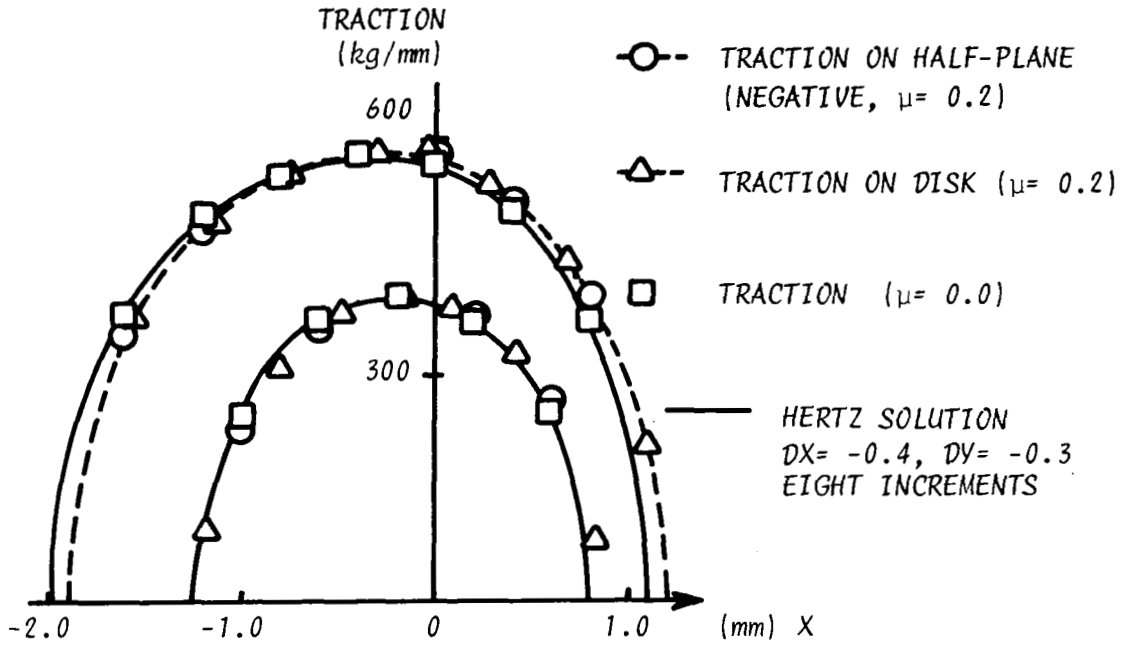

Figure 3.- Normal traction on contact surface.

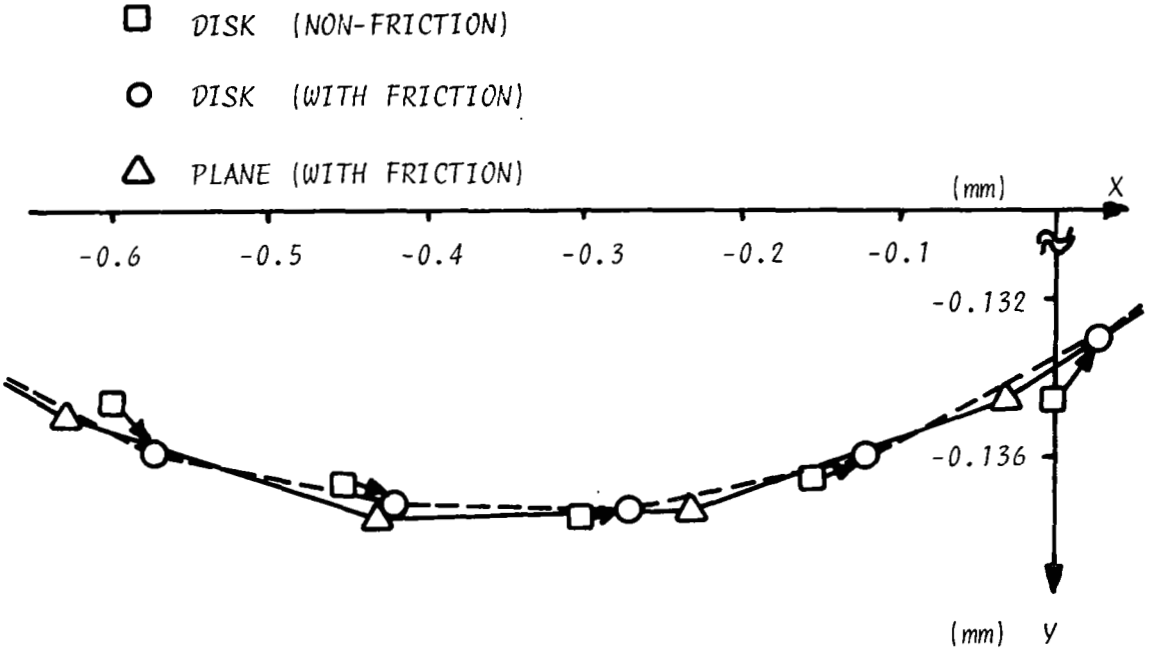

Figure 4.- Location of nodes.

FINITE ELEMENTS FOR CONTACT PROBLEMS IN TWO-DIMENSIONAL ELASTODYNAMICS

Thomas K. Zimmermann
IPEN, Swiss Federal Institute of Technology, Lausanne, Switzerland

Wing Kam Liu
Div. of Eng. and Applied Science, CALTECH, Pasadena, USA

SUMMARY

This article summarizes some aspects of research in progress for developing finite element methods for contact problems. We propose a new"finite element approach" for contact problems in two-dimensional elastodynamics. Sticking, sliding and frictional contact can be taken into account. The method consists of a modification of the shape functions, in the contact region, in order to involve the nodes of the contacting body. The formulation is symmetric (both bodies are contactors and targets), in order to avoid interpenetration. Compatibility over the interfaces is satisfied. The method is applied to the impact of a block on a rigid target. The formulation can be applied to fluid-structure interaction, and to problems involving material nonlinearity. The extension to three dimensions presents additional difficulties, but it is possible.

INTRODUCTION

The approach presented in this article was developed while trying to simulate the movement of a gas bubble in a liquid. The original idea was to introduce the compatibility of the velocities over the gas-liquid interface via a constraint equation and to handle it by the Lagrange multiplier method. In a second step, the Lagrange multiplier method was replaced by a penalty method, which is easier to implement. In both cases, the constraint equation is a geometric relationship between gas and liquid velocities. No local remeshing was performed; the bubble and liquid meshes were simply superposed. This resulted in poor pressure fields along the interface. Looking for an improvement of this situation, remeshing appeared as the best but also the most cumbersome solution. Alternatively, a modification of the shape functions appeared to have the advantages of remeshing, without its inconveniences. This latter approach is described herein as it is applied to contact problems in two-dimensional elastodynamics. Frictional contact results in an exchange of momentum between the two contacting bodies, and can be realised by direct introduction of a contribution of the contactor's velocity into the target's equation of motion. This is conveniently done by means of a modification of the shape functions, as described in the next paragraphs.

The proposed approach has the advantage, as compared to the Lagrange multiplier method, of maintaining a constant size of the linear system to be solved. Compared to a penalty method, it has the advantage that we get automatic compatibility of the field variables over the interface. When the formulation is symmetric (i.e., both bodies are targets and contactors), interpenetration is totally avoided.

MODIFIED SHAPE FUNCTIONS FOR QUADRILATERAL FINITE ELEMENTS

Figure 1 shows a two-dimensional contact problem. Node C contacts element (1-2-3-4) of the target and from then on contributes to its shape functions. We start from the initial 4-nodes interpolation function

$$v = \sum_{a=1}^{4} N_a \, v_a \tag{1}$$

with

$$N_a = 0.25 \left(1 + \text{sign}\left(\xi_a\right) \xi\right) \left(1 + \text{sign}\left(\eta_a\right) \eta\right) \tag{2}$$

where ξ, η are local coordinates, and v are the velocities.
In order to take the contribution of point C (node 5) into account, we modify the interpolation function as follows :

$$v = \sum_{a=1}^{5} N_a^{*} \, v_a \tag{3}$$

Notice that from a global point of view there is no new node appearing.

Obviously, a "hat shape function" at node 5 is the most adequate for our purpose. This yields automatic compatibility of the velocities at the interface, if a symmetric formulation is used. Further, we want to account for tangential sliding with friction at the contact point. Therefore, we introduce a factor μ which allows the shape function at node 5 to vary in amplitude between 0 and 1, which will lead to a partial exchange of momentum. The resulting shape functions are (assuming C is on side $\eta = +1$) :

$$N_5^{*} = \mu N_5 = \begin{cases} 0.5\,\mu\,(1+\eta)\left[1+(\xi-\xi_5)/(1+\xi_5)\right] & \text{if } \xi < \xi_5 \\ 0.5\,\mu\,(1+\eta)\left[1-(\xi-\xi_5)/(1-\xi_5)\right] & \text{if } \xi \geqslant \xi_5 \end{cases} \tag{4}$$

and

$$N_a^{*} = N_a - \alpha_a \, N_5^{*} \qquad a = 1 \longrightarrow 4 \tag{5}$$

with

$$\alpha_a = 0.5\left(1 + \text{sign}\, \xi_a \, \xi_5\right)$$

The local coordinates of C are $(\xi_5, 1)$. We can also assume, without restriction, that the contact point is associated with local coordinates (0, +1), N_5^{*}

then becomes†

$$N_5^* = 0.5\,\mu\,(1+\eta)\,(1-\text{sign}(\xi)\cdot\xi) \tag{6}$$

This shape function is shown on figure 2. Observe that $N_3^*(\xi_5, \eta_5)$ does not vanish at node 5 when $\mu \neq 1$, but $N_a = 1$ is preserved.

In the sequel, we separate normal (n) and tangential (t) directions and therefrom the following typical possible situations.

a. $\mu_n = 1$, $\mu_t = 0$, corresponds to frictionless sliding in the tangential direction and sticking in the normal direction. This yields :
$N_n^* = N_a$ $(a = 1 \to 5)$, the standard 5-nodes interpolation function,
$N_t^* = N_a$ $(a = 1 \to 4)$, the standard 4-nodes interpolation function.

b. $\mu_n = 1$, $\mu_t = 1$ corresponds to sticking, and yields :
$N_n^* = N_t^* = N_a$ $(a = 1 \to 5)$.

c. $\mu_n = 1$, $\mu_t \in]0.1[$ this accounts for frictional sliding.

Since μ depends on orientation, we introduce a second order tensor, which we need in order to define strain rates and stresses in global coordinates.

In a local orthogonal frame tangential to the target surface we write

$$\begin{Bmatrix} v_n^T \\ v_t^T \end{Bmatrix} = \begin{bmatrix} \mu_n & 0 \\ 0 & \mu_t \end{bmatrix} \begin{Bmatrix} v_n^C \\ v_t^C \end{Bmatrix} \tag{7}$$

where the superscripts T and C stand for target and contactor, respectively, and the subscripts n and t for normal and tangential.

Equation (7) defines the contribution of node 5 (contactor) to the target velocity while the true local velocity, at C, is given by

---

† $\text{sign}(\xi) = \begin{matrix} -1 & \text{if } \xi < 0 \\ +1 & \text{if } \xi \geqslant 0 \end{matrix}$

$$\left\{ v^n \right\} = \sum_{a=1}^{5} \left[N_a^n \right] \left\{ v_a^n \right\} \tag{8}$$

where[†]

$$\left\{ v^n \right\} = \left[v_n^T \quad v_t^T \right] \tag{9}$$

$$\left\{ v_a^n \right\} = \left[v_{1n}^T \; v_{1t}^T \; v_{2n}^T \; v_{2t}^T \; \ldots\ldots v_{4t}^T \; v_{5n}^C \; v_{5t}^C \right]^T \tag{10}$$

and $\left[N_a^n \right]$ is defined as follows[††]

$$\left[N_5^n \right] = N_5 \left[\mu^n \right] \tag{11}$$

$$\left[N_a^n \right] = N_a \left[I \right] - \alpha_a \left[N_5^n \right] \tag{12}$$

$$\left[\mu^n \right] = \begin{bmatrix} \mu_n & 0 \\ 0 & \mu_t \end{bmatrix} \tag{13}$$

$$\left[I \right] = \begin{bmatrix} 1 & 0 \\ 0 & 1 \end{bmatrix} \tag{14}$$

The matrix $\underset{\sim}{N}_5^n$ is diagonal when defined in a local referential, tangential to the contact surface. It does not induce a coupling of the normal and tangential components, but this would not be true in a global referential. We can, therefore, establish the stiffness in this local referential and rotate the element matrix before we assemble the elements. Alternatively we can make the derivation in a global coordinate system.

In practice, the whole effort essentially reduces to minor changes in the shape function routines.

TRANSIENT SOLUTION PROCEDURE

Search Algorithm

We need to determine at each time step the location of each node of each body in the contact zone with respect to the mesh of the other one. For that purpose a connectivity matrix is established in the input phase; this matrix lists all elements connected to each element. Assuming the time step to be small, we memorize the previous position of each node (by an element number), and search for its new position in adjacent elements. A 2-dimensional search path is shown on figure 3. Once the new position is known, we modify the shape functions of the target element as described in the previous paragraph and compute the updated stiffnesses.

---

† T as superscript of a matrix stands for transpose

†† α_a depends on the local coordinate of the fifth node

Predictor-Corrector Algorithm

We adopt here an explicit predictor-corrector algorithm, defined by the following equations, at time step (n + 1) (see ref. 1, 2 for details).

$$\underset{\sim}{M}\,\underset{\sim}{a}_{n+1} + \underset{\sim}{N}\left(\tilde{\underset{\sim}{d}}_{n+1}\,,\,\tilde{\underset{\sim}{v}}_{n+1}\right) = \underset{\sim}{F}_{n+1} \tag{15}$$

$$\tilde{\underset{\sim}{d}}_{n+1} = \underset{\sim}{d}_n + \Delta t\,\underset{\sim}{v}_n + \frac{\Delta t^2}{2}\left(1-2\beta\right)\underset{\sim}{a}_n \tag{16}$$

$$\tilde{\underset{\sim}{v}}_{n+1} = \underset{\sim}{v}_n + \Delta t\left(1-\gamma\right)\underset{\sim}{a}_n \tag{17}$$

$$\underset{\sim}{d}_{n+1} = \tilde{\underset{\sim}{d}}_{n+1} + \Delta t^2\,\beta\,\underset{\sim}{a}_{n+1} \tag{18}$$

$$\underset{\sim}{v}_{n+1} = \tilde{\underset{\sim}{v}}_{n+1} + \Delta t\,\gamma\,\underset{\sim}{a}_{n+1} \tag{19}$$

$$\underset{\sim}{d}_0 = \underset{\sim}{D} \tag{20}$$

$$\underset{\sim}{v}_0 = \underset{\sim}{V} \tag{21}$$

$$\underset{\sim}{a}_0 = \underset{\sim}{M}^{-1}\left(\underset{\sim}{F}_0 - \underset{\sim}{N}\left(\underset{\sim}{d}_0\,,\,\underset{\sim}{v}_0\right)\right) \tag{22}$$

Equations (16) and (17) are predictor equations (upper tilda), (18) and (19) are corrector equations, (20) to (22) are initial conditions, and $\underset{\sim}{N}$ is a nonlinear algebraic operator†. The implementation procedure can be found in (ref. 1).

If frictional contact occurs, we need in addition a predictor equation for $\tilde{\mu}_{n+1}$. Because of lack of space, this is not developed here. For the time being we adopt

$$\tilde{\mu}_{n+1} = \mu_n \tag{23}$$

NUMERICAL RESULTS

The analysis of an impact of a rectangular block on a rigid surface is performed (see ref. 3, for comparison). Figure 4 shows the mesh. The data are

density	$\rho = 0.01$
modulus of elasticity	$E = 1{,}000$
Poisson's coefficient	$\nu = 0.3$
dimensions	$L \,.\, W = 9.9$
time step	$\Delta t = 0.002725$

† If variables are to be memorized at element integration points, as often in nonlinear problems, remember that these are moving when node 5 moves.

Newmark parameters (explicit predictor-corrector algorithm)	$\gamma = 0.5 \qquad \beta = 0.25$
initial velocity	$v_0 = 1$
wave velocity	$C_d = \{[E(1-\nu)] / [(1+\nu)(1-2\nu)\cdot\rho]\}^{0.5} = 366.9$

The time step is defined by the transit time for a dilatational wave to cross one element. The impact takes place at t = 0. Frictionless contact is assumed ($\mu_t = 0$). This is introduced via isolated nodes, as shown on figure 4a. For the purpose of testing the new formulation, both node-to-node and distinct nodal positions are tested and yield the same results.

The anticipated solution is shown on figure 4b. This exact solution has two constant zones separated by the dilatational wave front emanating from the initial impact. The circular wave front is a result of reflections off the free boundary.

During the early steps of the computation, stresses in zone II are obtained from the impulse equation applied to a one-dimensional situation ($\sigma = c\cdot\rho\cdot v_0$) Stress results shown on figure 5.a confirm the validity of the new approach. Some overshoot appears, however, in the stress results of the lowest row of elements, probably due to the absence of a discrete impact condition in the algorithm. The deformed configuration at t = 0.0218 s.is shown on figure 5b.

CONCLUDING REMARKS

A new approach to contact problems involving friction in two-dimensional elastodynamics is proposed in this article. The basic idea obviously shows some analogies with local remeshing techniques, like the one proposed in (ref. 4). The treatment of friction via modified shape functions seems similar to the lines of thinking adopted in (ref. 5) for the treatment of shock waves.

The proposed formulation is symmetric (both bodies are contactor and target for each other) and satisfies compatibility of velocities over the contact interface (when possible), thus avoiding interpenetration. Completeness of the modified elements remains satisfied. Although no detailed comparison with different approaches has been made as yet, the following advantages can be mentioned : constant size of the system of equations (not true for local remeshing or Lagrange multiplier approach, important if an implicit solution is performed) and interface compatibility (not true in general for Lagrange multipliers or penalty methods).

The extension of the method to several contacting nodes per element is possible, but it is not trivial. The extension to contact problems in three dimensional space and inclusion problems in 2-D is possible, but at the cost of losing interface compatibility. As already mentioned, nonlinear analysis may present minor difficulties because of the fact that integration points can move.

Further research is needed on the predictor algorithm for sliding with friction and impact-release conditions have to be added.

Our main effort, at present, is directed towards testing the approach in problems involving friction.

REFERENCES

1. T.J.R. Hughes, K.S. Pister, R.L. Taylor : Implicit-explicit finite elements in nonlinear transient analysis.
FENOMECH 79 Symposium Proceedings, Stuttgart, West Germany, 1978.

2. T.J.R. Hughes, W.K. Liu : Implicit-explicit finite element in transient analysis. J. of Applied Mechanics, Vol. 45, 371-378, 1978.

3. T.J.R. Hughes, R.L. Taylor, J.L. Sackman, A. Curnier, W. Kanoknukulchai : A finite element method for a class of contact-impact problems. Computer Methods in Applied Mechanics and Engineering, No 8, 249-276, 1976.

4. P. Cundall, Joaquim Marti, Peter Beresford, Nigel Last, Margaret Asgian : Computer modelling of jointed rock masses, Dames and Moore Report NTIS N-78-4, Los Angeles, 1978.

5. L.C. Wellford, J.T. Oden : Discontinuous finite element approximations for the analysis of shock waves in nonlinearly elastic materials. J. of Computational Physics, No 19, 179-210, 1975.

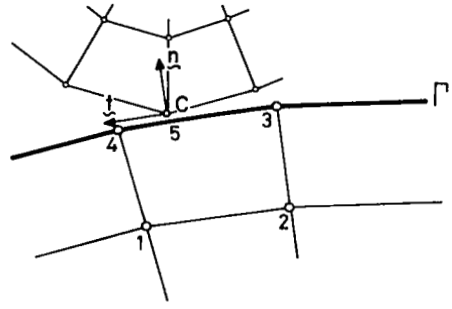

Figure 1.- Contact problem.

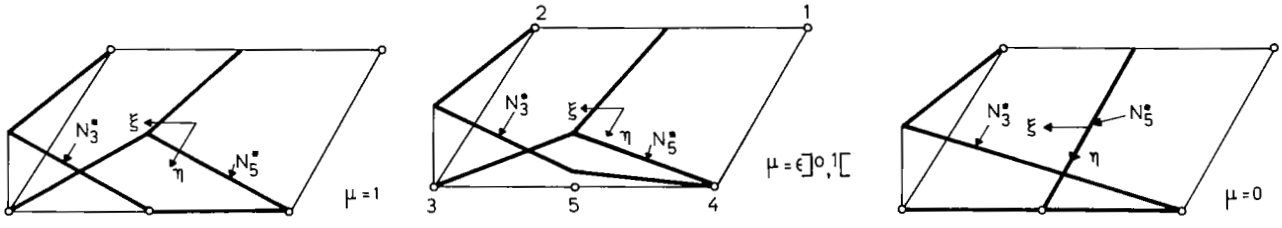

Figure 2.- Modified shape functions.

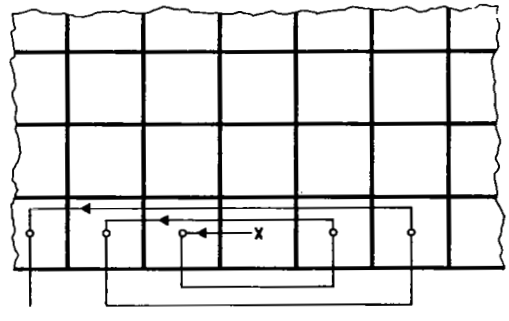

Figure 3.- Search path.

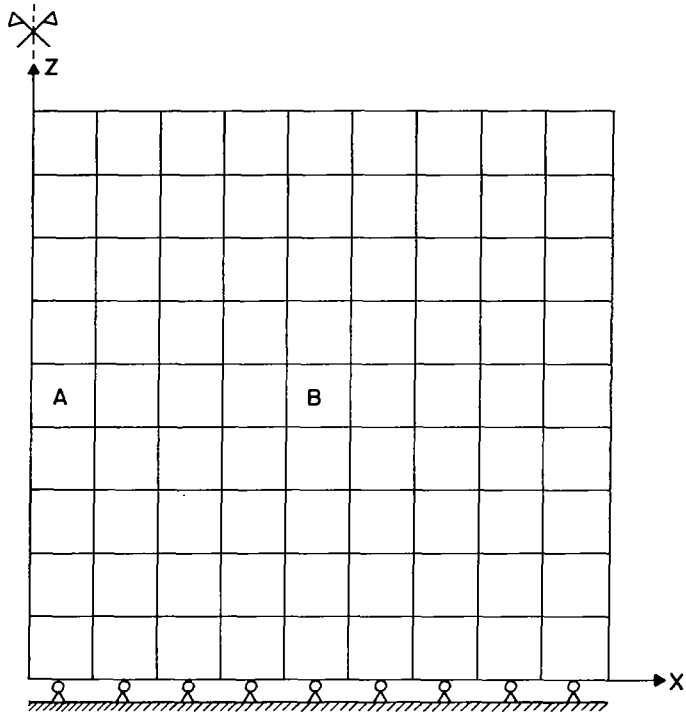

(a) Finite element mesh.

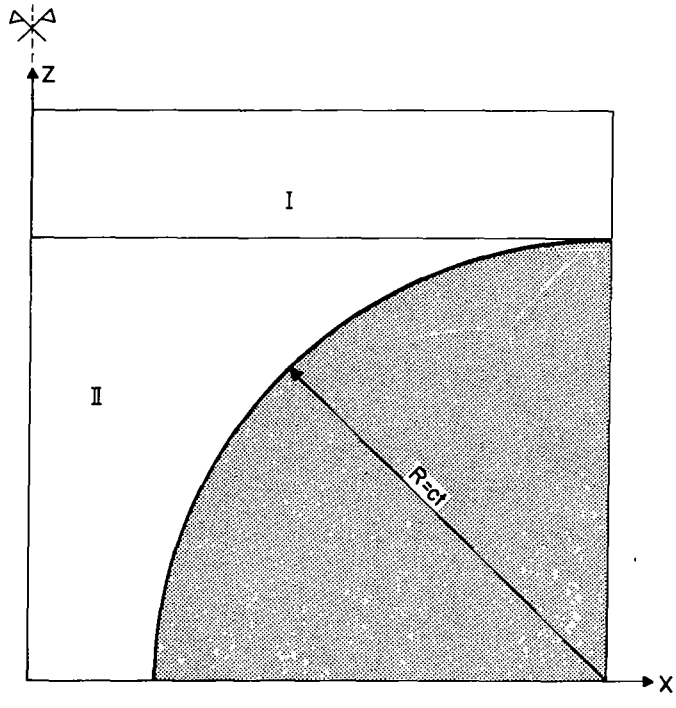

(b) Wave front diagram.

Figure 4.- Impact of rectangular block on a rigid surface.

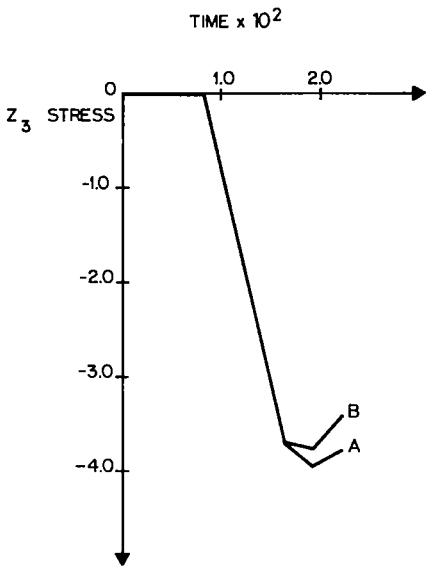

(a) Stress results.

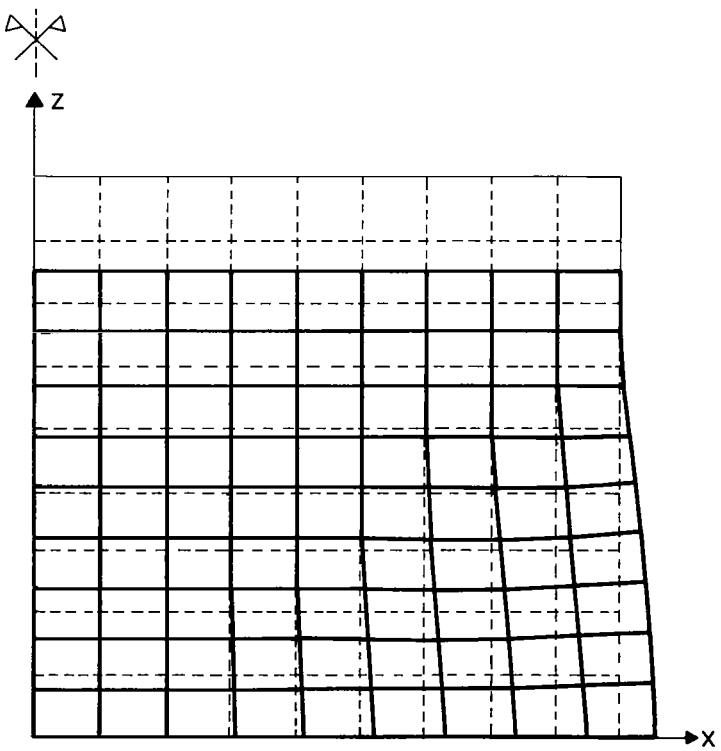

(b) Deformed mesh.

Figure 5.- Stress results and resulting deformed mesh.

INELASTIC BEHAVIOR OF STRUCTURAL COMPONENTS*

Noor Hussain, K. Khozeimeh and T. G. Toridis
School of Engineering and Applied Science
The George Washington University
Washington, DC 20052, USA

SUMMARY

The objective of this paper is to develop a more accurate procedure for the determination of the inelastic behavior of structural components. For this purpose, the actual stress-strain curve for the material of the structure is utilized to generate the force-deformation relationships for the structural elements, rather than using simplified models such as elastic-plastic, bilinear and trilinear approximations.

Force-deformation curves in the form of universal generalized stress-strain relationships are generated for beam elements with various types of cross sections. In the generation of these curves, stress or load reversals, kinematic hardening and hysteretic behavior are taken into account. Intersections between loading and unloading branches are determined through an iterative process.

Using the inelastic properties determined in this study, the plastic static response of some simple structural systems composed of beam elements is computed. Results are compared with known solutions, indicating a considerable improvement over response predictions obtained by means of simplified approximations used in previous investigations. The application of this procedure to the dynamic load case is currently in progress.

INTRODUCTION

Structural systems analyzed and designed for traditional loads and materials have been observed to undergo inelastic deformations when excessive load conditions are experienced. It is, therefore, an established fact now that inelastic deformations do occur in structures and are considered in the analysis in order to produce more economical and safe designs. For example, a generally accepted philosophy in the seismic analysis and design of structures is that a structure should remain elastic during earthquakes of small intensity that occur frequently; it should undergo limited plastic deformations during earthquakes of moderate intensity; however, it may undergo large plastic deformations but without major collapse during earthquakes of relatively high intensity that occur infrequently.

*This study has been partially supported by the National Science Foundation Research Grant No. PFR-79-16263.

At the same time, advances in naval, aerospace and nuclear reactor technology has led to the use of new materials such as stainless steel, alloys of aluminum and nickel, reinforced plastics, etc. The stress-strain curves for these materials are generally nonlinear. Therefore, an economical design of structures composed of such materials requires an accurate knowledge of the magnitude and distribution of the stresses and strains, as well as, the displacements. In all cases the effect of nonlinearities must be considered in the analysis.

In the study of the inelastic behavior of structures various idealizations to the actual stress-strain curves or force-deformation relations have been employed. The most extensively used model is the elastic perfectly plastic representation, principally due to its simplicity. When unloading occurs, this model neglects the strain hardening and Bauschinger effects. In general it produces conservative results and is mostly suitable for mild steel structures. Bilinear models with a nonzero slope for the inelastic branch have also been used widely. These models allow for the consideration of strain hardening effects (both isotropic and kinematic) due to loading and unloading cycles arising from static and dynamic loads. A trilinear model has also been used to simulate the stress-strain relationship of the material under static loads.

Simplified models often perform satisfactorily in predicting the inelastic behavior of special classes of structures. However, for general types of structures, an accurate representation of the stress-strain or force-deformation properties are needed for both the loading and unloading branches in the form of curvilinear or multilinear (piecewise linear) relations that follow as closely as possible the actual behavior of the system.

In the present study an accurate procedure is considered for the determination of the inelastic behavior of structural components. For this purpose, the actual stress-strain curve for the material of the structure is utilized to generate the force-deformation relationships for the structural elements, rather than using simplified models, such as elastic-plastic, bilinear and trilinear approximations. Applying this process to frame type structures, force-deformation curves in the form of universal generalized stress-strain relationships are generated for beam elements with various types of cross sections. In the generation of these curves stress or load reversals, more realistic strain hardening properties and hysteretic behavior are taken into account. Intersections between loading and unloading branches are determined through an iterative process. Based on the rather accurate force-deformation relationships of the individual elements, the governing equations for the structural system are established and used to compute the inelastic response of the structure.

GOVERNING EQUATIONS

Application of the Hamiltonian Principle to discrete systems in the context of the finite element method yields the basic dynamic equations governing the behavior of the structural systems. In matrix form these equations can be expressed as (ref. 1)

$$[m]\{\ddot{q}\} + ([K] + [K_G])\{q\} = \{F\} + \{F^O\} \tag{1}$$

where $[m]$ = consistent mass matrix of the structural system.

$[K]$ = elastic stiffness matrix of the structural system.

$[K_G]$ = geometric stiffness matrix of the structural system.

$\{q\}$ = vector of displacements at the structural degrees of freedom.

$\{\ddot{q}\}$ = vector of accelerations at the structural degrees of freedom.

$\{F\}$ = generalized nodal force vector corresponding to externally applied loads.

$\{F^O\}$ = equivalent generalized nodal force vector due to plastic strains, computed in accordance with the initial stiffness method.

In case of static loading the above equations take the form of

$$([K] + [K_G])\{q\} = \{F\} + \{F^O\} \tag{2}$$

PLASTICITY RELATIONS

Stress-Strain Curve

An experimentally determined virgin curve of the material is in general curvilinear. Starting with the experimental stress-strain data analytical expressions can be obtained to represent this data. Such expressions can be in the form of algebraic or other types of polynomials, exponential functions, or the widely used curvilinear relationship known as the Ramberg-Osgood approximation represented by

$$\varepsilon = \frac{\sigma}{E}\left[1 + D\left(\frac{\sigma}{\sigma_y}\right)^{R-1}\right] \tag{3}$$

in which ε and σ are the unit strain and unit stress, respectively, E represents the modulus of elasticity, σ_y denotes the yield stress of the material and D and R are real constants to be determined. However, this relationship is not explicit in stresses and, therefore, numerical procedures are needed to find the stresses corresponding to given strains. On the other hand, if the stress-strain data cannot be represented by an analytical expression, the curve is approximated by a series of line segments given by

$$\sigma = \sigma_i + k_{i+1}(\varepsilon - \varepsilon_i) \quad , \varepsilon_i < \varepsilon \leq \varepsilon_{i+1} \tag{4}$$

where, (σ_i,ε_i) are the stress-strain values at the beginning of the ith segment and k_{i+1} is the slope of the line segment between the points (σ_i,ε_i) and $(\sigma_{i+1},\varepsilon_{i+1})$ expressed as

$$k_{i+1} = \frac{\sigma_{i+1} - \sigma_i}{\varepsilon_{i+1} - \varepsilon_i} \quad , i = 0,1,2, \ldots, (n-1) \tag{5}$$

where n is total number of segments used to approximate the curve.

Moment-Curvature (Force-Deformation) Relationship

Figure 1 shows a general elasto-plastic doubly symmetric cross section of a beam member. A linear strain distribution over the depth of the cross section up to ultimate behavior is assumed. Tensile stresses are considered positive and curvatures causing positive strains at bottom fibers are also positive. The x- and y-axes are the principal axes and the z-axis is the geometric centroidal axis of the cross section. The bending moment acting on the cross section is the sum of moments of the stresses acting on the cross section about the geometric centroidal axis, i.e.

$$M = \int_A \sigma \, y dA \tag{6}$$

in which dA is an element of area. The integration is carried over the elastic and plastic parts of the area. Usually the stress-strain curve of the material cannot be represented explicitly for stresses; therefore, a numerical integration procedure is employed. For this purpose the section is divided into a series of rectangular slices, and the contribution of each slice to the moment acting over the cross section is found. Before indicating the details necessary for accomplishing this, certain definitions need to be established as follows. If ε_y, ε_u and σ_y are the yield strain, ultimate strain and yield stress, respectively, as observed in a tension test on a material and h is the distance to extreme fibers from z-axis, then

$$M_y = \sigma_y I_z/h = \sigma_y S \tag{7}$$

where M_y, I_z, S are the yield moment, moment of inertia and section modulus of the section, respectively. The yield curvature ϕ_y is obtained from

$$\phi_y = M_y/E I_z \tag{8}$$

Based on the assumption of a linear strain distribution over the cross section of the member, the ultimate curvature ϕ_u is given by

$$\phi_u = \varepsilon_u/h \tag{9}$$

In the present study the curvature range between ϕ_y and ϕ_u is divided into a suitable number of intervals to give enough data points to fit a curve. The strain ε_i at the center of ith rectangular slice, assumed to be uniformly distributed over the slice, corresponding to a curvature value ϕ_j is given by

$$\varepsilon_i = \phi_j y_i \tag{10}$$

where y_i is the distance to the centroid of the ith rectangular slice from the centroidal axis of the cross section. The strain ε_i in the ith slice due to curvature ϕ_j, at the jth discrete point along the member, is used to determine the stress σ_i assumed to act uniformly over the entire slice, from the stress-strain relationship as discussed previously. If A_i is the area of the ith slice, the force acting on the ith slice is given by

$$F_i = \sigma_i A_i \tag{11}$$

The moment of the force about the neutral axis is obtained from

$$M_i = F_i y_i \tag{12}$$

By summing over the total number of slices used to model the cross section, the total internal moment M_j on the cross section corresponding to a curvature ϕ_j is expressed as

$$M_j = \sum_{i=1}^{NS} M_i = \sum_{i=1}^{NS} \sigma_i A_i y_i \tag{13}$$

where NS is number of slices and j represents a typical discrete point along the member. Similarly the total internal axial force P at the cross section due to a prescribed strain field ε is obtained from

$$P = \sum_{i=1}^{NS} \sigma_i A_i \tag{14}$$

Equations (13) and (14) directly yield force P and moment M corresponding to a prescribed deformation field. However, to get the deformation corresponding to a given load history, equations (13) and (14) have to be solved iteratively. The moment curvature data generated through the use of equation (13) is then presented explicitly for curvature by a polynomial of the type

$$\phi = M/EI + \sum_{i=1}^{N} C_i M^i \tag{15}$$

where C_i are the polynomial coefficients to be determined and N is degree of the polynomial. Alternatively, an equation of the Ramberg-Osgood type

$$\phi = \frac{M}{EI}\left[\, 1 + D(M/My)^{R-1} \,\right] \tag{16}$$

can be fitted in which D and R are the real constants to be determined.

Normalized Moment Curvature Relationship

The moment-curvature data generated from Eq. (13) is normalized by using the quantities M_y and ϕ_y, so that

$$\bar{M} = M/M_y \tag{17}$$

$$\bar{\phi} = \phi/\phi_y \tag{18}$$

where $\bar{M}$ and $\bar{\phi}$ are normalized moment and normalized curvature, respectively. The normalized curvature is then separated into its elastic and plastic components $\bar{\phi}_e$ and $\bar{\phi}_p$, respectively, so that solving for $\bar{\phi}_p$

$$\bar{\phi}_p = \bar{\phi} - \bar{\phi}_e \tag{19}$$

Since $\phi_e = M/EI$, based on equation (17) the normalized elastic curvature is written in the form

$$\bar{\phi}_e = \bar{M} \tag{20}$$

Based on the normalized plastic components of curvature computed from equation (19), a polynomial of the form

$$\bar{\phi}_p = \sum_{i=0}^{N} d_i \bar{M}^i \tag{21}$$

is then fitted to approximate the data, where the d_i's are constants to be determined through regression analysis. Alternatively, an equation of the type

$$\phi_p = D\,\bar{M}^R \tag{22}$$

is also used to represent the data. The real constants D and R are determined by taking the logarithmic form of Eq. (22), so that

$$\ln \bar{\phi}_p = \ln D + R \ln \bar{M} \tag{23}$$

This is an equation of a straight line. Constants D and R are determined from linear regression analysis using the data for $\ln \bar{\phi}_p$ and $\ln \bar{M}$.

Using equations (19), (21), and (22), the following moment-curvature relations can now be formulated

$$\bar{\phi} = \bar{M} \quad , \quad \bar{M} < 1 \tag{24}$$

$$\bar{\phi} = \bar{M} + \sum_{i=0}^{N} d_i \bar{M}^i \quad , \quad \bar{M} > 1 \tag{25}$$

$$\bar{\phi} = \bar{M} + A\,\bar{M}^R = \bar{M}\,[1 + A\bar{M}^{R-1}] \quad , \quad \bar{M} > 1 \tag{26}$$

Slope of Generalized Stress-Strain Curve

A universal stress-strain curve usually represents the relationship between $\bar{\phi}^P$ and $\bar{M}$ expressed by Eqs. (21) or (22). Rewriting these equations in differential form and solving for the slope $\bar{K}_2$ yields

$$\bar{K}_2 = \frac{d\bar{M}}{d\bar{\phi}^P} = \frac{1}{\sum_{i=1}^{N} i\, d_i\, \bar{M}^{(i-1)}} \tag{27}$$

and

$$\bar{K}_2 = \frac{d\bar{M}}{d\bar{\phi}P} = \frac{1}{AR\,\bar{M}^{(R-1)}} \tag{28}$$

If a smooth analytical expression to fit the $\bar{\phi}^P - \bar{M}$ data is not possible within tolerable limits of accuracy, the slope $\bar{K}_2$ of the universal stress-strain curve is obtained as a series of approximate tangents drawn at discrete points representing the data, i.e.

$$(\bar{K}_2)_i = \frac{\bar{M}_{i+1} - \bar{M}_i}{\bar{\phi}^p{}_{i+1} - \bar{\phi}^p{}_i} \tag{29}$$

where i and i+1 are typical discrete points.

In eqs. (21), (22) and (24)-(29) the cross section is assumed to be subjected to a bending moment about the centroidal axis. However, in practical cases, structural elements are generally subjected to stress resultants acting in different directions. To extend the applicability of the above procedure, it is assumed that similar relationships exist between the effective stress f* and effective strain Θ* in a multi-axial stress case. The function f* in normalized form is also identified with the yield function.

Yield Function

When stress resultants in normalized form (instead of unit stresses) are considered to be generalized stresses in the context of plasticity theory, yielding at any section of a member is then assumed to occur when the critical combination of generalized stresses initiate inelastic deformations at that section. The yield function is expressed by an equation of the form

$$f^*(Q_i) = Y \tag{30}$$

where Q_i are the generalized stresses and Y is the initial yield value. To make the yield function independent of the cross section, the yield function equation is derived in terms of normalized (dimensionless) force parameters. A force component is normalized by its corresponding characteristic value (usually the value at first yield). In normalized form equation (30) takes the form of

$$f^*(\bar{Q}_i) = 1 \tag{31}$$

For a space frame member the cross section is subjected to a generalized force vector S having 6 components, so that

$$\{S\} = \{P_x, V_y, V_z, M_x M_y, M_z\} \tag{32}$$

where

P_x = axial force

V_y, V_z = direct or transverse shear forces

M_x, M_y = Bending moments

M_z = Twisting or torsional moment

Each of these forces influence the yield behavior at a cross section and the inelastic response depends upon the interaction between them. In the past, elliptical, parabolic, spherical (ref. 2) and other forms of yield functions have been used in inelastic analysis of structures. In the present study a spherical yield function is used as indicated below

$$f^* = \left[\left(\frac{P_x}{P_{ox}} \right)^2 + \left(\frac{M_x}{M_{ox}} \right)^2 + \left(\frac{M_y}{M_{oy}} \right)^2 + \left(\frac{M_z}{M_{oz}} \right)^2 \right]^{\frac{1}{2}} = \bar{Y} \qquad (33)$$

in which $\bar{Y}$ denotes the normalized yield value which may change during straining and P_{ox}, M_{ox}, M_{oy} and M_{oz} are the characteristic values of axial force, torsional moment, and bending moments about y and z axes, respectively. Similar expressions can be written for a plate element (ref. 1).

The above yield function can be used in conjuction with an average force model (refs. 1, 3) which assumes that an element undergoes plastic deformations if the loading function f* determined from average values of stress resultants acting at the member ends exceeds the current normalized yield value.

Flow Rule

A flow rule expresses the relationship between plastic strains and stresses. In the present study rather than solving the flow equations rigorously in terms of stress resultants, an approximate procedure (refs. 1, 3) is employed. In this method if f^*_{est} is the plastic potential at the end of a load increment in dynamic analysis (computed using member forces $P_{i_{est}}$ obtained from an elastic analysis), then the increment of plastic potential df^*_1 for an element already undergoing inelastic deformation is obtained from the equation

$$df_1^* = f_{est}^* - f_{prev}^* \qquad (34)$$

where f^*_{prev} is the plastic potential at the end of previous load or time increment. For a transitional element the equation for the increment of plastic potential is of the form

$$df_1^* = f_{est}^* - f_o^* \qquad (35)$$

where f_o^* is the initial yield value.

As shown in detail in reference 1, the correct value of the plastic potential increment df* can be computed from the relation

$$df^* = \frac{\bar{K}_2}{1 + \bar{K}_2} \, df_1^* \tag{36}$$

The current corrected value of the plastic potential f^*_{curr} is then obtained as

$$f^*_{curr} = f_{prev} + df^* \tag{37}$$

for an element already undergoing plastic deformations and

$$f^*_{curr} = f^*_o + d_f* \tag{38}$$

for an element entering the plastic range.

With the known value of the plastic potential f^*, the final values of member (element) forces are computed by a proportioning procedure represented as (refs. 1, 3)

$$P_{i_{curr}} = P_{i_{est}} \frac{f^*_{curr}}{f^*_{est}} \tag{39}$$

The overall numerical procedure utilized in the computation of the element and structural responses is the same as the one outlined in references 1 and 2.

NUMERICAL RESULTS

To determine the feasibility of the proposed method, two structures for which results are available in the literature were analyzed and the results were compared with the works of other investigators.

Example 1 - The first example considered consists of the simply supported beam with the I cross-section and material property, as shown in figure 1. The given stress-strain curve corresponds to material B as defined by Chajes (ref. 4) who had originally studied this structure. As in the case of the above reference, the stress-strain curve is idealized by a bilinear relationship. This is then utilized to obtain the moment curvature and the normalized universal stress-strain curves, as depicted in figure 2.

Subsequently, the response of beam when subjected to either a concentrated load at its midspan or a uniformly distributed load over its entire length is obtained. It should be mentioned that Chajes (ref. 4) has presented a "closed-form" solution for the deformation characteristic of the midspan of the beam when subjected to a concentrated load. However, his solution is based on the assumption that only the flanges resist the bending moment. In figure 3 are shown the deflection responses of the midspan as obtained in this study as well as that reported in reference 4. As can be observed, close agreement between the two sets of data is exhibited.

Example 2 - As a second example, a pin-based portal frame studied, both theoretically and experimentally, by Takahashi and Chiu (ref. 5) is analyzed. The structure consists of W12X27 sections, arranged to deform around their strong axes. The geometry of the structure and its loading are shown in figure 4a. The idealized structure and the equivalent nodal loading is shown in figure 4b. Note that the effect of the girder depth has been taken into account by introduction of an additional equivalent load and a bending moment at the top of the loaded column. In the analysis, a curve is fitted to the stress-strain relation for the mild steel with an average yield stress of 255 MN/m^2 and modulus of elasticity of $203.5X10^3$ MN/m^2. This is then used as a basis for determination of moment-curvature relationship for the structure. In figure 4c is shown the horizontal deflection response of the top of the unloaded column. Again, close correlation is observed.

REFERENCES

1. Khozeimeh, K., "Inelastic Response of Beam-Plate Assemblages Subjected to Static and Dynamic Loads," dissertation presented to the George Washington University, at Washington, D.C., in 1974, in partial fulfillment of the requirements for the degree of Doctor of Science.

2. Morris, G. A., and Fenves, S. J., "Approximate Yield Surface Equations," Journal of the Engineering Mechanics Division, ASCE, Vol. 95, No. EM4, Proc. Paper 6741, Aug., 1969, pp. 937-959.

3. Khozeimeh, K., and Toridis, T.G., "Models for Inelastic Response of Beam-Plate Assemblages," Journal of the Engineering Mechanics Division, ASCE, Vol. 104, No. EM5, October 1978, pp. 1001-1014.

4. Chajes, A., "Inelastic Deflection of Beams," Journal of the Structural Division, ASCE, Vol. 94, No. ST6, Proc. Paper 6012, June, 1968, pp. 1549-66.

5. Takahashi, S. K., and Chiu, R. H., "Static and Dynamic Behavior of Pinned-Based Portal Frames," NCEL TR336, Feb., 1965.

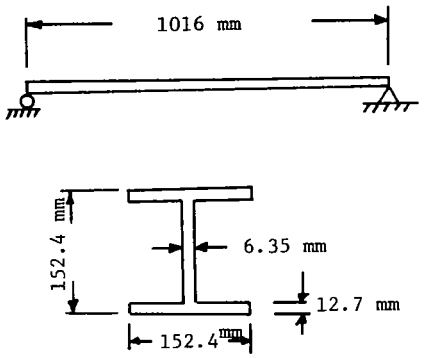

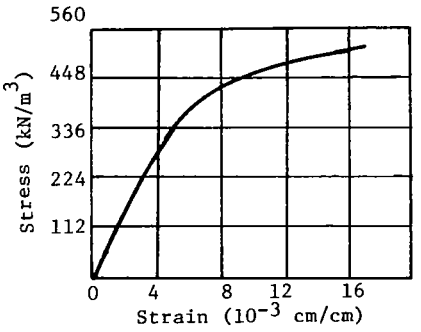

Figure 1.- Geometrical and material properties.

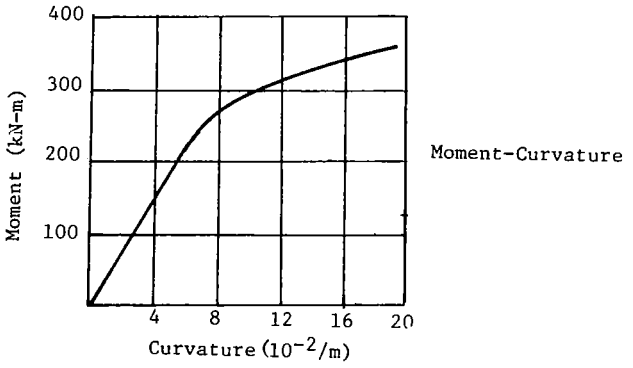

Moment-Curvature

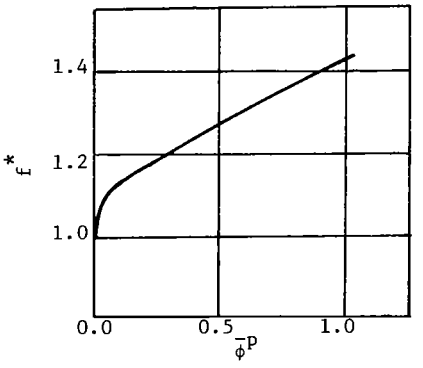

Universal Stress-Strain

Figure 2.- Moment-curvature and universal stress-strain curve.

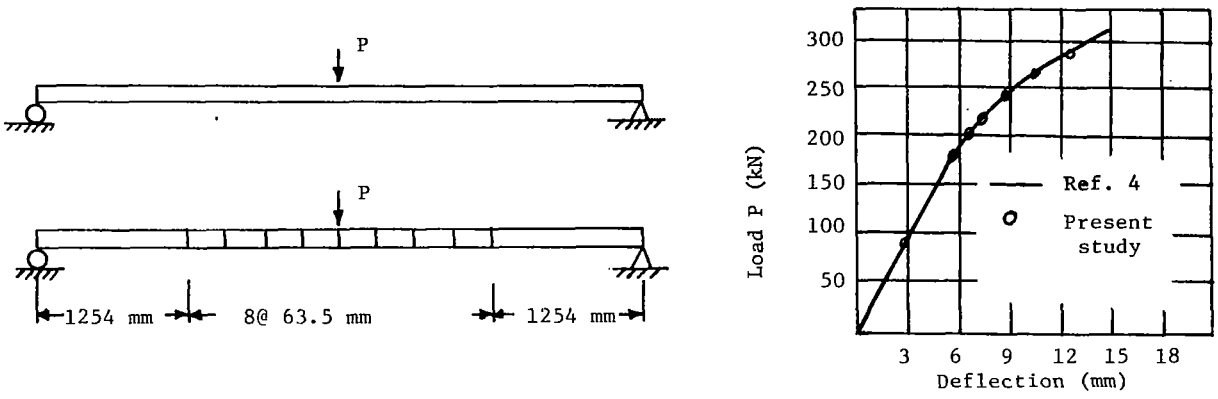

(a) Point load.

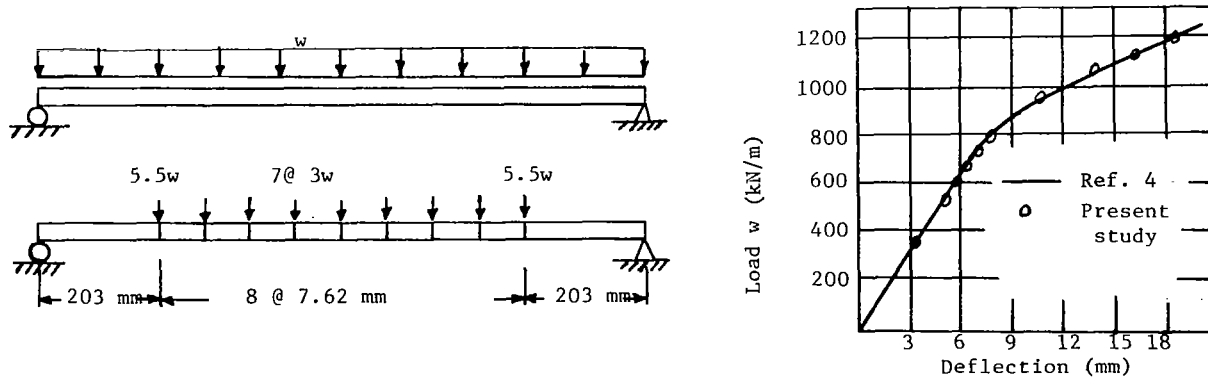

(b) Uniformly distributed load.

Figure 3.- Loading and mid-span deflection response.

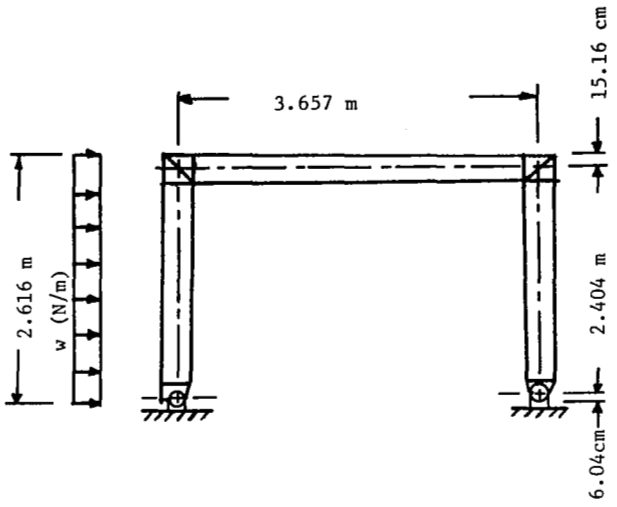

(a) Actual frame.

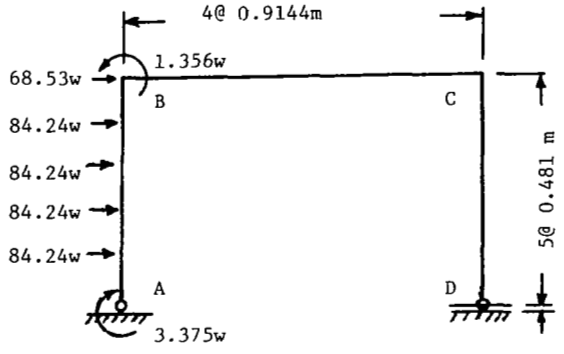

(b) Idealized frame.

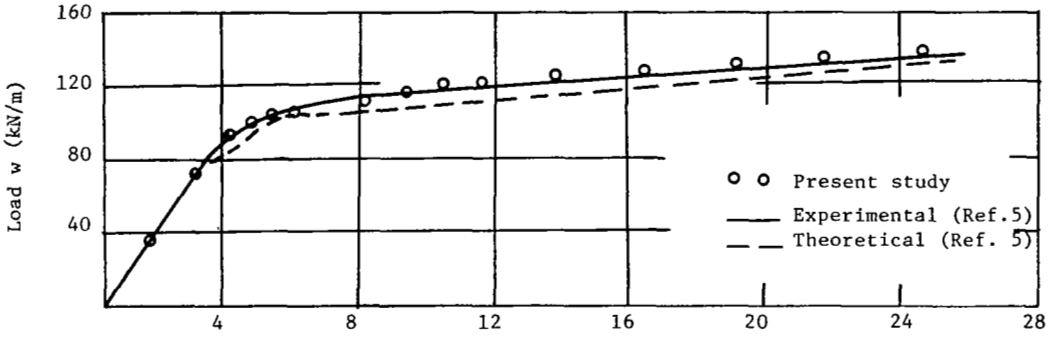

(c) Horizontal deflection of joint C (cm).

Figure 4.- Pin-based portal frame.

NONLINEAR FINITE ELEMENT ANALYSIS - AN ALTERNATIVE FORMULATION

Silvio Merazzi*
Ecole Polytechnique Fédérale de Lausanne, Switzerland

Peter Stehlin*
The Aeronautical Research Institute of Sweden, Stockholm, Sweden

SUMMARY

A geometrical nonlinear analysis based on an alternative definition of strain is presented. Expressions for strain are obtained by computing the change in length of the base vectors in the curvilinear element coordinate system. The isoparametric element formulation is assumed in the global Cartesian coordinate system. The approach is based on the minimization of the strain energy, and the resulting nonlinear equations are solved by the modified Newton method. Integration of the first and second variation of the strain energy is performed numerically in the case of two- and three-dimensional elements. Application is made to a simple long cantilever beam.

INTRODUCTION

The nonlinear finite element formulation described here represents a part of the development of the BASIS finite element analysis system (ref. 1). The basic idea was to combine linear and nonlinear behaviour in order to deal more efficiently with structural analysis. Thus, nonlinear elements had to be developed which fit into an existing system without loss of general validity. The Lagrange formulation has therefore been chosen (ref. 2), expressing the displacement variables directly in the global Cartesian coordinate system, although locally, for practical purposes, a skew coordinate system may be prescribed. The advantage of this formulation is the numerical method arising from it. By adopting the modified Newton method (ref. 3, 4) a clear solution process has been chosen, therefore minimizing errors due to a wrong understanding of nonlinear behaviour. The strains can be adapted to the nonlinearity of the problem. This feature may considerably reduce the computational effort.

---

* Research sponsored in part by the Swiss National Science Foundation (contract No. 2267-079) and the National Swedish Board for Energy Source Development under contract No. 5061-012.

A set of one-, two- and three-dimensional elements (in terms of curvilinear coordinates) can be derived from this formulation (Fig. 1). The elements presented here are based on the isoparametric approximation (ref. 3). One-dimensional elements are well suited to deal with cable and truss problems (ref. 5). Membrane and volume elements are mainly used to model elastic composite structures.

GOVERNING EQUATIONS

Consider a point P of the undeformed body (Fig. 2). The corresponding cartesian coordinate vector $\{r\}$ may be expressed as a function of the body's curvilinear coordinates Θ^α

$$\{r\} = \sum_{i=1}^{n} \{r\}_i \Psi_i(\Theta^\alpha) \tag{1}$$

where Ψ_i are the interpolation functions of the corresponding nodes. The base vectors at P are obtained by deriving $\{r\}$ with respect to the coordinates Θ^α

$$\{g\}_\alpha = \frac{\partial\{r\}}{\partial\Theta^\alpha} \tag{2}$$

For practical purposes, Eq. 2 can be rewritten

$$\{g\}_\alpha = [A]_\alpha \{s\} \tag{3}$$

$[A]_\alpha$ contains all functions $\Psi_{i,\alpha}$ and $\{s\}$ all Cartesian components of the node vectors $\{r\}_i$.

In order to define the strain energy the metric tensor at P

$$g_{\alpha\beta} = \{g\}_\alpha \cdot \{g\}_\beta \qquad \alpha = 1,3;\ \beta = 1,3 \tag{4}$$

and the infinitesimal volume

$$dV = \det(g_{\alpha\beta}) \cdot d\Theta^1 \cdot d\Theta^2 \cdot d\Theta^3 \tag{5}$$

are needed. In the deformed state the base vectors become (Fig. 1)

$$\{G\}_\alpha = \frac{\partial}{\partial\Theta} \sum_{i=1}^{n} (\{r\}_i \Psi_i + \{u\}_i \Psi_i) \tag{6}$$

Eq. 6 may be rewritten

$$\{G\}_\alpha = [A]_\alpha \cdot \{d\} + \{g\}_\alpha \tag{7}$$

where $\{d\}$ contains, similar to $\{s\}$, all Cartesian components of the node displacements. The metric tensor of the deformed body at P becomes

$$G_{\alpha\beta} = \{G\}_\alpha \cdot \{G\}_\beta \tag{8}$$

Substituting Eqs. 3 and 7 in Eq. 8,

$$G_{\alpha\beta} = \{d\}^T[D]_{\alpha\beta}\{d\} + \{d\}^T([D]_{\alpha\beta} + [D]_{\beta\alpha})\{s\} + g_{\alpha\beta} \tag{9}$$

with

$$[D]_{\alpha\beta} = [A]_\alpha^T \cdot [A]_\beta \tag{10}$$

The strains are now defined as the relative change of the base vectors:

$$\varepsilon_{\alpha\beta} = \frac{|\{G\}_\alpha + \{G\}_\beta| - |\{g\}_\alpha + \{g\}_\beta|}{|\{g\}_\alpha + \{g\}_\beta|} \tag{11}$$

or

$$\varepsilon_{\alpha\beta} = \left[\frac{G_{\alpha\alpha} + G_{\alpha\beta} + G_{\beta\alpha} + G_{\beta\beta}}{g_{\alpha\alpha} + 2g_{\alpha\beta} + g_{\beta\beta}}\right]^{\frac{1}{2}} - 1 \tag{12}$$

Eq. 12 can be expressed in terms of {d}

$$\varepsilon_{\alpha\beta} = \left[\frac{\{d\}^T[\bar{D}]_{\alpha\beta}(\{d\} + 2\{s\})}{\bar{g}_{\alpha\beta}} + 1\right]^{\frac{1}{2}} - 1 \tag{13}$$

with

$$[\bar{D}]_{\alpha\beta} = [D]_{\alpha\alpha} + [D]_{\alpha\beta} + [D]_{\beta\alpha} + [D]_{\beta\beta} \tag{14}$$

$$\bar{g}_{\alpha\beta} = g_{\alpha\alpha} + 2g_{\alpha\beta} + g_{\beta\beta} \tag{15}$$

Eq. 13 defines the strains $\varepsilon_{\alpha\beta}$ used to derive the numerical equations from the strain energy.

Note here that if the deformations are limited in size the root in Eq. 13 can be expressed as a series expansion according to

$$(X_{\alpha\beta} + 1)^{\frac{1}{2}} = 1 + \frac{1}{2} X_{\alpha\beta} + \ldots \tag{16}$$

Retaining only the first two terms of Eq. 16 leads to the quadratic approximation

$$\tilde{\varepsilon}_{\alpha\beta} = \frac{\{d\}^T[\bar{D}]_{\alpha\beta}(\{d\} + 2\{s\})}{2\bar{g}_{\alpha\beta}} \tag{17}$$

from which the linear solution may be obtained.

Assuming linear elastic behaviour, the variation of strain energy leads directly

to the nonlinear equilibrium equations of the element.

For ease of formulation the strains $\varepsilon_{\alpha\beta}$ are rewritten in vector form, $\{\varepsilon\} = \{\varepsilon_{11}, \varepsilon_{22}, \varepsilon_{33}, \varepsilon_{12}, \varepsilon_{13}, \varepsilon_{23}\}$. Furthermore, as the stress-strain relations are mainly formulated in a rectangular coordinate system the strain is transformed by

$$\{\gamma\} = [T]\{\varepsilon\} \tag{18}$$

The transformation matrix [T] is constant if the scalar products of the base vectors in the undeformed and in the deformed system are the same.

The strain energy density then becomes

$$dU = \frac{1}{2}(\{\sigma\}^T - \{\sigma_0\}^T)[E](\{\gamma\} - \{\gamma_0\})dV \tag{19}$$

or

$$dU = \frac{1}{2}(\{\varepsilon\}^T[T]^T[E] - \{\sigma_0\}^T)[T]\{\varepsilon\}dV \tag{20}$$

Eq. 20 is then integrated over the element. For one-dimensional elements an analytical solution is possible (ref. 5), whereas for two- and three-dimensional elements numerical integration must be performed. Using Gaussian integration the strain energy becomes

$$U \overset{\sim}{=} \frac{1}{2}\sum_{i=1}^{m}(\{\varepsilon\}_k^T[T]_k^T[E] - \{\sigma_0\}_k^T)[T]_k\{\varepsilon_k\}g_k w_k \tag{21}$$

where w_k designates the weight factor at the corresponding point Θ_k^α .

The set of nonlinear equations for one element is directly obtained from the first variation of the total potential energy with respect to the global variables

$$q_i(u_j) = \frac{\partial U}{\partial u_i} = f_i \tag{22}$$

{f} denotes the vector of external loads. It is worth mentioning here that in the case of dynamic analysis the equilibrium equations can also be obtained by applying Hamilton's principle and a suitable operator for discretization in time.

After rearrangement, Eq. 22 becomes

$$\{q\} = \sum_{k=1}^{m}(\{\varepsilon\}_k^T \cdot [\bar{E}] - \frac{1}{2}\{\sigma_0\}_k^T \cdot [T]_k^T) \cdot [P]_k \cdot g_k \cdot w_k \tag{23}$$

or

$$\{q\} = \sum_{k=1}^{m}\{\bar{\sigma}\}_k^T \cdot [P]_k \cdot g_k \cdot w_k \tag{24}$$

with

$$[P]^T = [\{p\}_{\alpha\beta}^T] \qquad \alpha = 1,3;\ \beta = \alpha,3 \tag{25}$$

and

$$\{p\}_{\alpha\beta} = \frac{(X_{\alpha\beta}+1)^{-\frac{1}{2}}}{\bar{g}_{\alpha\beta}} \cdot [\bar{D}]_{\alpha\beta} \cdot (\{u\}+\{s\}) \tag{26}$$

In order to solve Eq. 22 by the modified Newton method the Jacobian of {q} is needed:

$$[K] = \left[\frac{\partial^2 U}{\partial u_i \partial u_j}\right]$$

$$= \sum_{k=1}^{m} \left[[P]_k^T \cdot [\bar{E}] \cdot [P]_k + \bar{\sigma}_{\alpha\beta}(X_{\alpha\beta}+1)^{-\frac{1}{2}} \cdot \left\{\frac{1}{\bar{g}_{\alpha\beta}} [\bar{D}]_{\alpha\beta} - \{p\}_{\alpha\beta} \otimes \{p\}_{\alpha\beta}\right\}\right] \quad \alpha=1,3;\beta=\alpha,3 \tag{27}$$

For a set of several elements the stiffness matrices [K] are assembled to the global stiffness matrix and factored. Using the modified Newton method the n-th iteration becomes

$$\{d\}_{n+1} - \{d\}_n = \beta \cdot [K]_{\ell}^{-1} (\{f\} - \{q\}_n) \tag{28}$$

[K] being factored at iteration step $\ell \leq n$. The relaxation factor is computed using an extrapolation method for each iteration (ref. 5). Thus the final load level is reached stepwise, and for each new load step the solution is extrapolated quadratically. Convergence criteria are based on the Euclidean and maximum norms (ref. 6).

The computational procedure is essentially the same for all element types. However, for one-dimensional elements {q} and [K] can be determined analytically in terms of u_i, and the transformation [T] is not necessary. The [T] matrices for two- and three-dimensional elements are listed in the Appendix.

During the first assembly of [K] the [D], [T], [E] matrices as well as the geometry parameters $g_{\alpha\beta}$ and g are computed once for each Gaussian point and reused for further computations of [K] and {q}. For each iteration step {ε} and [P] are evaluated at each Gaussian point and the global {q} vector assembled. The global load vector contains not only external forces but also the first variation coming from linear elements. In fact, their contribution has to be evaluated only once for each load step, thus reducing the computing time.

NUMERICAL RESULTS

An application of the theory is demonstrated using results obtained by the BASIS computer program (ref. 1). A long thin cantilever beam (Fig. 3) has been idealized by 8-noded membrane elements. Its length is 1000 mm, height 10 mm and thickness 1 mm. The elastic modulus is 3000 N/mm^2 and the Poisson ratio 0.36. The beam is subjected to a load case consisting of a variable load Q at the node A and a case with constant Q and variable compression load P. Since the strains remain smaller than one in this example differences in the results are not detectable when using Eq. 17 instead of Eq. 13. The convergence criterion during iteration (Eq. 28) is based on the relative change of the displacement vector norm and has been set to 0.0001. The active load is applied stepwise. If convergence is rapid, the step is automatically increased. However, for highly nonlinear problems, it is preferable to recompute and refactor the stiffness matrix when the iteration diverges rather than to decrease the load step. The first and second variation of U has been computed using 2 by 2 Gaussian integration. Fig. 4 shows the load-displacement function at node A for transversal loading, and the same function for the divergence problem is exhibited in Fig.5. Note the good behaviour of the two-element approximation even for large nonlinearities.

To conclude, it should be mentioned that the problems currently being investigated include the influence of the integration order on numerical accuracy and convergence behaviour as well as the nonlinear creep of structures.

SYMBOLS

Vectors are symbolized by {}-brackets and matrices by []-brackets. $[]^T$ means transposed matrix, $[]^{-1}$ inverted or factored matrix, and ⊗ stands for dyadic product. Greek indices refer to the curvilinear coordinate system.

$[A]_\alpha$ matrix of form functions of curvilinear coordinate Θ^α

$[D]_{\alpha\beta}$ product of form function matrices (Eq. 11)

$\{d\}$ nodal displacement vector (global Cartesian components)

$\{\varepsilon\}$ strain vector, contains components $\varepsilon_{\alpha\beta}$

$[E]$ elasticity matrix

$g_{\alpha\beta}$ metric tensor of the undeformed body

$G_{\alpha\beta}$ metric tensor of the deformed body

$\{g\}_\alpha$ base vector of the undeformed body, coordinate Θ^α

$\{G\}_\alpha$	base vector of the deformed body
g	determinant of the metric tensor $g_{\alpha\beta}$
$\{\gamma\}$	strain vector in the local Cartesian system
$\{\gamma_0\}$	initial strain vector in the local Cartesian system
$[K]$	second variation of the strain energy (stiffness matrix)
$[P]$	matrix defined in Eq. 26
Ψ_i	interpolation functions for geometry and displacements
$\{q\}$	first variation of the potential energy
$\{r\}_i$	global Cartesian coordinate vector of node i
$\{s\}$	vector containing all Cartesian node coordinates
$\{\sigma\}$	stress vector in local Cartesian system
$\{\sigma_0\}$	initial stress vector in local Cartesian system
$[T]$	transformation matrix relating $\{\varepsilon\}$ to $\{\gamma\}$ (see Appendix)
Θ^α	curvilinear element coordinates
$\{u\}_i$	global Cartesian displacement at node i
U	strain energy
w_k	weighting factor for Gaussian integration
x^1, x^2, x^3	orthogonal Cartesian coordinates
$X_{\alpha\beta}$	expression defined in Eq. 13.

REFERENCES

1. BASIS User Manual. The Aeronautical Research Institute of Sweden, Stockholm, 1978.

2. Bathe, K. J.: An Assessment of Current Finite Element Analysis of Nonlinear Problems in Solid Mechanics. Numerical Solution of Partial Differential Equations, III, Academic Press, 1976.

3. Oden, J. T.: Finite Elements of Nonlinear Continua. McGraw-Hill, 1972.

4. Haisler, W.E., Stricklin J. A., Stebbins F. J.: Development and Evaluation of Solution Procedure for Geometrically Nonlinear Structural Analysis. AIAA Journal, Vol. 10, No. 3, March 1972, pp. 264-272.

5. Merazzi S., Stehlin P., Hanner K.: Nonlinear Analysis of Beam and Cable Structures. FFA AU-1499, Stockholm, 1978.

6. Bergan P. G., Clough R. W.: Convergence Criteria for Iterative Processes. AIAA Journal, Vol. 10, No. 8, August 1972, pp. 1107-1108.

APPENDIX

The strain is always transformed to a Cartesian coordinate system defined by $\{v\} = \{r\}_2 - \{r\}_1$ for two-dimensional elements and by $\{v\}$ and $\{r\}_4$ for three-dimensional elements. For membrane elements, [T] becomes

$$[T]^{-1} = \frac{1}{2}\left[\{1 + \cos 2\phi_\alpha\ ,\ 1 - \cos 2\phi_\alpha\ ,\ 2\sin\phi_\alpha \cos\phi_\alpha\}\right] \quad \alpha = 1,3$$

$$\cos\phi_\alpha = \frac{\{v\} \cdot \{g\}_\alpha}{|\{v\}| \cdot |\{g\}_\alpha|}$$

For volume elements the six strain components are transformed similarly.

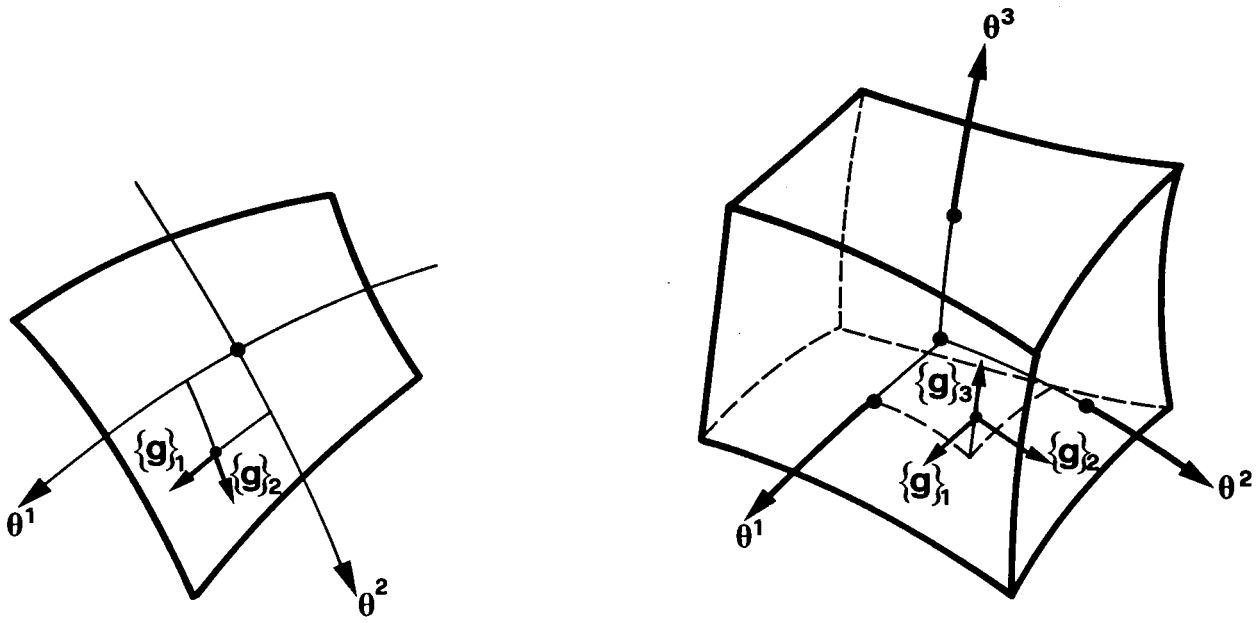

Figure 1.- Two- and three-dimensional elements.

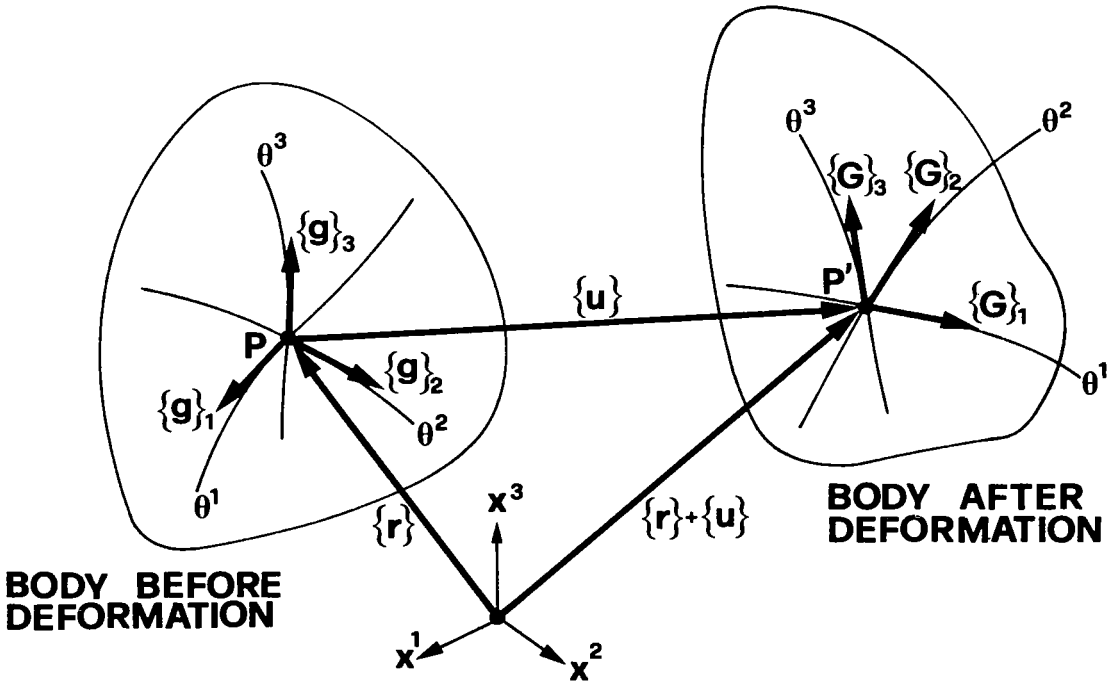

Figure 2.- Geometry of deformation.

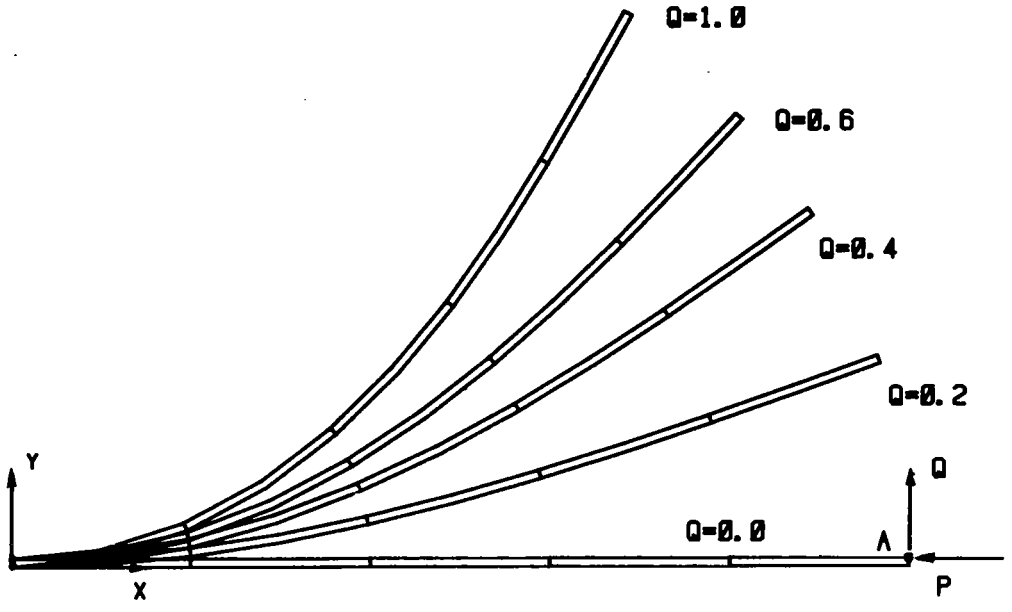

Figure 3.- Deformation of cantilever beam under transversal load Q.

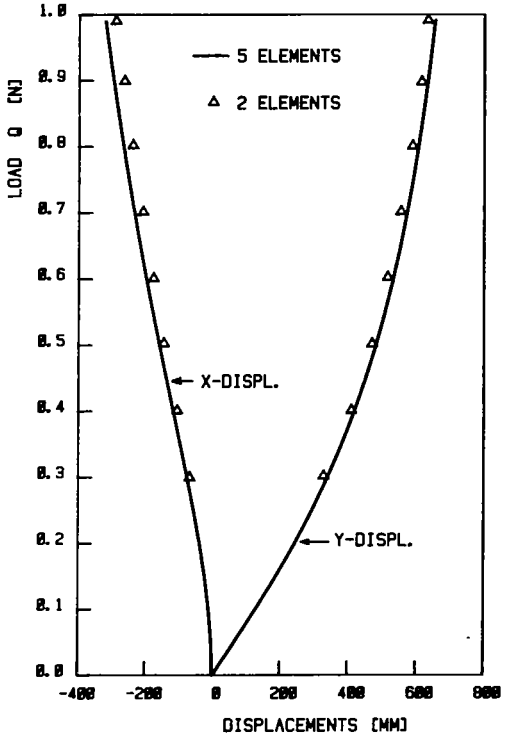

Figure 4.- Load-displacement function at node A under transversal load Q.

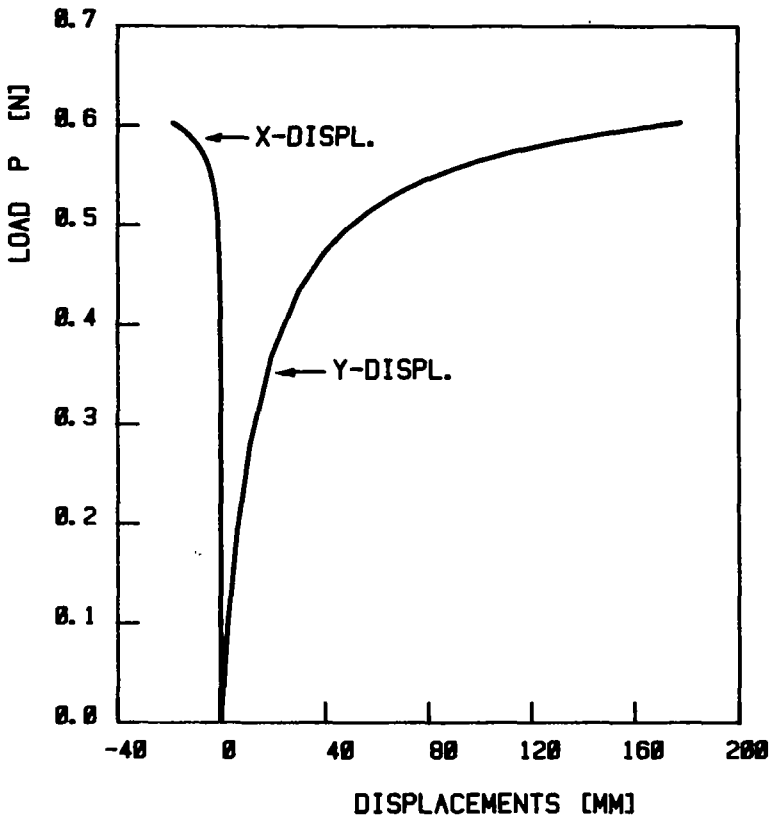

Figure 5.- Load-displacement function at node A under axial compression P.

COROTATIONAL VELOCITY STRAIN FORMULATIONS FOR NONLINEAR ANALYSIS OF BEAMS AND AXISYMMETRIC SHELLS*

Ted Belytschko
Department of Civil Engineering
Northwestern University, Evanston, Illinois

H. Stolarski
Institute of Fundamental Technological Research
Polish Academy of Sciences, Warsaw, Poland

C.S. Tsay
Northwestern University

SUMMARY

Finite element formulations for large strain, large displacement problems are formulated using a kinematic description based on the corotational components of the velocity strain. The corotational components are defined in terms of a system that rotates with each element and approximates the rotation of the material. To account for rotations of the material relative to this element system, extra terms are introduced in the velocity strain equations. Although this formulation is incremental, in explicitly integrated transient problems it compares very well with formulations that are not. Its simplicity, and its compatibility with constitutive equations found in "hydro" codes make it very attractive for this class of problems.

INTRODUCTION

Nonlinear structures are conventionally treated by kinematic descriptions that are essentially Lagrangian in nature, in that the measure of deformation is directly related to the total displacements. Several types of Lagrangian formulations are frequently used: formulations based on the Green strain or Almansi strain [1,2] and formulations based on corotational stretch [3,4].

Although velocity strain formulations have been used extensively for nonlinear solids, as exemplified in the work of Key [5], little study has been made of the application of these formulations to structures. Hughes and Liu [6] have presented a formulation based on the global components of the velocity strain.

In this paper, a corotational velocity strain formulation will be presented in which the components of the velocity strain are expressed in a framework that rotates with the material; formulations of this type have been studied by Green and Naghdi [7]. The formulation is then specialized to finite elements

*This work was supported by the Electric Power Research Institute.

by assuming that the rotation within an element is either constant or that the variation in the rotation field is small or moderate.

The potential benefits of these methods are significant. The basic equations are simpler than Green strain or Almansi equations, which endows the resulting computer programs with both simplicity and speed. The stress conjugate to the corotational velocity strain is the Cauchy stress tensor expressed in the corotational system. Any constitutive equations based on Cauchy stress and velocity strain can therefore be used. Furthermore, the corotational stress and stress-strain matrix are both materially objective, so no Jaumann type corrections need be made for the stress state and the formulation is directly applicable to anisotropic materials, which is not true of the formulations given in [5] or [8].

In the next section, the fundamental equations for the corotational velocity strain formulation are presented. Next, the general equations for a finite element application of this formulation is given. In order to illustrate the simplicity of the method, we then give the formulation for a beam element assuming a constant rotation in the element. More complex relations which account for the variation of rotation in an element are then given. The last section gives some examples of the application of this method to nonlinear transient problems.

BASIC EQUATIONS

We will use a kinematical and stress description by Green and Naghdi [7]. Let us denote the material coordinates of the structure by X_i, the spatial coordinates by x_i, the displacements by u_i and the velocities by v_i. Then

$$u_i = x_i - X_i \tag{1}$$

and the deformation gradient F_{ij} is given by

$$F_{ij} = \frac{\partial x_i}{\partial X_j} \tag{2}$$

From the polar decomposition theorem (see [9]) it follows that the deformation gradient can be expressed as a pure deformation, which is expressed by a symmetric matrix U_{kl}, and a rigid body rotation R_{kl} in the form

$$F_{ij} = R_{il}\, U_{lj} \tag{3}$$

The rotation matrix R_{il} is orthogonal, so that

$$R_{il} R_{im} = \delta_{lm} \tag{4}$$

where δ_{lm} is the Kronecker delta.

We will denote the coordinate system which is rotated by the rigid body motion of the material by $\hat{x}_i$ and call it a corotational coordinate system. This system is related to x_i by

$$\hat{x}_i = R_{ij} x_j \tag{5}$$

and its orientation varies from point to point in the material.

The velocity strain (rate of deformation) tensor is given by

$$D_{ij} = \frac{1}{2} \left(\frac{\partial v_i}{\partial x_j} + \frac{\partial v_j}{\partial x_i} \right) \tag{6}$$

and the corotational velocity strain, which is simply the same tensor with its components expressed in the corotational coordinates, is given by

$$\hat{D}_{kl} = R_{ik} R_{j\ell} D_{ij} \tag{7}$$

or

$$\hat{D}_{kl} = \frac{1}{2} \left(\frac{\partial \hat{v}_i}{\partial \hat{x}_j} + \frac{\partial \hat{v}_j}{\partial \hat{x}_i} \right) \tag{8}$$

The state of stress will be represented by the corotational stress $\hat{T}_{ij}$ which are the corotational components of the Cauchy (physical) stress T_{ij}; the two are related by

$$\hat{T}_{kl} = R_{ik} R_{j\ell} T_{ij} \tag{9}$$

The corotational components of the stress are frame invariant, so that the velocity strain is related to the rate of corotational stress by

$$\overset{\circ}{\hat{T}}_{ij} = \hat{C}_{ijkl} \hat{D}_{kl} \tag{10}$$

where the matrix $\hat{C}_{ijkl}$ for a material depends on the state of stress and state variables such as the yield stress but is independent of material rotation, regardless of whether the material is isotropic or anisotropic. This is a key advantage of corotational formulations. If the velocity strain and Cauchy stress are expressed in a fixed coordinate system, a Jaumann rate is required to provide frame invariance, but more importantly, the matrix $\hat{C}_{ijkl}$ must also be modified to account for the rigid body rotation. Furthermore, such formulations are quite awkward in structural theories where it is often convenient to distinguish velocities tangent and normal to the current configuration.

For a material in the domain Ω, the rate of internal work is given by

$$W = \int_{\Omega} D_{ij} T_{ij} \, d\Omega = \int_{\Omega} \hat{D}_{ij} \hat{T}_{ij} \, d\Omega \tag{11}$$

FINITE ELEMENT EQUATIONS

We consider an element which currently occupies a volume Ω^e. Its nodal displacements are u_{iI}, nodal velocities v_{iI} and nodal forces f^{int}_{iI}. We represent the velocities within the element by shape functions

$$\hat{v}_i = N_I (\hat{x}) \hat{v}_{iI} \tag{12}$$

where N_I are the shape functions which are expressed in terms of the corotational coordinates. Throughout this paper, upper case subscripts will refer to nodal values, as exemplified in Eq.(12), and the indicial summation convention will also apply to these subscripts.

The principle of virtual work gives

$$v_{iI}\, f^{int}_{iI} = \int_{\Omega^e} \hat{D}_{ij}\, \hat{T}_{ij}\, d\Omega \tag{13}$$

For elements other than the simplest, i.e. those with linear shape functions, the orientation of the corotational coordinates will vary within the element as shown in Fig. 1. Several alternatives are then available for handling the right hand side of Eq.(13):

i. a single corotational coordinate system $\bar{x}_i$ can be chosen for the element as shown in Fig. 1 and the relative rotations ignored;

ii. a single corotational coordinate system $\bar{x}_i$ can be chosen for the element and the rotations relative to $\bar{x}_i$ can be accounted for by modifying the velocity strain equations;

iii. the relative rotations can be accounted for by using the transformations (7) and (9) at each point of the element.

In this paper we will explore the first and second alternative; the third has been explored by Hughes and Liu [6].

For the first alternative, the use of Eq.(12) gives

$$v_{iI}\, f^{int}_{iI} = \int_{\Omega^e} \bar{v}_{iI}\, \frac{\partial N_I}{\partial \bar{x}_j}\, \bar{T}_{ij}\, d\Omega \tag{14}$$

so the use of the transformation (5) and the arbitrariness of of v_{iI} gives

$$f^{int}_{iI} = R_{ki} \int_{\Omega^e} \frac{\partial N_I}{\partial \bar{x}_j}\, \bar{T}_{kj}\, d\Omega \tag{15}$$

It should be observed that the stress is expressed in terms of a single corotational coordinate system throughout the element. Therefore, if we consider a beam with a constant axial stress $\bar{T}_x$, it follows that the only nonzero nodal forces lie along the $\bar{x}$ axis regardless of the curvature of the beam. This anomaly can yield spurious results whenever the flexural stiffness is small, since it introduces parasitic bending in states of pure membrane stress, cf [10].

The second alternative is to introduce velocity strain relations which account for the variation in rotations of the element but to express their components in the element system. If we represent these relations by

$$\bar{D}_{ij} = D_{ijkI}\,\bar{v}_{kI} \tag{16}$$

then Eq.(15) becomes

$$f^{int}_{iI} = R_{ki}\int_{\Omega^e} D_{mnkI}\,\bar{T}_{mn}\,d\Omega \tag{17}$$

In a subsequent section, forms of Eq.(16) for beams and axisymmetric shells will be presented. Higher order formulations as exemplified by Eq.(17) do provide better accuracy, particularly for relatively coarse meshes, but they do not eliminate parasitic bending.

A SIMPLE BEAM FORMULATION

In order to illustrate the application of a corotational velocity strain, we will first consider a beam element with the simplest corotational formulation where the nodal forces are evaluated by Eq.(15). The notation used is shown in Fig. 2. We will embed the element corotational coordinate within the element so that the $\bar{x}$ - axis always connects nodes 1 and 2. Euler-Bernoulli beam theory will be used, so that the velocities through the depth are completely defined by velocities of the middle surface $V_{\bar{x}}$ and $V_{\bar{y}}$

$$\bar{v}_x = \bar{V}_x - \hat{y}\,\bar{V}_{y,\bar{x}} \tag{18a}$$

so that

$$\bar{D}_x = \frac{\partial \bar{v}_x}{\partial \bar{x}} = \bar{V}_{x,\bar{x}} - \hat{y}\,\bar{V}_{y,\bar{x}\bar{x}} \tag{18b}$$

where commas denote differentiation with respect to the subsequent variables.

The velocity field $\bar{V}_{\bar{x}}$ will be approximated by linear shape functions, and the transverse velocity field of the midline by cubic shape functions so that

$$\bar{V}_x = \xi\,\bar{V}_{x2} \tag{19a}$$

$$\bar{v}_y = \ell(\xi^3 - 2\xi^2 + \xi)\,\phi_1 + \ell(\xi^3 - \xi^2)\,\phi_2 \tag{19b}$$

$$\xi = \bar{x}/\ell \tag{19c}$$

where the rigid body part of the velocity field has been omitted since it causes no strain. The nodal velocities associated with deformation are thus

$$\{\bar{v}\}^T = [\bar{V}_{x2},\ \phi_1,\ \phi_2] \tag{20}$$

and the conjugate nodal forces

$$\{\bar{f}^{int}\} = [f_{x2},\ m_1,\ m_2] \tag{21}$$

where m_I are the nodal moments. Combining Eqs.(18) and (19), we obtain

$$\bar{D}_x = \frac{\bar{V}_{x2}}{\ell} - \frac{\hat{y}}{\ell}\,[(6\xi-4)\phi_1 + (6\xi-2)\phi_2] \tag{22}$$

Equation (15) then gives

$$\begin{Bmatrix} \bar{f}_{x2} \\ m_1 \\ m_2 \end{Bmatrix} = \int_0^1 \int_A \begin{bmatrix} 1 \\ -\hat{y}\,(6\xi-4) \\ -\hat{y}\,(6\xi-2) \end{bmatrix} \bar{T}_x\, dA\, d\xi \tag{23}$$

where A is the cross-sectional area of the beam.

The remaining nodal forces can be obtained from equilibrium

$$\bar{f}_{x1} = -\bar{f}_{x2}$$

$$\bar{f}_{y1} = -\bar{f}_{y2} = \frac{m_1 + m_2}{\ell} \tag{24}$$

HIGHER ORDER VELOCITY STRAIN EXPRESSIONS

The velocity strain expression, Eq.(22), is exact for a beam only when the element's midline is coincident with the $\bar{x}$-axis, which corresponds to the chord between the two nodes. If the beam element is initially curved or if it deforms enough so that the midline displaces substantially from the $\bar{x}$-axis, these equations will be in error because of the following effects:

1. The $\bar{x}$ and $\bar{y}$ axes are no longer coincident with the midline and its normal, respectively, so Eqs.(18) are in error because $\bar{V}_x$ and $\bar{V}_y$ are not along the midline and its normal.
2. The volume integration neglects the deformation of the beam relative to the $\bar{x}$ axis.

In order to account for the first effect without transforming between coordinate systems within the element, higher order velocity strain relations are developed, using the same basic ideas employed in [4] for corotational stretch theories. For this purpose, the displacement of the midline relative to the chord, or $\bar{x}$ axis, is denoted by Y. It will be assumed that

$$\frac{Y}{\ell} = O(e) \qquad \bar{Y}_{,\bar{x}} = O(e) \qquad Y_{,\bar{x}\bar{x}} = O(e^2) \qquad Y_{,\bar{x}} = Y_{,\hat{x}} \tag{25}$$

and accuracy of order e^2 is assumed; terms of higher order and certain other terms are neglected. Because of space limitations, we omit the derivation, and give only the final result

$$\bar{D}_x = d_1 - \hat{y}\kappa_1 \tag{26a}$$

$$d_1 = \bar{V}_{x,\bar{x}} + Y_{,x}\,\bar{V}_{y,\bar{x}} \tag{26b}$$

$$\kappa_1 = (1 - \tfrac{1}{2} Y_{,\bar{x}}^2)\,\bar{V}_{y,\bar{x}\bar{x}} + \underline{Y_{,\bar{x}\bar{x}}\,\bar{V}_{x,x}} \tag{26c}$$

For an axisymmetric shell element, we let x correspond to the radial coordinate, r, and θ be the circumferential coordinate. The corresponding relations are

$$\bar{D}_x = d_1 - \hat{y}\kappa_1 \tag{27a}$$

$$\bar{D}_\theta = d_z - \hat{y}\kappa_2 \tag{27b}$$

where $\bar{D}_\theta$ is the hoop velocity strain. The terms d_1 and κ_1 are identical to those for the beam, Eqs.(26), while

$$d_2 = \frac{V_x}{r} = \frac{1}{r}\,(\bar{V}_x \cos\alpha + \bar{V}_y \sin\alpha) \tag{28a}$$

$$\kappa_2 = \frac{1}{r} Y_{,x}\, \bar{V}_{x,\bar{x}} \cos\alpha + \underbrace{\frac{1}{r}\,[r(\cos\alpha - Y_{,x}\sin\alpha) - Y\sin\alpha\cos\alpha]V_{y,\bar{x}}} \tag{28b}$$

where r is the current radial coordinate of a point, α the current angle between $\bar{x}$ and x, as shown in Fig. 2. For all applications we have considered so far, the second terms in the expressions for κ_1 and κ_2 have been insignificant.

EXAMPLES

Results are given for a clamped ring shown in Fig. 3, for which experimental results are reported in [11]; numerical results have been reported in [3]. Explicit time integration with the central difference method and a lumped mass matrix was used. The material model is elastic-plastic with a Mises yield condition and isotropic hardening. Because the width of the ring is large compared to its thickness, plane strain was assumed in the z-direction. Furthermore, the compressibility of the elastic strains was considered neglible, so the height h of the cross-section was modified by

$$h = h_o \ell_o / \ell \tag{29}$$

for both the velocity strain computations, Eq.(18b), and the nodal force computtations, Eq.(23). The nodal forces were obtained by numerical quadrature using five points through the thickness, and two points along the length with a trapezoidal rule.

The displacements for the midpoint of the clamped ring are compared for plane stress and plane strain, with and without the area correction of Eq.(29), in Table 1. As can be seen, the effects of the plane strain assumption are very significant, changing the result by 20%. The effect of the thickness correction is less pronounced but nevertheless not neglible.

TABLE 1

EFFECTS OF ASSUMPTIONS ON MIDPOINT DEFLECTION OF CLAMPED RING

Assumptions	Midpoint deflection (in)
Plane strain, variable thickness	2.99
Plane strain, constant thickness	3.06
Plane stress, variable thickness	3.43
Plane stress, constant thickness	3.53

The plane strain solution with thickness correction compares best with the experiment, so we will restrict all subsequent comparisons to this case. The time history of the midpoint is compared to the experiment in Fig. 4. The reported experimental results exhibit considerable snapback, which are absent in the computations. Figures 5 and 6 compare the deformed shape and strain time histories with the experiment. Overall, the agreement is quite good and comparable to that of the numerical results reported in [3].

REFERENCES

1. K.J. Bathe and H. Ozdemir, "Elastic-Plastic Large Deformation Static and Dynamic Analysis," Computers and Structures, Vol. 6, 1976, pp. 81-92.

2. S. Yaghmai and E.P. Popov, "Incremental Analysis of Large Deflections of Shells of Revolution," International Journal of Solid and Structures, Vol. 7, 1971, pp. 1375-1393.

3. T. Belytschko and B.J. Hsieh, "Nonlinear Transient Finite Element Analysis with Convected Coordinates," International Journal for Numerical Methods in Engineering, Vol. 7, 1973, pp. 255-271.

4. T. Belytschko and L.W. Glaum, "Applications of Higher Order Corotational Stretch Theories to Nonlinear Finite Element Analysis," Computers and Structures, Vol. 10, 1979, pp. 175-182.

5. S.W. Key, "HONDO - A Finite Element Computer Program for the Large Deformation Dynamic Response of Axisymmetric Solids," Report SLA-74-0039, Sandia Laboratories, April 1974.

6. T.J.R. Hughes, and Y.K. Liu, "Nonlinear Finite Element Analysis of Shells - Part I, Three Dimensional Shells," to be published Computer Methods in Applied Mechanics and Engineering.

7. A.E. Green and P.M. Naghdi, "A General Theory of an Elastic-Plastic Continuum," Archives of Rational Mechanics and Analysis, Vol. 18, 1965, pp. 251-281.

8. M.L. Wilkins, "Calculation of Elastic-Plastic Flow," Report UCRL-7322-Revision 1, Lawrence Radiation Laboratory, University of California, Livermore, 1969.

9. L. Malvern, Introduction to the Mechanics of a Continuous Medium, Prentice-Hall Incorporated, Englewood Cliffs, New Jersey, 1969.

10. T. Belytschko, "Nonlinear Analysis - Descriptions and Numerical Stability," in Shock and Vibration Computer Programs, edited by W. Pilkey and B. Pilkey, The Shock and Vibration Information Center, 1975, pp. 537-562.

11. H.A. Balmer and E.A. Witmer, "Theoretical-Experimental Correlation of Large Dynamic and Permanent Deformation of Impulsively Loaded Simple Structures," Report FDL-TDR-64-108, Air Force Flight Dyn. Lab., Wright-Patterson Air Force Base, Ohio, 1964.

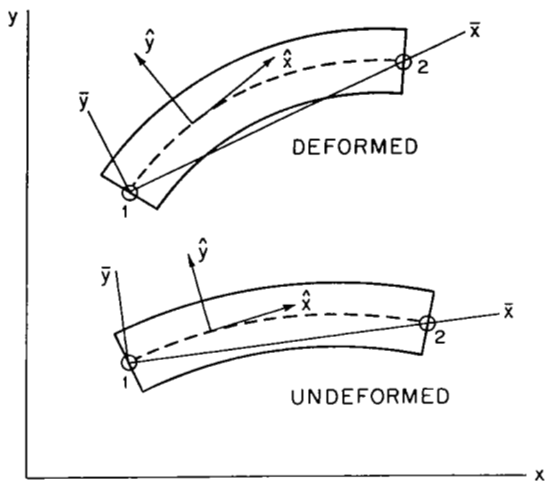

Fig. 1. Deformed and undeformed beam element showing element corotational coordinates $\bar{x},\bar{y}$ and local corotational coordinates $\hat{x},\hat{y}$.

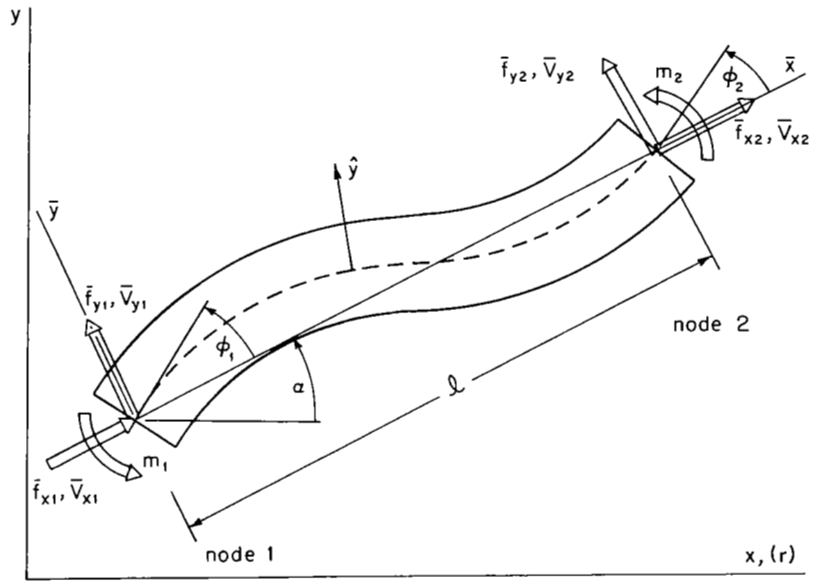

Fig. 2. Nomenclature for nodal forces and velocities.

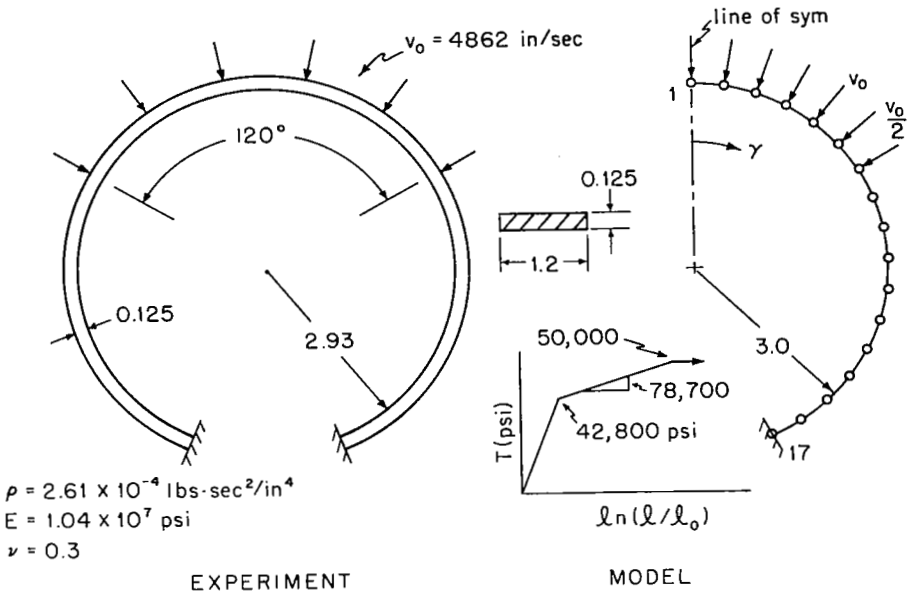

Fig. 3. Experiment [11] and model for clamped ring problem.

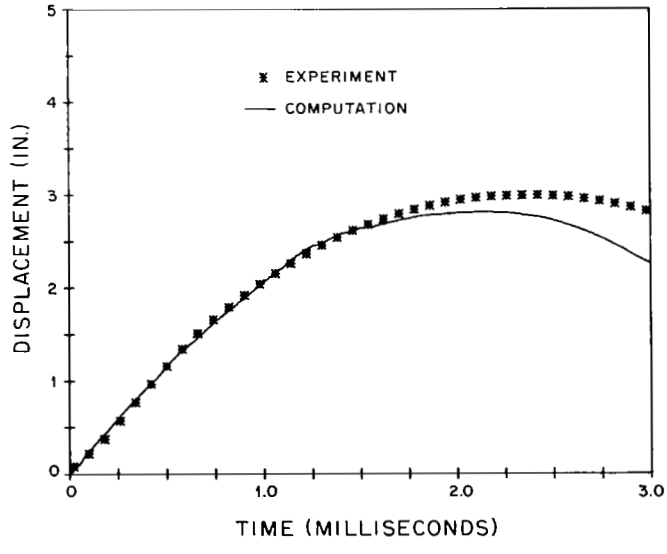

Fig. 4. Comparison of computed centerpoint (node 1 in Fig.3) vertical displacement with experimental results [11].

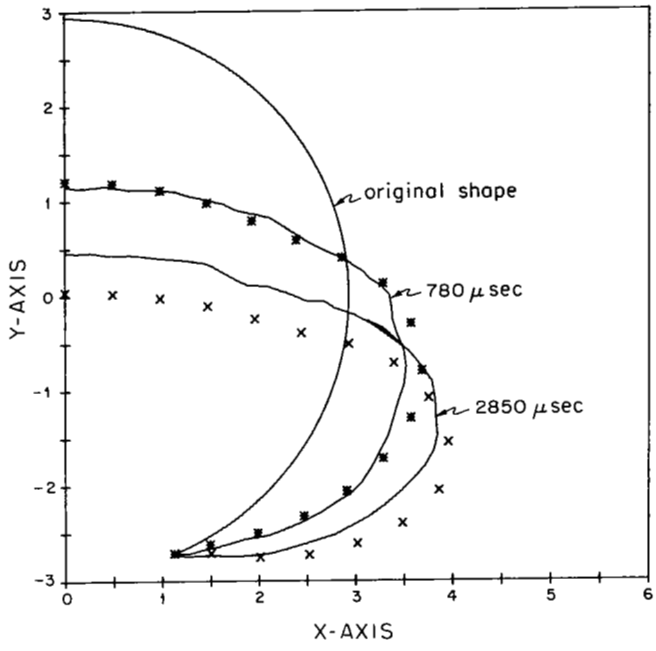

Fig. 5. Deformed configuration of clamped ring compared to experimental results [11].

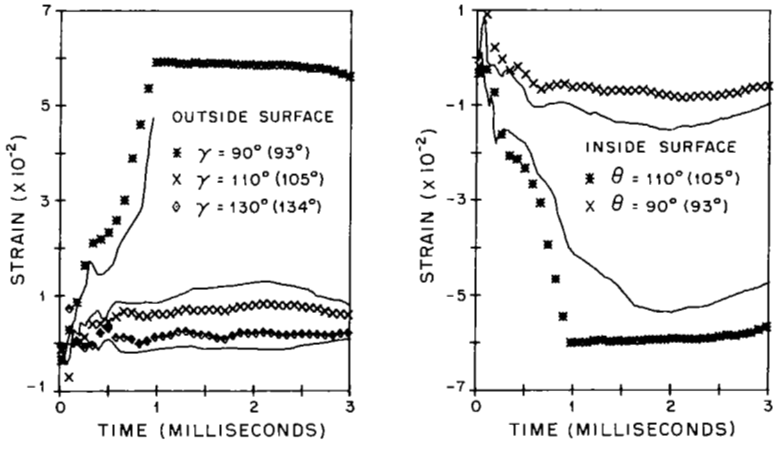

Fig. 6. Comparison of computed strains against experimental results [11]; angle in parenthesis is for the experimental record.

MICROCOMPUTER SYSTEM FOR MEDIUM-SIZED AND EXPERIMENTAL FINITE ELEMENT ANALYSIS

Yoshiaki Yamada and Hideto Okumura
Institute of Industrial Science, University of Tokyo

Tatsumi Sakurai
Japan Advanced Numerical Analysis Inc.

SUMMARY

A microcomputer system being developed by the authors is introduced. The parallel effort of compiling a series of compact finite element analysis programs enables the execution of most computation on inexpensive microcomputers. The system is practically maintenance free and can be sustained by individual laboratories of standard scale in the educational or academic environment. As for the programs, FEMN is discussed in some detail. The program is an extended version of the original linear analysis program FEM4 and is being tested for application to problems with material nonlinearities.

INTRODUCTION

The finite element analysis has reached the stage where the execution of the structural analysis is often considered routine. This is the case particularly in the industrial environment. However, so far the execution has relied largely on expensive hardware or costly remote time-sharing services. The role of the giant main-frame or super-computer in the solution of large scale problems, e.g. the inelastic analysis of pressure vessels and piping systems operated at elevated temperature, will not be changed even in future applications. But it has been an ambition of engineers to perform a great portion of their analysis jobs on inexpensive and hopefully personal computers and thus be freed from being slave to the large systems. The development of microcomputer and associated finite element analysis programs is a breakthrough in realizing this goal.

The microcomputer system should be stand alone and almost maintenance free so that it can be sustained by individual laboratories especially in the educational or academic environment. The medium-sized engineering problems should be solved within a reasonable time limit and the system could also be adapted to multi-purpose usages, i.e. interactive compilation of fundamental computation routines, data management, preparation of engineering documents and reports, letter writing and so forth. In the present paper a compact system is introduced which is being built by the authors. In a parallel effort, a series of microcomputer finite element analysis

programs are being developed. The original version is FEM4 which is an elastic analysis program of plane stress, plane strain and axisymmetric problems (ref. 1, 2). It is extended to the nonlinear analysis program FEMN by an addition of the restart capability. The results of this innovation are manifold. By an incorporation of user defined subroutine MTRLN specifying material data, problems with material nonlinearities can be easily handled. Mesh division can be modified in the course of computation and thus the simulation and/or pursuit, for example, of crack development in fracture mechanics becomes easier. In the following, some details of the microcomputer system and the program organization of FEMN are described with the example solution of a simple pilot problem.

MICROCOMPUTER SYSTEM STRUCTURE

Figure 1 illustrates the structure of the microcomputer system almost completed at the time, May 1980, of writing this paper. Zilog Z80 is used as the 8 bit CPU (Central Processing Unit), and the capacity of main memory, which is composed of a ROM (Read Only Memory) and several RAM (Random Access Memory) boards, totals 64 kilobytes. The transfer of control, address and data between the components of the system is performed exclusively via S-100 bus. For the purpose of connection and communication a number of interfaces are installed. The 8" floppy disk drive constitutes the secondary memory for mass storage and provides the housing of a compound of operating system, supporting language, finite element analysis and other computer programs. The standard disk operating system CP/M is used so that the problems in software exchange can be avoided. At the moment, program languages are BASIC and FORTRAN. It should be noted that two 240K dual disk systems are combined for commanding four floppy disk assemblage, although a dual system kit suffices to perform the standard operation. The authors intend to shorten the overall analysis time by an adoption of parallel processing that uses several CPUs and disk drives. The contemplated inclusion of the hard disk will increase the capacity of secondary memory to a great extent and may open the way to a novel system based on 16 bit microprocessors.

Among the peripherals for I/O (Input/Output) purposes shown in figure 1, CRT unit and printer are the essentials. The function of CRT unit is manifold, as it is used for input of the data, interactive operation of the system, compilation of program segments and/or subroutines, temporary display of the computed results, preparation of documents, e.g. the users' manual, and so on. The prepared data, the completed list of the programs and the results of computation can be plugged into the printer for permanent recording. Plotter and graphics terminal are optional, but both are useful for the finite element modeling and post-processing graphics, e.g. automatic mesh generation, model editing and plotting the computed results.

The general purpose programs compiled to date for mounting on the microcomputer system are COMPOL, COMPOS, CALM, FEM4, MICRO-FEM and FEMN. The first two, written in BASIC, are essentially the microcomputer version of 'COMPOsite material computation' being developed by Tsai on a magnetic card calculator (ref.3, 4). In the program names, L and S stand for the laminate

and sandwich composite structure respectively. CALM is a matrix operation program which is basically an interactive version of the first group operations in the program CAL (ref.5, 6). FEM4 and its microcomputer version MICRO-FEM are prepared to solve the plane stress, plane strain and axisymmetric problems and then converted to FEMN to conduct nonlinear analysis. Restart capability is implemented so that the inelastic material behavior can be handled. Complementary modification is an addition of the user defined subroutine MTRLN specifying the material properties which were formerly input through element data cards. The users who tailor the subroutine MTRLN according to their material data can perform conveniently the inelastic analysis on the microcomputer. An example of MTRLN is shown in the following section.

ORGANIZATION OF NONLINEAR ANALYSIS PROGRAM FEMN

FEMN is composed of two parts FEMAB and FEMCD which are concerned with the preparation of input data file and the solution procedure of the problem. The major feature of the program is that it uses dynamic storage allocation which means the complete elimination of common statement. This function is performed by subroutines OPENS, CLOSE, PSEEK and POOLWT as shown in figures 2a and 2b.

The program organization of FEMAB is shown in figure 2a. It reads title and control cards first. Then follows the input of node and element data from which the index or integer joint array is formed and stored on IFIL2. IFIL2 accommodates also load data and IFIL6 is essentially a storage of input and processed element data. The formation of strain-displacement matrix B from the data in IFIL6 is performed by subroutine MGN and the result is written on IFIL3 to be read in FEMCD subsequently. Finally the initial displacement data (usually the cleared zero displacement) are stored on IFIL5 for subsequent updating by the solution obtained through FEMCD. In the following the principal functions of individual subroutines in FEMAB are summarized.

PINPG Preparatory segment for subroutine INPUTG
INPUTG Input generation, read input data in sequence and compile index or integer joint array
RNODE Read node data
RELEM Read element data including material specification number and element thickness
MKIDX Make index for attributing merging point and coordinate to input and processed element data and also create index for skyline assemblage of stiffness matrix
RLOAD Read loading step sequence and nodal force and/or displacement data

OPENS Open storage area for array from bottom of POOL in main memory
CLOSE Close a part or whole storage area by deleting unused array
PSEEK Search for array data by its name
POOLWT Debug write wanted array data in POOL for inspection

PMGN Preparatory segment for subroutine MGN
MGN Command sequential generation of element matrices
ISOBMN Generate element strain-nodal displacement matrix B for 3-8 variable

node parametric element

STDMA Evaluate components of strain-nodal displacement matrix B and determinant of associated Jacobi matrix J

DISPI Initialize displacements, by either clearing for initial run or entering displacement data of preceding computation for restart run

After the execution of FEMAB described above, the next program block FEMCD is called by the main of FEMN. Functions of FEMCD, whose organization is shown in figure 2b, are the formation and assemblage of the element stiffness matrix and subsequently the solution of the problem. Material data are input via the user defined subroutine MTRLN and then the stress-strain matrix D for each incremental stage of loading is evaluated in subroutine DMXMKN. FEMCD starts its operation by a transfer or reading of the data stored on IFIL5, which are title of the problem, integer data, initial cleared displacement and load data or their values obtained in preceding step of loading sequence. The stress-nodal displacement matrix S and element stiffness matrix K are formed in subroutine SMXMKN, the latter being stored in the appropriate locations in the overall stiffness matrix by referring to the index prepared on IFIL2. IFIL3 and 4 are used as the seesaw external memory for integer data and the element strain-displacement matrix B. Skyline or profile active column method of data acquisition is used for saving area in the main memory. Therefore all subroutines prefixed by capitals SK in SOLVEN, SKDCNP etc., take advantage of the skylined form of storage for the manipulation of data. Newton-Raphson iteration procedure is incorporated in subroutine SOLVEN, some details of which are discussed in the next section concerned with the solution of an elementary sample problem. The following summarises the function of individual subroutines relevant to FEMCD.

PSOLVN Preparatory segment for subroutine SOLVEN

SOLVEN Solve overall stiffness equation for unknown nodal displacement and compute reaction at constrained node; iterative procedure is incorporated in this solver for nonlinear problems

VECTWN Print out computed displacement and reaction vector at each stage of loading

SMXMKN Evaluate stress-nodal displacement matrix S and element stiffness matrix K, synthesize overall stiffness matrix by referring to merging point index stored on IFIL2, and also determine equivalent nodal force from current stress data for equilibrium check

SWRITE Write components for debugging of active columns in matrix S stored by skyline method

BWRITE Write components of vector B for debugging

SKDCNP Cholesky decomposition of symmetric positive definite matrix by skyline method

SKXMLU Multiply, add and/or subtract matrix components in skyline storage

CONVCK Check convergence of solution being obtained by Newton-Raphson iterative procedure

SKFWD Forward elimination by skyline method

SKBKW Backward substitution by skyline method

DMXMKN Evaluate components of stress-strain matrix D of constitutive equation

MTRLN User defined subroutine specifying elastic and inelastic material properties

STRSUM Add stress/strain increments to update values of stress/strain
PRINST Compute principal stresses and their directions
STRPRN Print out stress/strain solutions at respective Gauss integration points, together with coordinates of Gauss points

Finite element used in FEM4 as well as in FEMN is 4-8 variable nodes parametric quadrilateral with the following interpolation functions (ref.7).

For corner nodes 1-4

$$N_1 = S_1 - (N_8+N_5)/2, \quad N_2 = S_2 - (N_5+N_6)/2$$

$$N_3 = S_3 - (N_6+N_7)/2, \quad N_4 = S_4 - (N_7+N_8)/2$$

for midedge nodes 5-8

$$N_5 = S_5, \quad N_6 = S_6, \quad N_7 = S_7, \quad N_8 = S_8$$

where S_i stands for the trial functions defined as (ref.8, 9)

$$S_1 = (1-\xi)(1-\eta)/4, \quad S_2 = (1+\xi)(1-\eta)/4$$

$$S_3 = (1+\xi)(1+\eta)/4, \quad S_4 = (1-\xi)(1+\eta)/4$$

$$S_5 = (1-\xi^2)(1-\eta)/2, \quad S_6 = (1+\xi)(1-\eta^2)/2$$

$$S_7 = (1-\xi^2)(1+\eta)/2, \quad S_8 = (1-\xi)(1-\eta^2)/2$$

By coalescing an edge of the quadrilateral to a single point a triangular element is produced. It can be shown (ref.8, 9) that the resulting element coincides with the conventional constant stress/strain element when the primary quadrilateral element is four-noded. The number of integration points in Gauss quadrature can be one to five by five in accordance with the users' specification.

The input card or data sequence in FEMN is summarized in table I. An example of input data preparation as well as the user defined subroutine MTRLN is illustrated in the next section.

SOLUTION OF SAMPLE NONLINEAR PROBLEM AND REMARKS

As a sample problem, nonlinear behavior of a composite block specimen shown in figure 3 is analysed. The block consists of an ideally plastic element 101 and a nonlinear one 501 with a negative slope segment at a large strain as depicted in figure 4 based on the material data of figure 3. Loading sequences are summarized in figure 3 and the solid curve in figure 4 is the theoretical load-displacement relation of the block under axial tensile loading. It is noted that the loading condition in numerical analysis is given by the force increment for step 1-3 and 7-9, while in step 4-6 it is given by the displacement increment.

Table II is the image of input cards prepared for the solution of the sample problem and serves to illustrate simplicity of the data preparation.

Specifically table II is concerned with the first loading sequence, i.e. step 1-3. The solution for consecutive loading conditions, step 4-6 and 7-9 in the present example, is obtained by restarting the execution with the renewal of input data and the use of the solution obtained in the preceding step and stored on an appropriate file. Table III is the subroutine MTRLN written for this sample problem. The program FEMN is versatile because the user can easily tailor the subroutine MTRNL so that it characterizes particular nonlinear properties of the material of interest. It must be emphasized that the anisotropic material behaviors are easily incorporated in the program.

Figure 5 depicts solution convergence in the sample problem. The iterative procedure that the present version of FEMN employs is a modified Newton-Raphson method with incorporation of equivalent nodal force $\{F^a\}$. It compensates the imbalance of force equilibrium at the nodes and is given by

$$\{F^a\} = \{F\} - \int [B]^T \{\sigma\} dV$$

where $\{F\}$ denotes the prescribed nodal force, $[B]$ and $\{\sigma\}$ are the strain-nodal displacement matrix and the current stress. Convergence is satisfactory in the present example and it should be noticed that the computed results lie on the theoretical curve exhibiting sharp turning points.

Test of convergence in case of the large scale problem, sophistication of iterative procedure and extension of the program to three dimensions are the next steps that are to be taken. Moreover, the development of parallel processing and the installation of suitable hard disk will increase the speed and capacity of the system.

REFERENCES

1. Yamada, Y., Hirakawa, T., Nishiguchi, I. and Okumura, H.: Nonlinear Analysis by Finite Elements and a Microcomputer System Development, Comp. Appl. in Civil Engng., Nem Chand and Bros, Roorkee, India.
2. FEM4 Users Manual, Nonlinear Analysis Program Research Association, c/o JANA Inc., 1-1-71 Nakamegro, Megro-ku, Tokyo, 153 Japan.
3. Tsai, S.W. and Hahn, H.T.: Introduction to Composite Materials, vol.1, AFML-TR-78-201, 1978 Wright-Patterson AFB, Ohio.
4. Tsai, S.W. and Hahn, H.T.: TI-59 Magnetic Card Calculator Solutions to Composite Materials Formulas, AFML-TR-4040, 1979, Wright-Patterson AFB, Ohio.
5. Wilson, E.L.: CAL-A Computer Analysis Language for Teaching Structural Analysis, Computers and Structures, vol.10, 1979, pp.127-132.
6. Wilson, E.L.: CAL 78, User Information Manual, Rep. no. UC SESM 79-1, Univ. of California, Berkeley.
7. Bathe, K.J. and Wilson, E.L.: Numerical Methods in Finite Element Analysis, Prentice-Hall, Inc., Englewood Cliffs, 1976.
8. Yamada, Y., Ezawa, Y., Nishiguchi, I. and Okabe, M.: Reconsiderations on Singularity or Crack Tip Elements, Int. J. Num. Meth. Engng., vol.14, 1979, pp.1525-1544.
9. Yamada, Y.: Matrix Method of Mechanics of Materials, Baifukan, 1980.

TABLE I INPUT DATA FORMAT OF FEMN

(1) TITLE CARD (18A4)

COL		
1-72		PROBLEM IDENTIFICATION ETC BY ALPHANUMERIC CHARACTER

(2) CONTROL CARD (23I1)

COL		
1	=0	AXISYMMETRIC
	=1	PLANE STRAIN
	=2	PLANE STRESS
2		NUMBER OF INTEGRATION POINTS (1-5) FOR GAUSSIAN QUADRATURE
3*	=0	INITIAL START
	>0	RESTART
4- 5*		NUMBER OF ITERATION IN NEWTION-RAPHSON METHOD
6-20		BLANK
21	>0	DEBUG WRITE IN MODULE INPUG
22	>0	DEBUG WRITE IN MODULE MG
23	>0	DEBUG WRITE IN MODULE SOLVEN

(3) NODE HEADER CARD (A4)

COL	
1-4	'NODE'

(4) NODE DATA CARDS (A4, I6, 2F10.0, 10X, F10.0, 10X, 2I1)

COL		
1- 4		'NODE'
7-10		NODE NUMBER
11-20		X(R) COORDINATE
21-30		Y(Z) COORDINATE
41-50		OBLIQUE ANGLE (DEG) OF LOCAL COORDINATE
61	=1	X-DOF CONSTRAINED OR X(R)-DISPL GIVEN
	=0	OR BLANK FREE OR X(R)-LOAD GIVEN
62	=1	Y-DOF CONSTRAINED OR Y(Z)-DISPL GIVEN
	=0	OR BLANK FREE OR Y(Z)-LOAD GIVEN

(5) ELEM HEADER CARD (A4)

COL	
1- 4	'FLEM'

(6) ELEM DATA CARDS (A4, I6, 8I5, I5*, 2I5*, F8.0)

COL	
1- 4	'ELEM'
7-10	ELEMENT NUMBER
11-15	1ST NODE NO.
16-20	2ND NODE NO.
21-25	3RD NODE NO.
26-30	4TH NODE NO.
31-35	5TH NODE NO.
36-40	6TH NODE NO.
41-45	7TH NODE NO.
46-50	8TH NODE NO.
51-55*	MATERIAL SPECIFICATION NUMBER
56-65*	FOR EXTENSION OF PROGRAM BY USERS
66-73	ELEMENT THICKNESS

(7) LOAD HEADER CARD (A4)
COL 1- 4 'LOAD'

(8) LOAD OR DISPLACEMENT STEP CARD (A4, I6, 6F10.0)*
COL 1- 4 'STEP'
5-10 STEP NUMBER
11-70 FOR PROGRAM EXTENSION

(9) LOAD OR DISPLACEMENT DATA CARD (A4, I6, 2F10.0)
COL 1- 4 'LOAD'
5-10 NODE NUMBER ON WHICH GIVEN LOAD OR DISPLACEMENT IS APPLIED
11-20 X(R) GIVEN NODAL FORCE OR DISPLACEMENT
21-30 Y(Z) GIVEN NODAL FORCE OR DISPLACEMENT

(10) END CARD (A4)
COL 1- 3 'END'

* INDICATES ADDITION OR MODIFICATION APPLIED TO LINEAR ANALYSIS PROGRAM FEM4 AND/OR MICRO-FEM

TABLE II INPUT DATA IMAGE OF SAMPLE PROBLEM OF FIGURE 3

```
    2-ELEMENT NONLINEAR MODEL TEST 1980-5-16 (ITER MAX= 8)
22  8
NODE
NODE      1      0.000      0.000                                          11
NODE      2      0.000     20.000                                          10
NODE      3      0.000     40.000                                          10
NODE     11     25.000      0.000                                          01
NODE     13     25.000     40.000                                          00
NODE     21     50.000      0.000                                          01
NODE     22     50.000     20.000                                          00
NODE     23     50.000     40.000                                          00
ELEM
ELEM    101      1   21    23     3    11    22    13     2     0     0..
ELEM    501      1   21    23     3    11    22    13     2     1     0 .
LOAD                                                                      .
STEP      1                                                  ..............
LOAD     21   4000.000      0.000                           .   (65)
LOAD     22  16000.000      0.000                           -->  0  6.000
LOAD     23   4000.000      0.000                                0  6.000
STEP      2
LOAD     21   2000.000      0.000
LOAD     22   8000.000      0.000
LOAD     23   2000.000      0.000
STEP      3
LOAD     21   2000.000      0.000
LOAD     22   8000.000      0.000
LOAD     23   2000.000      0.000
END
```

TABLE III EXAMPLE OF USER DEFINED SUBROUTINE MTRLN

```
      SUBROUTINE MTRLN(KK,IK,EK,ITER,ISTP)
C     .....................................................
C     . IK(4)       MATERIAL IDENTIFICATION NUMBER        .
C     . EK(IK(9))   COMPUTED STRAIN VALUE                 .
C     . EK(IK(8))   CORRESPONDING STRESS VALUE            .
C     . ITER=0, ROUTINE DETERMINES TANGENT MODULUS        .
C     . ITER)0, ITERATES STRESS FOR COMPUTED STRAIN VALUE .
C     .....................................................
      DIMENSION KK(1),IK(1),EK(1)
      MID=IK(4)
      IK8=IK(8)
      IK9=IK(9)
      IF(ITER.GT.0) GO TO 6000
C     **-** SLOPE OF STRESS-STRAIN CURVE **-**
      IF(MID.GT.0) GO TO 3000
C     **-** PERFECTLY PLASTIC **-**
      EK(2)=0.3
      IF(EK(IK9).GT.10.0E-3) GO TO 2100
      EK(1)=2.0E4
      GO TO 9000
 2100 EK(1)=0.0
      GO TO 9000
C     **-** NONLINEAR MATERIAL **-**
 3000 EK(2)=0.3
      IF(EK(IK9).GT.3.0E-3) GO TO 3100
      EK(1)=2.0E4
      GO TO 9000
 3100 IF(EK(IK9).GT.6.0E-3) GO TO 3200
      EK(1)=0.0
      GO TO 9000
 3200 EK(1)=-1.0E+4
      GO TO 9000
C     **-** STRESS VALUE FOR COMPUTED STRAIN **-**
 6000 IF(MID.GT.0) GO TO 7000
C     **-** PERFECTLY PLASTIC **-**
      IF(EK(IK9).GT.10.0E-3) GO TO 6200
      EK(IK8)=2.0E4*EK(IK9)
      GO TO 9000
 6200 EK(IK8)=200.0
      GO TO 9000
C     **-** NONLINEAR MATERIAL **-**
 7000 IF(EK(IK9).GT.3.0E-3) GO TO 7200
      EK(IK8)=2.0E4*EK(IK9)
      GO TO 9000
 7200 IF(EK(IK9).GT.6.0E-3) GO TO 7400
      EK(IK8)=60.0
      GO TO 9000
 7400 EK(IK8)=120.0-1.0E4*EK(IK9)
 9000 RETURN
      END
```

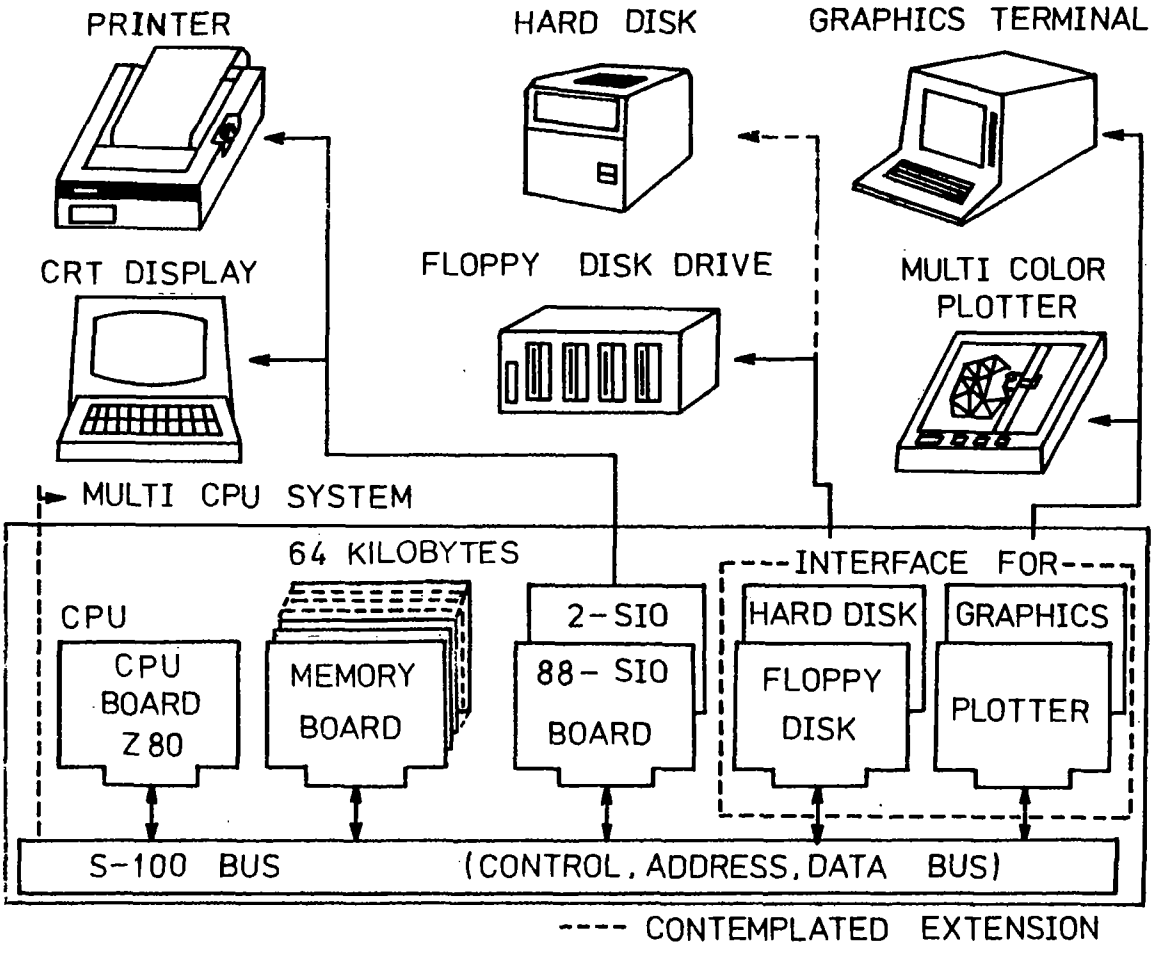

Figure 1.- Structure of microcomputer system.

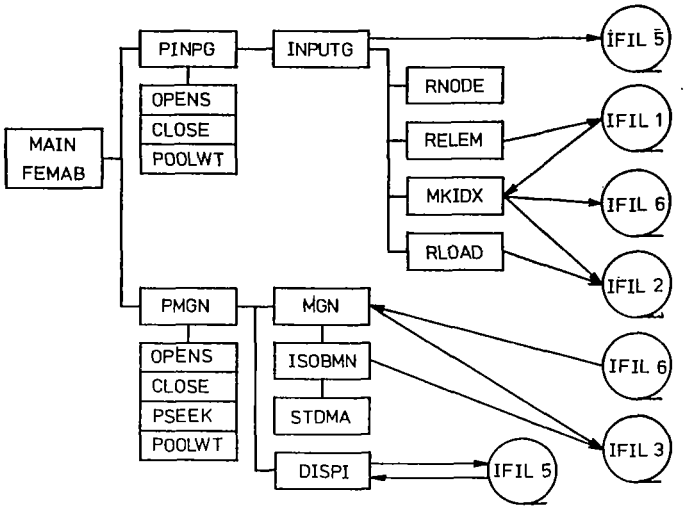

(a) FEMAB.

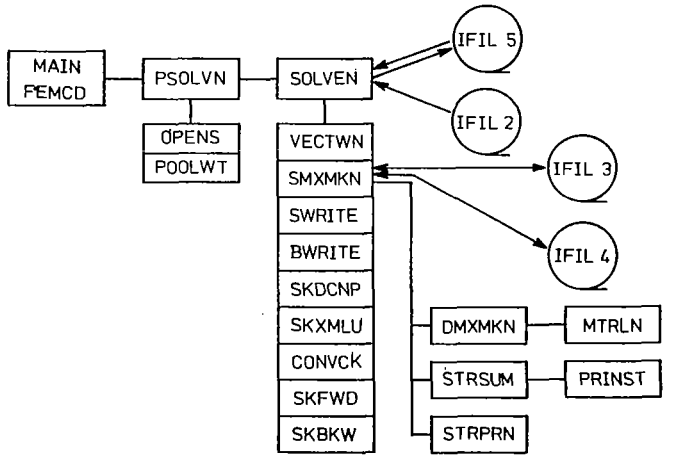

(b) FEMCD.

Figure 2.- Organization of FEMAB and FEMCD.

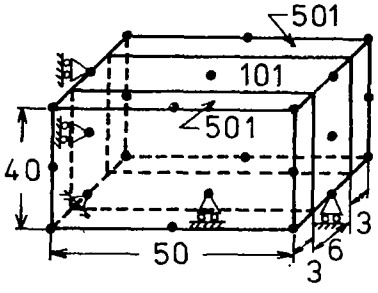

MODULUS H'_o OF MATERIALS, kgf/mm²

STRAIN RANGE	H'_o OF ELEMENT 101	501
$\varepsilon < 3\times10^{-3}$	20×10^3	20×10^3
$3\times10^{-3} < \varepsilon < 6\times10^{-3}$	20×10^3	0
$6\times10^{-3} < \varepsilon < 10\times10^{-3}$	20×10^3	-10×10^3
$10\times10^{-3} < \varepsilon$	0	-10×10^3

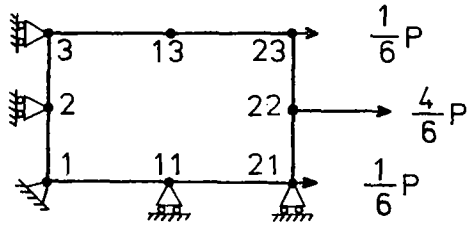

SPECIFIED LOADING SEQUENCE

LOAD STEP	TOTAL LOAD INCREMENT	DISPLACEMENT INCREMENT
1	24×10^3 (kgf)	—
2	12×10^3	—
3	12×10^3	—
4	—	0.2 (mm)
5	—	0.2
6	—	0.2
7	-12×10^3	—
8	-12×10^3	—
9	-12×10^3	

Figure 3.- Composite block of nonlinear material.

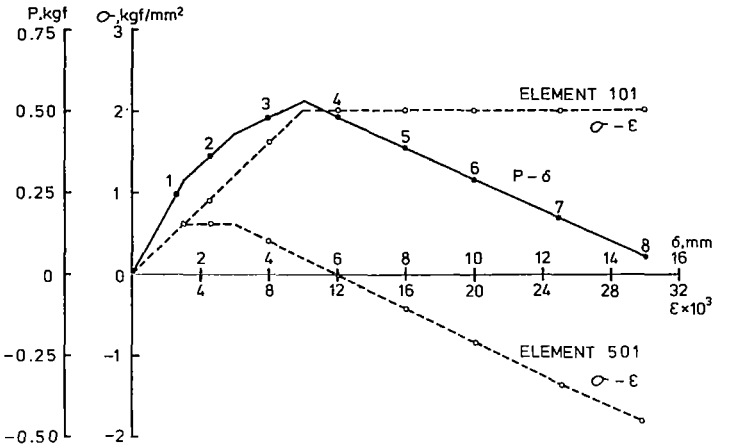

Figure 4.- Nonlinear material properties and load-displacement curve.

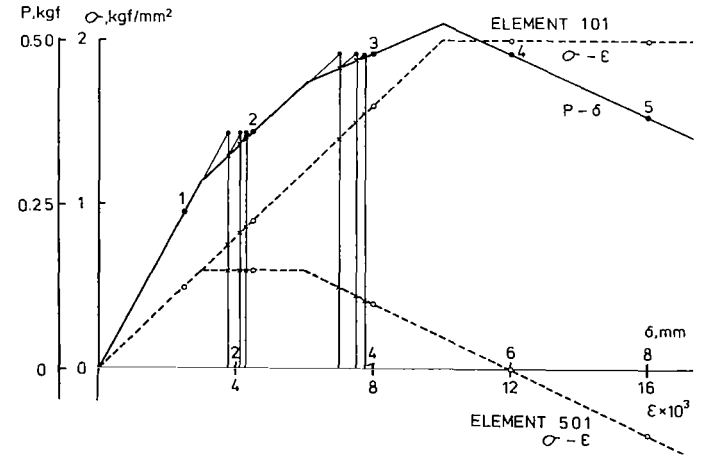

Figure 5.- Convergence of solution.

1. Report No.	2. Government Accession No.	3. Recipient's Catalog No.
NASA CP-2147		

4. Title and Subtitle	5. Report Date
RESEARCH IN NONLINEAR STRUCTURAL AND SOLID MECHANICS	October 1980
	6. Performing Organization Code

7. Author(s)	8. Performing Organization Report No.
Harvey G. McComb, Jr., and Ahmed K. Noor, compilers	L-13950
	10. Work Unit No.
9. Performing Organization Name and Address	506-53-53-03
NASA Langley Research Center Hampton, VA 23665	11. Contract or Grant No.
	13. Type of Report and Period Covered
12. Sponsoring Agency Name and Address	Conference Paper
National Aeronautics and Space Administration Washington, DC 20546	14. Sponsoring Agency Code

15. Supplementary Notes

Harvey G. McComb, Jr.: NASA Langley Research Center.
Ahmed K. Noor: The George Washington University, Joint Institute for Advancement of Flight Sciences, NASA Langley Research Center.

Most of the papers presented at the symposium are contained in Noor, Ahmed K.; and McComb, Harvey G., Jr. (eds.): Computational Methods in Nonlinear Structural and Solid Mechanics. Pergamon Press, Ltd., 1980.

16. Abstract

A Symposium on Computational Methods in Nonlinear Structural and Solid Mechanics was held in Washington, D.C., on October 6-8, 1980. NASA Langley Research Center and The George Washington University sponsored the symposium in cooperation with the National Science Foundation, the American Society of Civil Engineers, and the American Society of Mechanical Engineers. The purpose of the symposium was to communicate recent advances and foster interaction among researchers and practioners in structural engineering, mathematics (especially numerical analysis), and computer technology. This conference publication includes 20 papers; 15 were presented at research-in-progress sessions and 5 at other sessions. The papers deal with (1) nonlinear analysis of building structures (2 papers), (2) numerical solution of nonlinear algebraic equations and Newton's method (1 paper), (3) nonlinear interaction problems (2 papers), (4) solution procedures for nonlinear problems (4 papers), (5) crash dynamics and advanced nonlinear applications (3 papers), (6) material characterization, contact problems, and inelastic response (5 papers), and (7) formulation aspects and special software for nonlinear analysis (3 papers).

17. Key Words (Suggested by Author(s))	18. Distribution Statement
Nonlinear mechanics Structural mechanics Solid mechanics Computational methods	Unclassified - Unlimited Subject Category 39

19. Security Classif. (of this report)	20. Security Classif. (of this page)	21. No. of Pages	22. Price
Unclassified	Unclassified	308	A14

For sale by the National Technical Information Service, Springfield, Virginia 22161

NASA-Langley, 1980